LAURA A. TOOKMAN

THE ROLE OF THE DNA DAMAGE AND REPAIR PATHWAYS IN THE EFFICACY OF ONCOLYTIC ADENOVIRUS FOR OVARIAN CANCER

THE ROLE OF THE DNA DAMAGE AND REPAIR PATHWAYS IN THE EFFICACY OF ONCOLYTIC ADENOVIRUS FOR OVARIAN CANCER

LAURA A. TOOKMAN

Centre for Molecular Oncology
Barts Cancer Institute
Queen Mary University of London

June 2016

DECLARATION

I, Laura Tookman, confirm that the work presented in this thesis is my own. Where information has been derived from other sources, I confirm that this has been indicated in the thesis.

London, UK, June 2016

Laura A. Tookman

ABSTRACT

Defects within the DNA damage response (DDR) pathways are common in human malignancies. This is especially true in high-grade serous ovarian cancer (HGSOC) where defects within the Homologous Recombination (HR) pathway may be present in up to 50% of tumours. Oncolytic adenovirus is a potential novel therapy for human malignancies. These viruses infect malignant cells and multiply selectively within them causing cell death and release of mature virions. Here, I have investigated the role of the DDR in determining the efficacy of the E1A-CR2 deleted adenovirus type 5 (Ad5) vector, *dl*922-947, in ovarian cancer.

I show that infection with *dl*922-947 stimulates a robust DDR within the host cell, which the virus manipulates in order to ensure optimal viral replication. In a panel of HGSOC cell lines, the extent of over-replication of genomic DNA and the degree of genomic damage following infection with *dl*922-947 was shown to correlate closely with viral efficacy. Functional HR, however, promoted viral DNA replication and augmented overall anti-cancer efficacy. Mechanistically, both BRCA2 and RAD51 localised to viral replication centres within the infected cell nucleus. RAD51 co-localisation was also demonstrated in cells with defective HR and occurred independently of BRCA2. In addition, a direct interaction was identified between RAD51 and adenovirus E2 DNA binding protein. Using functional assays of HR competence, I show that Ad5 infection does not alter cellular ability to repair DNA double-strand break damage via HR. These data suggest that oncolytic adenoviral therapy may be most clinically relevant in tumours with intact HR function.

Using a high-throughput siRNA DNA repair screen, potential novel targets have been identified that can increase the efficacy of *dl*922-947 (for example: NONO) and also result in increased resistance (RPA).

These results highlight the complex interplay between adenovirus and host cell. Further understanding of these pathways is vital to increase efficacy, develop biomarkers and improve patient selection into clinical trials for these therapies.

PUBLICATIONS

Some ideas and figures have appeared previously in the following publications:

- **Tookman LA**, Browne AK, Connell CM, Bridge G, Ingemarsdotter CK, Dowson S, Shibata A, Lockley M, Martin SA, McNeish IA. RAD51 and BRCA2 Enhance Oncolytic Adenovirus Type 5 Activity in Ovarian Cancer. *Molecular Cancer Research*. 2016 Jan;14(1):44-55.
- Connell CM, Shibata A, **Tookman LA**, Archibald KM, Flak MB, Pirlo KJ, Lockley M, Wheatley SP, McNeish IA. Genomic DNA damage and ATR-Chk1 signaling determine oncolytic adenoviral efficacy in human ovarian cancer cells. *Journal of Clinical Investigation*. 2011 Apr;121(4):1283-97.

ACKNOWLEDGMENTS

I have many people that I must thank, without whom this thesis could not have been written.

I feel very lucky to have the support and guidance from two inspirational supervisors, Iain McNeish and Sarah Martin. Thank you to Iain McNeish for introducing me to science, the joys of lab meetings with cake and his unwavering support despite geographic distances. I am very grateful to Sarah Martin for accepting me so readily in her group, her encouragement, understanding and scientific guidance during my project. Thank you to Michelle Lockley for allowing me to be part of her lab meetings, her support and career advice.

I must also thank all members of the Department of Molecular Oncology for creating such a friendly and open working environment and for help with answering lots of daft/ridiculous questions from a medic with limited pipetting experience. Thank you to all members of 'Team McNeish' and 'Team Martin' both past and present. I would particularly like to thank Ashley for all her technical help and support throughout the years.

Thanks also to the MRC for funding me and giving me the opportunity to enter the world of research.

Thank you to my family, especially my husband, Mike, for putting up with me - this thesis could definitely not have been written without you.

CONTENTS

I INTRODUCTION 27

1 INTRODUCTION 28

1.1 Ovarian cancer 28

1.1.1 Epidemiology and genetics 28

1.1.2 Pathology and molecular characteristics of epithelial ovarian cancer 30

1.1.3 Low grade serous ovarian cancer 31

1.1.4 Mucinous carcinomas 32

1.1.5 Clear cell and endometrioid ovarian cancers 32

1.1.6 Molecular characteristics of high grade serous ovarian cancers 33

1.1.7 Ovarian cancer and genomic instability 36

1.1.8 The spread of ovarian cancer and the tumour microenvironment 37

1.1.9 Current treatment of Ovarian Cancer 41

1.2 HR pathway and DNA damage response 45

1.2.1 Signalling DSB damage 48

1.2.2 Repair of DSBs: Classical NHEJ 51

1.2.3 Alt-NHEJ and SSA 52

1.2.4 Homologous recombination 52

1.2.5 Regulation of HR 54

1.2.6 Negative regulators of HR 58

1.2.7 Repair of DSBs: Pathway choice 59

1.2.8 HR defects and cancer 61

1.2.9 Therapeutic targeting of the DDR 62

1.2.10 Targeting the HR pathway in ovarian cancer 62

1.3 Oncolytic Viruses 68

1.3.1 The development of oncolytic adenoviral vectors 69
1.4 Adenovirus 70
1.4.1 Structure 70
1.4.2 Adenoviral DNA 71
1.4.3 Adenoviral life cycle 73
1.4.4 Early phase: cell entry 73
1.4.5 Early phase: S phase induction 75
1.4.6 Viral replication 79
1.4.7 Inhibition of apoptosis by adenovirus 80
1.4.8 Adenoviruses and the immune response 82
1.4.9 The adenoviral E4 region 87
1.4.10 Adenovirus and the DNA damage response 87
1.4.11 Oncolytic adenoviruses summary and rationale for this project 92
1.5 Aims 94

II MATERIALS AND METHODS 95

2 MATERIALS AND METHODS 96
2.1 Cell lines 96
2.2 Adenoviral mutants 97
2.3 Cell Survival assays 97
2.3.1 MTT assay 97
2.3.2 Sulforhodamine B assay 98
2.3.3 CellTitre-Glo 99
2.3.4 Analysis 99
2.4 Immunoblot Blot analysis 99
2.4.1 Preparation of protein lysates 99
2.4.2 Protein concentration evaluation 100
2.4.3 SDS polyacrylamide gel electrophoresis (SDS PAGE) 100
2.5 Co-Immunoprecipitation 102

2.6 Viral life cycle 103
2.6.1 Virus Infectivity assay 103
2.6.2 $TCID_{50}$ assay 103
2.6.3 Extraction of viral DNA for qPCR for viral proteins 105
2.6.4 Quantitative PCR for viral DNA 106
2.7 Southern Blot 107
2.8 Immunofluorescence 107
2.9 Experiments using small interference RNA 108
2.10 RNA harvest for BRCA2 transcription 110
2.10.1 RNA analysis 111
2.10.2 Reverse transcription of RNA to yield cDNA 111
2.10.3 Quantitative RT-PCR 112
2.11 Homologous Recombination Reporter assay 113
2.12 High-throughput siRNA screen 115
2.12.1 siRNA screen validation 118

III RESULTS 119

3 DNA DAMAGE AND VIRAL CYTOTOXICITY 120
3.1 Introduction 120
3.2 Results 121
3.2.1 *dl*922-947 is cytotoxic to ovarian cancer cell lines 121
3.2.2 Cellular infectivity to *dl*922-947 121
3.2.3 Cell cycle following infection with *dl*922-947 125
3.2.4 Cell cycle changes following iso-infection with *dl*922-947 130
3.2.5 Genomic damage following infection with *dl*922-947 131
3.2.6 Genomic damage assessed by Immunofluorescence 135
3.2.7 Genomic damage following iso-infection with *dl*922-947 138

3.2.8 Differences in background DNA damage do not correlate with adenoviral efficacy 140
3.2.9 Genomic damage following infection with a non-replicating virus 142
3.2.10 Genomic damage following infection with E1A wild type virus 144
3.2.11 DNA damage induced by chemotherapeutics and sensitivity to *dl*922-947 146
3.3 Discussion 148
4 HOMOLOGOUS RECOMBINATION AND VIRAL CYTOTOXICITY 153
4.1 Introduction 153
4.2 Results 154
4.2.1 Adenoviral cytotoxicity in HR competent and incompetent cells 154
4.2.2 HR competence and viral efficacy 161
4.2.3 Viral infectivity and cytotoxicity in HR competent and incompetent cells 163
4.2.4 Viral lifecycle in HR competent and incompetent cell lines 166
4.2.5 DNA damage and cell cycle in PE01 and PE04 cells 169
4.2.6 PARP inhibitor and *dl*922-947 172
4.2.7 MRE11 is degraded following infection with *dl*922-947 175
4.2.8 NHEJ function in the HR competent and incompetent cell lines 177
4.2.9 RAD51 is maintained at early time points 179
4.2.10 BRCA2 co-localises with VRC 180
4.2.11 BRCA2 influences adenovirus efficacy in HR competent cells 183
4.2.12 RAD51 co-localises with VRC 185
4.2.13 RAD51 influences adenovirus efficacy 190

4.2.14 RAD51 influences adenovirus replication 194
4.2.15 *dl*922-947 does not inhibit HR function 197
4.3 Discussion 200
5 HIGH-THROUGHPUT DNA DAMAGE AND REPAIR SCREEN 208
5.1 Introduction 208
5.2 Results 209
5.2.1 Experimental setup 209
5.2.2 Optimisation experiments 212
5.2.3 DNA damage and repair screen 214
5.2.4 Hits from screen that resulted in increased sensitivity to *dl*922-947 219
5.2.5 Screen hits that resulted in resistance to *dl*922-947 222
5.2.6 Validation of siRNA hits 225
5.2.7 Further validation of hits 228
5.3 Discussion 230
IV DISCUSSION 236
6 DISCUSSION 237
6.1 A brief summary 237
6.2 Conclusions and future work 238
6.2.1 The mechanism of cell death 239
6.2.2 Identification of biomarkers 241
6.2.3 The role of the immune system 243
6.3 Potential future directions 244
6.3.1 Development of experimental models 244
6.3.2 Extending findings to other viruses and DNA repair pathways 245
6.3.3 Combination treatment 247
6.3.4 Development of future clinical trials 248
6.4 Concluding remarks 250

V APPENDIX 251

A APPENDIX 252

A.1 Publications 252

A.2 Results from screen 280

BIBLIOGRAPHY 294

LIST OF FIGURES

Figure 1.1 The origins of ovarian cancer 31
Figure 1.2 Molecular characteristics of HGSOC 34
Figure 1.3 The immune microenvironment in ovarian cancer 38
Figure 1.4 The molecular and physiological consequences of the DDR 46
Figure 1.5 Main pathways involved in repair of DNA damage 47
Figure 1.6 Signalling DNA damage to cell cycle checkpoints 50
Figure 1.7 Key factors involved in repair of DSBs by HR 53
Figure 1.8 Repair of DSBs by HR 55
Figure 1.9 Cell cycle and DNA repair pathway choice 60
Figure 1.10 Synthetic lethality 65
Figure 1.11 Tumour specific killing by oncolytic adenovirus 70
Figure 1.12 Structure of adenovirus 71
Figure 1.13 Adenoviral DNA 72
Figure 1.14 Cell cycle control and E1A 76
Figure 1.15 E1A regions bind to a variety of cellular proteins 78
Figure 1.16 The adenoviral mutant, *dl*922-947 79
Figure 1.17 The E3 region of the viral genome 83
Figure 1.18 The E4 region of the viral genome 88
Figure 1.19 Regulation of the DDR by adenovirus type 5 92
Figure 2.1 Reporter assay to assess homologous recombination function 114
Figure 2.2 HTS method 116
Figure 3.1 Cytotoxicity of adenoviruses in ovarian cancer cells 122
Figure 3.2 Permissiveness of cell lines to adenoviral infection 123

Figure 3.3 Cytotoxicity in cells equally infected with *dl*922-947 124
Figure 3.4 Cell cycle profiles following *dl*922-947 infection 126
Figure 3.5 Cell cycle changes following infection with *dl*922-947 127
Figure 3.6 Cell cycle changes following *dl*922-947 infection and correlation with overall efficacy 129
Figure 3.7 Cell cycle changes following iso-infection with *dl*922-947 131
Figure 3.8 Cell cycle and genomic damage assessed by flow cytometry following *dl*922-947 132
Figure 3.9 Relationship between genomic DNA damage and cellular sensitivity to *dl*922-947 134
Figure 3.10 DNA damage assessed by IF following infection with *dl*922-947 136
Figure 3.11 Quantification of DNA damage assessed by IF 137
Figure 3.12 Correlation between sensitivity to *dl*922-947 and γH2AX intensity 138
Figure 3.13 DNA damage following iso-infection with *dl*922-947 139
Figure 3.14 Background genomic damage and viral efficacy 141
Figure 3.15 DNA damage following infection with a non-replicating virus 143
Figure 3.16 DNA damage following infection with E1A wild type virus 145
Figure 3.17 Correlation between adenovirus efficacy and DNA damage induced by chemotherapy agents 147
Figure 4.1 HR competence assessed in PE01 and PE04 cells 157
Figure 4.2 Cisplatin and rucaparib dose response curves 158
Figure 4.3 Sensitivity of PE01 and PE04 cells to type 5 adenovirus 160

Figure 4.4 Sensitivity of PE01 and PE04 cells to group B adenovirus 161
Figure 4.5 HR compentence of a panel of ovarian cancer cell lines 162
Figure 4.6 Association between IC_{50} *dl*922-947 and HR competence 163
Figure 4.7 Viral infectivity in an HR competent and incompetent cell pair 164
Figure 4.8 Viral cytotoxicty following iso-infection with *dl*922-947 in an HR competent and incompetent cell line 165
Figure 4.9 Viral replication in an HR competent and incompetent cell line 166
Figure 4.10 Protein expression in an HR competent and incompetent cell line 167
Figure 4.11 Viral DNA in an HR competent and incompetent cell line 168
Figure 4.12 Assessment of viral DNA in an HR competent and incompetent cell line 169
Figure 4.13 DNA damage and cell cycle in a HR competent and incompetent cell pair 170
Figure 4.14 Cell cycle and DNA damage in an HR competent and incompetent pair at baseline 171
Figure 4.15 DNA damage and cell cycle following isoinfection with *dl*922-947 172
Figure 4.16 PARP inhibitor does not increase cytotoxicity to *dl*922-947 174
Figure 4.17 MRE11 is degraded following infection with *dl*922-947 176
Figure 4.18 Sensitivity of BRCA2 deficient and proficient cells to DNA PK inhibitor 178
Figure 4.19 Effect of inhibition of DNA PK to viral cytotoxicity 178

Figure 4.20 RAD51 is maintained at early time-points following infection 180
Figure 4.21 BRCA2 co-localises with VRC 181
Figure 4.22 Assessment of HR function in TOV21G and HeLa cells 182
Figure 4.23 BRCA2 co-localises with VRC 183
Figure 4.24 BRCA2 knockdown 184
Figure 4.25 BRCA2 knockdown decreases adenovirus efficacy 185
Figure 4.26 RAD51 co-localises with VRC in HR competent cells 186
Figure 4.27 RAD51 co-localises with VRC in the HR incompetent PE01 cell line 187
Figure 4.28 Assessment of HR function in IGROV1 cells 188
Figure 4.29 RAD51 co-localises with VRC in the the HR incompetent, IGROV1 cell line 189
Figure 4.30 Co-immunoprecipitation of RAD51 and viral E2 DBP 189
Figure 4.31 RAD51 knockdown in PE01 and PE04 cell lines 190
Figure 4.32 RAD51 knockdown reduces cytotoxicity to *dl*922-947 191
Figure 4.33 RAD51 knockdown reduces cytotoxicity to *dl309* 192
Figure 4.34 RAD51 knockdown reduces cytotoxicity in HR competent cell lines 193
Figure 4.35 RAD51 knockdown reduces cytotoxicity in an incompetent cell line 194
Figure 4.36 Viral replication is reduced following knockdown of RAD51 196
Figure 4.37 γH2AX and RAD51 foci following infection with *dl*922-947 197
Figure 4.38 *dl*922-947 infection does not alter the function of HR 198

Figure 4.39 Adenovirus infection does not increase sensitivity to PARP inhibitor or cisplatin 199
Figure 5.1 Sensitivity of OVCAR4 and COV318 cells to *dl*922-947 210
Figure 5.2 HR competence assessed in OVCAR4 and COV318 cells 211
Figure 5.3 Sensitivity of OVCAR4 and COV318 cells to cisplatin and rucaparib 212
Figure 5.4 Optimisation of transfection reagents 213
Figure 5.5 Optimisation of dose of virus 214
Figure 5.6 Reproducibility of HTS 216
Figure 5.7 Scatter plot showing average ΔZ scores 217
Figure 5.8 Waterfall plot of Scatter plot showing average ΔZ scores 218
Figure 5.9 Genes selected from the HTS that resulted in sensitization to *dl*922-947 220
Figure 5.10 Cell survival following infection with *dl*922-947 in the siControl wells 223
Figure 5.11 Genes selected from the HTS that resulted in resistance to *dl*922-947 224
Figure 5.12 Further genes selected from the HTS that resulted in resistance to *dl*922-947 225
Figure 5.13 High-throughput screen validation 227
Figure 5.14 NONO siRNA increases cytotoxicity to *dl*922-947 229
Figure 5.15 Immunoblot showing knockdown of NONO 230

LIST OF TABLES

Table 2.1 Components of SDS PAGE resolving (10% and 15%) and stacking gels 101
Table 2.2 Antibodies used for Immunoblot analysis 102
Table 2.3 Oligonucleotides and probes for E1A and Ad5 106
Table 2.4 Antibodies used in Immunofluorescence experiments 108
Table 2.5 BRCA2 primer and probe sequences 112

ABBREVIATIONS

53BP1	p53-binding protein 1
γH2AX	γ H2A histone family, member X
Ad5	Adenovirus Type 5
Ad5-WT	Wild type adenovirus
ADP	Adenovirus death protein
alt-NHEJ	Alternative NHEJ
ARID1A	AT-rich interaction domain 1A
ATM	Ataxia telangiectasia mutated
ATP	Adenosine triphosphate
ATR	Ataxia telangiectasia and RAD3-related protein
ATRIP	ATR interacting protein
AUC	Area under the curve
BARD	BRCA1-associated RING domain protein
BAX	BCL2-associated X protein

BCL2	B-cell lymphoma 2
BER	Base excision repair
BLM	Bloom syndrome
BIR	Break-induced replication
BRAF	B-Raf proto-oncogene, serine/threonine kinase
BRCA1	Breast cancer type 1 susceptibility protein
BRCA2	Breast cancer type 2 susceptibility protein
BRCT	BRCA1 C Terminus
BRIP1	BRCA1 interacting protein C-terminal helicase 1
BSA	Bovine serum albumin
CA125	Cancer antigen 125
CAR	Coxsackie Adenovirus Receptor
CBP	CREB-binding protein
CCNE1	Cyclin E1
CCT5	Chaperonin Containing TCP1, Subunit 5
CDK1	Cyclin-dependent kinase 1
CDK2	Cyclin-dependent kinase 2
cDNA	complementary DNA
CETN2	Centrin 2
CHK1	Checkpoint kinase 1
CHK2	Checkpoint kinase 2
CIN	Chromosome instability
CMV	Cytomegalovirus

C-NHEJ	Classical-NHEJ
Co-IP	Co-immunoprecipitation
CPE	Cytopathic effect
CR	Conserved region
CtIP	C-terminal binding protein
CTL	Cytotoxic T lymphocytes
CTLA4	Cytotoxic T-lymphocyte-associated protein 4
Cul2	Cullin2
Cul5	Cullin5
CXCL12	Chemokine (C-X-C motif) ligand 12
DAPI	4′,6-Diamidino-2-phenylindole
DBP	DNA binding protein
DC	Dendritic cell
DDR	DNA damage response
dHJ	Double Holliday junction
DMEM	Dulbecco's modified Eagle's medium
DNA	Deoxyribonucleic acid
DNA-PK	DNA-dependent protein kinase
DNA-PKcs	DNA-dependent protein kinase catalytic subunit
dNTP	Deoxyribonucleotide
DSB	Double strand break
DSBR	Double strand break repair
dsDNA	Double strand DNA

E1A	Early region 1A
E2 DBP	E2 DNA binding protein
EBV	Epstein Barr virus
ERCC1	Excision repair cross-complementing protein 1
EXO1	Exonuclease 1
FACS	Fluorescence-activated cell sorting
FBS	Foetal bovine serum
FIGO	The International Federation of Gynecology and Obstetrics
GFP	Green fluorescent protein
HGSOC	High-grade serous ovarian cancer
HNPCC	Hereditary nonpolyposis colon cancer
hnRNPUL1	Heterogeneous Nuclear Ribonucleoprotein U-Like 1
HR	Homologous recombination
HRP	Horse radish peroxidase
HSV	Herpes simplex virus
IAP	Inhibitors of apoptosis proteins
IC50	Inhibitory concentration, 50%
ICL	Intra-cross and inter-cross links
IDO	Indoleamine 2,3-dioxygenase
IF	Immunofluorescence
IL	Interleukin
IP	Intraperitoneal

IR	Ionizing radiation
IT	Intratumoural
ITR	Inverted terminal repeats
KRAS	Kirsten rat sarcoma viral oncogene homolog
LOH	Loss of heterozygosity
MAD	Median absolute deviation
MBD1	Methyl-CpG binding domain protein 1
MDC1	Mediator of damage checkpoint 1
MHC I	Major histocompatibility complex class one
MLP	Major late promoter
MMP9	Matrix metalloproteinase 9
MMR	DNA mismatch repair
MOI	Multiplicity of infection
MRN	MRE11-RAD50-NBS1
mTOR	Mammalian target of rapamycin
NADPH	Nicotinamide adenine dinucleotide phosphate
NER	Nucleotide excision repair
NF	Nuclear factor
NF1	Neurofibromin 1
NHEJ	Non-homologous end joining
NK cells	Natural killer cells
NONO	Non-POU domain containing, octamer-binding
NUP205	Nucleoporin 205kDa

orf	Open reading frame
OS	Overall survival
PAGE	Poly acrylamide gel electrophoresis
PALB2	Partner and localizer of BRCA2
PARI	Proliferating cell nuclear antigen
PARP1	Poly(ADP-ribose) polymerase 1
PAX5	Paired box protein 5
PBS	Phosphate buffered saline
PCNA	Proliferating cell nuclear antigen-interacting factor
PCR	Polymerase chain reaction
PD-L1	Programmed death ligand 1
PFU	Plaque forming units
PFS	Progression free survival
PI	Propidium iodide
PI3K	Phosphoinositide 3-kinase
PIK3CA	Phosphatidylinositol-4,5-Bisphosphate 3-Kinase, Catalytic Subunit Alpha
PIKK	Phosphatidylinositol 3-kinase related kinase
PLD	Liposomal doxorubicin
PLK1	Polo-like kinase 1
PML	Promyelocytic leukaemia protein
pol	polymerase
pRB	Retinoblastoma protein

PTEN	Phosphatase and tensin homolog
qRT-PCR	Quantitative reverse transcriptase PCR
RBM4	RNA Binding motif protein 4
Rbx1	RING-box 1
RGD	Arginine-glycine-aspartate
RID	Receptor internalisation and degradation
RNA	Ribonucleic acid
RNF168	Ring Finger Protein 168
ROS	Reactive oxygen species
RPA	Replication protein A
RPMI	Roswell Park Memorial Institute medium
RTKi	Receptor tyrosine kinase inhibitor
RT-PCR	Reverse transcriptase PCR
SD	Standard deviation
SDS	Sodium dodecyl sulfate
SDSA	Synthesis-dependent strand-annealing
SEM	Standard error of the mean
SFPQ	Spicing factor proline/glutamine-Rich
siCrl	Non-targeting control siRNA
siRNA	Small interfering RNA
SMC1	Structural maintenance of chromosomes protein 1A
SNP	Single nucleotide polymorphism
SSA	Single-strand annealing

SSB	Single strand breaks
ssDNA	Single strand DNA
TCID50	Tissue Culture Inhibitory Dose, 50%
TGCA	The Cancer Genome Atlas
TGF	Transforming growth factor
TIC	Tubal intraepithelial carcinoma
TNF	Tumour necrosis factor
TNFR1	TNF receptor 1
TOPBP1	Topoisomerase 2-binding protein 1
TP	Terminal protein
TP53	Tumour protein 53
TRAIL	TNF related apoptosis inducing ligand
Tregs	Regulatory T cells
VA RNA	Viral associated RNAs
VEGF	Vascular endothelial growth factor
VRC	Viral replication centres
XLF	XRCC4-like factor
XRCC2	X-ray repair cross-complementing protein 2
XRCC4	X-ray repair cross-complementing protein 4
YB1	Y-Box Binding Factor-1

Part I

INTRODUCTION

1

INTRODUCTION

1.1 OVARIAN CANCER

Ovarian cancer is the most lethal gynaecological malignancy. It is the eighth most common type of cancer and the seventh most common cause of cancer-related death in women worldwide (5th among women in Western countries) (Jemal et al., 2011). Although patient prognosis has improved for many solid cancers, survival for women with ovarian cancer has changed little since the introduction of platinum based chemotherapy over 30 years ago (Lowe et al., 2013; Coleman et al., 2011). Many women present with advanced disease with only 27% of women with distant disease surviving 5 years post diagnosis (Jemal et al., 2010). There is clearly a need for new and more effective therapies.

1.1.1 *Epidemiology and genetics*

The age-standardised incidence of developing ovarian cancer is approximately 9.4 per 100 000 population in developed areas and 5 per 100 000 populations elsewhere (Jemal et al., 2011; Soerjomataram et al., 2012). In the UK, 7000 women develop ovarian cancer and 4200 die from the disease each year (Jelovac and Armstrong, 2011). Age and genetics are the most well established risk factors for ovarian cancer. It most commonly occurs in peri- or post-menopausal women, with the median age of diagnosis being 63 years, although some hereditary tumours are often diagnosed approximately 10 years earlier (Boyd et al., 2000).

The lifetime risk of developing ovarian cancer is <2% for the average woman and 4-5% among women with a single family member with the disease (Lowe et al., 2013). Germ line genetic mutation syndromes are a major cause of increased risk of epithelial ovarian cancer. Approximately 10-12% of all ovarian cancers are familial and most of these are linked to mutations in the breast and ovarian cancer susceptibility genes, *BRCA1* or *BRCA2*. These genes are involved in the repair of deoxyribonucleic acid (DNA) double strand breaks (DSB) (Venkitaraman, 2009). The lifetime risk of developing ovarian cancer is 12-25% in women with a *BRCA2* mutation and 35-60% among women with *BRCA1* mutations (Antoniou et al., 2003; King et al., 2003). More recently, mutations in further genes have also been implicated in increasing ovarian cancer risk including *RAD51C, RAD51D* and BRCA1 Interacting Protein C-Terminal Helicase 1 *(BRIP1)* (Pennington and Swisher, 2012). For women with germline *BRCA1* or *BRCA2* mutations, prophylactic oophorectomy has been shown to be associated with a 90% reduction in the risk of ovarian cancer (Rebbeck et al., 2002). However a small percentage of women may develop disseminated peritoneal disease (Piver et al., 1993). Other hereditary cancer syndromes that increase ovarian cancer risk include Lynch syndrome where mutations are found in DNA mismatch repair (MMR) genes. This syndrome has been estimated to increase risk of ovarian cancer by up to 20% but the risk depends on the gene involved (Bonadona et al., 2011). These mutations are found to be present in less than 1% of ovarian cancers and are more common in endometrioid and clear cell subtypes.

Although genetic factors have the most significant impact on ovarian cancer risk, epidemiological studies have also shown that the risk of developing ovarian cancer is proportional to the number of lifetime ovulations (Titus-Ernstoff et al., 2001; Jelovac and Armstrong, 2011). Factors that increase ovulations and/or oestrogen exposure, such as nulliparity, early menarche, late menopause and the use of

hormone replacement therapy, all increase the risk of ovarian cancer (Titus-Ernstoff et al., 2001; Morch et al., 2009; Salehi et al., 2008). Conversely, factors associated with suppression of ovulations such as increasing numbers of full term pregnancies, longer duration of lactation and oral contraception use are associated with decreased risk (Titus-Ernstoff et al., 2001; Hinkula et al., 2006). Tubal ligation and hysterectomy have also been shown to decrease the risk (Hankinson et al., 1993; Van Gorp et al., 2004). There are some studies that suggest that chronic inflammation in the reproductive tract is involved in ovarian cancer development (reviewed in Knutson et al. (2015)). These studies suggest that inflammation as a result of incessant rounds of ovulation lead to oncogenic events. This is supported by the association of the inflammatory conditions endometriosis and polycystic ovaries with ovarian cancer (Chittenden et al., 2009; Munksgaard and Blaakaer, 2012).

1.1.2 *Pathology and molecular characteristics of epithelial ovarian cancer*

Epithelial ovarian cancer is not a single disease but is composed of a diverse group of tumours that can be classified based on morphological and molecular genetic features (Kurman and McConnell, 2010). High grade serous, low grade serous, endometrioid, clear-cell and mucinous ovarian cancers are the five most common histotypes (Figure 1.1). These different subtypes have distinct clinical characteristics and are characterised by different molecular abnormalities. It was previously thought that these tumours arose from ovarian tissue. However, pathological and molecular studies have recently provided a different view of epithelial ovarian cancer and the majority of invasive tumours are now thought to arise from non-ovarian tissues. Although the actual contribution of the ovary to the spectrum of epithelial cancers is still debated, it is now apparent that the different histotypes should be considered distinct diseases originating from different cell

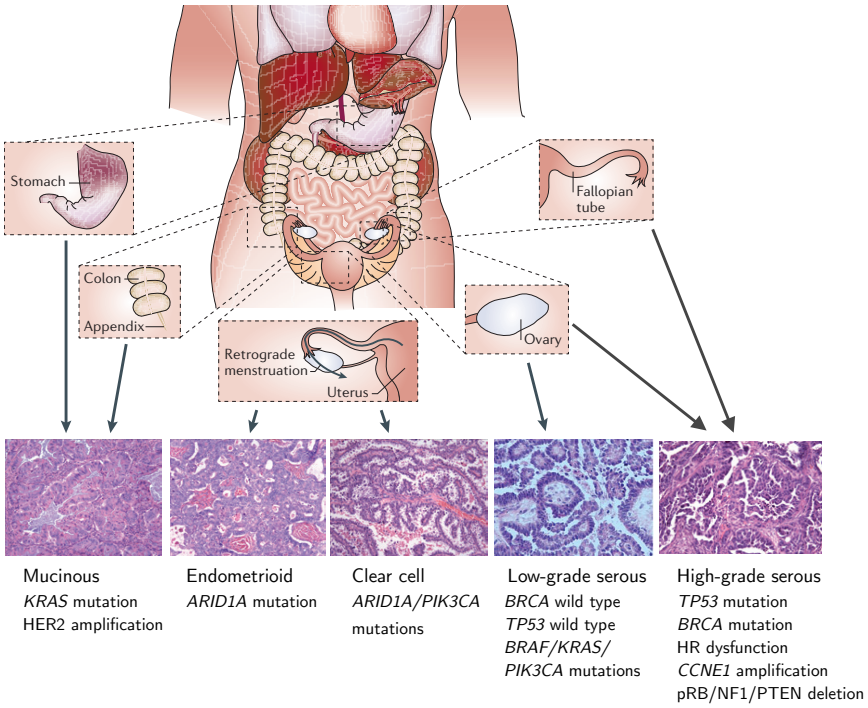

Figure 1.1: The origins of ovarian cancer. Ovarian cancer is not a single disease. It consists of a diverse group of tumours with different origins and distinct pathological and molecular features. Image shows five subtypes of ovarian cancer with their likely site of origin and lists key molecular features. Image adapted from Vaughan et al. (2011).

types (Vaughan et al., 2011). Key features of the main subtypes of ovarian cancer are outlined below.

1.1.3 *Low grade serous ovarian cancer*

Low grade invasive tumours are thought to arise from the ovary although their initiating cell is unknown. This subtype accounts for around 4% of ovarian cancers. It shows a much more indolent behaviour compared to high grade tumours and most studies show poor response rates to chemotherapy (Gershenson et al., 2009; Malpica et al., 2004). In addition, low grade serous cancers are not precursor

lesions for high grade serous cancers, as they have a distinct range of molecular events (Bowtell, 2010). Unlike high grade serous cancers, low grade serous ovarian cancer is generally *TP53* and *BRCA* wild-type and chromosomally stable (Singer et al., 2005; Gilks and Prat, 2009; Kuo et al., 2009). Mutations are often found in phosphatidylinositol-4,5-bisphosphate 3-kinase, catalytic subunit alpha *(PIK3CA),* B-Raf proto-oncogene, serine/threonine kinase *(BRAF)* and Kirsten rat sarcoma viral oncogene homolog (*KRAS*) *(Singer et al., 2003)*.

1.1.4 *Mucinous carcinomas*

Mucinous ovarian cancers account for 3-4% of ovarian cancers and are often diagnosed at an early stage when they are confined to the ovary. *KRAS* mutations are common and HER2 amplification has been reported in 18-35% of cancers (Gilks, 2010; Chao et al., 2014). Most invasive mucinous ovarian cancers are believed to represent metastases to the ovary from other cancer types including gastrointestinal tumours, in particular appendiceal cancers (Lee and Young, 2003; Kelemen and Kobel, 2011). The ability to distinguish mucinous ovarian cancers from those from the gastrointestinal tract has improved with the development of immunohistochemistry for the cytokeratins CK7 and CK20 (Jayson et al., 2014) and therefore the incidence of true mucinous ovarian cancers appears to have fallen. Studies have shown poor response rates to chemotherapy and a poorer prognosis compared to high grade serous cancers in patients with advanced stage mucinous cancers (Pignata et al., 2008; Bamias et al., 2010).

1.1.5 *Clear cell and endometrioid ovarian cancers*

Clear cell and endometrioid carcinomas each account for approximately 10% of ovarian cancers. They bear frequent mutations in the

tumour suppressor gene, AT-rich interaction domain 1A (*ARID1A*), a chromatin remodelling gene, and about a third of clear cell ovarian cancers also have *PIK3CA* mutations (Kuo et al., 2009; Wiegand et al., 2010). Pathological and epidemiological data have associated endometrioid and clear cell ovarian cancer with endometriosis. This association has been strengthened by identification of high-frequency somatic mutations in *ARID1A* in adjacent endometriotic and precancerous lesions (Wiegand et al., 2010). Ovarian clear cell cancers have expression phenotypes similar to renal cell cancers (Anglesio et al., 2011) and this may impact treatment choices for this group of patients (for example the use of tyrosine kinase inhibitors frequently used in renal cell cancers) .

1.1.6 *Molecular characteristics of high grade serous ovarian cancers*

Most patients with epithelial ovarian cancer have high grade serous ovarian cancer (HGSOC), a disease that has now been shown to be characterised by specific molecular events (Figure 1.2). By examining focal premalignant lesions and carcinoma *in situ* in the fallopian tubes of women with germ-line *BRCA1/2* mutations who were undergoing prophylactic risk-reducing surgery, the secretory cells of the distal fallopian tubes are the likely progenitor of HGSOC (Lee et al., 2007; Levanon et al., 2008). In addition, disseminated peritoneal cancers are histologically similar and share molecular findings to HGSOC (Birrer, 2010).

The Cancer Genome Atlas (TGCA) project analysed mRNA expression, miRNA expression, promoter hypermethylation and DNA copy number in 489 HGSOCs and the DNA sequences of exons from coding genes in 316 of these tumours (TGCA, 2011). This revealed that HGSOC is characterised by *TP53* mutations in almost all tumours (96%), confirming earlier data (Ahmed et al., 2010). *TP53* mutations have been found to be present in the distal, fimbriated end of the fal-

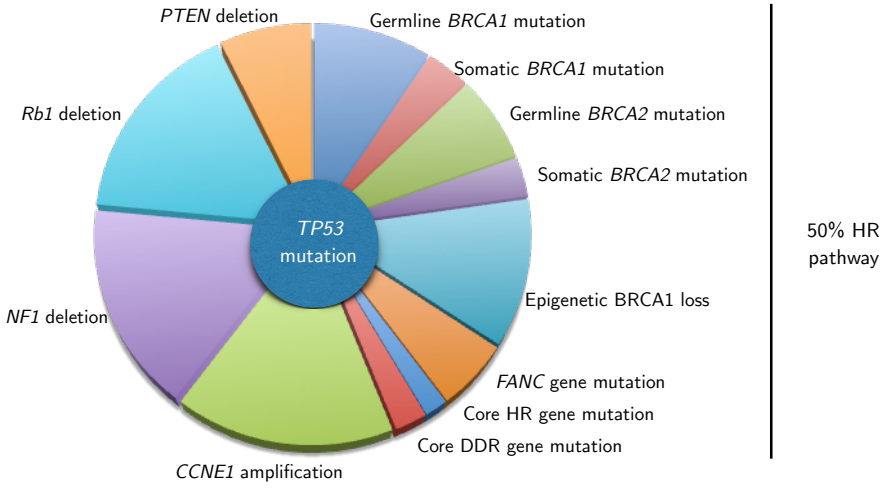

Figure 1.2: Molecular characteristics of HGSOC. The majority have a *TP53* mutation and approximately 50% have mutations affecting the HR pathways. Image created by Prof I. McNeish, data from (TGCA, 2011; Etemadmoghadam et al., 2009; Patch et al., 2015)

lopian tube and these areas, known as tubal intraepithelial carcinoma (TIC), are the probable precursors of many HGSOC (Crum et al., 2007; Lee et al., 2007; Folkins et al., 2008). *TP53* mutation is therefore both an early and necessary event for the development of HGSOC (Bowtell, 2010).

Beyond *TP53* mutations, the TGCA project revealed the importance of the homologous recombination (HR) pathway (discussed in detail below). This pathway is responsible for the repair of DNA double stand breaks (DSBs) and key components of this pathway are BRCA1 and BRCA2. It was shown that 20% of HGSOC have germ-line or somatic mutations in *BRCA1/2*, the majority of which are frame-shift insertions or deletions (Rebbeck et al., 2015). Promoter hypermethylation resulting in loss of BRCA1 (but not BRCA2) expression was seen in 11% of tumours and appears to be mutually exclusive of *BRCA1/2* mutations. (TGCA, 2011; Baldwin et al., 2000). Genomic alterations were seen in other HR genes including *RAD51C,* Ataxia Telangiectasia and RAD3-related protein/Ataxia Telangiectasia Mu-

tated *(ATR/ATM)* and mutations of the Fanconi anaemia genes. Overall pathway analysis suggests that the HR pathway is defective in about half of tumours (TGCA, 2011) (Figure 1.2) HGSOC with defects within the HR pathway may represent a subset of tumours with a more favourable prognosis as they respond better to cytotoxic chemotherapy and may be candidates for more targeted treatment. This is discussed in more detail below.

The molecular characteristics of the HR competent tumours are less well defined. Approximately 30% of this group have amplification of Cyclin E1 (*CCNE1*) (Etemadmoghadam et al., 2013; Ciriello et al., 2013; TGCA, 2011). Cyclin E1 forms a complex with, and regulates, CDK2 to facilitate G1/S progression of the cell cycle (Siu et al., 2012). A further study looking at chemo-resistant ovarian cancers confirmed that *CCNE1* amplification is confined to HR competent tumours as it appeared to be exclusive of *BRCA1/2* mutation (Patch et al., 2015).

Further classification of HGSOC has been investigated by the use of gene expression analysis. Microarray gene expression profiling of 300 HGSOCs as part of the Australian Ovarian Cancer Study identified distinct molecular subtypes (C1/mesenchymal, C2/immune, C4/differentiated, C5/proliferative) linked with clinical and pathological features (Tothill et al., 2008). Further studies have confirmed distinct gene expression patterns which partially overlap with those found by Tothill et al (Tothill et al., 2008) including TGCA and the prognostic gene expression profile 'Classification of Ovarian Cancer' (CLOVAR) (Verhaak et al., 2013; Helland et al., 2011). Although it is currently not clear what is driving these gene expression profiles, specific subtypes may respond to particular treatments. Currently, however, this classification has not been applied to clinical care.

1.1.7 *Ovarian cancer and genomic instability*

One of the most striking features of HGSOC is that it is characterised by considerable genomic instability (Ciriello et al., 2013), with frequent DNA gains and losses resulting in loss of heterozygosity (LOH), aneuploidy and intra-tumour heterogeneity. Structural change is an important mechanism for the loss or inactivation of tumour suppressor genes in HGSOC (TGCA, 2011). For example, gene breakage commonly inactivates the tumour suppressors Neurofibromin 1 (*NF1*), retinoblastoma protein (pRB), *RAD51B* and phosphatase and tensin homolog (*PTEN*) (Patch et al., 2015).

There is a complex relationship between genomic instability and prognosis. Studies have shown that genomic instability has been associated with a poorer prognosis in many tumours (Carter et al., 2006). However, in HGSOC (and basal-like breast cancer), which show extreme level of genomic instability, a high level of LOH was associated with a better prognosis and low platinum chemotherapy resistance rates (Wang et al., 2012; Baumbusch et al., 2013). In contrast to platinum chemotherapy, ovarian cancer with a gene expression signature reflecting higher chromosomal instability (CIN70) showed resistance to taxanes in a trial of taxane monotherapy (Swanton et al., 2009).

Widespread chromosomal changes that are seen in HGSOC are likely a result of mutations in *TP53* along with *BRCA1* or *BRCA2* (Bowtell, 2010). Basal like breast cancers, the most common subtype arising in women with *BRCA* mutation, also show widespread copy number changes (Natrajan et al., 2009) and they also have a high frequency of *TP53* mutation (Manie et al., 2009; Holstege et al., 2009). Deletion of BRCA1 or BRCA2 in cell lines has been shown to result in significant chromosomal instability and aneuploidy (Patel et al., 1998; Xu et al., 1999). In addition, mutations in a variety of DNA repair genes in addition to *BRCA1* and *2* result in genomic instability syndromes with heightened risk of developing cancer (for example

Bloom's syndrome, xeroderma pigmentosum, Neijmegen breakage syndrome and Fanconi anaemia), reviewed in (Martin et al., 2010). Defects within these DNA repair pathways, which normally maintain the integrity of the genome, result in genomic instability and are thought to promote tumorigenesis through accumulation of mutations in tumour suppressor genes and oncogenes (Charames and Bapat, 2003). It is proposed that DNA copy number change as a result of *BRCA* and *TP53* mutation is a vital step in the development of HGSOC (Bowtell, 2010).

1.1.8 *The spread of ovarian cancer and the tumour microenvironment*

HGSOC spreads either by direct extension from the primary tumour or when malignant cells shed from the ovarian/fallopian tube surface. Peritoneal fluid then facilitates their spread throughout the peritoneal cavity. Tumour deposits can therefore be found across all peritoneal surfaces and in draining lymph nodes, and frequently the development of increased peritoneal fluid (ascites) occurs. This ascitic fluid is rich in immune cells and inflammatory cytokines. In contrast, blood-borne dissemination to extra-abdominal sites is uncommon (Lengyel, 2010).

The immune microenvironment and immune cells in ovarian cancer disease play an important part in disease prognosis. The balance between the tumour promoting effects of the tumour evading the immune system verses the immune system mediating an anti-tumour response is complex (Figure 1.3). An understanding of this complex interplay is opening up potential avenues of new immune therapies in ovarian cancer.

T cell infiltration into ovarian tumours has been associated with improved survival (Zhang et al., 2003a). CD8 cytotoxic T lymphocytes (CTL) are thought to be the main mediators of anti-tumour responses. These cells recognise antigens displayed on major histocompatibil-

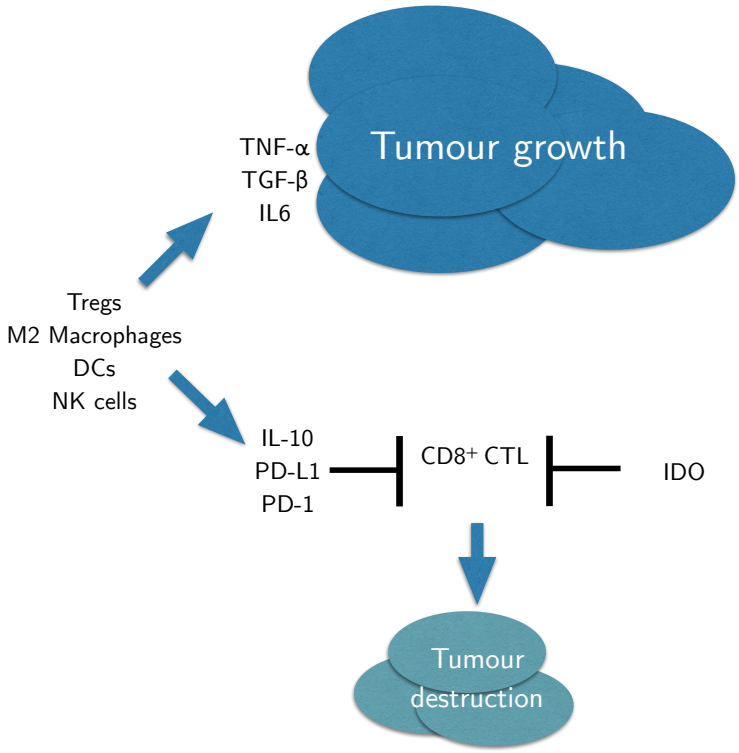

Figure 1.3: The immune microenvironment in ovarian cancer. Simplified diagram showing the balance between tumour suppressive factors and tumour promoting factors in ovarian cancer. The balance favours ovarian cancer progression. Figure adapted from Knutson et al. (2015).

ity complex (MHC) class I expressed on ovarian cancer cells. It has been shown that patients with higher CD8+ T cells have improved survival compared to those without infiltrating T cells (55 months vs 26 months) (Sato et al., 2005). The role of CD4 helper T cells is less clear. Some studies have shown similar outcomes among patients with and without CD4+ staining in tumours while others have shown increased CD4 cells is associated with improved survival. High levels of interleukin-17 (IL-17) in ascites has been shown to be associated with improved survival suggesting that a subset of CD4 helper cells may have a role in eradicating tumour (reviewed in Knutson et al. (2015)).

Other specific subsets of potential anti-tumour effectors have been studied. Antibody responses to ovarian cancer are a common observation, suggesting a role for B cells (Knutson et al., 2015). Studies, however, evaluating whether B cell infiltration is associated with improved survival show mixed results. Some have suggested that these cells are involved in modulating CTL recruitment or activity (Milne et al., 2009). Recently published data has shown that the presence of antibody producing plasma cells are associated with the most prognostically favourable CD8+ tumour infiltrating lymphocyte responses in HGSOC (Kroeger et al., 2016). It is suggested that the co-localisation of B and T cells within tertiary lymphoid structures facilitates their antitumour responses (Kroeger et al., 2016). Natural killer (NK) cells are also found in the immune microenvironment. Nearly all ovarian cancers express NK ligands (MICA, MICB and ULBP2) (Li et al., 2009a). However, increased numbers of NK cells in peritoneal and pleural effusions have been associated with poor prognosis (Dong et al., 2006).

Immune evasion in ovarian tumours involves a complex collection of immune factors that suppress the generation of the anti-tumour response (Knutson et al., 2015). Immune suppression is mediated by factors released from the tumour or by a variety of suppressor or reg-

ulatory cells. The role of CD4+ regulatory T cells (Tregs) in ovarian tumours has been well documented. These cells are a T cell subpopulation that functions to suppress the immune response through release of immune suppressive mediators such as transforming growth factor β (TGFβ) and Interleukin-10 (IL10). They also prevent T cell responses through cytokine dependent or cell contact-dependent mechanisms (Knutson et al., 2015). Tumours with increased numbers of Tregs have a poor prognosis (Li et al., 2005; Preston et al., 2013) .

Multiple regulatory cells, including macrophages and dendritic cells (DCs) are dervived from the myeloid arm of the immune system. Infiltration of tumours with macrophages of the M2 phenotype is characterised by immune suppression and is tumour promoting (Ko and Naora, 2014). Human ovarian cancers have been shown to recruit a subset of DCs that induce T cells to release large amounts of IL-10 preventing local T cell activation (Wei et al., 2005). In addition, depletion of DCs has been shown to delay ovarian cancer progression in a murine model (Huarte et al., 2008). Tumour cells also express a variety of molecules that directly block the immune response. These include programmed death ligand 1 (PD-L1) (Hamanishi et al., 2007), Cancer antigen 125 (Ca125 also known as MUC16) (Patankar et al., 2005) and indoleamine 2,3-dioxygenase (IDO) (Inaba et al., 2009).

The role of the inflammatory cytokine network has also been assessed. The 'tumour necrosis factor (TNF) network', consisting of TNFα, chemokine (C-X-C motif) ligand 12 (CXCL12) and interleukin 6 (IL-6), has paracrine actions on angiogenesis, infiltration of myeloid cells and NOTCH signalling in ovarian cancer (Kulbe et al., 2012). High levels of IL-6 in the serum of ovarian cancer patients have been associated with shorter survival (Plante et al., 1994; Coward et al., 2011). IL-6 is also associated with the generation of thrombocytosis that is associated with shortened survival (Stone et al., 2012).

An understanding of this complex relationship between the tumour and the immune system is important in the development of new treat-

ments and particularly novel treatments such as oncolytic viral therapy as they have a complex interaction with the immune system that is discussed in more detail below.

1.1.9 *Current treatment of Ovarian Cancer*

1.1.9.1 *Surgery*

Currently epithelial ovarian cancer is treated as a single disease entity. The mainstay of treatment, in both early and advanced ovarian cancer, is surgery. Data from retrospective studies show that minimal residual disease following surgery is associated with improved outcome (Chi et al., 2009; du Bois et al., 2009). There is some debate over whether this association is causal or due to the fact that resectable tumours may be less aggressive or more responsive to chemotherapy (Schorge et al., 2010). Nevertheless, the aim of surgery is therefore for complete removal of all cancer tissue (optimal debulking) (du Bois et al., 2009).

In cases where optimal debulking is not possible, neoadjuvant (preoperative) chemotherapy is an option (Chi et al., 2009). Interval debulking can then be considered after 3 cycles of treatment. This strategy is supported by large randomised trials that show non-inferiority in survival and reduced surgical morbidity when compared to upfront surgery in advanced ovarian cancer (Hou et al., 2007; Vergote et al., 2010; Kehoe et al., 2015; Fagotti et al., 2016).

1.1.9.2 *Chemotherapy*

EARLY STAGE DISEASE There have been several randomised controlled trials looking at the role of platinum based chemotherapy following surgery in early stage disease. A recent meta analysis of these trials has concluded that the addition of adjuvant chemotherapy in early stage disease (The International Federation of Gynecology and

Obstetrics (FIGO) stage I/IIa) improves both progression free survival (PFS) and overall survival (OS) (Lawrie et al., 2015). It is unclear whether this benefit is confined to women with intermediate and high-risk disease and the role of chemotherapy in those with low risk disease (stage Ia/ grade 1 disease) is currently debated (Lawrie et al., 2015).

ADVANCED DISEASE Platinum based chemotherapy treatment has been the standard of care in ovarian cancer for around 40 years. Currently, standard chemotherapy consists of a combination of paclitaxel ($175mg/m^2$) and carboplatin (area under the curve (AUC) 5-6), both administered intravenously every 3 weeks (Ozols et al., 2003). This has been the standard of treatment for more than 15 years, and clinical trials adding a third conventional chemotherapy drug have been shown not to improve PFS or OS in these patients (Bookman et al., 2009). The combination of cisplatin and paclitaxel is equally effective but more toxic. There is no evidence to suggest that more than 6 cycles result in better outcome (Bookman et al., 2009).

A number of recent trials are now beginning to influence first line treatment of advanced ovarian cancer. Large randomised trials inhibiting angiogenesis with bevacizumab (a monoclonal antibody targeting vascular endothelial growth factor, VEGF) (GOG218 and ICON-7) or pazopanib (a VEGF receptor tyrosine kinase inhibitor (VEGF RTKi)) have shown improved PFS (Burger et al., 2011; Perren et al., 2011; du Bois et al., 2014). Fractionating paclitaxel into a dose dense weekly regime has also shown an improvement in PFS and OS and it has been suggested that this regime should be standard of care (Katsumata et al., 2013). Two further trials (ICON8 and GOG262) are currently evaluating the role of dose dense weekly paclitaxel together with bevacizumab (Suh et al., 2014).

Since ovarian cancer is often confined within the abdomen, the role of intraperitoneal treatment in ovarian cancer has been investi-

gated. A catheter is placed into the peritoneal cavity and remains in place for the duration of therapy. A 'turning protocol' can be used in which the patient spends 1.5 to 2 hours lying in different positions to maximise exposure of peritoneal surfaces to the drugs (Alberts et al., 2006). A phase III trial comparing intraperitoneal (IP) and intravenous cisplatin and paclitaxel therapy with intravenous paclitaxel and cisplatin showed an improvement in both PFS and OS in the group that received IP treatment (Armstrong et al., 2006). Toxicities were higher in the IP group and as a result the IP regime was only deliverable in 42% of patients. Despite the potential for this approach to deliver higher concentrations of cytotoxic treatment to the tumour, general uptake has been poor and more tolerable regimes are needed (Jayson et al., 2014).

1.1.9.3 *Recurrent disease*

Despite optimal upfront surgery and administration of chemotherapy, approximately 70% of patients will relapse in the first 3 years and the median PFS is around 18 months. Detection of relapse could be by the rising serum tumour marker, CA125 level (Meyer and Rustin, 2000), the development of symptoms or by imaging. A rising of CA125 levels can often predate symptoms; however, early intervention on the basis of a rising CA125 alone without the presence of symptoms did not improve survival and reduced quality of life in these patients (Rustin et al., 2010).

The choice of chemotherapy regime for relapsed disease is largely dictated by the interval from the last cycle of platinum based chemotherapy to the point of development of disease (Eisenhauer et al., 1997). For those patients with a late relapse (more than 6 months after chemotherapy), carboplatin combination is the treatment of choice. Randomised trials have shown that options for platinum sensitive recurrence include the combination of carboplatin with paclitaxel (Par-

mar et al., 2003), gemcitabine (Pfisterer et al., 2006) or liposomal doxorubicin (Pujade-Lauraine et al., 2010).

Chemotherapy resistance is a major problem and treatment for platinum resistant (progressing within 6 months of platinum based chemotherapy) or platinum refractory (progressing during or within 4 weeks of platinum chemotherapy) patients are limited and prognosis is poor. Options include chemotherapy with paclitaxel (Thigpen et al., 1994), topotecan (Bookman et al., 1998), liposomal doxorubicin (PLD) (Gordon et al., 2000) and gemcitabine (Markman et al., 2003). Overall response rates are poor and median PFS is 3-4 months (Ushijima, 2010).

The angiogenesis inhibitor, bevacizumab, has shown to improve PFS of recurrent ovarian cancer in two randomised phase III trials (Aghajanian et al., 2012; Pujade-Lauraine E, 2012). An improvement in OS was, however, not seen and this may be due to cross- over and further lines of treatment at progression. Currently the addition of bevacizumab in recurrent disease is not standard of care. Other angiogenesis inhibitors such as cediranib, vandetanib and aflibercept are being assessed in ovarian cancer but currently their efficacy is yet to be determined.

Currently the options for patients with relapsed disease and especially those with platinum refractory disease are limited, and there is a need for newer treatments. A variety of chemotherapeutic agents and novel targeted drugs are currently being developed and evaluated in ovarian cancer. Although a number of newer chemotherapy agents have been assessed in platinum resistant ovarian cancer (eg. Ixabepilone) the response rates have been poor and none have been incorporated into the standard of care (Mantia-Smaldone et al., 2011).

With the increasing understanding of the molecular basis of ovarian cancer, trials have focused on a variety of molecularly targeted treatments. One focus has been to exploit the overexpression of the folate receptorα (Konner et al., 2010; Lorusso et al., 2012) and large

randomised trials are underway. Targeting CA125 has also been investigated but unfortunately trials with the anti-CA125 antibody, oregovamab have been negative (Berek et al., 2009).

Immune therapies are currently receiving a great deal of attention in the treatment of cancer and these also starting to be investigated in ovarian cancer. As discussed in more detail earlier, the immune microenvironment has been shown to be important in the biology of ovarian cancer, the status of T-cell infiltration in the immune microenvironment (Zhang et al., 2003a, 2015), along with reduced expression of the programmed cell death ligand-1 (PD-L1) (Hamanishi et al., 2007; Maine et al., 2014) are associated with improved prognosis. Based on this rationale, clinical trials are currently underway with immune checkpoint inhibitors (anti-PD-L1/PD-1, anti anti-cytotoxic T-lymphocyte-associated protein 4 (anti-CTLA4)) (e.g. NCT02608684, NCT02440425, NCT02537444).

What is now clear is that ovarian cancer is a heterogeneous disease and for treatments to be effective they need to be developed and targeted towards appropriately selected patients. The knowledge that the DNA repair pathway, HR, is frequently compromised in ovarian cancer has lead to the development of treatments targeted to this particular group of patients. The role of poly(ADP)ribose polymerase (PARP) inhibitors in ovarian cancer demonstrates the importance of defects within this pathway and this is discussed in more detail below. Given the importance of HR in HGSOC, the next section will discuss this DNA repair pathway with a particular focus on how knowledge of defects within the DDR is now influencing therapy.

1.2 THE HOMOLOGOUS RECOMBINATION PATHWAY AND THE DNA DAMAGE RESPONSE

The DNA damage response (DDR) is vitally important for maintaining the integrity of the genome (Friedberg et al., 2006). The genome is

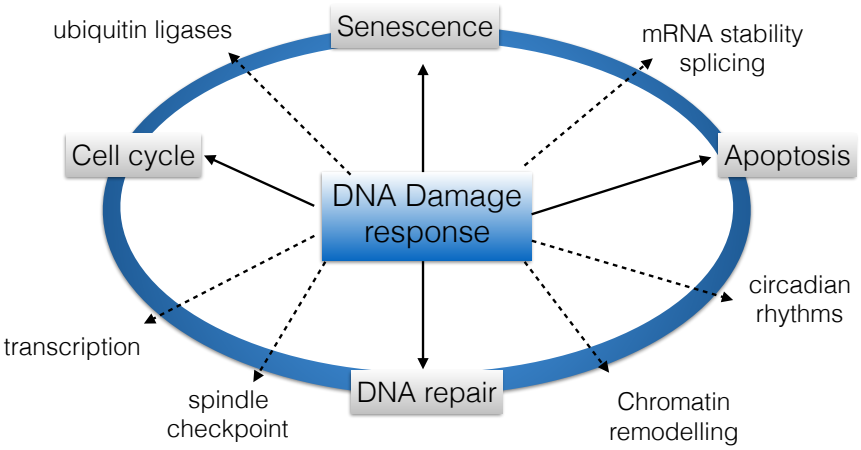

Figure 1.4: The molecular and physiological consequences of the DDR. Adapted from Harper and Elledge (2007).

constantly exposed to endogenous and exogenous genotoxins. Unless repaired by an error-free process, DNA damage can result in mutations and altered cellular behaviour. Consequently, cells respond to DNA damage by activating a number of interconnecting pathways. These pathways not only involve the DNA repair process itself but also integrate with regulatory pathways such as cell cycle control and apoptosis. This is summarised in Figure 1.4. Together, these pathways ensure that mutated DNA is not duplicated, and therefore ensure the lesion is repaired, or if damage is too great, trigger cell death (Harper and Elledge, 2007).

A human cell undergoes tens of thousands of DNA lesions per day (Hoeijmakers, 2009; Jackson and Bartek, 2009). These lesions can block replication and transcription, and if they are not repaired or repaired incorrectly, can lead to mutation or cell death. Different forms of DNA damage evoke different repair mechanisms and signalling pathways (Jackson and Bartek, 2009). In human cells there are five major repair pathways (shown in Figure 1.5). The most common form of DNA damage is single strand breaks (SSBs), which are repaired by the base excision repair (BER) pathway (Caldecott, 2014). The nucleotide excision repair (NER) pathway deals with mod-

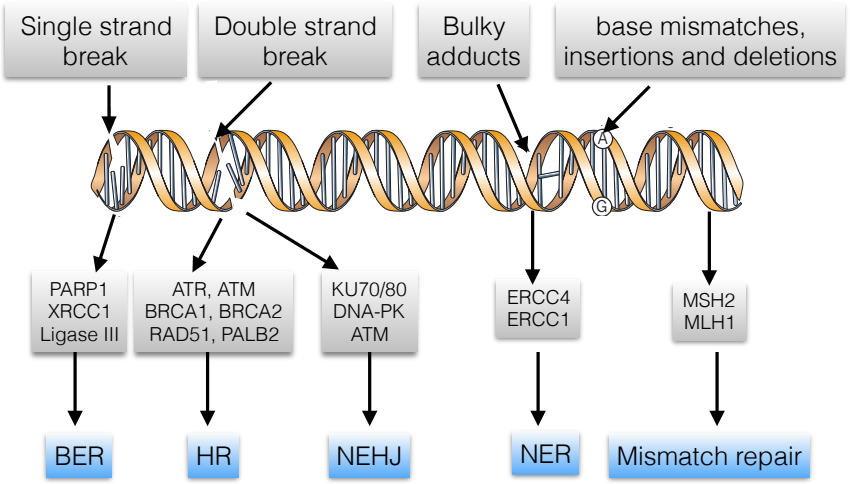

Figure 1.5: Illustration of the five main pathways involved in repair of DNA damage. DNA is continuously exposed to a variety of forms of DNA damage. Different forms of DNA damage trigger different repair pathways and signalling mechanisms. Adapted from Lord and Ashworth (2012)

ified nucleotides that distort the structure of the DNA double helix. This pathway deals with ultaviolet (UV)–induced damage and also plays a role in dealing with the damage induced by platinum agents (O'Connor, 2015). The mismatch repair (MMR) pathway is involved in repairing replication errors, including mismatch base-pairing as well as nucleotide insertions and deletions (Jiricny, 2006).

The most genotoxic lesions are DNA double strand breaks (DSBs). A single unrepaired DSB can lead to aneuploidy, genetic aberrations or cell death. DSBs can be generated by a number of sources, including genotoxic chemicals (for example chemotherapeutics) and ionizing radiation. In addition, many other types of DNA lesions impede replication fork progression, leading to replication fork collapse and DSBs (Krejci et al., 2012). There are two main pathways that repair these lesions: HR and classical non-homologous end joining (C-NHEJ). In addition, other error prone DSB repair pathways, namely alternative-NHEJ (alt-NHEJ) and single-strand annealing (SSA), have

recently been shown to operate in many different conditions and contribute to genome rearrangements and oncogenic transformation (Ceccaldi et al., 2016).

1.2.1 *Signalling DSB damage*

Following a DSB, proteins are rapidly recruited to the DSB and histone modifications take place. At least four, partially independent, sensors detect DSBs: PARP, Ku70/80, MRN complex (MRE11/ RAD50 / NBS1) and, the if end processing occurs, replication protein A (RPA). Ku localises within seconds to DSBs where it loads and activates DNA dependent protein kinase (DNA-PK) to initiate C-NHEJ. PARP1/2 act to promote alt-NHEJ, which functions as a back-up pathway of C-NHEJ. DSB resection and formation of 3'ssDNA ends results in RPA accumulation and activation of the ATR pathway leading to SSA or HR (Ciccia and Elledge, 2010). The MRN complex is the major DSB sensor and recruits and activates ATM. MRE11 has endonuclease and exonuclease activity important for the initial steps of DNA end resection that is essential for HR (Williams et al., 2007).

Once DSB have been detected, key proteins that mediate the DDR include proteins of the phosphatidylinositol 3-kinase-like protein kinase (PIKKs) family – ATM and ATR (Ciccia and Elledge, 2010). ATM and ATR coordinate a wide number of cellular processes through phosphorylation of a large number of mediator proteins. ATM is activated by DSBs created by DNA damaging agents (like irradiation). ATR, together with ATRIP, is activated following recruitment to RPA-coated ssDNA regions particularly at stalled replication forks (Cimprich and Cortez, 2008). These proteins initially amplify the DDR by acting as recruiters of ATM/ATR substrates (Zhou and Elledge, 2000). Effector proteins of the DDR are then either directly phosphorylated by ATM/ATR or by kinases such as checkpoint kinase 1 and 2 (CHK1 and CHK2) (Ciccia and Elledge, 2010). As a result, ATM and ATR co-

ordinate a wide variety of cellular activities in response to DNA damage including modulating the cell cycle and apoptosis (Figure 1.6).

ATM and ATR promote DSB repair in part through phosphorylation dependent recruitment of DDR factors to the sites of DNA damage (Ciccia and Elledge, 2010). A critical aspect of the process involves rapid phosphorylation of Ser139 on histone H2AX, a variant of H2A, by ATM. This promotes chromatin binding of mediator of damage checkpoint 1 (MDC1); MDC1 interacts with MRE11, tethering MRN and also ATM at the DSB (Shibata and Jeggo, 2014). The DDR signal is amplified as ATM extends the region of phosphorylated H2AX (γH2AX) (Harper and Elledge, 2007). Formation of extensive γH2AX is important for sustaining the DDR. In addition, γH2AX recruits chromatin remodelling enzymes that stabilise DDR factors at the site of DSBs (Ciccia and Elledge, 2010).

MDC1 phosphorylation and recruitment to γH2AX initiates a ubiquitin cascade at sites of DNA damage. Recruitment of the ubiquitin ligase, ring finger protein 168 (RNF168) by MDC1 mediates the formation of p53-binding protein 1 (53BP1) foci at damaged chromatin, promoting C-NHEJ. 53BP1 has recently been shown to be an important regulator of the cellular response to DSB (Panier and Boulton, 2014). 53BP1 also binds to the RAD50 component of MRN (Shibata and Jeggo, 2014). Additional proteins, including BRCA1, RAP80, Abraxas and BRCC36, assemble at DSBs and some of these are cell cycle dependent, being more abundant in G2/S phase (Shibata and Jeggo, 2014). BRCA1 is required to relieve the barrier that 53BP1 poses to resection, thereby promoting homologous recombination (Bunting et al., 2010). Together, this plethora of factors meditating phosphorylation, ubiquitination, sumoylation and acetylation, carefully regulate the repair of the DSB and play an important role in determining the most appropriate pathway to repair the damage (Ciccia and Elledge, 2010). The different pathways involved to repair DSBs are discussed below, with a focus on HR.

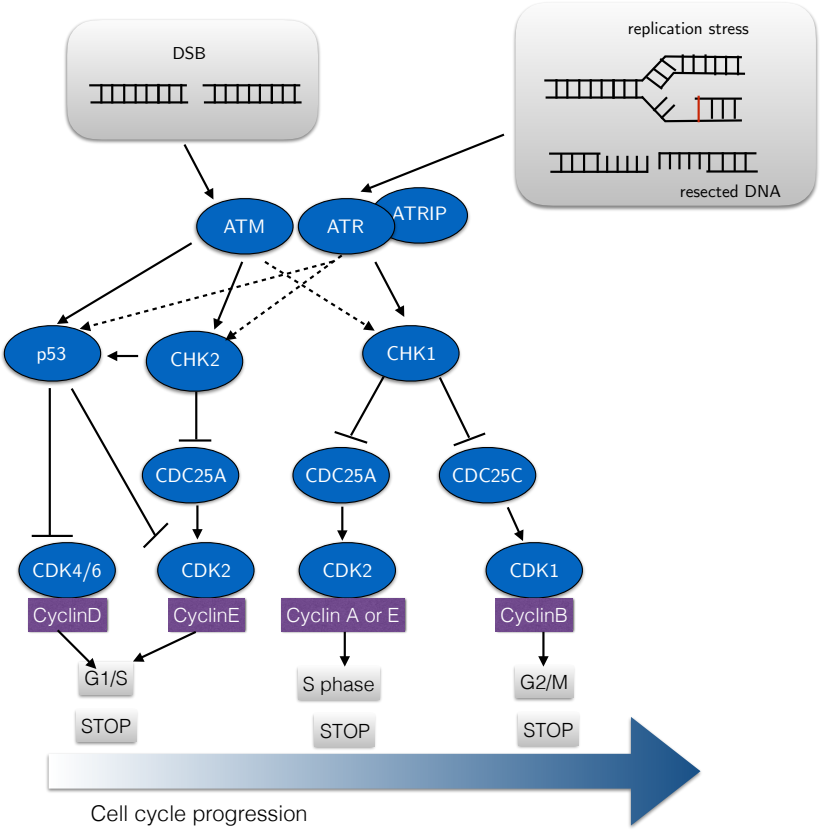

Figure 1.6: Signalling DNA damage to cell cycle checkpoints. ATM is activated by DSBs and triggers the G1 checkpoint by phosphorylating CHK2 and p53. ATM and ATR are activated by resected DSBs and stalled replication forks. This results in phosphorylation of CHK1 and activates the intra-S phase and G2 checkpoints. CHK1 also phosphorylates and inactivates CDC25 to inhibit cell cycle progression through suppression of CDK activity (Curtin, 2012). There is also cross talk between the pathways and dashed arrows show secondary targets. (Figure adapted from Curtin (2012))

1.2.2 *Repair of DSBs: Classical NHEJ*

Of the four known pathways that repair DSBs, the C-NHEJ pathway represents the major DSB repair pathway in mammalian cells, a feature demonstrated by the dramatic radiosensitivity shown by defective mutants (Jeggo and Lavin, 2009). NHEJ ligates DSBs with minimal end-processing. The DSB is repaired by blunt end ligation independent of sequence homology. It is not error free but is active in all phases of the cell cycle, predominating in Go and G1 (Branzei and Foiani, 2008).

NHEJ is initiated by sequence independent binding of the heterodimeric Ku70/80 protein to the double strand ends. This is achieved through the Ku's ring structure, which enables Ku to loop onto the DNA end. DNA-bound Ku recruits the catalytic component of the DNA–dependent protein kinase catalytic (DNA-PK) complex DNA-PKcs, activating the kinase activity (Shibata and Jeggo, 2014). Autophosphorylation of DNA-PKcs regulates end-processing together with artemis nuclease, polynucleotide kinase 3' phosphatase (PNKP) and polymerases (including polλ and polμ) (Radhakrishnan et al., 2014). Once DNA ends have been processed, they are covalently joined by DNA ligase IV, which exists in a complex with X-ray repair cross-complementing protein 4 (XRCC4). XRCC4 is required for stabilisation of DNA Ligase IV and stimulates its activity (Grawunder et al., 1997). XRCC4 also interacts with XLF (XRCC4-like factor), which is required to repair a subset of breaks involving mismatched or non-cohesive ends (Ahnesorg et al., 2006; Tsai et al., 2007).

The abundance of Ku 70 and DNA-PKcs together with Ku's capacity to bind double-stranded DNA ends make C-NHEJ an important mechanism of DSB repair (Shibata and Jeggo, 2014). Despite the potential for mutagenicity of C-NHEJ, its fast kinetics means that it plays a role in protecting genomic integrity by suppressing chromosomal translocations (Difilippantonio et al., 2000).

1.2.3 *Alt-NHEJ and SSA*

Recent studies have shown that, following end resection, DSB can be repaired by two error-prone end-joining pathways, Alt-NHEJ and SSA (Ceccaldi et al., 2016). Alt-NHEJ occurs in various cellular conditions but the mechanistic details of the pathway remain unclear (Ceccaldi et al., 2016). Alt-NHEJ predominantly occurs when NHEJ is compromised by the loss of Ku or ligase IV. This pathway requires end resection by CtBP-interacting protein (CtIP) and uses DNA ligase I or III, XRCC1 and PARP1 (Ceccaldi et al., 2016). The process involves two ssDNA re-joining events using microhomology to tether the ends. It has harmful consequences on genomic integrity due to the possibility of joining DSBs on different chromosomes thus generating chromosomal translocations and deletions (Deriano and Roth, 2013). SSA can occur when end resection reveals flanking homologous sequences and it involves reannealing of RPA coated ssDNA by the RAD52 protein. It therefore mediates end joining between interspersed nucleotide repeats in the genome resulting in deletion of the intervening sequences (Mehta and Haber, 2014) and subsequent loss of genetic information (Ceccaldi et al., 2016).

1.2.4 *Homologous recombination*

In contrast to NHEJ, HR exploits the use of an undamaged homologous template to restore any lost sequence information (Shibata and Jeggo, 2014). It functions in the S and G2 phases of the cell cycle when an intact sister chromatid is available. The central reaction of HR is homology search and DNA strand invasion mediated by RAD51 (Shibata and Jeggo, 2014). There are three phases of HR: pre-synapsis, synapsis and post-synapsis, and RAD51 is involved in all stages (Sung et al., 2003). The presence of DSBs is signalled by

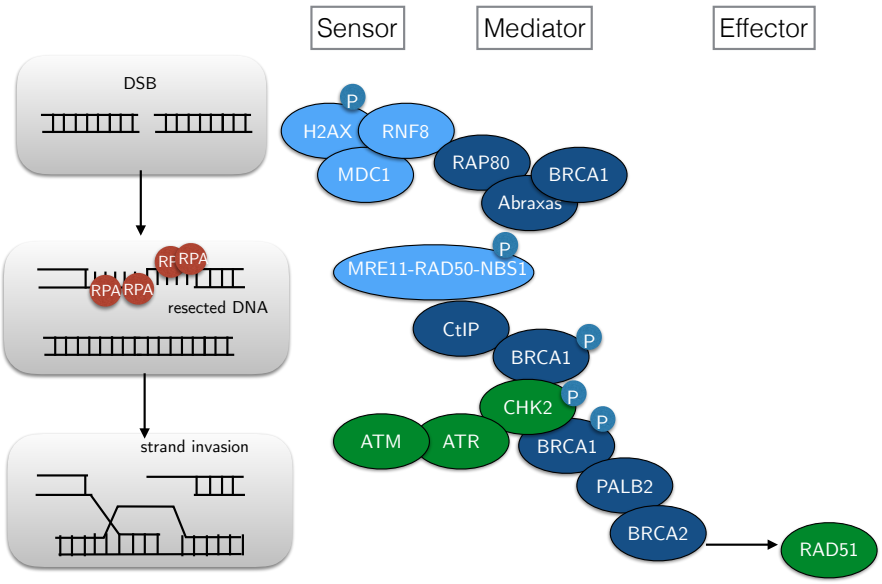

Figure 1.7: Representation of the key factors involved in repair of DSBs by HR. In response to DSBs, sensors (light blue) detect the damage, and signalling mediators recruit or activate effectors that repair the damage through RAD51 mediated process. Figure adapted from Roy et al. (2012).

the factors such as γH2AX (described in more detail Section 1.2.1) and HR is initiated by CtIP/MRE11-dependent resection of double-stranded DNA ends. The extension of the resection is highly regulated and involves the repositioning of 53BP1 via a BRCA1-dependent process (Bunting et al., 2010). The resulting single-stranded 3′ tails generated by resection are rapidly bound by RPA. In the presynapsis phase, RAD51 displaces RPA and is loaded onto ssDNA. The resulting RAD51-ssDNA filament (the presynaptic filament) mediates homology search (Krejci et al., 2012) (Figure 1.7).

During synapsis, RAD51 facilitates the formation of a physical connection between the invading DNA substrate and the homologous DNA template, leading to the generation of heteroduplex DNA (D-loop). At this point, RAD51-dsDNA filaments are formed by accommodating both the invading and donor ssDNA strands within the filament. Finally, during post synapsis, RAD51 dissociates from the

dsDNA to expose the 3'-OH end, which is required for DNA synthesis (Krejci et al., 2012).

At least three different routes can be used once DNA synthesis is initiated. In double strand break repair (DSBR), the second end of DSB can be used to stabilise the D–loop structure, leading to the generation of a double Holliday junction (dHJ) (Krejci et al., 2012). The dHJ is subsequently resolved by enzyme complexes such as BLM in complex with topoisomerase IIIα (Wu and Hickson, 2003) or GEN1 to produce crossover or noncrossover products (Krejci et al., 2012; Ip et al., 2008). Alternatively, the invading strand can be displaced from the D loop after DNA synthesis and then anneal with its complementary strand. This is known as the synthesis-dependent strand-annealing mode of HR (SDSA) (Krejci et al., 2012). In break-induced replication (BIR), the D-loop structure can assemble into a replication fork and copy the entire chromosome arm to result in loss of heterozygosity (Li and Heyer, 2008) (Figure 1.8).

1.2.5 *Regulation of HR*

There are multiple regulatory mechanisms that control HR at many points along the pathway. One level of regulation occurs between RAD51 and RPA complex. RPA has a higher affinity for ssDNA and has been shown to arrive at DSB sites prior to RAD51 (Krejci et al., 2012). The presence of RPA blocks RAD51 binding and therefore needs to be removed for HR to take place. Once RAD51 is loaded onto ssDNA, however, RPA has also been shown to promote recombination by protecting DNA ends from resection and removing secondary structures formed on ssDNA that could impede RAD51 filament formation (Sung et al., 2003).

Recombination mediators are proteins that can overcome the inhibitory effect of RPA on RAD51. These mediators can facilitate RAD51 loading onto ssDNA, increase intrinsic stability of RAD51 presynap-

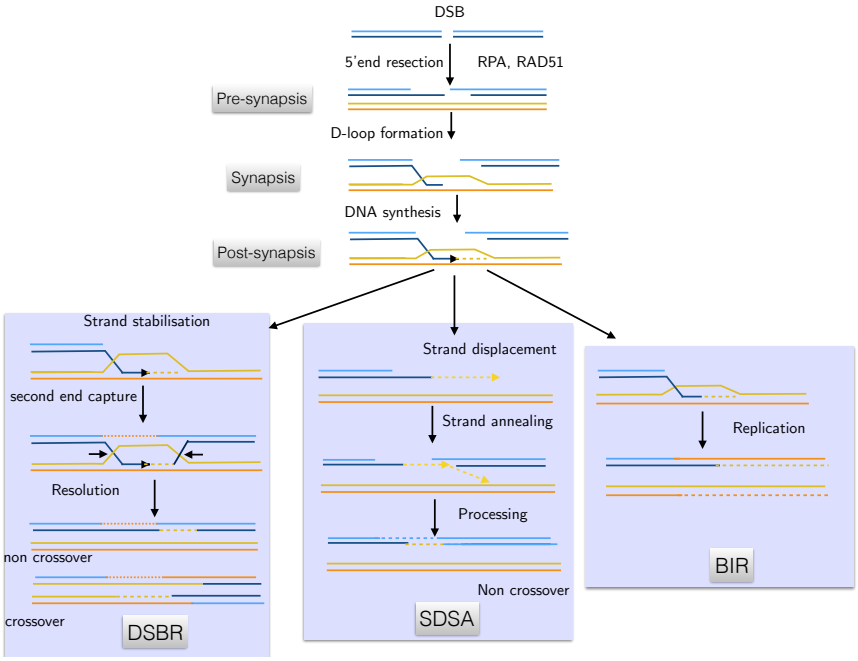

Figure 1.8: Models for the repair of DSBs by HR. DNA DSBs are resected to generate 3′ ends followed by the formation of RAD51 filaments that invade the homologous strand to form a D loop structure. After priming DNA synthesis, three pathways can be followed. In the DSBR pathway, the second end is captured and a dHJ is formed. Resolution of the dHJs can generate cross over or non crossover products. In the SDSA, pathway the newly extended strand is displaced, followed by pairing with the other 3′ single stranded tail and DNA synthesis completes the repair. The third pathway, BIR, can act when the second end is absent. The D-loop intermediate turns into a replication fork capable of both lagging and leading strand synthesis. Figure adapted from Krejci et al. (2012).

tic filament and prevent RAD51 from being removed by factors such as helicases. Mediators include RAD52, RAD51B, RAD51C, and X-ray repair cross-complementing protein 2/3 (XRCC2/3) but the most important mediator in mammalian cells is BRCA2 (Ceccaldi et al., 2016).

1.2.5.1 *BRCA2*

BRCA2 is the main mediator of RAD51 nucleofilament formation and strand exchange. BRCA2 contains a DNA binding domain that binds to ssDNA and dsDNA and interacts with RAD51 through a series of eight evolutionary conserved motifs, the BRC repeats (Roy et al., 2012). The repeats have subtle differences and bind RAD51 with varying affinity by mimicking the structure of RAD51 monomers (Pellegrini et al., 2002). The BRC repeats facilitate the recruitment of RAD51 to ssDNA, and also accelerate the displacement of RPA by RAD51, and facilitate RAD51 filament formation on ssDNA by maintaining the active ATP-bound form of RAD51 on ssDNA (Roy et al., 2012; Carreira et al., 2009). In addition to the BRC domains, BRCA2 also interacts with RAD51 through its C-terminal part, but this region can only interact with RAD51 in the nucleoprotein filament form and in a cell cycle dependent fashion (Krejci et al., 2012).

The primary function of BRCA2 is to promote HR repair (Roy et al., 2012). BRCA2 deficient cells are defective in recruiting RAD51 to sites of DSBs and in repairing DSBs by HR (Yuan et al., 1999). Recently work has also shown that BRCA2 may also have a second role in protecting replication forks by preventing degradation of the nascent strand at stalled replication forks (Schlacher et al., 2011).

Partner and localizer of BRCA2 (*PALB2*) interacts with the N-terminus of BRCA2 and plays a role in HR by regulating BRCA2 and possibly affecting RAD51 function (Krejci et al., 2012). Germline mutations in *PALB2* in breast and ovarian cancer patients lead to loss of BRCA2-PALB2 binding and BRCA2 function in HR (Xia et al., 2006).

In addition both PALB2 and BRCA2 have been shown to influence cell cycle checkpoints (Menzel et al., 2011).

Further regulators of BRCA2 function include deleted in split hand/split foot protein 1 (DSS1), which has been shown to facilitate BRCA2 in RAD51-ssDNA filament formation (Krejci et al., 2012). P53 has also been shown to interact with multiple regions of BRCA2 and suppress HR (Rajagopalan et al., 2010).

1.2.5.2 *BRCA1*

BRCA1 interacts with tumour suppressors, DNA repair proteins and cell cycle regulators has multiple functions that link DNA damage sensing and DDR effectors. (Roy et al., 2012). BRCA1 contains an amino-terminal RING domain that has E3 ubiquitin ligase activity and a BRCA1 C Terminus (BRCT) domain that facilitates phosphoprotein binding. Mutations in the RING and BRCT domain have been linked to the development of ovarian cancer (Friedman et al., 1994).

BRCA1 is directly involved in HR through a number of interactions. BRCA1 binds to DSBs through its association with abraxas which in turn binds to ubiquitylated histones at DNA DSBs through RAP80 (Roy et al., 2012). BRCA1 is involved in end resection of DSBs through the interaction with CtIP and the MRN complex. BRCA1 also promotes HR (and inhibits NHEJ) by removing 53BP1 from DSBs (Bunting et al., 2010). BRCA1 is also required for RAD51 recruitment to the sites of DSBs through its interactions with PALB2 and BRCA2 (Roy et al., 2012).

BRCA1 has an important role in cell cycle checkpoint activation. The BRCA1-BRCA1-associated RING domain protein (BARD1) complex is involved in the activation of G1/S, S-phase and the G2/M checkpoints. The G1/S checkpoint requires phosphorylation of BRCA1 by ATR or ATM, which facilitates phosphorylation of p53 on S15. P53-S15 phosphorylation is necessary for transcriptional induction of the CDK inhibitor p21 and G1/S checkpoint activation (Roy et al.,

2012). The exact mechanism of BRCA1 control of the S and G2/M checkpoint is less well characterised (Roy et al., 2012). The BRCA1-BRIP1-DNA topoisomerase 2-binding protein 1 (TOPBP1) complex appears to be necessary for S phase checkpoint activation in response to stalled or collapsed replication forks. The G2/M checkpoint control involves the BRCA1-abraxas–RAP80 complex (Roy et al., 2012). These roles of BRCA1 in the cell cycle along with HR may account for the increased severity of genomic instability found in BRCA1 deficient tumours relative to BRCA2-deficient tumours (Roy et al., 2012).

1.2.6 *Negative regulators of HR*

There are a number of factors that negatively regulate RAD51 and consequently HR. Several mammalian helicases including the RecQ helicase and Proliferating Cell Nuclear Antigen (PCNA)-interacting factor (PARI) have been shown to dismantle RAD51 nucleofilaments (Ceccaldi et al., 2016). The polymerase polυ has been shown to act at the presynaptic step as an anti recombinase. These factors have been shown also to promote error-prone repair pathways (such as alt-NHEJ and SSA).

Even after RAD51 nucleofilament formation, HR can be modulated at the level of strand exchange (Ceccaldi et al., 2016). D-loop displacement by specific DNA helicases prevents cross over events and can inhibit HR (Ceccaldi et al., 2016). After strand exchange, RAD51 needs to be removed from dsDNA to allow for the downstream steps of strand extension, junction resolution and chromatin assembly. ATM regulates these last steps of HR possibly through RAD54 activation. The HELQ helicase removes RAD51 from dsDNA and promotes strand exchange in an ATP-dependent manner (Ward et al., 2010).

HR is therefore a tightly controlled process and RAD51 is central to all aspects of the process.

1.2.7 *Repair of DSBs: Pathway choice*

There are multiple mechanisms that control DSB pathway choice and it is an area of ongoing research. HR only functions after DNA replication in the late S/G2 phase of the cell cycle and therefore the cell cycle phase plays a crucial role in pathway choice decision (Shibata and Jeggo, 2014) (summarised in Figure 1.9).

Since three of the DSB pathways require end resection, it is likely that the control of end resection dictates pathway choice and repair outcome (Symington and Gautier, 2011). C-NHEJ will repair DSBs unless end-resection occurs (Kakarougkas and Jeggo, 2014). ATM promotes end resection by recruiting and phosphorylating all members of the MRN complex, which subsequently leads to ATM-dependent phosphorylation of other HR components including BRCA1, CtIP, EXO1 and Bloom syndrome protein (BLM), (Ceccaldi et al., 2016). MRE11 and CtIP carry out the initial phase of end resection followed by a more extensive resection mediated by helicases and exonucleases (including DNA2, BLM, CtIP and EXO1). This commits the cells to HR or SSA (Ceccaldi et al., 2016).

One mechanism underlying the regulation of HR is the control of resection by cyclin-dependent kinases (CDKs) (Aylon et al., 2004). In the S/G2 phases of the cell cycle, end resection is stimulated by CDKs through phosphorylation of multiple substrates. For example, CDK-phosphorylation of CtIP favours the CtIP-BRCA1 interaction in G2/S phase and therefore promotes HR. In addition, CDK dependent phosphorylation of EXO1 promotes end resection and thus HR (Ceccaldi et al., 2016). Conversely, impairment of EXO1 phosphorylation attenuates resection, cell survival and HR but greatly increases NHEJ upon DNA damage (Ceccaldi et al., 2016).

The balance between 53BP1 and BRCA1 also modulates end resection and therefore pathway choice. In the G1 phase of the cell cycle, 53BP1 proteins localise to DSB, inhibit BRCA1 recruitment, block

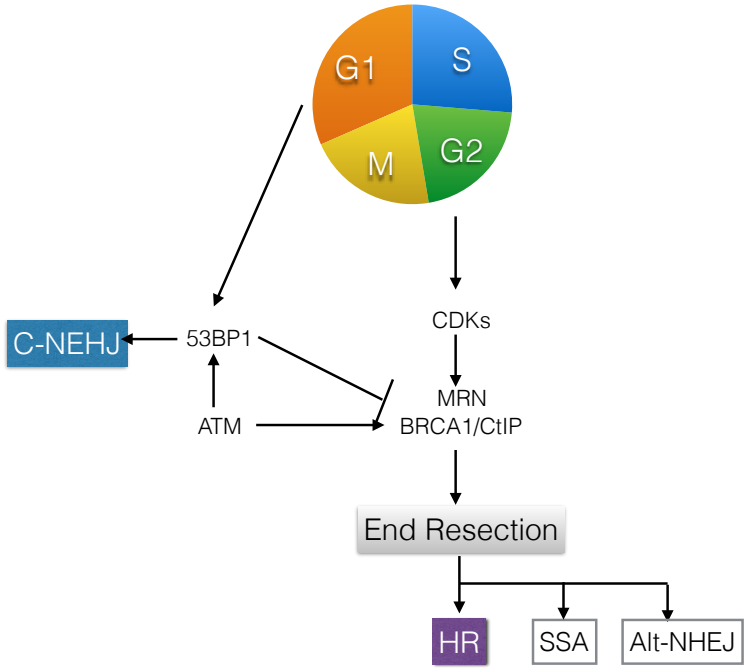

Figure 1.9: Cell cycle regulation of DNA end resection and DNA repair pathway choice. The cell cycle controls the competition between C-NHEJ and HR. Extensive end resection is stimulated in the S/G2 phase of the cell cycle. This is controlled by CDK activity which mediates phosphorylation of multiple substrates such as components of the MRN complex and CtIP. In G1 phase of the cell cycle, 53BP1 foci localise to DSBs, inhibit BRCA1 recruitment, block DNA end resection and therefore promote C-NHEJ. In the S and G2 phase of the cell cycle, ATM kinase, which phosphorylates members of the MRN complex, BRCA1, CtIP or BLM, favours the three resection-dependent pathways (HR/SSA/Alt-NHEJ). Adapted from Ceccaldi et al. (2016)

end resection and favour C-NHEJ (Panier and Boulton, 2014). Loss-of-function mutations in factors that control end resection, such as 53BP1, result in reduced C-NHEJ and restored DNA end resection. This results in HR activity and induces PARP inhibitor resistance in BRCA1-deficient cells (Bunting et al., 2010).

Although it has been assumed that HR plays the major role in repair of DSBs in G2, recent work has suggested that the situation may be more complex. Cells lacking NHEJ proteins such as DNA ligase IV, display a marked G2 phase repair defect and conversely cells defective in HR only show a subtle G2 repair defect (Shibata et al., 2011). It has therefore been suggested that NHEJ initially attempts to repair in G2, but if re-joining is delayed then resection and HR repair occur (Kakarougkas and Jeggo, 2014). Factors influencing the switch from NHEJ to HR include the heterochromatic status and the complexity of DNA damage (Kakarougkas and Jeggo, 2014).

1.2.8 *HR defects and cancer*

HR has a key role in repair of DNA lesions and preventing inappropriate recombination that could otherwise lead to oncogenic transformation. It is therefore not surprising that mutations of the genes involved in the HR pathway can predispose of a variety of cancers. Mutations in *BRCA1* and *2* increase the risk of ovarian cancer (as discussed earlier) but also lead to increased risk of breast cancer. BRCA2 mutations also increase the risk of prostate (Edwards et al., 2003) and pancreatic cancer (Carnevale and Ashworth, 2015).

Mutations of other *RAD51* mediators including *RAD51C*, *RAD54B*, *RAD51B* along with *PALB2* have also been shown to increase the risk of breast, pancreatic and ovarian cancer (reviewed in Krejci et al. (2012)). Although mutations in *RAD51* have not been linked to any disease, many cancer cell lines show evidence of elevated levels of RAD51 (Raderschall et al., 2002). It is postulated that high levels

of RAD51 may lead to uncontrolled HR and destabilisation of the genome in the early events in carcinogenesis (Richardson et al., 2004). An alternative view is that high levels of RAD51 maintain the genome during tumourigenesis (Krejci et al., 2012; Schild and Wiese, 2010).

1.2.9 *Therapeutic targeting of the DDR*

Knowledge of the DDR in tumours is influencing treatment choice. Deregulation of the pathways involved not only affects responses to DNA-damaging chemotherapy but can be a targeted for therapeutic intervention (Curtin, 2012). Loss of elements of one DNA repair pathway may be compensated for by increased activity of other elements or pathways. The resulting upregulation of these other DNA repair pathways can cause resistance to DNA damage chemotherapy or radiotherapy (Curtin, 2012). Specific inhibitors of these up-regulated pathways have the potential to sensitize cells to these therapies. In addition, tumour cells may be 'addicted' to compensatory DDR pathways for survival. Exploiting this dependence and using the concept of synthetic lethality has resulted in the development of DNA repair inhibitors (Curtin, 2012). These principles have been applied to the HR pathway in ovarian cancer.

1.2.10 *Targeting the HR pathway in ovarian cancer*

1.2.10.1 *Response to chemotherapy*

Tumours with HR defects are sensitive to cross-linking agents such as carboplatin and cisplatin (Clauson et al., 2013). This is highlighted in ovarian cancer where large studies have shown that *BRCA*-mutated ovarian cancer demonstrate superior response to platinum chemotherapy and longer platinum-free durations than wild-type *BRCA* ovarian cancer patients, with *BRCA2* mutation carriers having the best

prognosis (Tan and Kaye, 2015; Yang et al., 2011; Bolton et al., 2012). Post-treatment secondary mutations that result in gain of function of BRCA1 and BRCA2 restoring the function of HR are associated with platinum resistance (Sakai et al., 2008; Swisher et al., 2008). It is, however, unclear which functions of BRCA1/2 proteins are required for therapy resistance and which *BRCA1/2* genotypes are more likely to undergo reversion mutations. It is also unclear whether certain *BRCA1/2* mutations result in differing sensitivities to platinum.

Although the improved response to platinum agents in *BRCA*-mutated ovarian cancer has been well documented, there are only limited clinical data as to whether *BRCA*-mutated cancers also have improved response to other chemotherapy agents. Two retrospective studies on patient outcomes following the topoisomerase IIα inhibitor, pegylated liposomal doxorubicin (PLD), have demonstrated improved response rates and PFS when compared with patients with non-*BRCA* mutated cancers (Adams et al., 2011; Safra et al., 2011). Treatment of *BRCA*-mutated cancers with topotecan, a topoisomerase I inhibitor, however, showed no differences in PFS compared to non *BRCA*-mutated cancers (Safra et al., 2011). There is also some data to suggest that patients with BRCA deficiency have increased sensitivity to other DNA damaging agents such as mitomycin C (induces DNA cross links) and melphalan (alkalyating agent that induces inter-and intra-strand DNA cross links) (Tan and Kaye, 2015). The data on the use of taxanes (microtubule-interfering drugs) are conflicting. There are a number of preclinical and clinical studies that suggest that mutations in *BRCA1* and 2 may confer resistance to taxanes (Tagliaferri et al., 2009; Tan et al., 2013). However, benefit has been seen with the use of paclitaxel in *BRCA*-mutated cancers (Tan et al., 2013) and therefore they continue to have a therapeutic role.

1.2.10.2 *PARP inhibitors*

A promising approach for targeting the HR pathway is the exploitation of dysregulated DDR through a synthetic lethal approach. This is illustrated by the use of poly(ADP)ribose polymerase (PARP) inhibitors in HR defective tumours. The best-documented role of the PARP enzymes is their role in the repair of DNA single strand breaks (SSB) in the base-excision repair/single strand break repair (BER/SSBR) pathway. PARP enzymes catalyse the transfer of adenosine diphosphate (ADP)-ribose moieties from cellular NAD+ forming ADP-ribose polymers (Dianov and Hubscher, 2013). By inhibiting repair of SSBs, PARP inhibition results in accumulation of these lesions. The unrepaired SSBs can be converted to double strand breaks (DSBs) at replication forks (Boulton et al., 1999). In cells with defective HR pathways (for example, *BRCA1* and *BRCA2* mutant cancers), these DSBs accumulate and cannot be repaired resulting in cell death (McCabe et al., 2006). However, PARP inhibition is not toxic in cells with functioning HR pathways (McCabe et al., 2006; Bryant et al., 2005). This is the concept of synthetic lethality where cell death only occurs when there is loss of two genes (or pathways) but loss of each gene independently does not affect cell survival (Figure 1.10). PARP inhibitors should therefore be synthetically lethal in patients with cancers that have defective HR function (Fong et al., 2009), and as discussed earlier, this could be in up to 50% of HGSOCs.

Recent reports have challenged this view of the mechanism of action of PARP inhibitors and have proposed alternative mechanisms of synthetic lethality (reviewed in De Lorenzo et al. (2013)). For example, it is now known that PARP inhibitors can be toxic to cells by trapping PARP1 and 2 at the sites of DNA damage. These trapped complexes obstruct replication forks, which require the HR pathway to be resolved (Murai et al., 2012). Several studies also suggest a role of non-homologous end joining (NHEJ) in PARP inhibitor induced

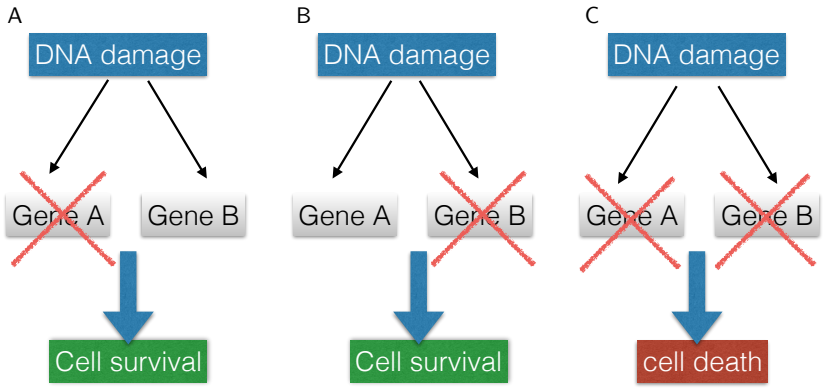

Figure 1.10: Synthetic lethality. A: Loss of gene A alone, such a mutation in the DDR, is compatible with cell survival. B: loss of gene B alone is compatible with cell survival. C: loss of gene A and gene B causes cell death.

killing (Patel et al., 2011). An understanding of the contribution of these different mechanisms to PARP inhibitor sensitivity will help in determining their use in a clinical setting. Despite the possible incomplete understanding of the mechanism of action of PARP inhibitors, these drugs have showed promising results in clinical trials.

The activity of PARP inhibitors has been assessed in phase I and II trials in showing PARP inhibitors have shown activity in BRCA mutated ovarian cancer (Gelmon et al., 2011; Kaye et al., 2012; Ledermann et al., 2012; Kaufman et al., 2015a; Domchek et al., 2016). Activity has also been seen in sporadic BRCA non-mutated cancers (Gelmon et al., 2011). However, this was associated with platinum sensitivity suggesting that these patients had defects within the HR pathway and highlighting the need for a marker for HR function. Several PARP inhibitors are currently being investigated, the most studied of which is olaparib. The pivotal phase II study investigated olaparib maintenance therapy in platinum sensitive recurrent cancer (study 19) which demonstrated improved PFS compared to placebo (4.8 months vs 8.4 months for patients treated with olaparib) with the largest benefit seen in the BRCA mutated groups. (Ledermann et al.,

2012). A further trial of olaparib given with paclitaxel and carboplatin followed by a period of olaparib maintance compared to chemotherapy alone also led to a significant improvement in PFS (12.2 months in the olaraprib maintainance group compared to 9.6 months in those given chemotherapy alone) (Oza et al., 2015).

Two other PARP inhibitors, niraparib and rucaparib, have been shown to have activity in ovarian cancer (Sandhu et al., 2013; McNeish et al., 2015). Phase III trials maintenance trials (NOVA study for niraparib and ARIEL3 study of rucaparib) are currently underway in platinum sensitive disease. Both trials include cohorts of patients with *BRCA* mutations and ARIEL3 is stratified by homologous recombination defects determined on tumour biopsies. The results of these and other trials are awaited.

The optimal timing of the use of PARP inhibitors is debated, in particular whether PARP inhibitor or bevacizumab should be used at first relapse (Tan and Kaye, 2015). It is hoped that further clinical trials will help in answering this question. A further question surrounding PARP inhibitor use is whether development of resistance to PARP inhibitors might also confer resistance to other chemotherapy agents and therefore compromise benefit to subsequent chemotherapy. The significance of this remains to be determined (Tan and Kaye, 2015).

Knowledge about the molecular basis of ovarian cancer is therefore beginning to influence treatment options in *BRCA*-mutated cancer. There are, however, several important questions that remain. Firstly, there are other mechanisms that result in HR deficiency in ovarian cancer and should these HR defective patients be considered as having a similar phenotype to *BRCA1/2* mutated cancers and therefore be treated similarly. If this is the case it raises the question of how should these HR defective cancers be identified. A number of approaches have been taken to address this problem, including gene expression profiles (Konstantinopoulos et al., 2010) and the use of a functional HR assay measuring RAD51 foci that predicts sensitivity to PARP

inhibitors (Naipal et al., 2014; Mukhopadhyay et al., 2010). In addition, given that the potential effects of the mechanisms of *BRCA1/2* inactivation may influence clinical phenotype, should patients also be stratified according to their underlying mutation when considering treatment options?

1.2.10.3 *Inhibitors of the HR pathway*

The sensitivity of HR defective tumours to chemotherapy provides the rationale for the development of HR inhibitors. Specific inhibition of the HR pathway has proved technically difficult. Mirin is an inhibitor of MRE11 endonuclease function and therefore inhibits HR function but it is non-specific, also inhibiting NHEJ. RAD51 inhibitors are in development (Curtin, 2012). The HR pathway has also been targeted by ATM inhibitors. Studies have shown that the ATM inhibitor, KU55933, sensitizes cells to IR and topoisomerase inhibitors (Hickson et al., 2004). Recently ATR inhibitors have been identified and have been shown to sensitize cells to a variety of DNA damaging agent (Charrier et al., 2011; Reaper et al., 2011).

When developing new treatments for ovarian cancer it is therefore important to consider the DDR. Manipulation of the DDR may offer ways of improving treatment efficacy and also may be important in patient stratification and selecting patients who would most benefit from the therapy. There is a significant unmet clinical need for treatments targeting HR competent tumours. These patients, especially those with platinum resistant disease, have a poor prognosis and have limited therapeutic options (Bolton et al., 2012). This thesis addresses the role of the DDR in the efficacy of oncolytic viruses, a novel therapy for ovarian cancer.

1.3 ONCOLYTIC VIRUSES

Oncolytic viruses represent a novel class of anti-cancer agent for the treatment of cancer. Interest in the use of viruses as possible agents for tumour destruction has been present for over a hundred years. The idea was derived from reports that following an infectious disease, patients with cancer (often leukaemia) occasionally had periods of clinical remission (reviewed in Kelly and Russell (2007)). The use of viruses to treat cancer then began to take hold in the 1950s when tissue culture systems were developed (Russell et al., 2012). Cancer patients at this time were treated with impure oncolytic virus preparations and, in some cases, patients were even inoculated with viruses from previous patients (Larson et al., 2015). The majority of viruses were usually destroyed by the host immune system but sometimes the infection took hold and the tumours responded. This usually occurred in immunocompromised individuals, although frequently they subsequently became unwell when the infection spread to normal tissues (Kelly and Russell, 2007; Russell et al., 2012). Unfortunately, enthusiasm for viral gene therapy waned as any anti-tumour effects were short lived and new chemotherapy agents were being developed.

More recently, however, as knowledge of viral biology and mechanisms of oncogenesis has accumulated, there has been a development of more rationally designed, tumour specific viruses that have entered clinical trials. Several different oncolytic viruses, from 10 different virus families, have been identified to date and entered clinical trials including herpesvirus, reovirus, polio virus, parvovirus and vaccinia along with adenovirus (Russell et al., 2012). Different viruses have differing structures, lifecycles, tropisms and toxicities and each may possess several advantages as well as disadvantages for use as an oncolytic viral therapy. In addition, to enhance efficacy, these oncolytic

viruses may be 'armed' with additional therapeutic genes that can drive systemic anti-tumour immune responses. (Russell et al., 2012).

This thesis focuses on replication-selective Adenovirus based on human serotype 5 of group C. Adenoviruses replicate very efficiently in human cells and are well characterised. In addition, human adenoviruses are associated with relatively mild respiratory illnesses, their genomes can be easily manipulated and they can be purified to a high titre, making them an attractive vector for oncolytic viral therapy (Alemany et al., 2000).

1.3.1 *The development of oncolytic adenoviral vectors*

Early adenoviral vectors were designed to deliver transgenes, and thus had complete E1 deletions in order to prevent replication (Robert-Guroff, 2007). The transgenes inserted into the deleted region included tumour suppressor genes, antisense oligonucleotides to block oncogene expression, prodrug activating genes and antiangiogenic factors. Although preclinical results were encouraging, therapeutic benefit in clinical trials was minimal and thought to be due to the inability of these non-replicating viruses to access every malignant cell (Robert-Guroff, 2007).

More recent adenoviral gene therapy have used replicating viruses. This harnesses the property of adenovirus to infect cells, multiply within them, cause death and infect neighbouring cells. One method to achieve tumour selectivity uses the principal that viral replication and oncogenesis both require inactivation of the same proteins. This has resulted in the development of viral mutants deleted in parts of their genome that are not required for replication within tumour cells with specific genetic defects. (Wong et al., 2010). These viruses should not replicate in normal cells that do not have the tumour associated mutations. This ability of adenoviral replication to be tumour

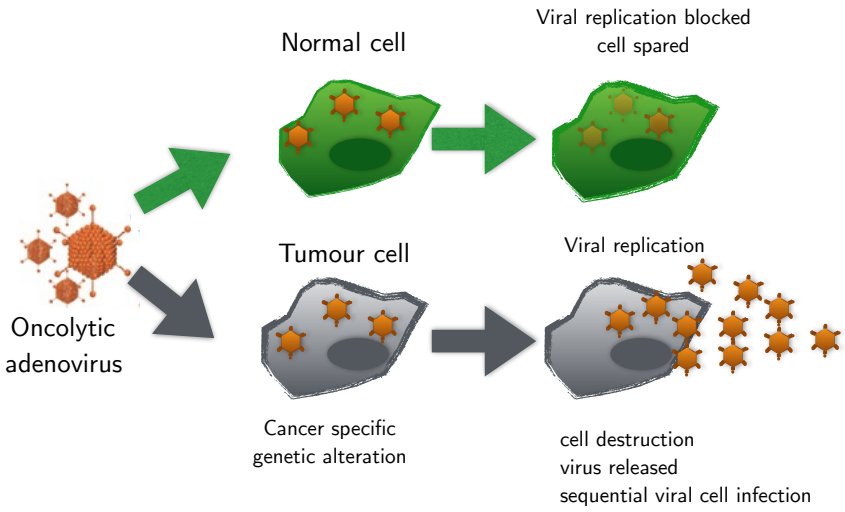

Figure 1.11: Tumour specific killing by oncolytic adenovirus. Replication-competent oncolytic adenoviruses specifically replicate within, and lyse tumour cells releasing mature virions that can then spread throughout a tumor. Image taken from Choi and Yun (2013).

selective should result in therapeutic efficacy but would be minimally toxic (Figure 1.11).

1.4 ADENOVIRUS

1.4.1 *Structure*

Human adenoviruses comprise a large family of 51 different serotypes originally classified on the basis of their ability to be neutralised by specific animal antisera. These can be further subdivided into six subgroups (A-F) based on their sequence homology and ability to agglutinate red blood cells (Flint et al., 2004). The adenovirus genome is contained within a capsid that has a characteristic icosahedral appearance. The capsid is comprised of three major proteins: hexon (II), penton base (III), and a knobbed fibre (IV) along with a number of

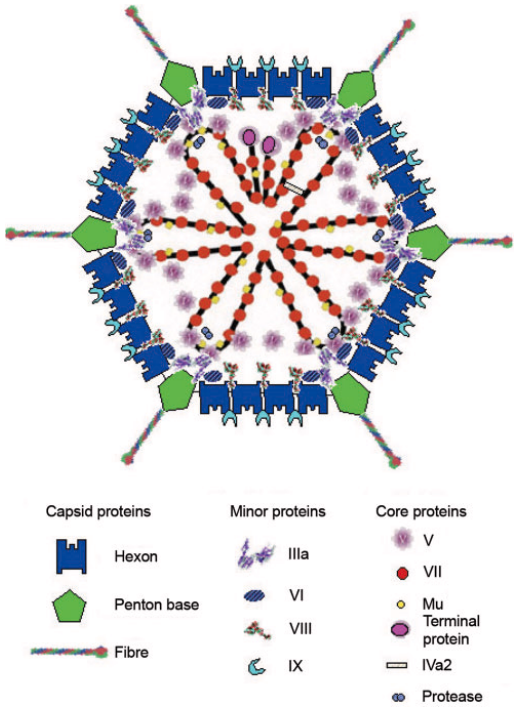

Figure 1.12: Structure of adenovirus. A schematic depiction of the structure based on electron microscopy and crystallography. Taken from Russell (2009)

other minor proteins (VI, VII, IX, IIIa and IVa2). There are 240 hexons on the faces and edges of the capsid with 12 pentons on the apices. Extended fibres arise from each penton base located at the 12 vertices of the capsid. Each fibre terminates at a distal knob that binds the virus to the cell surface receptor on the host cell (Russell, 2000, 2009) (Figure 1.12).

1.4.2 *Adenoviral DNA*

Linear, double-stranded adenoviral DNA is 35-36 Kb long and is tightly wrapped around viral proteins V and VII in the adenoviral core. Terminal proteins (TP) are covalently attached to the 5′ ends and the adenoviral genome is flanked by inverted terminal repeats (ITR), which contain sequences that serve as the origin of replication.

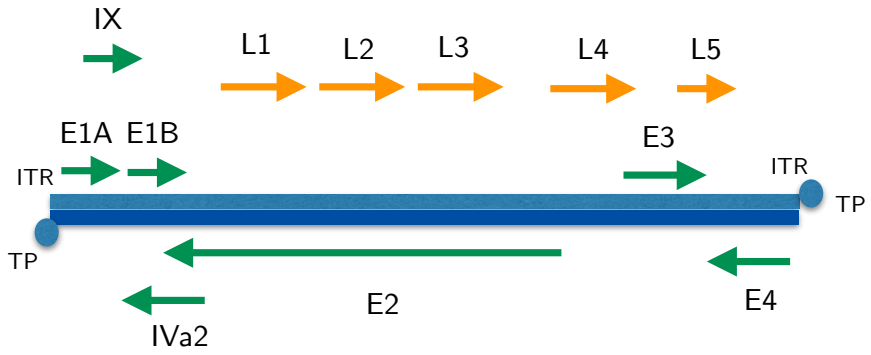

Figure 1.13: Adenoviral DNA. The double stranded DNA adenoviral linear genome is covalently linked at its ends to terminal proteins via inverted terminal repeats (ITRs). The first viral transcription unit to be expressed is E1A that activates the other early adenovirus transcripts (E1B, E2, E3 and E4). Late gene transcription (L1-L5) is activated after the onset of DNA replication and is under the control of major late promoter (MLP). Arrows indicate the direction of transcription.

The genes are grouped into transcriptional units: five early transcription units named E1A, E1B, E2, E3 and E4, two delayed early units, IX and IVa2, and the major late transcription unit that produces five groups of mRNA designated L1 to L5 (Shenk, 2001) (Figure 1.13). All of these units are transcribed by cellular RNA polymerase II, the early regions are transcribed before the late ones (Flint et al., 2004). Each region is transcribed to yield multiple mRNAs through the use of alternative splicing and differential polyadenylation. There are also two viral-associated (VA) RNAs, which play a role in regulating translation, transcribed from a polymerase III promoter (Thimmappaya et al., 1982). Transcription occurs from both the leftward and rightward stand of the adenoviral chromosome (Flint et al., 2004).

With the exception of E4 region, transcription units encode proteins with similar functions. The early regions are involved with viral replication and late regions encode viral structural proteins such as hexon and penton bases (McConnell and Imperiale, 2004). In addition to

promoting the expression of key viral and cellular genes, early genes also suppress the ability of the host cell to mount a viral response. For example, early viral genes block host protein synthesis, inhibit apoptosis, inhibit the DNA damage repair response and the immune response. These effects facilitate the ultimate aim of successful replication and virion production (Weitzman and Ornelles, 2005) and is discussed in more detail below. This interaction between the virus and host is important when considering the development of an oncolytic virus.

1.4.3 *Adenoviral life cycle*

The adenovirus infectious cycle can be divided into two phases. The first 'early' phase consists of the entry of the virus into the host cell and the passage of the viral genome to the nucleus followed by the selective transcription and translation of the early genes (E1-E4). This phase can take around 6-8 hours. The late phase leads to the assembly within the nucleus of structural proteins and the maturation of the infectious virus and takes around 4-6 hours (Russell, 2000).

1.4.4 *Early phase: cell entry*

The capsid fibre is the first component to interact with the host. Adenoviruses from groups A, C, D, E and F bind to host cells via an interaction between the fibre and cell surface coxsackie adenovirus receptors (CAR) (Bergelson et al., 1997). CAR is widely expressed on human tissues, it is a member of the immunoglobulin family and is involved *in vivo* in the formation of tight junctions (Coyne and Bergelson, 2005). Most of the species B viruses bind to a ubiquitously expressed, CD46. Members of the group D viruses can use the sialic acid receptor (Russell, 2000).

Binding to these initial receptors occurs along with the attachment of the five arginine-glycine-aspartate (RGD) motifs on each penton base to cell surface $\alpha v\beta 3$ and $\alpha v\beta 5$ integrins. This results in viral internalisation within clathrin-coated vesicles into endosomes for further processing. This interaction with integrins also induces a variety of cellular responses, for example activation of PI3K and Rho GTPases (Li et al., 1998). These responses are important in altering the cytoskeleton of the cell to facilitate internalisation. Following permeabilisation of the vesicles, the virus is released into the cytoplasm where the viral capsid is disrupted (Stewart et al., 1997). The viral genome, associated with core protein VII, is then transported via cellular dynein and microtubules to the nuclear pore whereby the adenovirus particle disassembles (Leopold et al., 2000). Viral DNA is then released which can enter the nucleus via the nuclear pore (Trotman et al., 2001; Kelkar et al., 2004). Viral DNA can be detected within the nucleus between 1 and 2 hours after infection (Matthews and Russell, 1998). Once inside the nucleus the genome is targeted to the nuclear matrix (Russell, 2000).

1.4.4.1 *Oncolytic adenovirus and enhancing entry into host cells*

There is evidence that CAR expression on malignant cells is variable. Low CAR expression could therefore affect the efficient infection of tumours by group C adenoviral vectors (Akiyama et al., 2004). To address this problem, modifications have been made to the adenoviral fibre protein. Δ24-RGD, has a RGD peptide motif inserted into the fibre, which allows the virus to bind to cell surface integrins rather than just CAR(Jiang et al., 2009). In models of glioma, this mutant showed imporved infectivity and cytotoxicity when compared with Δ24 in both low and high CAR-expressing cell lines (Jiang et al., 2009, 2003). A phase I clinical trial of Δ24-RGD in patients with recurrent ovarian cancer demonstrated overall safety and potential anti-tumour

efficacy with stable disease seen in 71% of patients after 1 month (Kimball et al., 2010).

A further approach to increase infection involves creating an adenovirus containing a chimeric fiber with the knob domain of Ad3 in the Ad5 capsid (Kanerva et al., 2002). This virus was found to infect ovarian cancer cell lines more efficiently than Ad5. In addition, in ascitic fluid samples from four patients with ovarian cancer, infection by Ad5/3 was greater than that of Ad5 (Kanerva et al., 2002).

1.4.5 *Early phase: S phase induction*

Once inside the cell, the priority for adenoviruses is to promote replication of their DNA. The proteins encoded by early region 1A (E1A) of human adenovirus type 5 (Ad5) activate viral transcription and reprogram cellular gene expression in the infected cell which provides the optimal environment for viral replication (Flint and Shenk, 1989). E1A is the first adenoviral protein to be expressed after viral DNA has been transported to the nucleus (Flint and Shenk, 1997). Only host proteins are required for E1A expression. It is transcribed by cellular RNA polymerase, and following alternative splicing and export of the mRNAs to the cytoplasm, it is synthesised by cellular translation machinery. Ad5 E1A is expressed as two alternately spliced isoforms, referred to as 12S and 13S, and shares four highly conserved regions (CR1-CR4) with E1A proteins from other serotypes. These proteins, which are extensively modified by phosphorylation, are imported into the nucleus where they regulate transcription of both cellular and viral genes.

E1A proteins bind to cellular proteins, most of which regulate host cellular transcription (Flint and Shenk, 1997). One such protein is the retinoblastoma protein (pRb). The tumour suppressor pRb is part of the retinoblastoma family of proteins, which includes p107 and p130, that regulate transition into S phase (Felsani et al., 2006). In quies-

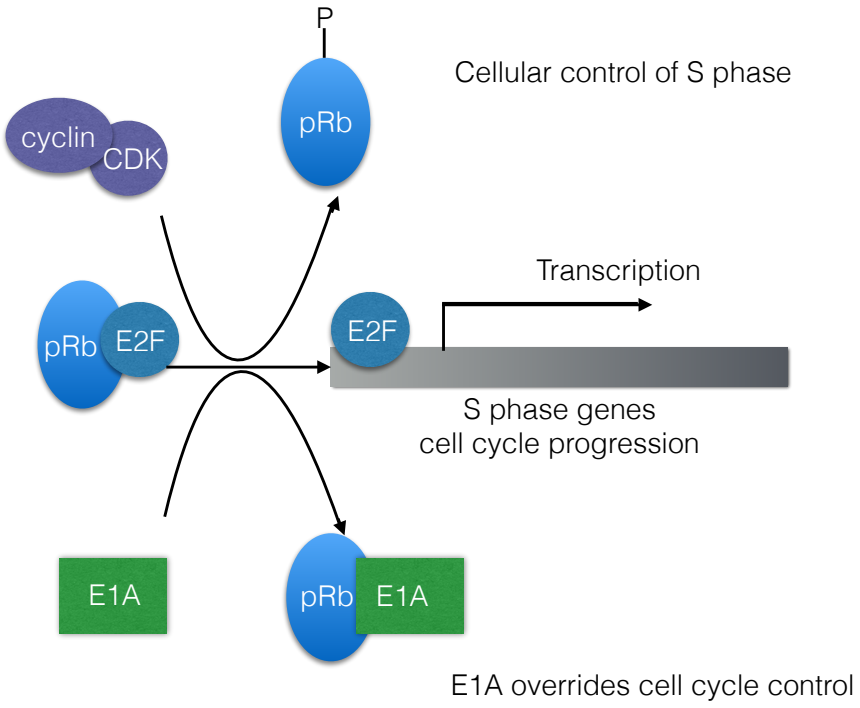

Figure 1.14: Cell cycle control and E1A. In G_0-G_1 phase of the cell cycle, hypophosphorylated RB protein (pRB) forms a complex with the transcription factors of the E2F family (E2F), which prevents their ability to activate transcription. Phosphorylation of pRB is controlled by cell cycle dependent cyclin/cyclin dependent kinases (CDKs) and releases pRB from E2F resulting in S phase progression. Infection by adenovirus overrides this control by binding to pRB releasing E2F. Adapted from Frisch and Mymryk (2002).

cent cells, un- or hypophosphorylated pRb binds to and inhibits the E2F family of transcription factors, holding the cell in G1. In early stages of adenoviral infection CR2 binds with high affinity to the pRB pocket domain and subsequently, E1A CR1 displaces E2F from pRB by binding with pRB at the E2F binding site. This overrides the normal phosphorylation dependent regulation of the pRB-E2F transcription by cyclin dependent kinases (CDKs) (Figure 1.14).

The release of E2F also transactivates genes (E1B, E2, E3 and E4) necessary for DNA replication and S-phase entry. This stimulates the

transcription of cellular genes that encode enzymes that make substrates for DNA synthesis, therefore driving viral DNA replication. The virus therefore bypasses the normal control of the cell cycle, facilitating preferential replication of the viral genome (Flint and Shenk, 1997).

In addition to RB, E1A interacts with an impressive collection of cellular proteins. Figure 1.15 shows some of the cellular proteins bound to the conserved regions of E1A (Frisch and Mymryk, 2002). Many of these cellular proteins are critical regulators of gene expression, cell signalling and cell cycling, and by altering their activity, the adenovirus prepares the host cell for maximal production of viral progenies (Berk, 2005). For example, E1A CR3 activates transcription by interacting with the MED23 subunit of the Mediator of transcription complex (Boyer et al., 1999b). This stimulates pre-initation complex (PIC) assembly (Cantin et al., 2003) and may also increase the rate at which PICs initiate transcription. This results in an increase in the rate of re-initiation at early viral promoters. CR1 binds to the cyclin dependent kinase (CDK) inhibitors p21 (Chattopadhyay et al., 2001) and p27 (Nomura et al., 1998), which prevents them from binding and inhibiting CDK-cyclin complexes, and thus promotes cell cycling. CR1 also influences transcription by binding several cellular protein complexes involved in chromatin structure, including p300 (Barbeau et al., 1992) and CBP (CREB-binding protein) (Arany et al., 1995) The CR4 region of E1A also binds and inactivates the transcription co repressor, CtIP (Frisch and Mymryk, 2002; Bruton et al., 2007).

1.4.5.1 *E1A deletions and Oncolytic adenovirus: dl922-947*

Based on the principle that both viral replication and oncogenesis proceed due to inactivation of the same regulatory proteins, adenoviral mutants have been developed targeting regions of the adenoviral genome that are dispensable for replication in tumour cells. This project focuses on the adenoviral mutant, *dl*922-947. *dl*922-947 has a

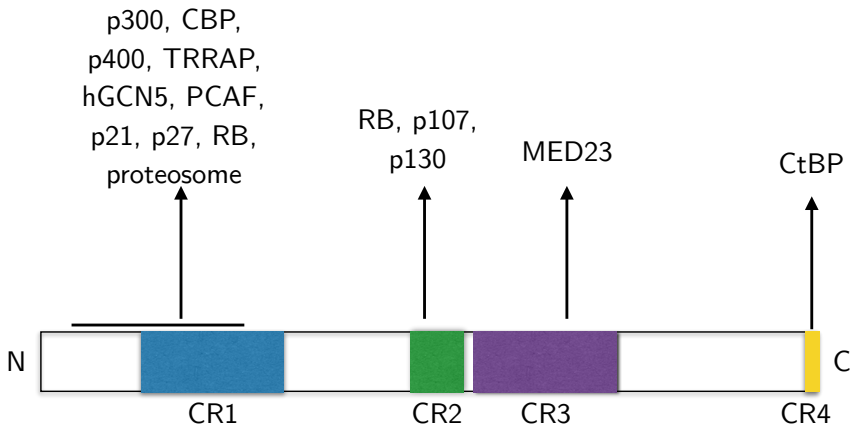

Figure 1.15: E1A regions bind to a variety of cellular proteins to manipulate cell signalling, cell cycling and gene expression to prepare the host cell for the production of virus. Adapted from Berk (2005).

24 base pair deletion in the early region 1A (E1A) CR2 region between amino acids 122 and 129 (Figure 1.16). As discussed, in wild type adenovirus, the CR2 region binds to retinoblastoma protein, dissociating it from E2F and inducing S phase induction. *dl*922-947 should therefore not induce S phase induction and subsequent viral replication in normal cells. However, the pRb pathway is disrupted in the majority of cancers (Sherr and McCormick, 2002), including ovarian cancer (D'Andrilli et al., 2004) therefore *dl*922-947 should replicate selectively in pRb-deregulated malignant cells.

*dl*922-947 has shown to have activity in both ovarian (Lockley et al., 2006) and non ovarian cell lines (Heise et al., 2000). It has shown efficacy that exceeded that of wild-type adenovirus (Ad5 WT) and ONYX-015. It has also shown activity when given by intraperitoneal (IP) injection in a mouse model of ovarian cancer (Lockley et al., 2006). In contrast, in growth arrested normal cells dl922-947 was significantly less toxic than Ad5-WT (Heise et al., 2000). A similar adenovirus, Δ24, with the same E1A deletion as *dl*922-947, has also been investigated. This virus has been shown to be capable of inducing S

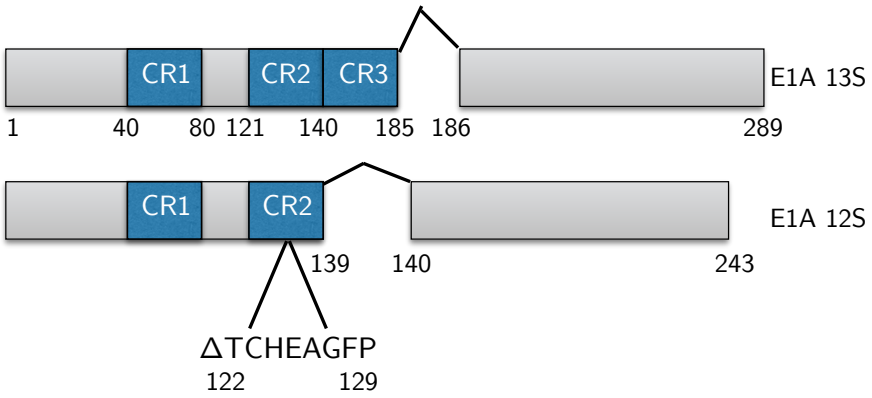

Figure 1.16: The adenoviral mutant, *dl*922-947. *dl*922-947 has a 24 base pair deletion in the early region 1A (E1A) CR2 region between amino acids 122 and 129. The diagram represents the two Ad5 E1A isoforms (12S and 13S) showing the location of the deletion.

phase, replicating in and lysing several glioma cell lines and shows activity *in vivo* in a mouse model (Fueyo et al., 2000).

1.4.6 *Viral replication*

Following S phase induction, preferential replication of the adenoviral genome occurs. Adenovirus replicates very efficiently in human cells, a property that makes it an attractive and frequently used vector for gene therapy. Up to 10^6 new DNA molecules can be synthesised within 48 hours after infection. This efficiency is achieved through a mechanism that requires three viral proteins and at least three cellular proteins (De Jong and Van der Vliet, 1999). The E2 region encodes proteins necessary for replication of the viral genome. These are the pre-terminal protein, pTP, the 72-kDa single-stranded DNA-binding protein, DBP, and DNA polymerase (pol) (de Jong et al., 2003). Cellular proteins are, however, needed for efficient replication. These include nuclear factors (NF) I, NFII (a topoisomerase) and Oct-1. Adenoviral DNA replication is initiated by a protein priming mechanism

involving the viral pTP, which is covalently attached to the 5′ end of the genomic DNA, together with NF1 and Oct-1. Viral DNA is synthesised by the E2b DNA polymerase (De Jong and Van der Vliet, 1999). DBP is required for viral DNA replication and also regulates transcription and translation of viral genes during the late stages of infection (Kruijer et al., 1983).

1.4.7 *Inhibition of apoptosis by adenovirus*

The expression of E1A alone results in short lived proliferation prior to cell death by apoptosis (Rao et al., 1992). E1A causes stabilisation of p53 (Lowe and Ruley, 1993) due to a variety of mechanisms (Gallimore and Turnell, 2001) including the inhibition of MDM2 (a p53 inhibitor) and proteosome modification by E1A CR1 (Zhang et al., 2004). The response to stabilisation of p53 as a result of E1A includes cell cycle arrest in G1 through activation of the CDK inhibitor, p21 or cell death via the intrinsic apoptotic pathway (Berk, 2005). p53 results in apoptosis by a complex series of mechanisms including activating cellular proapototic genes (such as BAX and BAK) (Berk, 2005). BAX is also activated by the release of its binding partner MCL-1 (Cuconati et al., 2003). BAK and BAX cooperate to form pores in the outer mitochondrial membrane. This causes the release of the proapototic proteins, cytochrome C and Smac/DIABLO. This initiates apoptosis through caspases and blocks the inhibitor of apoptosis proteins (IAPs) (White, 2001). The viral genome must, therefore, prevent this p53 stabilisation to inhibit apoptosis function to keep the cell alive for as long as possible in order to allow maximal viral replication (White, 2001). This is achieved through E1B-19K and E1B-55K, the two main proteins encoded by E1B (Berk, 2005) along with the E4 region product E4orf6 (Querido et al., 2001; Ben-Israel and Kleinberger, 2002).

The apoptotic pathway is blocked in wild-type virus infected cells by the binding of E1B-19K to both BAX and BAK, preventing them

from co-oligomerising and forming pores in the outer mitochondrial membrane (Cuconati et al., 2003). In adenoviral infected cells, E1B 55K is found in a complex with E4orf6 (Sarnow et al., 1984). In infected cells, this complex is assembled with several cellular proteins into ubiquitin ligase complex with elongins B and C, cullin5 (Cul5) and RING-box 1 (Rbx-1) (Berk, 2005). P53 along with the MRN complex (discussed in more detail below), are the two substrates for this complex targeting these proteins for proteosomal degradation (Berk, 2005). It is interesting to note that in the case of Ad12, cullin 2 (Cul2) rather than Cul5 is recruited to the E3 ligase (Blackford et al., 2008; Forrester et al., 2011). The reason for these differences between adenoviral serotypes has not yet been determined.

1.4.7.1 *E1B deleted oncolytic adenovirus*

The first replication competent oncolytic virus to enter clinical trials was ONYX-015 (*dl*1520). ONYX-015 was generated by deletion of the viral E1B 55K gene, which results in a complete lack of E1B 55K expression (Bischoff et al., 1996). As discussed above, the E1B region of the viral genome has crucial p53 inhibitory functions. ONYX-015 should therefore not be able to prevent p53-induced apoptosis of normal cells, resulting in cell death of infected cells prior to completion of the viral replication cycle. Since over 50% of human cancers have abnormalities of the p53 pathway (Sherr and McCormick, 2002), E1B-55K should not be required for viral replication in many malignant cells. This deletion should allow ONYX-015 to selectively kill p53 deficient cancer cells without damaging normal cells (Bischoff et al., 1996). However, results from clinical trials were disappointing: although some tumour selection was seen, durable responses were rare. In addition ONYX-015 was also shown to replicate in some p53 wild-type tumour cells (O'Shea et al., 2004). It is now known that E1B 55K has functions that are essential to viral replication, in particular promoting export of late adenoviral mRNA in normal cells (O'Shea

et al., 2004). The tumour selectivity is thought to be due to the expression of Y-Box Binding Factor-1 (YB1) which is expressed on tumour cells but not on normal cells (O'Shea et al., 2004). YB1 substitutes for the mRNA export function of E1B-55K only in tumours (but not all tumours are positive for YB1). This initial incomplete understanding of the virus may explain its lack of efficacy (Larson et al., 2015).

Despite this, phase I and II clinical studies showed that the toxicity profile of ONYX 015 was promising and dose limiting toxicity was rarely reached (even at the highest dose of $3x10^{11}$ pfu) (Kirn, 2001). The most common side effects were short-lived 'flu'-like symptoms (Larson et al., 2015). An oncolytic virus virtually identical to ONYX-015 called H101 has been assessed in a phase III trial in 160 patients with advanced head and neck squamous cancer. The patients were randomised to chemotherapy with or without H101. Patients treated with the virus with 5-FU/cisplatin had a 78.8% response rate, compared to 39.6% in the chemotherapy alone group. Based on these results, H101 has been approved in China for treatment of head and neck squamous cell cancer (Lu et al., 2004).

1.4.8 *Adenoviruses and the immune response*

Following adenoviral infection, rapid immune responses are induced to protect the host from further infection. In general, this immune response represents a major challenge when using adenoviral vectors (Hendrickx et al., 2014) as it could result in both clearance of the virus as well as inducing toxicity. However, this inflammatory response may also increase the therapeutic potential of oncolytic viruses (Russell et al., 2012). These defence mechanisms are divided into innate and adaptive, and their ultimate aim is destruction of virally infected cells. With respect to the former, the nature of the innate response network triggered by virus varies depending on receptor usage and cell type, yielding a complex signalling cascade with diverse outcomes.

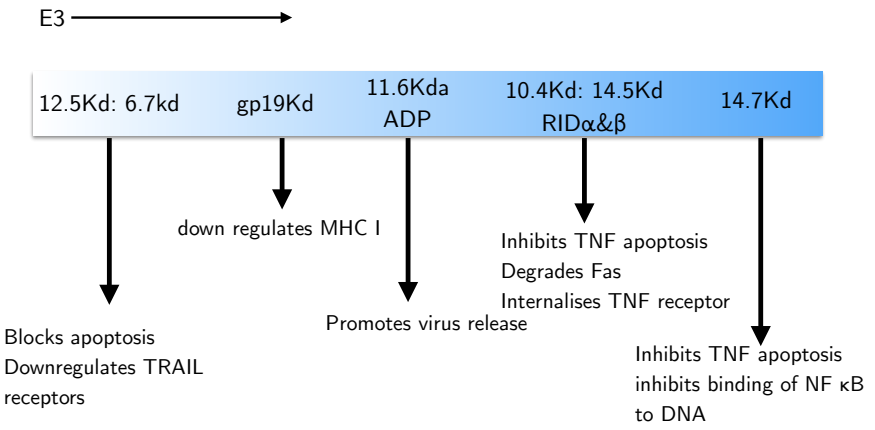

Figure 1.17: The E3 region of the viral genome. Products of the viral E3 region function to inhibit aspects of the host immune response to allow persistence of virally infected cells. Once viral replication is complete the E3 protein ADP facilitates cell lysis .

Multiple genes within the virus are involved in ensuring that the host cell does not recognise viral infection and therefore continues to replicate the viral genome. For example, in addition to its action on p53, E1B-55K interferes with the induction of IFN-inducible genes (Chahal et al., 2013). The E1a proteins also inhibit activation of genes induced by interferon and IL-6 (Ackrill et al., 1991; Takeda et al., 1994) and therefore may reduce the effect of the inflammatory cytokines and chemokines. Products of the viral E3 region also function to subvert the host immune response and allow persistence of infected cells (Lichtenstein et al., 2004). A summary of the function of the viral E3 region is shown in Figure 1.17.

One host response against viral infection is the presentation of antigens by virally infected cells to cytotoxic T lymphocytes by major histocompatibility complex class one (MHC I). The viral protein E3 gp19 down regulates MHC I. This reduces antigen presentation to cytotoxic T-lymphocytes, thereby preventing T cell recognition of infected cells (Burgert and Kvist, 1987). E3-gp19 also lowers the cell surface levels of receptors for natural killer cells (McSharry et al., 2008).

A major component of the host cell response to virus is lysis of infected cells caused by inflammatory cytokines and CTLs binding to death receptors (DRs). Proteins encoded by the E3 region also protect cells from the lytic effects of tumour necrosis factor-α (TNFα) (Deryckere and Burgert, 1996). These proteins act to prevent the induction of the extrinsic apoptotic pathways and possibly classical TNFα induced necrosis by binding to death receptor signalling. For example RIDα binds strongly to the Fas receptor and RIDβ interacts with TNF receptor type 1 (TNFR1). Once bound these death receptors are internalised and targeted for lysosomal destruction. This prevents the induction of apoptosis by TNFα and the Fas ligand on the surface of CTLs (reviewed in Benedict (2003)). The inflammatory response is also inhibited by E3 proteins by a number of mechanisms including the interaction of 14.7K with NF-κB to prevent its binding to DNA (Carmody et al., 2006).

Adenoviral E3 therefore protects infected cells from the host immune system to allow viral replication and mature viral particles to be produced. Spread of mature virions to adjacent cells requires cell lysis and this is facilitated by a further E3 protein, the adenoviral death protein (ADP) (Tollefson et al., 1996). The E3 genes are, however, dispensable for replication of virus in tissue culture and parts of this viral region are commonly deleted in viral vectors including *dl*922-947. A full assessment of the impact of this deletion is beyond the scope of this project, however it is possible that the E3B deletion may affect their therapeutic potency either by permitting premature immune-mediated lysis of infected cells or by preventing release of mature progeny by ADP.

1.4.8.1 *Oncolytic adenovirus and the immune response*

Treatment of patients with systemic adenoviral therapy results in dose limiting inflammatory toxicities, which can be severe and in some cases has resulted in death (Reid et al., 2002; Raper et al., 2003).

These toxicities have understandably hindered the development of oncolytic viruses. Liver toxicity as a result of oncolytic adenovirus is also of particular concern. Ad5 is extensively sequestered by the liver by macrophages (Kupffer cells), leading to acute transaminitis and vascular damage (Shayakhmetov et al., 2005). In female nude mice with human ovarian cancer IP xenografts treated with *dl*922-947, high levels of ascitic cytokines were seen and marked hepatotoxicity occurred (Lockley et al., 2006). In an attempt to modulate these side effects, inhibitors of TNFα were combined with the oncolytic virus. Although improved viral efficacy was seen, liver toxicity still occurred (Salako et al., 2011). More recently, in a murine ovarian cancer model, systemic cytokines and hepatic toxicity have been shown to be reduced by pharmacological inhibition of $\beta 3$ integrin without compromising efficacy (Browne et al., 2015).

Along with mediating toxicities to adenoviral vectors, the immune system is also a barrier to delivery of virus. Neutralising antibodies (nAbs) directed against the primary antigenic epitopes in the three major capsid proteins target the systemically-delivered therapeutic vector for elimination, thus limiting therapeutic efficacy (Uusi-Kerttula et al., 2015)). Administering the virus directly to the tumour by intratumoral injection may partly overcome this problem (Turnbull et al., 2015). In ovarian cancer, IP injection of virus may be the route of choice to maximize delivery of virus to the tumour. Further approaches to limit antibody neutralisation is to coat the virus in chemical conjugates (Fisher and Seymour, 2010) or encapsulate the adenovirus into liposomes (Wan et al., 2013). To address the problem of the prevalence of preexisting anti-Ad5 nAbs alternative serotypes have been developed. ColoAd1 is a chimeric Ad3/Ad11p virus generated through forced evolution via recombination of a pool of Ads from different serotypes on tumour cell lines (Di et al., 2014). Clinical trials of this virus are now underway in both ovarian cancer (NCT02028117) and other solid tumours.

Although aspects of the immune system mediate toxicity to adenoviral vectors, it is also recognised that oncolytic viruses exert an immunogenic, in addition to a directly cytotoxic, effect (Turnbull et al., 2015; Kaufman et al., 2015b). The immune response to oncolytic viruses is complex and could be innate, driven by cytokine release causing migration of immune cells such as NK cells or adaptive via a response to tumour associated antigens. Following oncolytic cell death, tumour cells release tumour-associated antigens that serve to promote an adaptive immune response that could mediate tumour regression at distant sites that are not exposed to the virus. The response to oncolytic viruses has the potential to overcome the immune evasion seen in tumours. By altering the cytokines and immune cells within the tumour microenvironment oncolytic viruses could promote immune recognition of tumour cells (Kaufman et al., 2015b).

To further stimulate an immune response and overcome the immune evasion seen in tumours, there are a number of adenoviral vectors in development that are armed with factors that stimulate the immune response including GM-CSF (Cerullo et al., 2010), and IL12 (Yang et al., 2012). In a trial of Ad5-Δ24-GMCSF in 20 patients, 2 patients had a complete response, 1 a minor response and 5 had stable disease. Responses were frequently seen in both injected and uninjected tumours (Cerullo et al., 2010). Combining oncolytic virus with immune checkpoint inhibitors, for example, antibodies targeting CTLA-4 and PD-1/PD-L1 may offer a further approach to enhance therapeutic efficacy (Turnbull et al., 2015).

The importance of the immune system in oncolytic adenovirus highlights the need for immunocompetent models. Murine cells do not support productive replication of human adenovirus (Young et al., 2012). This has been a significant barrier to the development of preclinical models and more fully understanding how the immune system contributes to adenoviral efficacy.

1.4.9 *The adenoviral E4 region*

The E4 region produces transcripts for six proteins named after their open reading frames: orf1, orf2, orf3, orf4, orf6 and orf6/7. These proteins that play a role in DNA replication, transcription, apoptosis, host cell protein shut off, regulation of cell cycle signalling and regulation of the DNA damage response (discussed in more detail below)

In early stages of infection, E4orf6/7 binds to the displaced E2F from pRb and E1A, and promotes viral DNA replication by stabilising the binding of E2F to the E2 promotor (Weitzman and Ornelles, 2005). The E4orf3 protein associates with the nuclear matrix and induces the reorganisation of nuclear bodies into tract-like structures (Doucas et al., 1996). These structures contain proteins implicated in multiple cellular functions and it is thought that this reorganisation is advantageous for viral replication (Russell 2000). E4orf3 has been shown to bind E1B 55K, re-localising it to the nucleus and it also has a role in regulating late viral gene expression (Weitzman and Ornelles, 2005). E4orf6 cooperates with E1B-55K and is involved in viral replication, RNA processing, nucleo-cytoplasmic transport of late viral mRNA and the shut off of host protein synthesis (Gonzalez and Flint, 2002; Russell, 2000). In addition, E4orf6 and E1B-55K together with cellular factors (Cul5, elongin B and C) mediate polyubiquintinylation and degradation of cellular targets including p53 and MRE11 (discussed below) (Harada et al., 2002). A summary of some of the functions of the E4 regions is shown in Figure 1.18.

1.4.10 *Adenovirus and the DNA damage response*

The adenoviral genome mainly exists as monomers of dsDNA throughout infection. At late stages of infection, amplification of this linear

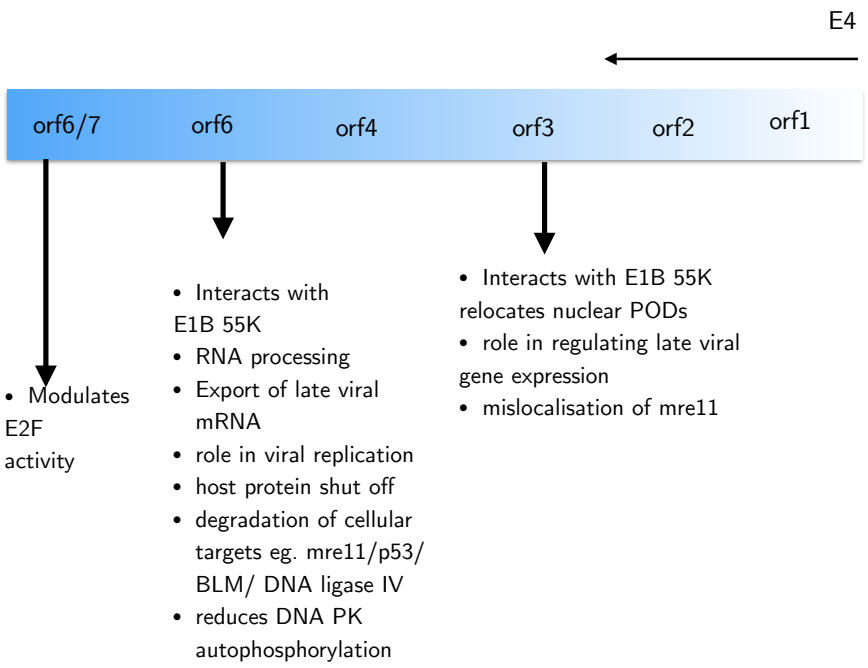

Figure 1.18: The E4 region of the viral genome. Schematic showing the six proteins encoded by the E4 region of the viral genome and their interaction with host proteins.

genome presents the cell with a huge number of free DNA ends (Weitzman and Ornelles, 2005). The host cell responds to this challenge by activation of the DNA damage response (Weitzman and Ornelles, 2005). There is a complex interplay between the host cell's DDR and adenoviral infection. Infection by many viruses is sufficient to trigger a DDR, activating some or all the repair pathways and this has been seen as the host cell recognising viral DNA as its own damaged DNA (Weitzman and Ornelles, 2005). This cellular response is an obstacle to efficient viral replication and, therefore, viruses have a complex series of mechanisms that, in turn, have evolved to combat and inactivate the cellular damage response pathways.

During the first few hours after infection, the host cell responds to adenovirus, possibly due to recognition of viral DNA or due to cellular stress, by activating various DNA damage response signals. These include phosphorylation of H2AX, structural maintenance of chromosomes protein 1 (SMC1) and RPA32 (Turnell and Grand, 2012). Full

activation of the DSB machinery, however, only occurs in the absence of the E4 region of the adenovirus (Stracker et al., 2002). Following infection with a mutant adenovirus lacking the E4 region, activation of MRE11 occurs (Carson et al., 2003) together with activation of the ATM kinase (as demonstrated by autophosphorylation on S1981) and many of the known substrates for ATM and ATR become phosphorylated (Weitzman and Ornelles, 2005). Proteins involved in the cellular response to DNA damage are thought to be recruited to sites of DSB in the host genome and appear as foci within the nucleus of infected cells. Many of these proteins, including MRE11 and autophosphorylated ATM, are found to form foci surrounding viral replication centers (VRC) during infection with an E4 deleted virus (Carson et al., 2003; Stracker et al., 2002).

The result of this activation of the DDR in an E4 mutant virus is that viral DNA genomes are joined end to end to form high molecular weight concatamers of viral DNA that cannot be packaged into viral capsids (Weiden and Ginsberg, 1994). The junctions of the concatamers also have deletions (Weiden and Ginsberg, 1994), suggesting that the ends of the Ad genomes are degraded or end-resected. Since the origins of replication are located at the termini of the viral genome, this would inhibit viral replication. The ligation of viral genomes into concatamers seen following infection with E4 mutant virus is thought to be due to the function of the NHEJ pathway. This is supported by the fact that the concatameric junctions had variable sized deletions, with little or no sequence homology (Karen et al., 2009a). In addition, concantamers are not formed in cells with mutant DNA-PK (Boyer et al., 1999a) and ligase IV (Stracker et al., 2002) following infection with an E4 mutant virus.

Together these observations imply that the viral genome is a substrate for DNA repair processess and proteins from the E4 region are necessary to block the DNA repair response. Mechanisms employed by the virus to inhibit NHEJ, and thus prevent concatamer for-

mation, include proteosomal degradation of DNA Ligase IV (Baker et al., 2007) whilst both E4-34kDa and E4-11kDa bind and inactivate DNAPK, which is an essential kinase for NHEJ (Boyer et al., 1999a).

A major target of the virus following Ad5 infection is the MRN complex (comprised of MRE11, RAD50 and NBS1) (Stracker et al., 2002). In uninfected cells, the MRN complex is a sensor and central player in the response to DSBs (Williams et al., 2007). The MRN complex is inactivated by several mechanisms following Ad5 infection. E1B-55K together with E4orf6 form an E3 ubiquitin ligase complex with the cellular proteins Cul5, Rbx1 and elongins B and C and targets MRE11 (along with p53, and DNA-ligase IV) for proteosomal degradation (Harada et al., 2002; Karen et al., 2009b). A second mechanism is the mislocalization of the MRN complex by E4-orf3 from the nucleoplasm to promyelocytic leukaemia protein (PML)-containing 'nuclear tracks' (Araujo et al., 2005; Stracker et al., 2005; Evans and Hearing, 2005). This sequesters the MRN complex away from the viral genomes, which are located in the VRC (Stracker et al., 2005; Evans and Hearing, 2005). These VRCs do not co-localise with the redistributed MRN proteins (Stracker et al., 2005).

E1B-55K and E4orf3 are also involved in re-localising MRE11 to cytoplasmic aggresomes (Araujo et al., 2005), resulting in degradation. Degradation of the MRN complex has been shown to occur early in infection, prior to the accumulation of viral DNA (Karen et al., 2009b). E1B-55K/E4orf6–dependent degradation of MRN is sufficient to prevent ATM activation (Carson et al., 2003). Inhibition of ATR signalling, such as CHK1 phosphorylation, occurs due to mislocalisation of MRN by Ad5 E4orf3 prior to MRN degradation by E1B-55K/E4orf6 (Blackford et al., 2008). Adenoviral inhibition of MRE11 prevents both the DDR signalling and the formation of viral genome concatamers (Stracker et al., 2002; Carson et al., 2003).

Further proteins involved in the DNA damage response that have been shown to be degraded include BLM (Orazio et al., 2011) and

SPOC1 (a regulator of DNA damage response and chromatin structure (Mund et al., 2012; Schreiner et al., 2013). During adenoviral infection, a number of DDR proteins are recruited to viral VRC. These include RPA32, ATR, ATRIP, RAD9, DNA topoisomerase 2-binding protein 1 (TOPBP1), RAD17 and heterogeneous nuclear ribonucleaoprotein U-Like 1(hnRNPUL1) (Blackford et al., 2008). It is unclear whether re-localisation of these DDR proteins to VRC may alter or inhibit their function (Weitzman and Ornelles, 2005) or whether their presence facilitates viral replication. It has been shown that the E1B 55K associated protein, E1B-AP5, is required for the ATR-dependent phosphorylation of RPA32 and it is postulated that RPA32 may aid DNA elongation (Blackford et al., 2008).

Different adenoviral serotypes affect the host cell DNA damage repair mechanisms differently. For example p53 is not degraded following infection with Ad3, Ad7, Ad9 and Ad11 but shows a pronounced increase in expression (Forrester et al., 2011). MRE11 is degraded in Ad5, Ad4 and Ad12 infected cells but is not degraded by group B and group D viruses (Forrester et al., 2011). In addition, the mechanism of ATR inhibition also varies; Ad5 E4orf3 protein inhibits ATR activation by re-localizing and immobilizing MRN subunits before their targeted degradation by E1B-55K/E4orf6. In contrast to Ad5, TOPBP1, an activator of ATR, is degraded by Ad12 and results in inhibition of ATR signalling (Blackford et al., 2010). The reasons for these differences await further investigation.

Adenoviruses, therefore, go to considerable lengths to disable the DDR (summarised in Figure 1.19) yet some DDR proteins are recruited to VRCs suggesting that they may be required for viral replication (Weitzman and Ornelles, 2005). Further investigation into the DDR following viral infection may identify key components that could shed further light into the lifecycle of adenovirus and importantly could identify targets to enhance oncolytic viral efficacy. As discussed earlier, DNA repair pathways are frequently abnormal in ovarian can-

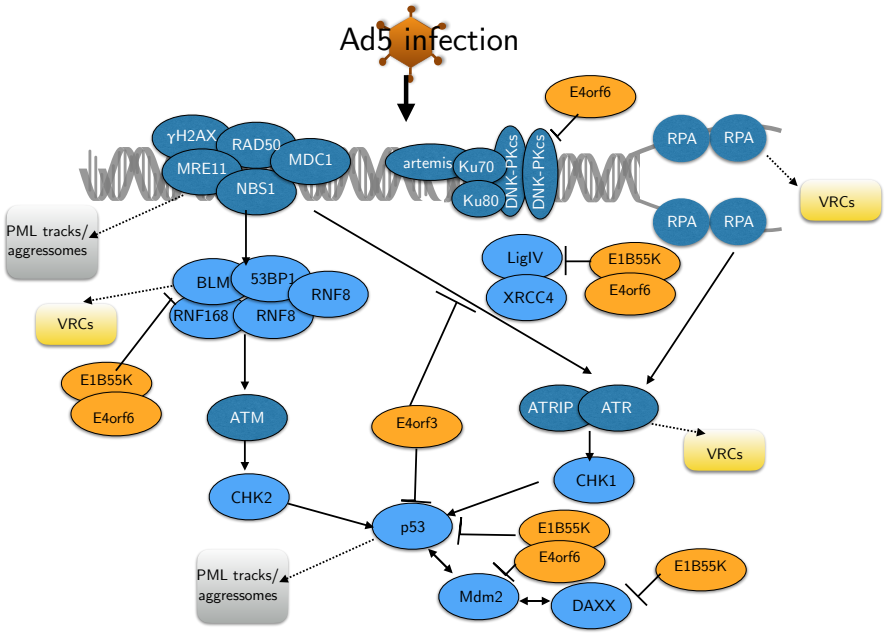

Figure 1.19: Regulation of the DDR by adenovirus type 5. Adenoviral genes (E1B55K and E4orf6) promote degradation of p53, BLM, MRE11 and DNA Ligase IV. E4orf6 inactivates DNAPK by reducing phosphorylation. Ad5 E4orf3 sequesters MRN to aggresomes to inhibit MRN–dependent activation of ATR. Components of the ATM and ATR pathways are recruited to VRC or PML-containing nuclear tracks and aggresomes. Viral replication proteins are shown in orange, cellular proteins in blue. Broken arrows shown proteins recruited to VRCs, PML-tracks or aggresomes. Figure adapted from Turnell and Grand (2012).

cer and investigation into these pathways may also aid patient selection for future clinical trials of oncolytic adenoviruses.

1.4.11 *Oncolytic adenoviruses summary and rationale for this project*

Adenovirus replication ultimately results in death of the infected cell. Although the mechanism of cell death and the pathways involved are complex and yet to be fully elucidated (Baird et al., 2008), harnessing this cell killing in a tumour specific fashion is the goal of oncolytic viral therapies. The oncolytic nature of adenoviruses reflects

an intrinsic property of the cancer cell. Cancer cells arise from the deregulation of multiple pathways that regulate cell growth and survival. Adenoviruses express genes that achieve these same changes in the host cell during the course of infection. Consequently, due to the intrinsic properties of cancer cells, viral replication can still occur despite genetic manipulation of the virus and deletion of specific key genes needed for viral replication in normal cells. Why some tumour cells display acute sensitivity to viral cytotoxicity whereas other cells are resistant is currently not know.

What is clear is that adenoviruses, including the E1A CR2 adenoviral mutant *dl*922-947, interact with, and deregulate multiple cellular processes. Investigation into these pathways will not only shed light on adenoviral biology but could identify targets that could enhance efficacy. It may also lead to the identification of patients who are most likely to respond to oncolytic viral therapy.

The DDR is a key pathway that is deregulated by oncolytic viruses. This pathway is also frequently abnormal in tumours, particularly ovarian cancer. Previous work has shown that, following infection with *dl*922-947, profound deregulation of the cell cycle is observed in sensitive cells (Connell et al., 2011). This is associated with the presence of extensive genomic DNA damage. Inhibition of the ATR-Chk1 pathway promoted genomic DNA damage and over-replication in resistant cells, which was accompanied by increased adenovirus toxicity both *in vitro* and *in vivo* (Connell et al., 2011). It appears that virus-induced host cell DNA damage signalling may be key determinants of viral efficacy and understanding this further could identify the factors which could promote viral efficacy. This is particularly important in the treatment of patients with ovarian cancer, where the DDR is frequently abnormal.

1.5 AIMS

1. To assess the role of DNA double strand break damage following infection with the oncolytic adenovirus, *dl*922-947, in a panel of ovarian cancer cell lines.

2. To assess the role of the homologous repair pathway in the efficacy of *dl*922-947.

3. To assess the role of components of the DDR in their response to the oncolytic adenovirus, *dl*922-947, through the use of a DNA repair siRNA screen.

Part II

MATERIALS AND METHODS

2

MATERIALS AND METHODS

2.1 CELL LINES

Cell lines were maintained at 37°C in a humidified atmosphere with 5% CO_2. There were routinely passaged twice a week using 0.5% trypsin in PBS (PAA Laboratories) to detach monolayers.

All cell lines were routinely tested for mycoplasma and human cell lines underwent short tandem repeat profiling (LGC Standards) to verify their authenticity. For long term storage, cells were pelleted by centrifugation, and the cell pellet resuspended in 10% dimethyl sulphoxide (DMSO) and 90% foetal bovine serum (FBS) (Biosera). Cell were stored overnight at−80°C, and then transferred to liquid nitrogen.

The human ovarian cancer cell line, SKOV3ip1, was provided by Dr Janet Price (University of Texas-MD Anderson Cancer Center, Texas) and SKOV3 cells were obtained from Cancer Research UK Cell Services (Clare Hall, South Mimms, Hertfordshire, UK). TOV21G cells were obtained from Prof F Balkwill (Centre for Cancer and Inflammation, BCI). OVCAR4 cells were obtained from Dr R. Camalier (NCI-Frederick, MD, USA). IGROV1 cells were obtained from NCI. The PE01 and PE04 cells were kindly provided by Dr Simon Langdon (School of Molecular, Genetic and Population Health Sciences, University of Edinburgh, UK). UWB 1.289 and UWB 1.289 + BRCA1 cells were obtained from ATCC.

Of these cell lines, IGROV1, PE01, PE04 and SKOV3 cells were maintained in RPMI with 10% heat-inactivated FBS. The UWB 1.289 cells were maintained in 50% RPMI and 50% mammary epithelial

growth medium (Medium 171 and mammary epithelial growth supplement (MEGS), ThermoFisher Scientific) with 3% FBS and Penicillin 100 units/mL streptomycin 100 μg/mL (PAA laboratories). To maintain expression of BRCA1, UWB + BRCA1 cells were also cultured with G418 (200 μg/ml) (Geneticin, ThermoFisher Scientific). The remainder of the cell lines were cultured in DMEM with 10% FBS.

2.2 ADENOVIRAL MUTANTS

The adenoviral 5 (Ad5) mutant *dl*922-947 is deleted in the region encoding amino acids 122-129 of the E1A CR2 domain. It also has a 745bp deletion in E3B between base pairs 30,005 and 30,750 that is substituted for by a 642bp non-coding DNA fragment (Heise et al., 2000). The adenoviral 5 mutant, *dl*309 has the same E3B deletion as *dl*922-947 but has wild-type E1A. Wild type adenovirus 5 (Ad5WT) and the E3B-deletion mutant *dl*309 were kindly provided by Dr. W.S. Wold (St. Louis University, St. Louis, MO, USA). Ad5 GFP is deleted in E1 and E3B and has green fluorescent protein (GFP) in the E1 position under control of the cytomegalovirus (CMV) promoter. Ad5 LM-X has a complete deletion of E1, it is therefore non-replicating, and its E3 region is intact. The construction has been described previously (McNeish et al., 2001).

2.3 CELL SURVIVAL ASSAYS

2.3.1 *MTT assay*

Cell survival was measured using an MTT (3-(4,5-Dimthylthiazol-2-yl)-2,5-17 diphenyltetrazolium bromide) (Sigma) assay. MTT assays were performed in 24 well tissue culture plates and cells plated at a density of $1 \times 10^4 - 4 \times 10^4$ cells per well depending on the cell

line used, in 1ml of complete medium. Cells were treated with virus or drug 24 hours after plating and cell survival measured after 120 hours by adding 100 μl of a 5 mg/ml solution of MTT (final concentration 500μg/ml) to each well. After 3 hours of incubation at 37^{o}C the medium was then aspirated and crystals dissolved in 100-500 μl of DMSO depending on the colour intensity of the crystals. Plates were read at 560 nm on a Wallac 1420 Multilabel counter plate reader (PerkinElmer Life and Analytical Sciences). Cell survival was normalised for background absorbance and expressed as a percentage of untreated cells (100% survival).

2.3.2 *Sulforhodamine B assay*

Sulforhodamine B assays were performed in a 24 well plate. Cells were seeded at a density of $1 \times 10^4 - 4 \times 10^4$ cells per well depending on the cell line used in 1 ml of complete medium. Cell survival was assessed 72-120 hours following drug treatment by removing medium and fixing cells in 100μl/well trichloroacetic acid for 1 hour at 40^{o}C. Cells were washed 3 times with water, allowed to air dry at room temperature. They were then stained with 250 μl of 0.4% w/v sulphorodamine B in 1% acetic acid for 30 minutes at room temperature. Excess dye was removed by washing with 1% acetic acid, the plates air dried and then the amount of incorporated dye within the cells was dissolved in 1ml/well 10 mM tris base solution. Plates were read on Wallac 1420 Multilabel counter plate reader (PerkinElmer Life and Analytical Sciences). Cell survival was normalised for background absorbance and expressed as a percentage of untreated cells (100% survival).

2.3.3 *CellTitre-Glo*

Cell viability was also measured using the ATP-based luminescent CellTiter-Glo assay (Promega). The luciferase reaction for this assay is shown by the following formula:

$$beetle\,luciferin + ATP + O_2 \rightarrow Oxyluciferin$$

CellTiter-Glo reagent was diluted 1 in 4 in PBS prior to use. Cells were cultured in a 96 well plate and cell survival measured 72-120 hours following treatment with drug, siRNA or virus. The medium was removed from the cells and 100 μl diluted CellTiter-Glo was added. The plates were mixed for 2 mins using a plate shaker (Grant-bio) and incubated for 10 mins at room temperature. Luminescence was read using a Wallac 1420 Multilabel counter plate reader (PerkinElmer Life and Analytical Sciences). Luminescence data were expressed as a percentage of untreated cells (100% survival).

2.3.4 *Analysis*

Dose response curves were created using GraphPad Prism version 6 (GraphPad Software San Diego CA, USA). The IC_{50} (inhibitory concentration, 50%) was calculated from the equations of the sigmoidal curves generated by GraphPad Prism software.

2.4 IMMUNOBLOT BLOT ANALYSIS

2.4.1 *Preparation of protein lysates*

For preparation of whole protein lysates, cells were washed twice in cold PBS and scraped into cold western lysis buffer (150 mM NaCl,

50 mM Tris Base, 0.05% SDS and 1% TritonX-100) containing one protease and one phophatase inhibitor tablets (Roche) per 10 ml buffer. Samples were put on ice for 10 min and sonicated for 10 seconds. Samples were then centrifuged for 5 mins at 8000 rpm at 4^{o}C and the supernatant stored at -80^{o}C.

2.4.2 *Protein concentration evaluation*

The protein concentration of cell lysates was measured using the Bio-Rad assay. Dilutions of protein ranging from 0.1 mg/ml to 1.0 mg/ml were made using bovine serum albumin (BSA) as positive, protein standard controls. Reagent A' was prepared by adding 20 μl Bio-Rad reagent S to 1 ml Bio-Rad reagent A. 5 μl of each protein lysate sample was added per well of a 96 well plate in triplicate, with the protein standards added in triplicate plus a control well of 5 μl water. To each 5 μl of sample, 25 μl of A' and 200 μl Bio-Rad reagent B was added and the plate incubated at room temperature for 5minutes. Absorbance was measured at 630 μm on Wallac 1420 Multilabel counter plate reader. The absorbance of the protein standards was used to construct a standard curve and the equation for this line was used to calculate the protein concentrations of the cell lysates.

2.4.3 *SDS polyacrylamide gel electrophoresis (SDS PAGE)*

Samples were run on either a NuPAGE 4-12% Bis-Tris precast gel (Invitrogen) or a poured 10% - 15% polyacrylamide gel (Table 2.1). Resolving gels were poured as shown in (Table 2.1) and allowed to set in a multiple gel caster system (Amersham Biosciences). Once set, a stacking gel (Table 2.1) was poured on the top of the gel a comb inserted to creat the wells and the gel set at room temperature.

REAGENT	10%	15%	STACKING GEL
water	4 ml	2.3 ml	3.4 ml
30% Proto- Gel (National Diagnostics)	3.3 ml	5 ml	0.83 ml
1.5MTris (pH 8.8)	2.5 ml	2.5 ml	-
1M Tris (pH 6.8)	-	-	0.63 ml
10% SDS (Bio-Rad, Ca. USA)	0.1 ml	0.1 ml	0.05 ml
10% Ammonium persulphate (Sigma)	0.1 ml	0.1 ml	0.05 ml
TEMED	0.004 ml	0.004 ml	0.005 ml

Table 2.1: Components of SDS PAGE resolving (10% and 15%) and stacking gels

Up to 30 μg of the protein lysates were mixed with 6x loading buffer (375 mM Tri-HCL pH 6.8, 6% SDS, 48% Glycerol, 9% mercaptoethanol and 0.03% Bromophenol Blue) and made up to a total of 24 μl with distilled water. Samples were boiled on a heating block at 95°C for 5 mins, then transferred to ice and centrifuged briefly before loading. Electrophoresis took place at 120 V for 90-120 mins in 1× running buffer diluted from a 10× stock (30.2g Tris Base, 94 g Glycine and 100 ml 10% SDS in 1 litre) or MOPS buffer (Invitrogen) (for precast gels). Molecular weight rainbow markers (Amersham Biosciences) were loaded alongside the protein samples to allow size comparison of bands. Proteins were transferred onto nitrocellulose membranes (GE Healthcare) using a semi-dry transfer system (Trans-Blot, Bio-Rad) set at 20 V for 40 mins. After being soaked in transfer buffer (39 nM Glycine, 48 mM Tris Base and 20% Methanol in 1 litre). Membranes were blocked with a solution of 4% (w/v) skimmed milk powder in 0.1% Tween 20 (Fluka Analytical) in PBS (PBS-T) for at least 1 hour at room temperature.

The primary antibody was diluted in a 1.5% solution of BSA (Sigma) in 0.1% PBS-T or 4% (w/v) non-fat milk and incubated for either 1 hour at room temperature or 4°C overnight on a gentle rocker (Table 2.2). Primary antibody was removed by three washes with 0.1% PBS-T for 5, 10 and 15 mins. Secondary horseradish peroxidise

ANTIBODY	COMPANY	DILUTION	SPECIES
E1A	Becton Dickinson (cat 554155)	1:1000	mouse
Ad5	Abcam (ab36851)	1:5000	goat
RAD51	Santa-Cruz (sc-8348)	1:500	rabbit
RAD51	Abcam (ab213)	1:500	mouse
MCM3	Abcam (ab97282)	1:1000	rabbit
Ku70	Santa Cruz (sc-1486)	1:1000	goat
MRE11	Cell signalling (4895)	1:500	rabbit
NONO	Abcam (ab70335)	1:2000	rabbit
E2-DBP	kind gift of Dr. David Ornelles	1:500	mouse
Anti-rabbit HRP	Dako	1:1000	goat
Anti-goat HRP	Dako	1:1000	rabbit
Anti-mouse HRP	Dako	1:1000	rabbit

Table 2.2: Antibodies used for Immunoblot analysis

(HRP)-conjuated antibody (Table 2.2) was diluted at a concentration of 1:1000 in a solution of 1.5% BSA in 0.1% PBS/Tween and incubated with the membrane for one hour at room temperature. Three washes with 0.1% PBS/Tween were repeated as before. The detection of HRP-conjugated secondary antibodies was performed by ECL Plus Western Blotting Detection Reagent (GE Healthcare) and visualised by exposure of the member to Hyperfilm ECL (GE Healthcare) prior to developing in a Curix 60 Developer (Agfa, Middlesex, UK).

2.5 CO-IMMUNOPRECIPITATION

2×10^6 cells were infected with *dl*922-947 (MOI 10) and lysed 24 hours later in 800 µl RIPA lysis buffer (with complete protease inhibitors, Roche, Herts, UK). 35 µl Sepharose beads (Santa Cruz, CA, US) were incubated with anti-RAD51 antibody (Santa Cruz, H-92, sc8349) or control antibody (anti-HA, sigma H6908) for 1 hour at 4°C. Lysates were then incubated with the IP matrix beads for 1 hour at room temperature and washed with RIPA lysis buffer. SDS loading buffer was added, samples boiled and proteins detected by Western blot as

described in Section 2.4. Primary antibodies used: rabbit anti-Ad5 E2 DBP and anti-RAD51 (Abcam, ab213).

2.6 VIRAL LIFE CYCLE

2.6.1 *Virus Infectivity assay*

5×10^5 cells were plated in 6 cm plates. 24 hours later, cells were infected with an E1 deleted adenovirus type 5 containing the green fluorescent protein gene driven by the cytomegalovirus (CMV) immediate early promoter (Ad GFP) or mock infected. 24 hours post infection the cells were trypsinised, re-suspended in medium and centrifuged for 5 mins in a centrifuge at 1500 rpm. The supernatant was removed and the cell pellet re-suspended in 2 mls warm phosphate buffered saline (PBS) and centrifuged for 5 mins at 1500 rpm. The supernatant was removed and the cells re-suspended in 400 μl PBS. Samples were processed in a Florescence-activated cell sorting (FACS) Caliber (Becton Dickinson, CA, USA). Infectivity was determined after 10,000 total events were recorded. The percentage of GFP positive events was determined from the total count. All conditions were repeated in triplicate and analysed using FLOWJO software.

2.6.2 *$TCID_{50}$ assay*

The $TCID_{50}$ assay (tissue culture inhibitory dose 50%) is a limiting dilution assay that enables the quantification of any infectious particles in the test sample. To quantify intracellular production of mature viral particles, 2×10^5 cells were seeded in 6 well plates. Cells were infected 24 hours later with *dl*922-947 at the stated MOI in serum free medium and re-fed 2 hours later with serum containing medium. 24, 48 and 72 hours post infection, cells were washed twice with PBS and

then scraped into 0.5 ml 0.1 M Tris pH 8.0, all time points were harvested in triplicate. The collected samples were freeze/thawed three times and samples spun in a microfuge at 8000 rpm for 5 mins to pellet out the cell debris.

The quantity of replicating virus (measured in pfu/ml) was determined by titrating 10 fold serial dilutions of virus onto JH293 cells in a 96 well plate. JH293 cells were seeded in 96 well plates at 1×10^4 cells per well in 200 μl medium per well. The test samples were prepared by diluting in DMEM. Dilutions started at 10^{-3} for the 24 hour sample and 10^{-6} for the 48 and 72 hour sample. The samples were added to the second row of the plate (22 μl) and serial dilutions within the same plate were made by taking 10% of the volume of each well of the second row (22 μl) and adding it to the third row and so on until the final row. The top row of each plate was left uninfected.

The JH293 cells were scored for cytopathic effect (CPE) 10-12 days later. The observed number of wells displaying CPE at each dilution were counted and the $TCID_{50}$ calculated with the formula:

$$Log\, TCID_{50} = A - D\,(S - 0.5)$$

where:

A = Log of the highest dilution showing CPE in more than 50% of the wells

D = Log of the dilution factor.

S = summation of the proportion of positive wells in each row.

This gives a value for 22 μl of virus and the value is therefore divided 0.022 to give $TCID_{50}$/ml. Since $TCID_{50}$ overestimates viral titre by 0.7 log compared to plaque assay, $TCID_{50}$/ml is converted to pfu/ml using the following formula:

$$Pfu/ml = 10^{n-0.7}$$

Where: n = log $TCID_{50}$/ml

This result is only valid if the lowest dilution gives greater than 50% CPE, and the highest dilution gives less than 50% CPE.

2.6.3 *Extraction of viral DNA for qPCR for viral proteins*

$2x10^5$ cells were plated and infected 24 hours later with *dl*922-947. Cells were harvested at 24-72hours following infection. Cells were washed twice in ice cold PBS and scraped into 500 μl PBS. Extraction of viral DNA was performed using QIAmp DNA Blood Mini Kit (Qiagen). 20 μl of proteinase K (Qiagen) was added to 200 μl of virus, followed by 200 μl of Buffer AL (supplied with the extraction kit) and then incubated at56°C for 10 mins in a heat block. 200 μl of ethanol was added to the sample and the mix was pulse-vortexed for 15 sec and transferred to a QIAmp spin column in a 2 ml collection tube. After centrifugation for 1 min at 8000 rpm, the QIAmp spin column was transferred to a new collection tube. 500 μl of Buffer AW1 (supplied) was added and the sample centrifuged again at 8000 rpm for 1 min. 500 μl of buffer AW2 (supplied) was added and the colum was centrifuged at 1300 rpm for 3 mins, followed by another 1 mins after transfer to a new collection tube. After placing the column in a sterile Eppendorf tube, 40 μl of distilled H_2O was added and the column centrifuged at 8000 rpm for 1 min to elute the purified DNA. DNA concentration was measured using a Nanodrop ND-1000 spectrophotometer and stored at -20°C.

	E1A	Ad5
5′ primer sequence	CCACCTACCCTTCACGAACTG	GGTGGCCATTACCTTTGACTCT
3′ primer sequence	GCCTCCTCGTTGGGATCTTC	GGGTAAGCAGGCGGTCATT
Probe	ATGATTTAGACGT GACGGCC	CTGTCAGCTGGCCTGG

Table 2.3: Oligonucleotides and probes for E1A and Ad5

2.6.4 *Quantitative PCR for viral DNA*

DNA samples were all diluted to 10 ng/μl in 100 μl. Triplicates were prepared for each sample.

The volumes used to prepare each sample are:

- Total volume = 20μl
- Template volume = 2μl
- Forward primer = 10μM
- reverse primer = 10μM
- 2× reaction buffer =10μM (TaqMan Universal PCR Master Mix, Applied Biosystems)

Oligonucleotides and probes for E1A and Ad5 are shown in Table 2.3

Samples, were plated in a 96 well plate. The plate was covered with an adhesive lid and centrifuged briefly to remove air bubbles. Real-time PCR was performed on an ABI Prism 7500 (Applied Biosystems, Foster 23 City, CA). PCR conditions were:

- 50°C for 2 minutes,
- 95°C for 10 minutes,
- followed by 40 cycles of: 95°C for 15 secs and 60°C for 60 secs.

A standard curve using $10^3 - 10^9$ *dl*922-947 genomes was used for quantification.

2.7 SOUTHERN BLOT

1×10^6cells plated and infected with *dl*922-947 (MOI 10 for PE04, MOI 100 for PE01 cells). 24 and 48 hours later cells were trysinised and washed in PBS. DNA was extracted as described above. DNA concentration was measured using Nanodrop ND-1000 spectrophotometer and $10\,\mu g$ genomic DNA was run on a 1% agarose gel with DNA ladder. The gel was soaked in 200 ml 0.2 M HCl for 10 mins, with constant gentle agitation and washed with distilled water. The gel was then soaked for 15 mins at room temperature in Alkaline Transfer buffer (0.4 M NaOH, 1 M NaCl) 500 ml. The buffer was changed and the gel was again soaked in fresh Alkaline Transfer buffer (0.4 M NaOH, 1 M NaCl) 500 ml, with constant gentle agitation.

Hybond N+ membrane (GE Healthcare Life Sciences) was cut to exactly the same size as the gel. The membrane was floated in ddH2O for 2 mins, and then immersed in Alkaline Transfer buffer (0.4 M NaOH, 1 M NaCl) for at least 5 mins. DNA was transferred onto the membrane by conventional capillary transfer over 48 hours. Probe Labelling against viral DNA, hybridization and detection were performed using the Amersham ECL Direct Nucleic Acid Labelling and Detection systems. This was performed by Atsushi Shibata at the Genome Damage and Stability Centre, Life Sciences at University of Sussex, Brighton BN19RQ, UK.

2.8 IMMUNOFLUORESCENCE

Coverslips were placed in 24 well plates and were treated with 0.01% (w/v) poly-L-lysine (Sigma) for 5 mins. Poly-L-lysine was removed and the coverslips dried and then exposed to UV light to sterilize. Alternatively premade polylysine coated coverslips were used.

ANTIBODY	COMPANY	DILUTION	SPECIES
RAD51	Santa-Cruz (sc-8348)	1:200	rabbit
γH2Ax	Millipore (05-636)	1:800	mouse
E2 DBP	kind gift of Dr. David Ornelles	1:500	mouse
BRCA2	Millipore (OP95)	1:200	rabbit

Table 2.4: Antibodies used in Immunofluorescence experiments

2×10^5 cells were cultured on coverslips and infected 24 hours later with *dl*922-947 or treated with etoposide (100 μM for 1 hour), hydroxyurea (2 mM for 24 hours), or rucaparib (10 μM for 24 hours). 24 or 48 hours post treatment, the medium was aspirated and 0.04% Triton (Sigma) in PBS was added for 1 min. The Triton was removed and immediately the cells were fixed in 3% paraformaldehyde and 2% sucrose (Sigma) for 10 mins and then washed three times in PBS. The cells were stained with primary antibodies as detailed in Table 2.4 in 1.5% BSA PBS 0.1% tween for 45 mins at 37°C. The cells were washed three times in PBS and incubated for 45 min at 37°C with antimouse ALEXA 488 (invitrogen) and antirabbit ALEXA 568 (Invitrogen) secondary antibody (1:1000 in 1.5% BSA PBS tween). Cells were washed again three times with PBS and co-stained with DAPI (1 in 10 000) to define the nucleus. Coverslips were mounted on slides using mowiol mounting medium and left overnight for the mounting solution to set. Images were captured using a Zeiss 510 confocal microscope and foci counted using Image J software.

2.9 EXPERIMENTS USING SMALL INTERFERENCE RNA

Small interference RNA (siRNA) targeted against BRCA2, RAD51, NONO and CETN2 were obtained from either Dharmacon (siGENOME SMARTpool; GE Lifesciences) or Qiagen. A non-targeting (NT) pool of siRNA was also used (Qiagen). All cell lines were transfected using lipofectamine 2000 (Invitrogen) or RNAiMAX (invitrogen), apart

from IGROV1 cells where DharmaFECT1 (Dharmacon) was used. A final concentration of 10 nM RAD51 siRNA or 30 nM or 50 nM (depending on cell line) siRNA was used for the Dharmacon SMARTpool SiRNA. All experiments with RAD51 were repeated using a second siRNA (Qiagen) at a concentration of 50 nM.

Depending on the experiment, cells were transfected in a 24 or 6 well plate. For experiments in a 24 well plate (cell survival experiments), $1 \times 10^4 - 3 \times 10^4$ cells (depending on cell line) were plated and 24 hours later transfected with siRNA as follows; the appropriate amount of siRNA (at a concention of 10-50nM) was diluted in 50 μl/well in OptiMEM (invitrogen). 1 μl/well DharmaFECT1 (dharmacon), lipofectamine 2000 or RNAiMAX (invitrogen) was added to 50 μl/well of OptiMEM in a separate tube. Following a 5 min incubation at room temperature, siRNA solution and transfection solution were mixed by pipetting and incubated for 20 mins at room temperature. 100 μl of this solution was added to each well (containing 500 μl medium). 24 hours following transfection cells were infected with *dl*922-947 or *dl*309. Cell survival was assessed 96 hours following infection by MTT assay. Cells survival following siRNA was compared to the non targeting control (siControl). Transfection efficiency was determined by the use of a polo-like kinase 1 (PLK1) targeting siRNA (siPLK1). PLK1 is a polo-like kinase and is involved in mitosis and apoptosis, its silencing causes cell death in most cell lines (Liu and Erikson, 2003).

Wells were also transfected for protein collection to assess knockdown concurrently with cell survival. This was performed as follows; the appropriate amount of siRNA (at a concention of 10-50 nM) was diluted in 250 μl/well of OptiMEM. 5 μl/well DharmaFECT1 or lipofectamine 2000 was added to 250 μl/well of OptiMEM in a separate tube. Following a 5 min incubation at room temperature, siRNA solution and transfection solution were mixed by pipetting and incubated for a further 20 mins at room temperature. 500 μl of this solu-

tion was added to each well. 24-48 hours following transfection cells were lysed and proteins assessed as described in Section 2.4.

Experiments assessing viral DNA following knockdown of RAD51 were performed in 6 well plates. 2×10^5 cells were plated and transfected 24 hours later with SiRNA as described above for protein collection after siRNA knockdown. 24 hours following transfection cells were infected with *dl*922-947. 48 hours following infection wells were harvested to assess viral DNA as described in Section 2.6.3.

2.10 RNA HARVEST FOR BRCA2 TRANSCRIPTION

2×10^5 cells were transfected with BRCA2 siRNA. Cells were trypsinised 48 hours later, spun and washed in PBS. Ribonucleic acid (RNA) was harvested using the RNeasy kit (Qiagen). Briefly, 350 μl Buffer RLT lysis buffer (with 10 μl per ml mercaptoethanol) was added to each sample. The lysate was added onto a QIA shredder (supplied) and spun according to the protocol. 350 μl of 70% ethanol was added and the sample applied to an RNeasy mini column (supplied) and spun at 10,000 rpm for 15 secs. Buffer RW1 (supplied) was added to the column and the column was again centrifuged at 10,000 rpm for 15 secs. 10 μl DNase I was added to 70 μl buffer RDD (supplied) per sample and this was added to directly to the RNeasy silica-gel membrane and then incubated at 20-30^{o}C for 15 mins. 350 μl buffer RW1 was added to the RNeasy mini column and the samples centrifuged at 10,000 rpm for 15 secs before transferring the column to a new collection tube. 500 μl Buffer RPE was then added samples centrifuged for 15 secs at 10,000 rpm. 500 μl Buffer RPE was again added following by centrifugation for 2 mins at 10 000 rpm. To elute the RNA the column was transferred to a new collection tube. 30 μl RNase- free water was added directly to the membrane and the sample centrifuged for 1 min at 10,000 rpm.

2.10.1 *RNA analysis*

Purity and quantity was analysed using the ND1000 Spectophotometer, reading absorbance at 260/280 nm (NanoDrop, Wilmington, US) with a ratio of greater or equal to 1.8 indicating purity.

2.10.2 *Reverse transcription of RNA to yield cDNA*

cDNA synthesis was carried out using the Applied Biosystems High Capacity cDNA Reverse Transcription Kit on a thermal cycler as per the manufacturer's instructions. For each sample 1 μg RNA was made up with the following components to result in a final volume of 20 μl:

- 10$\times$ reverse transcription buffer (2 μl)
- 25 $\times$(100nM) deoxynucleiotide mix (0.8 μl)
- 10 $\times$ reverse transcription random primers (2 μl)
- reverse transcriptase (1 μl)
- RNase inhibitor (1 μl)
- and RNase free water (to make up to a final volume of 20 μl)

The tubes which contained 50 ng/μl were then set up in a DNA Engine (PTC-200) Peltier thermo cycler (Bio-Rad), under the following conditions:

- 25°C for 10 min
- 37°C for 50 min
- 85°C for 5 min
- 4°C for at least 5 min

PRIMER/PROBE	SEQUENCE
BRCA2-Fwd 1	CAGAAGCCCTTTGAGAGTGGA
BRCA2-Rev 1	TGAGACCATTCACAGGCCAA
BRCA2-Fwd 2	CCACAGCCAGGCAGTCTGTAT
BRCA2-Rev 2	AGAACACGCAGAGGGAACTTG
BRCA2-PROBE 2	(6FAM) CCACTCTGCCTCGAAT(TAM)
BRCA2-PROBE 1	(6FAM) CCAAGGAAGTTGTACCGTC(TAM)

Table 2.5: BRCA2 primer and probe sequences

2.10.3 *Quantitative RT-PCR*

Analyses were performed using the ABI Prism 7500 Sequence Detection system Instrument and software (PE Applied Biosystems). RT-PCR was performed as described in Section 2.6.4 using primers and probes as shown in Table 2.5 and 18S as an internal control (Applied Biosystems):

BRCA2 mRNA was normalised (ΔCT) to 18sRNA by subtracting the cycle threshold (CT) of the 18sRNA sample from the cycle threshold (CT) of each sample. The expression level of BRCA2 in the treatment group samples was determined relative to the scrambled controls:

$$\Delta\Delta CT = \Delta CT\, treatment - \Delta CT\, control\, group$$

This was expressed as a fold change in gene expression using the formula:

$$Fold\, change = 2^{-\Delta\Delta CT}$$

2.11 HOMOLOGOUS RECOMBINATION REPORTER ASSAY

To assess the function of homologous recombination, a recombination substrate DR-GFP was used (Pierce et al., 1999). Briefly, pDR-GFP (a gift from Maria Jasin (Addgene plasmid 26475)) contains two differently mutated GFP genes orientated as direct repeats and separated by a puromycin resistance gene. One of the GFP constructs, SceGFP, is mutated to contain the recognition site for the rare cutting endonuclease I-SceI. Exposure to I-SceI will therefore induce a unique double strand break. The I-SceI site is incorporated at a BcgI restriction site by substituting 11bp of wild type GFP sequence with those of the I-SceI recognition site. These substituted base pairs also supply two in frame stop codons, which terminate translation and inactivate the protein. Downstream of SceGFP gene is an 812 bp internal GFP fragment termed iGFP. Homologous sequences in the two mutated GFP genes are separated by 3.7kb. When I-SceI-induced DSB occurs, iGFP sequence can act as a donor strand to allow homology-mediated repair and generation of a functional GFP open reading frame. GFP expression can be detected by flow cytometry (Figure 2.1).

PEO1 and PEO4 cells were transfected with pDR-GFP using Fugene HD. Following puromycin selection, 1×10^6 cells were plated and 24 hours later transfected with either 1 μg pI-SceI or pCAAGs (negative empty vector control). 24 hours later, cells were infected with *dl*922-947 (MOI 50 for PE04 cells MOI 500 for PE01 cells). 24 hours thereafter, cells were analysed for GFP events using a FACSCaliber. 100,000 events were recorded and results analyzed using FlowJo software.

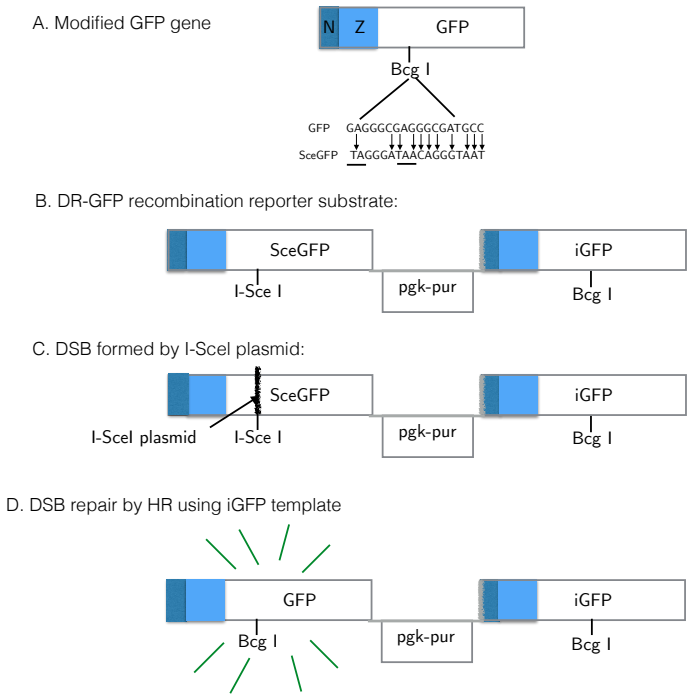

Figure 2.1: Reporter assay to assess homologous recombination function. (A) Modified GFP gene. The modified GFP gene encodes the GFP protein fused to a nuclear localization signal (N) and zinc finger domain (Z). It is expressed from a CMV promoter. The GFP is modified to contain an I-SceI site and in-frame termination codons (underlined) and termed SceGFP. (B) DR–GFP recombination substrate. Downstream of the SceGFP gene is iGFP, a 5′ and 3′-truncated GFP gene. (C) When exposed to I-SceI plasmid, a double strand break (DSB) at the I-SceI site is created. (D) If homologous recombination pathways are functional, this DSB is repaired from the iGFP gene on the same chromatid or sister chromatid, to result in a functional GFP gene. Image is adapted from Pierce et al. (1999).

2.12 HIGH-THROUGHPUT SIRNA SCREEN

The Human DNA repair library Set V1.0 siRNA library (Qiagen, UK) targets 230 known and putative DNA repair proteins. The library consisted of 7× 96 well plates, each well containing 5 μl of an individual siRNA at a concentration of 2 μM. The first and last columns of each plate were left empty and 5 μl of 2 μM non-targeting control siRNA (siCtrl), or siPLK1 were added. Each well of the screen contains enough siRNA for 2 plates (one to be infected with *dl*922-947, the other mock infected) to give a final concentration of 50 nM.

14 plates each of COV318 (4000 cells per well) and OVCAR4 (2000 cells per well) cells were plated on day 1. The following day, cells were transfected with the siRNA library using lipofectamine RNAiMAX transfection reagent (Invitrogen) Briefly, transfection medium was prepared as follows; 0.25 μl RNAiMAX and 50 μl OptiMEM medium (Invitrogen) per well were incubated in a 50 mL tube for 5 mins. 50 μl of this transfection mix was added to the 96 well plates containing the siRNA. After 20 mins incubation, 160 μl complete medium was added (no antibiotics). The medium was then removed from 2 plates of the same cell line and replaced by 100 μl of the siRNA/transfection mix for a final siRNA concentration of 50 nM. Medium was changed 6 hours after transfection. 24 hours following transfection cells were infected with *dl*922-947 at MOI 5 or mock infected. Cell viability was measured 96 hours following infection, using the CellTiter-Glo assay (Figure 2.2).

Luminescence readings from each well were log transformed and normalised according to the median signal on each plate and then standardized by use of a Z-score statistic. This was done using the median absolute deviation (MAD) to estimate the variation in each screen (Zhang et al., 1999b):

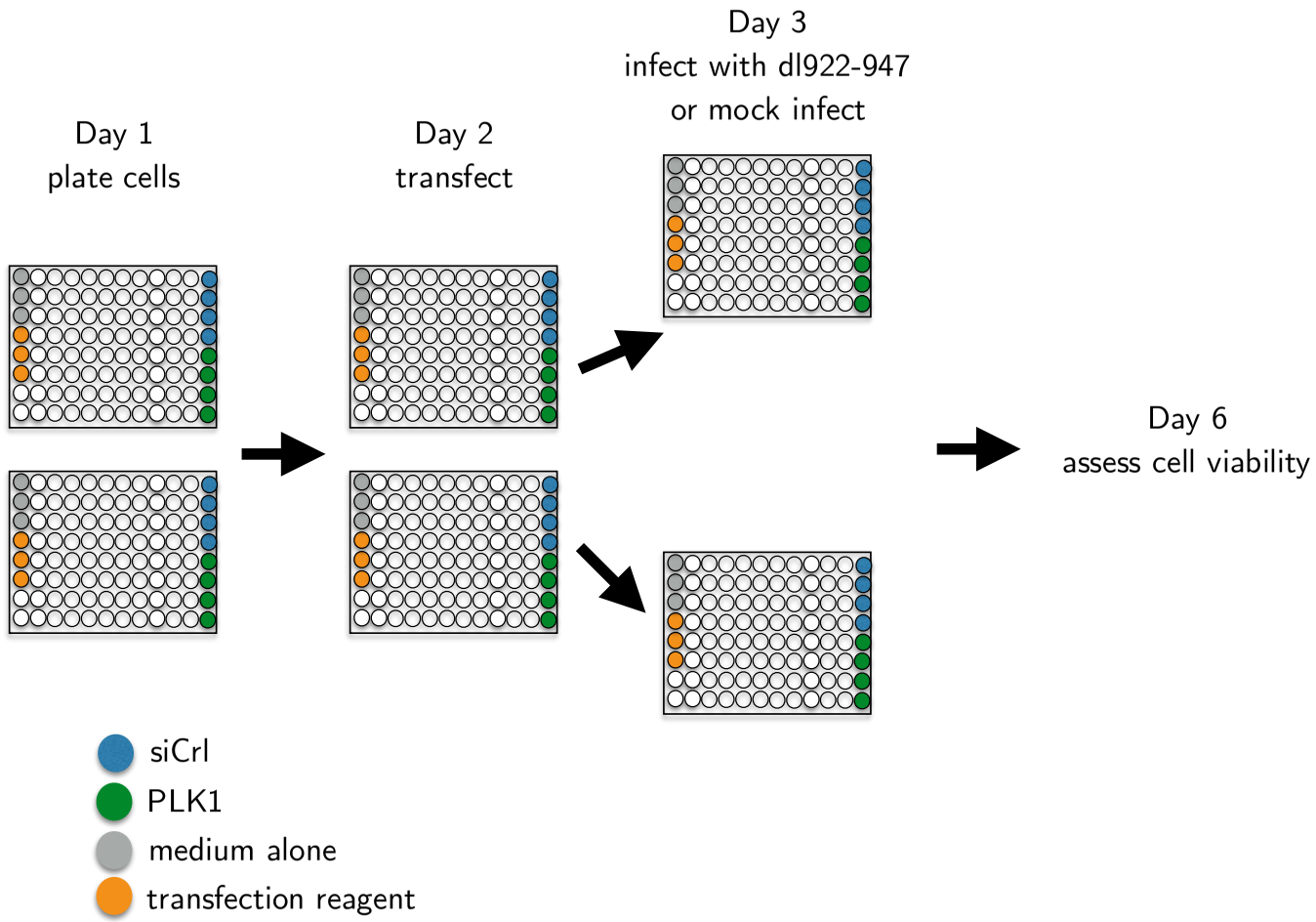

Figure 2.2: HTS method. 2000 OVCAR4 cells or 4000 COV318 cells were plated in 96 well plates. 24 hours later cells were transfected with the SiRNA in duplicate and medium changed after 6 hours. 24 hours following infection, cells were infected with *dl*922-947 or mock infected. Cell viability was assessed on day 6 (120 hours following tranfection). Control SiRNA and siPLK1 were included on each plate for transfection controls.

$$Z_{score} = X - \frac{median(sample)}{MAD(sample)}$$

where:

$$MAD(sample) = median_i(\left|X_i - median_j(X_j)\right|)$$

Z-score analysis has been described as a reliable method to analyse high-throughput screens (Zhang et al., 1999b). In this experiment, the Z-score represented the difference between one siRNA and the rest of the screen. This is based on the assumption of a normal distribution of cell viability. The standardization and normalization of the data in each condition resulted in a Z score for each siRNA in mock infected and virus infected cells. To establish genes synthetically lethal with *dl*922-947 a ΔZ- score was calculated:

$$\Delta Z\,score \;=\; Z\,score_x \;-\; Zs\,core_y$$

where

$$x = virus\,infected\,cells, \;\; y = mock\,infected\,cells$$

Negative ΔZ-scores represent genes synthetically lethal with *dl*922-947. ΔZ score of 0 represents no effect of the siRNA on viral efficacy. Positive ΔZ score represents genes that if silenced result in resistance to viral cell death. A threshold of ΔZ-score <-2 was used to select potential hits.

2.12.1 *siRNA screen validation*

Following analysis of the siRNA screen ΔZ-score data, 5 genes were selected for validation. A custom made 96-well plate (Qiagen) was used to validate the hits. This plate contains 4 single siRNAs per hit gene (one siRNA per well). The siRNA was aliquoted into 10× 96 well plates with 5 μl of 2 μM siRNA per well. siControl and siPLK1 were added to the plates as controls. In brief, OVCAR4 and COV318 cells were seeded on day 1, followed by siRNA transfection using RNAiMAX (as described above), the medium was replaced 6 hr after transfection and cells infected with *dl*922-947 or mock infected 24 hours thereafter. Cell viability was measured by CellTitre-Glo assay, 96 hours after infection.

Part III

RESULTS

3

DNA DAMAGE AND VIRAL CYTOTOXICITY

3.1 INTRODUCTION

Replication selective oncolytic adenoviruses are a novel treatment for ovarian cancer. The adenoviral mutant, *dl*922-947, has a 24 base pair deletion in the in E1A-CR2 region. This region normally interacts with host cell pRB, dissociating it from E2F, thereby enabling S-phase entry and viral DNA replication (Fattaey et al., 1993). Since the RB pathway is abnormal in nearly all ovarian cancers (Sherr and McCormick, 2002), *dl*922-947 should replicate in malignant cells but not quiescent normal cells. Although previous work has shown that *dl*922-947 and other oncolytic adenoviral mutants have activity in ovarian cancer (Lockley et al., 2006), the factors that determine tumour sensitivity to oncolytic adenovirus are currently unknown.

Once inside the cell, adenoviruses hijack control of the host cell and reprogram cellular gene expression to provide the optimal environment for viral replication and production of new virions (Weitzman and Ornelles, 2005; Berk, 2005). Adenoviruses promote cell cycle progression, stimulate unscheduled DNA synthesis and present the cell with a huge amount of exogenous DNA. The host cell, in turn, mounts a response to adenoviral infection in an attempt to inhibit viral gene expression (Weitzman and Ornelles, 2005). This results in a complex interplay between the virus and host cellular responses. Increased knowledge of this interaction may lead to the identification of factors that increase the therapeutic efficacy of oncolytic viruses.

Previous work has demonstrated that following infection with *dl*922-947, deregulation of multiple cell cycle checkpoints occurs, which ac-

celerates cell cycle progression (Connell et al., 2011, 2008). The over-replication of genomic DNA induced by the oncolytic adenovirus, *dl*922-947, is associated with the presence of extensive genomic DNA damage (Connell et al., 2011). These results suggest that virus-induced host cell DNA damage signalling may be a key determinant of viral efficacy, and understanding this further could identify the factors that promote viral cytotoxicity.

Using a panel of ovarian cancer cell lines, this chapter aims to investigate the role of genomic DNA replication and cellular DNA damage following viral infection in determining overall viral efficacy.

3.2 RESULTS

3.2.1 *dl922-947 is cytotoxic to ovarian cancer cell lines in vitro, but the sensitivity varies between the cell lines*

To evaluate the sensitivity of ovarian cancer cells to *dl*922-947, a panel of cell lines was infected with *dl*922-947 and cell survival was measured 120 hours post-infection. The sensitivity of the cell lines varied considerably (IC_{50} for TOV21G = 0.01 pfu/cell, IC_{50} SKOV3 = 438 pfu/cell) (Figure 3.1a). The same range of sensitivities was seen with an E1A wild-type virus (*dl309*), although *dl309* is less potent (Figure 3.1b), in keeping with previous data (Lockley et al., 2006).

3.2.2 *Cellular infectivity to dl922-947 is not the only determinant of cytotoxicity*

The ability of *dl*922-947 to infect cells varies and this could be an important determinant of cell sensitivity to the virus. Permissiveness to Ad5 infection was therefore evaluated by infecting cells with an E1 deleted Ad5 vector encoding green fluorescent protein (GFP) under

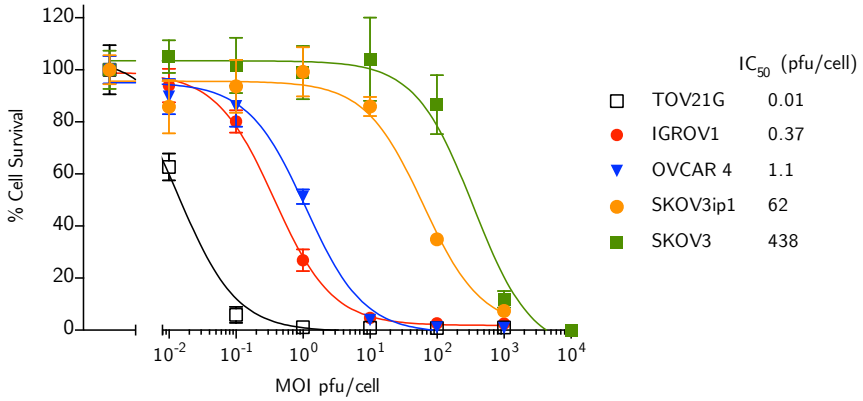

(a)

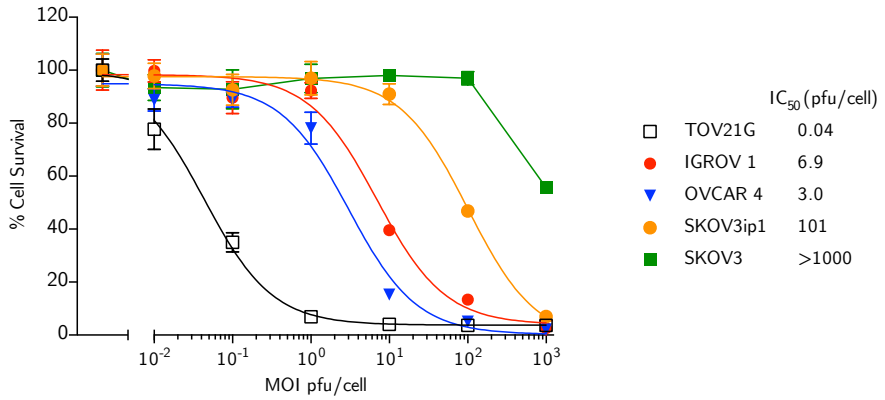

(b)

Figure 3.1: Cytotoxicity of adenoviruses in ovarian cancer cells.1×10^4 cells were infected with *dl*922- 947 **(a)** and *dl309* **(b)** at MOI $0.01 - 1000$ pfu/cell. Cell survival was assessed by MTT 120 hours post infection. Results are presented as percentage cell survival compared to mock infected cells (mean +/- s.d. n=3).

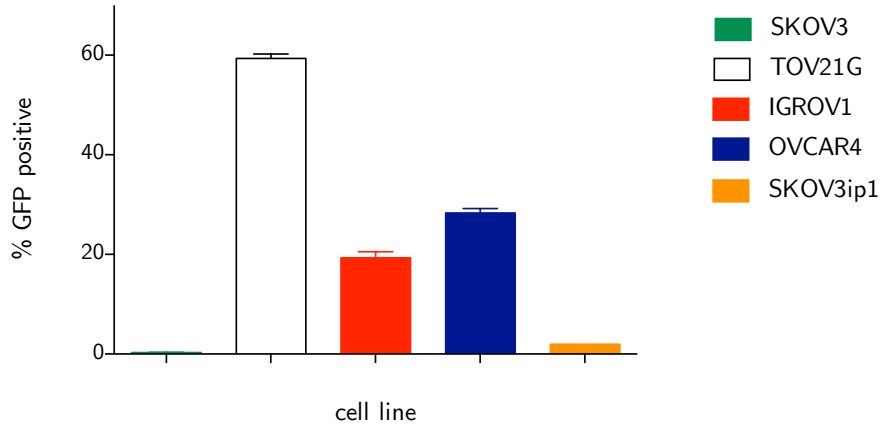

Figure 3.2: Permissiveness to infection with Ad5 vectors varies between cell lines. TOV21G, IGROV1, SKOV3ip1, SKOV3 and OVCAR4 cells were infected with Ad5 GFP MOI 7.5 in triplicate. Percentage of GFP expressing cells was quantified by flow cytometry (bars represent mean GFP expression +/- s.d.).

the control of the cytomegalovirus (CMV) immediate early promoter (Ad5 GFP). Infectivity is then assessed by GFP expression measured using flow cytometry.

Figure 3.2 shows the difference in infectivity across a panel of cell lines. All cell lines were infected with *dl*922-947 at an MOI of 7.5. Infectivity ranged from 60% (TOV21G) to less than 2% (SKOV3). To determine whether factors other than just the permissiveness of the cell to viral infection play a part in determining viral sensitivity this difference in infectivity needed to be accounted for.

To control for differences in infectivity between the cell lines, SKOV3, TOV21G and IGROV1 cells were infected with an MOI that permits 50-60% infection (Figure 3.3a) (iso-infection) and cell survival assessed 120 hours post infection. Even when differences in infectivity are controlled for, there remained significant differences in cell survival (Figure 3.3b) indicating that factors other than infectivity determine sensitivity to *dl*922-947.

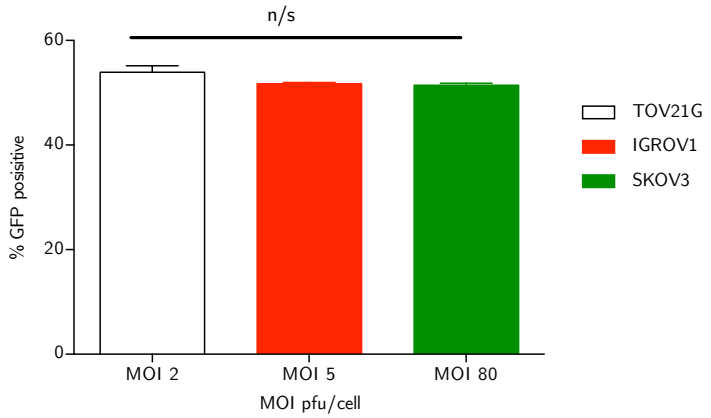

(a)

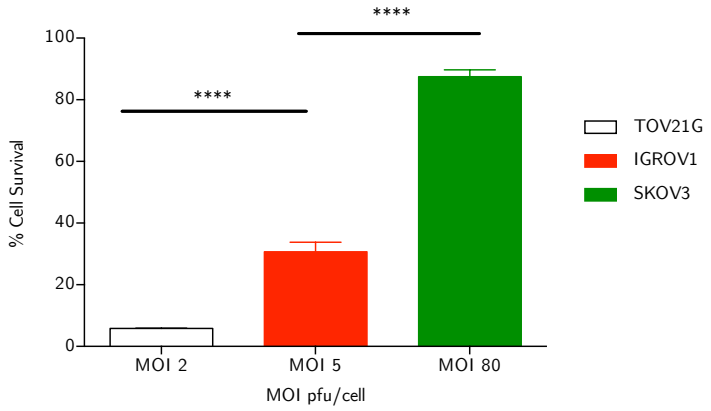

(b)

Figure 3.3: Cytotoxicity in cells equally infected with *dl*922-947. **(a)** Equal infection of TOV21G, IGROV1 and SKOV3 cells by GFP flow cytometry (MOI 2, 5, 80 respectively). Bars represent mean GFP expression +/- s.d. n/s: no significant difference between infection of the cell lines. **(b)** Survival of TOV21G, IGROV1 and SKOV3 120 hours following infection with *dl*922-947 with an MOI that permits $50-60\%$ infection (MOI 2, 5, 80) showing a significant difference in cell survival between the isoinfected cells; **** 2 tailed t-test, p=0.0001, **** 2 tailed t test, p= 0.0001. Bars represent mean cell survival +/- s.d.

3.2.3 *Cell cycle following infection with dl922-947*

Previous results have shown that *dl*922-947 causes deregulation of the cell cycle and over-replication of genomic DNA in highly sensitive cells, with appearance of populations of cells with >4N DNA content (Connell et al., 2011). This analysis has now been extended to a wider panel of ovarian cancer cell lines to determine whether the differences in cytotoxicity could be explained by abnormal cell cycle and genomic DNA replication.

A panel of ovarian cancer cell lines was infected with *dl*922-947 at MOI 7.5. Cell cycle was assessed 48 hours later by propidium iodide staining and flow cytometry. The results revealed that cell lines more sensitive to *dl*922-947 readily accumulated DNA contents of more than 4N after viral infection. By 48hrs post infection, over 25% of the most sensitive cells, TOV21G, demonstrated 4N or greater DNA content. In comparison, in the insensitive SKOV3 cells, less than 5% of the cell cycle exceeded 4N with little change of the cell cycle. Examples of cell cycle profiles are shown in Figure 3.4. Figure 3.5a shows the proportion of the cell cycle with 4N or more DNA contents following viral infection for each cell line. To control for differences in the cell cycle that are seen at baseline between the different cell lines, Figure 3.5b shows the change in the proportion of the cells with >4N DNA content following viral infection.

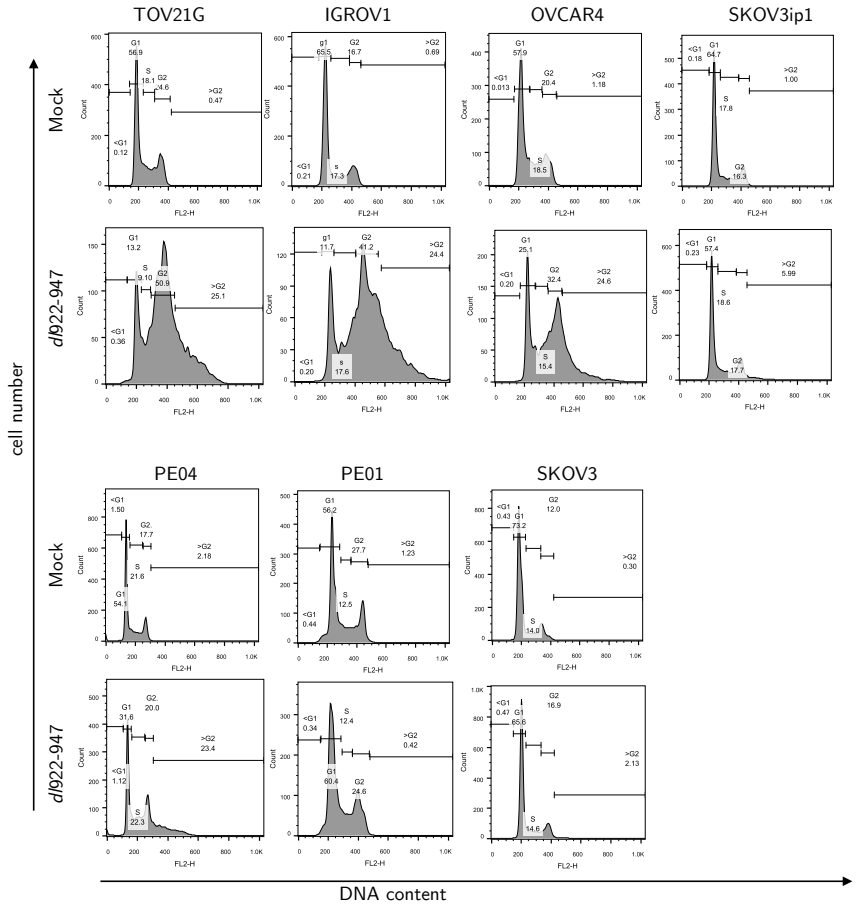

Figure 3.4: Cell cycle profiles following *dl*922-947 infection. Ovarian cancer cell lines (TOV21G, OVCAR4, IGROV1, SKOV3, SKOV3ip1, PEO1 and PEO4) were harvested 48 hours following infection with *dl*922-947 (MOI 7.5), fixed in 100% cold ethanol, stained with propidium iodide (PI) and analysed by flow cytometry. Cell cycle was visualised using Flowjo software. Representative cell cycle image for each cell line shown.

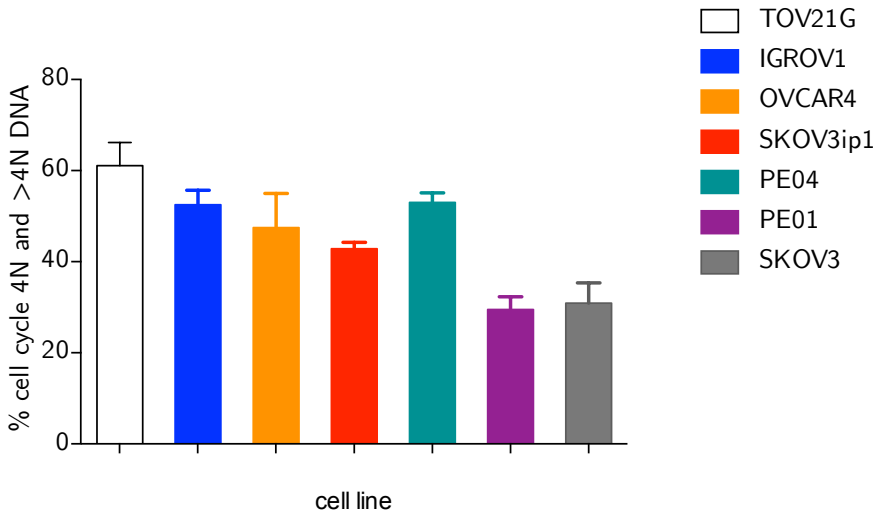

(a)

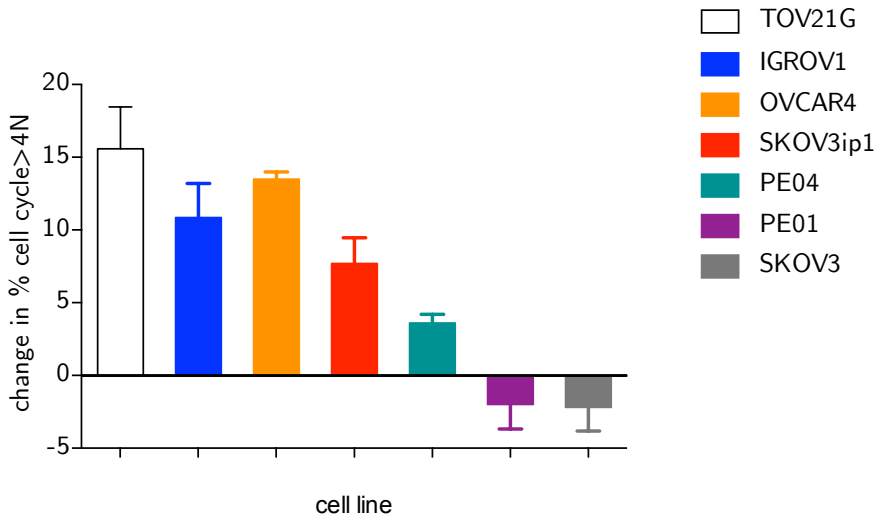

(b)

Figure 3.5: *dl*922-947 results in DNA over-replication. Ovarian cancer cell lines (TOV21G, IGROV1, OVCAR4, SKOV3ip1, PE01, PE04 and SKOV3) were infected with *dl*922-947 at MOI 7.5. 48 hours later cells were fixed, stained with propidium iodide and analysed by flow cytometry. Cell cycle changes were assessed using Flowjo software. **(a)** The proportion of cells with 4N or greater contents following infection with *dl*922-947. Each bar shows an individual cell line (mean +/- S.E.M). **(b)** Change in percentage of cells with more than 4N DNA contents following *dl*922-947 infection. Each bar shows an individual cell line (mean +/- S.E.M).

To determine whether the differences in cytotoxicity to *dl*922-947 could be explained by abnormal cell cycle and genomic DNA replication, the change in the cell cycle following infection with *dl*922-947 was correlated with the sensitivity of each cell line to the virus. The results from the panel of cell lines tested demonstrated a trend of an association between viral efficacy and DNA over-replication (as determined by percentage cells with 4N and >4N DNA) 48h post-infection with *dl*922-947 was observed; however this did not reach statistical significance; Spearman r = -0.68, p=0.055 (Figure 3.6a). A close correlation between viral efficacy (as determined by IC_{50} for *dl*922-947 at 120hr) and change in the percentage of cells with greater than 4N DNA content following infection was demonstrated; Spearman r= -0.96, p= 0.003 (Figure 3.6b).

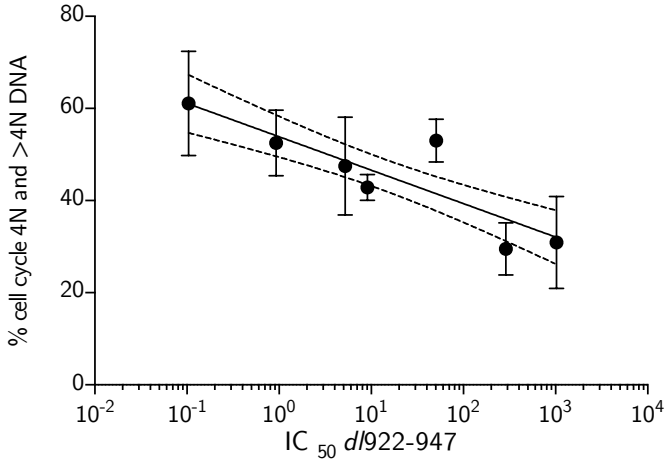

(a)

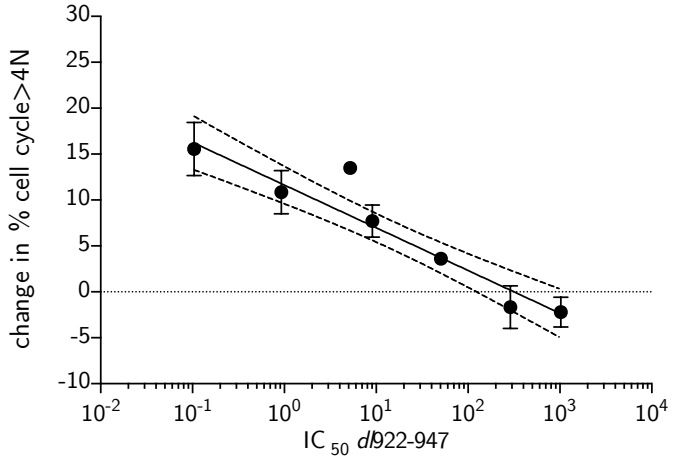

(b)

Figure 3.6: Cell cycle changes following *dl*922-947 infection and correlation with overall efficacy. Ovarian cancer cell lines (TOV21G, OVCAR4, IGROV1, SKOV3, SKOV3ip1, IGROV1, PEO1 and PEO4) were harvested 48 hours following infection with *dl*922-947 (MOI 7.5), fixed in 100% cold ethanol, stained with propidium iodide (PI) and analysed by flow cytometry. **(a)** Correlation between IC_{50} *dl*922-947 and percentage of cells with 4N or more than 4N DNA contents. Points represent the IC_{50} of each cell line plotted against % of cells with at least 4N DNA contents following infection +/- S.E.M. Solid line shows linear regression, $r^2 = 0.56$, $p < 0.0001$. Dotted line represents 95% CI. Spearman r= -0.75, p = 0.06. **(b)** Correlation between IC_{50} *dl*922-947 and change in percentage of the cell with more than 4N DNA contents. Points represent the IC_{50} of each cell line plotted against % change in >4N DNA contents following infection +/- S.E.M. Solid line shows linear regression, $r^2 = 0.72$, $p < 0.0001$. Dotted line shows 95% C.I. Spearman $r = -0.94$, $p = 0.0003$.

These results demonstrate that infection with *dl*922-947 results in abnormal replication of cellular DNA with the appearance of cells with greater than 4N DNA contents. This abnormal replication is clearly greater in sensitive cells. These findings therefore suggest that deregulation of the cell cycle may be an important determinant of viral efficacy.

3.2.4 *Cell cycle changes following iso-infection with dl922-947*

To further investigate the relationship between cell cycle changes and viral efficacy, experiments were performed to control for differences in viral infectivity between cell lines. Cell cycle changes were assessed in cells equally infected with *dl*922-947 as determined by Figure 3.3a (the iso-infective dose). TOV21G, IGROV1 and SKOV3 were iso-infected with *dl*922-947 (MOI 2, 5 and 80 respectively). 48 hours later, cell cycle was assessed by flow cytometry. A significant difference in the change in the proportion of the cells with DNA content of >4N was seen following infection between the iso-infected cells (Figure 3.7). This confirmed the above findings that *dl*922-947 results in abnormal replication of cellular DNA with the appearance of populations with >4N DNA contents. These cell cycle changes are most profound in sensitive cells and appear to be due to intrinsic differences in the host cell and not just due to differences in the ability of the virus to infect cell.

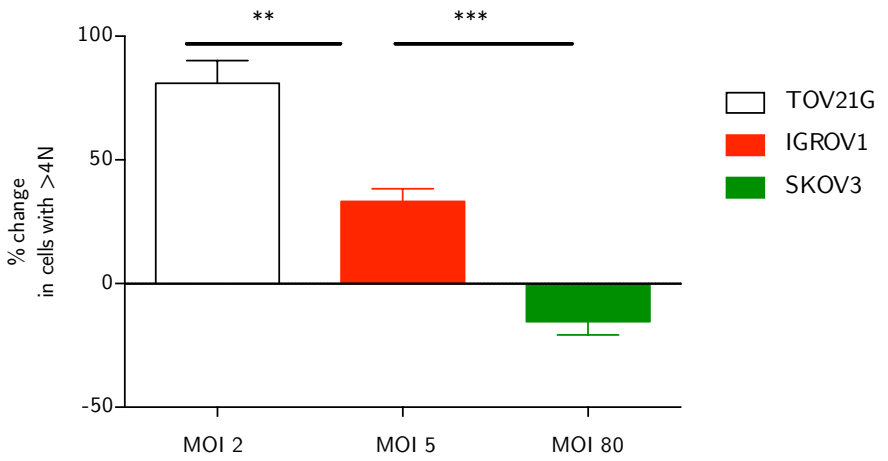

Figure 3.7: Cell cycle changes following iso-infection with *dl*922-947. TOV21G, IGROV1 and SKOV3 cells were harvested 48 hours following infection with *dl*922-947 (MOI 2, 5 and 80 respectively) fixed in 100% cold ethanol, stained with propidium iodide and analysed by flow cytometry. Cell cycle was analysed using Flowjo software and the change in the percentage of the cells with >4N contents calculated (bars represent mean +/- s.d.) ** p = 0.014, *** p = 0.0003, 2 tailed t-test.

3.2.5 *Genomic damage following infection with dl922-947*

Cell cycle control and the DNA damage response are closely interlinked (Shaltiel et al., 2015; Harper and Elledge, 2007). In addition, abnormal cellular replication is associated with the accumulation of replication-associated double strand DNA breaks (Truong and Wu, 2011). Since *dl*922-947 causes deregulation of the cell cycle that is more profound in the sensitive cells, the next step was to assess genomic DNA damage following infection.

Phosphorylation of H2AX (γH2AX) is considered one of the earliest indications of a DSB (Paull et al., 2000). Phosphorylation of H2AX has been shown following adenoviral infection (Nichols et al., 2009; Connell et al., 2011) but the exact relationship between the degree of double strand break damage and viral cytotoxicity has not yet been

determined. To assess this, γH2AX staining 48 hours following *dl*922-947 infection was analysed in a panel of ovarian cancer cell lines by flow cytometry with propidium iodide counterstaining to define cell cycle stage. Examples of the cell cycle profiles with γH2AX staining is shown in Figure 3.8.

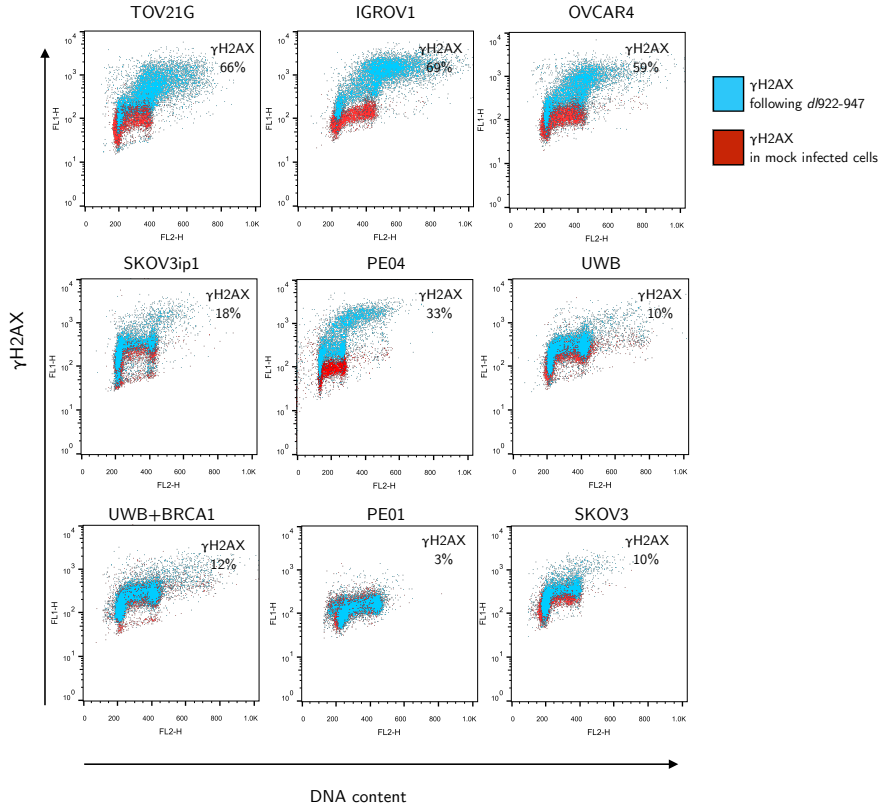

Figure 3.8: Cell cycle and genomic damage following *dl*922-947. Ovarian cancer cell lines (TOV21G, OVCAR4, IGROV1, PE01, PE04, SKOV3ip1, SKOV3, UWB and UWB +BRCA1) were infected with *dl*922-947 (MOI 7.5). 48 hours later, cells were fixed, stained with γH2AX and counterstained with propidium iodide. Cells were assessed using flow cytometry and analysed using Flowjo software. Representative images are shown illustrating cell cycle and γH2AX in mock infected cells (red) and following *dl*922-947 (blue). Percentages show increase in cells positive for γH2AX following infection.

Results demonstrated that the amount of γH2AX induced following viral infection varied across the cell lines tested. Sensitive cells (for example TOV21G, OVCAR4) showed a large increase in γH2AX 48 hours after infection with *dl*922-947 but there was very little γH2AX in the more resistant cells (SKOV3). Interestingly γH2AX staining predominately occurred in cells with 4N or more than 4N DNA content.

Figure 3.9a shows the percentage of cells positive for γH2AX in each cell line 48 hours following infection with *dl*922-947 (MOI 7.5). A correlation was also demonstrated between the increase in γH2AX (determined by flow cytometry) 48 hours following viral infection and the sensitivity of those cells to *dl*922-947 (as determined by IC_{50}) (Figure 3.9b). These results suggests that cellular susceptibility to virus-induced DNA damage may determine the potency of oncolytic adenovirus.

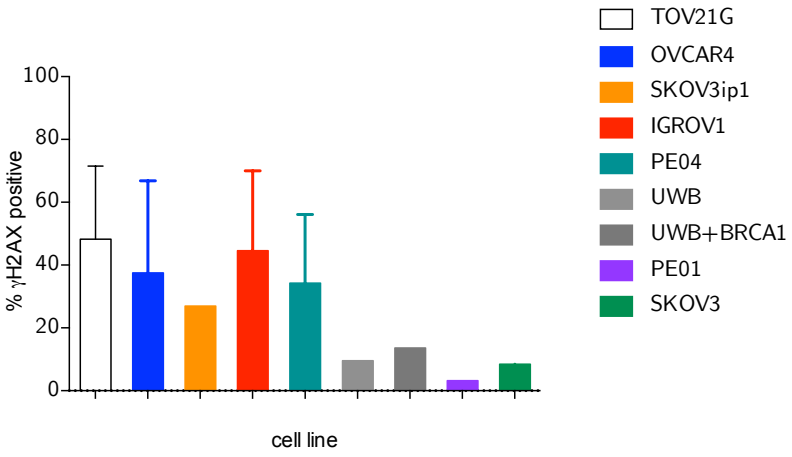

(a)

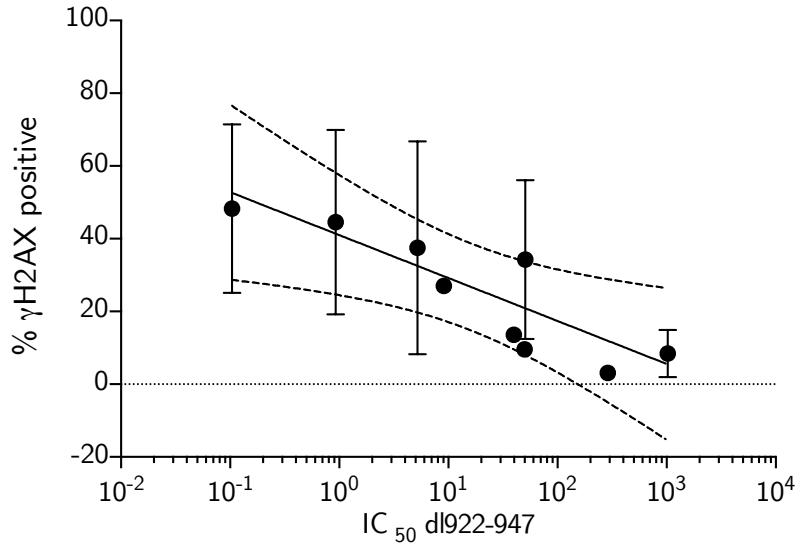

(b)

Figure 3.9: Relationship between genomic DNA damage and cellular sensitivity to oncolytic adenovirus. **(a)** DNA damage following infection with *dl*922-947 (MOI 7.5) was assessed in ovarian cancer cell lines by γH2AX using flow cytometry. Bars represent % H2AX positive following infection with *dl*922-947 +/- S.E.M. **(b)** Correlation between DNA damage (γH2AX by flow cytometry) following infection with *dl*922-947 and sensitivity to *dl*922-947. Points represent the IC_{50} of each cell line plotted against % of cells positive for γH2AX following infection +/- S.E.M. Solid line shows linear regression, $r^2 = 0.35$, dotted line represents 95% CI. Spearman r = -0.88, p = 0.0031.

3.2.6 *Genomic damage assessed by Immunofluorescence*

To further examine the relationship between virus-induced DNA damage and cellular sensitivity, γH2AX was also analysed by immunofluorescence 48 hours after infection with *dl*922-947 at MOI 7.5. The pattern of staining seen at 48 hours following infection is pannuclear rather than that of discrete foci. Figure 3.10 shows a representative image of γH2AX staining across the panel of cell lines tested. This staining pattern is consistent with previously published data, that showed pannuclear γH2AX following group C adenoviral infection (Nichols et al., 2009). Assessment of γH2AX staining was quantified by intensity of γH2AX within the nucleus because counting of γH2AX foci was not possible. To control for differences in background staining of γH2AX the fold change in γH2AX intensity following infection with *dl*922- 947 was calculated. Figure 3.11 shows the change in intensity of γH2AX staining following viral infection in each cell line. Results revealed a strong correlation between viral efficacy (as determined by IC_{50}) and fold change in intensity of γH2AX following viral infection (Spearman r = -0.96, p = 0.0028) (Figure 3.12).

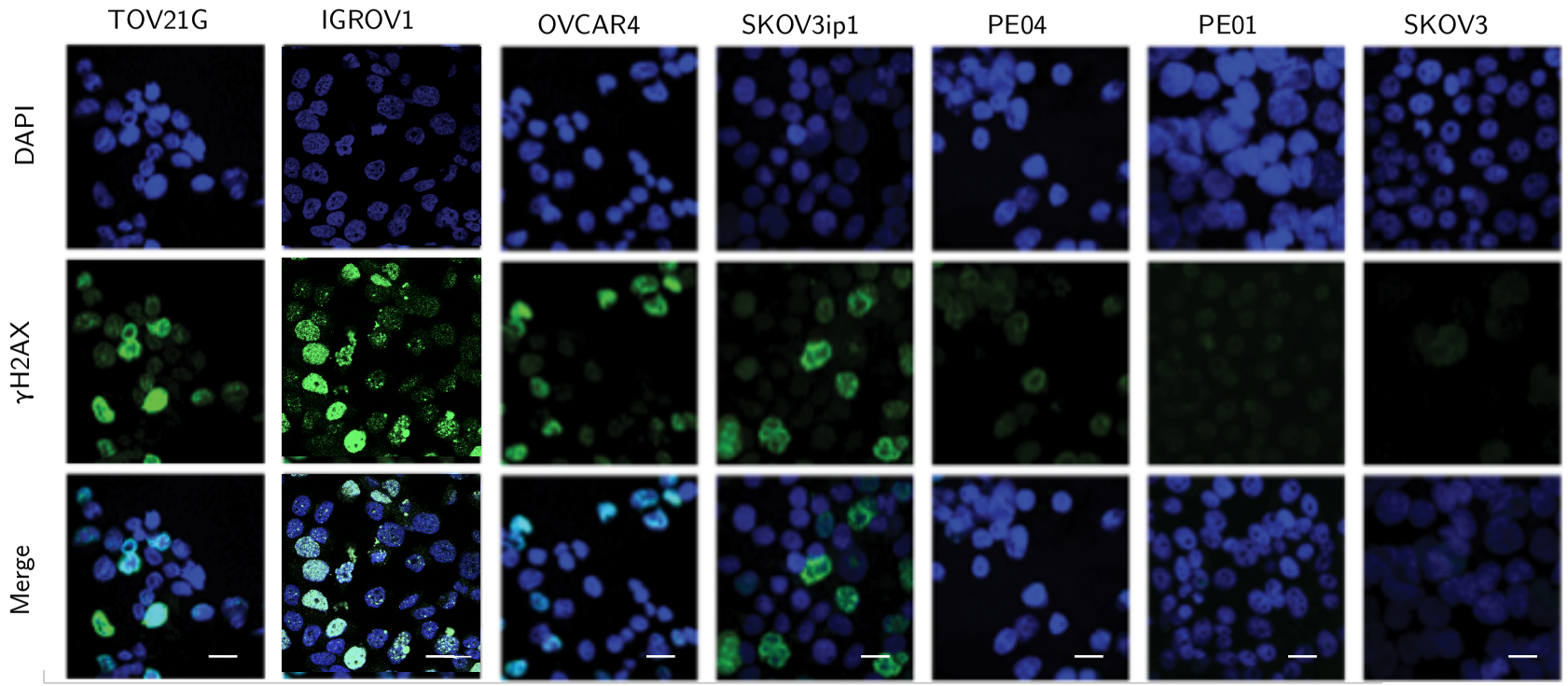

Figure 3.10: DNA damage following infection with *dl*922-947. Presence of γH2AX 48 hours following infection with *dl*922-947 was detected in a panel of ovarian cancer cell lines by immunofluorescence. Images were captured on a Zeiss 510 confocal microscope. Images arranged from cells sensitive to *dl*922-947 (on the left) to most resistant (right). Scale bar = 20 μm

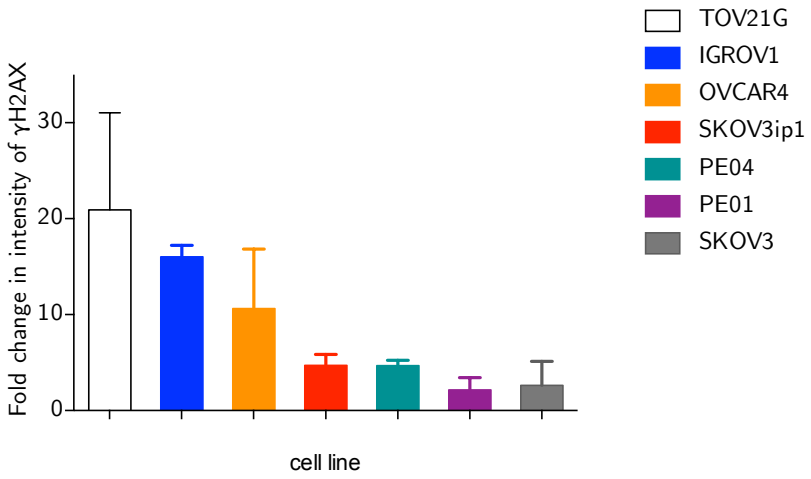

Figure 3.11: Quantification of DNA damage assessed by immunofluorescence following infection with *dl*922-947. Presence of γH2AX 48 hours following infection with *dl*922-947 was detected in a panel of ovarian cancer cell lines by immunofluorescence. Intensity of nuclear γH2AX staining was assessed using Image J software in at least 50 cells per condition. Fold increase in γH2AX following *dl*922-947 was calculated. Bars represent average intensity of γH2AX +/- S.E.M for each cell line.

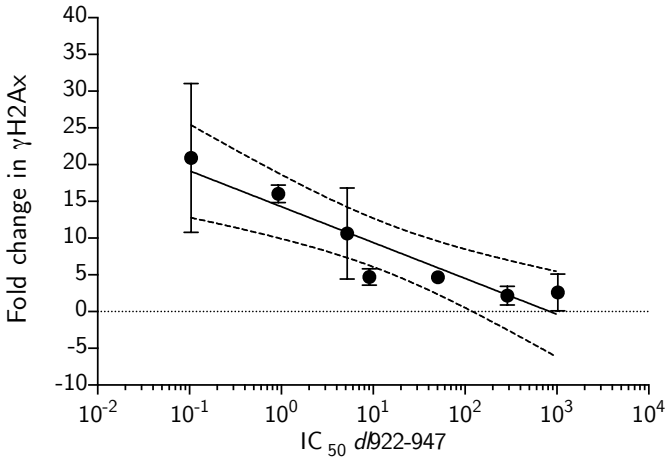

Figure 3.12: Correlation between IC_{50} *dl*922-947 and γH2AX intensity following viral infection. Points represent the IC_{50} of each cell line plotted against change in intensity of γH2AX following infection +/- S.E.M. Solid line shows linear regression, $r^2 = 0.59$, $p < 0.0013$ dotted line represents 95% C.I. Spearman r = -0.96, p =0.0028.

3.2.7 *Genomic damage following iso-infection with dl922-947*

To further investigate the relationship between viral efficacy and genomic damage I also performed experiments using cells equally infected with *dl*922-947. Intensity of γH2AX staining was quantified following iso-infection in TOV21G (MOI 2), IGROV1 (MOI 5) and SKOV3 (MOI 80). Significant differences were seen between the sensitive and resistant cells (Figure 3.13b). This suggests that DNA damage following infection with *dl*922-947 is an important marker of viral sensitivity and is independent of the ability of the virus to infect the cells.

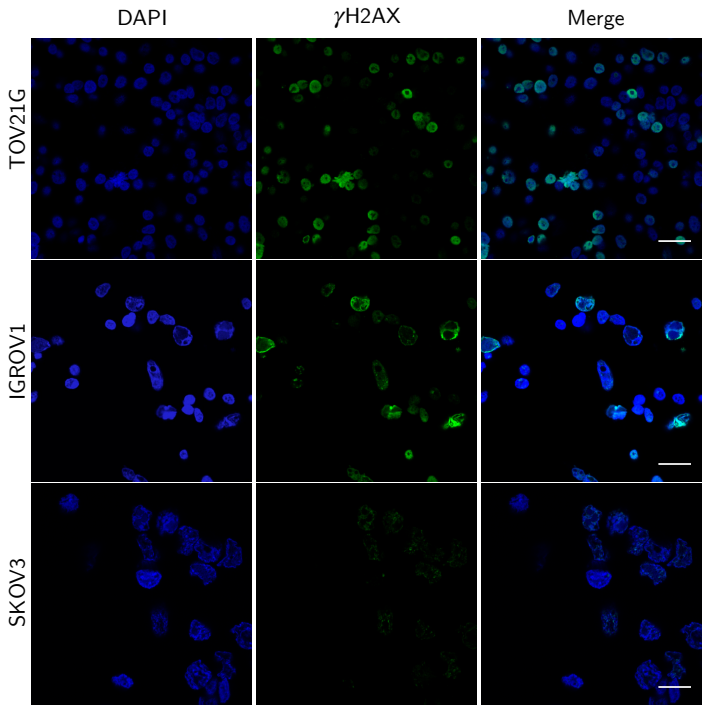

(a)

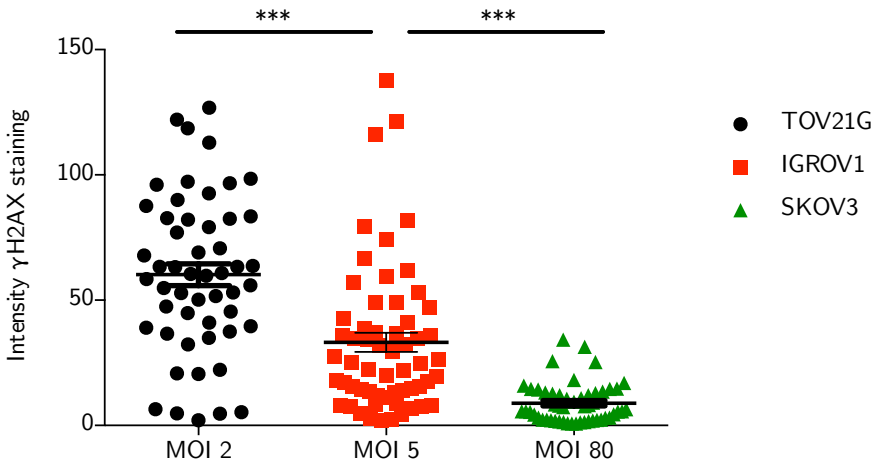

(b)

Figure 3.13: DNA damage following iso-infection with *dl*922-947. **(a)** Presence of γH2AX in TOV21G, IGROV1 and SKOV3 cells 48 hours following iso-infection with *dl*922-947 (MOI 2, 5, 80 respectively) was detected by immunofluorescence Scale bar = 20 μm. **(b)** γH2AX intensity was quantified using ImageJ in TOV21G, IGROV1 and SKOV3. Each symbol represents intensity of a single nucleus, *** $p < 0.0001$, 2-tailed t-test.

3.2.8 *Differences in background DNA damage do not correlate with adenoviral efficacy*

To assess whether there was a relationship between the extent of endogenous γH2AX and adenovirus efficacy, γH2AX was assessed in the untreated cells. Differences in background staining were clearly visible between the cell lines and quantification of this is shown in Figure 3.14a. There was however, no association between baseline γH2AX and adenoviral efficacy (Figure 3.14b). Baseline, endogenous γH2AX levels may reflect genomic instability (Podhorecka et al., 2010). This suggests that the degree of genomic stability does not influence oncolytic adenoviral efficacy.

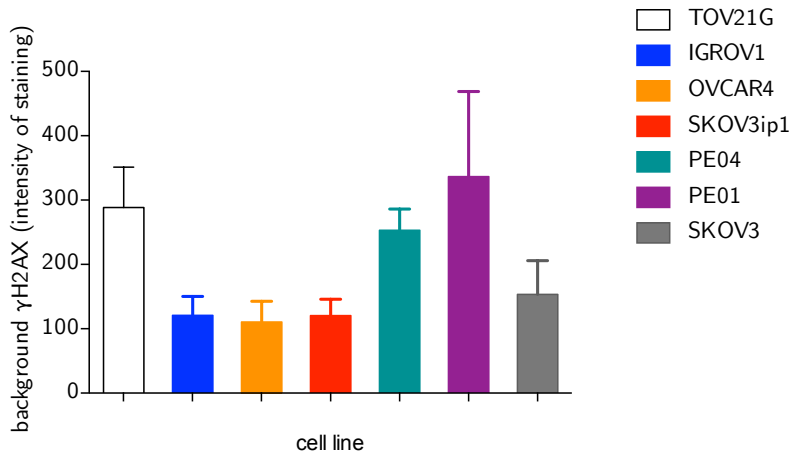

(a)

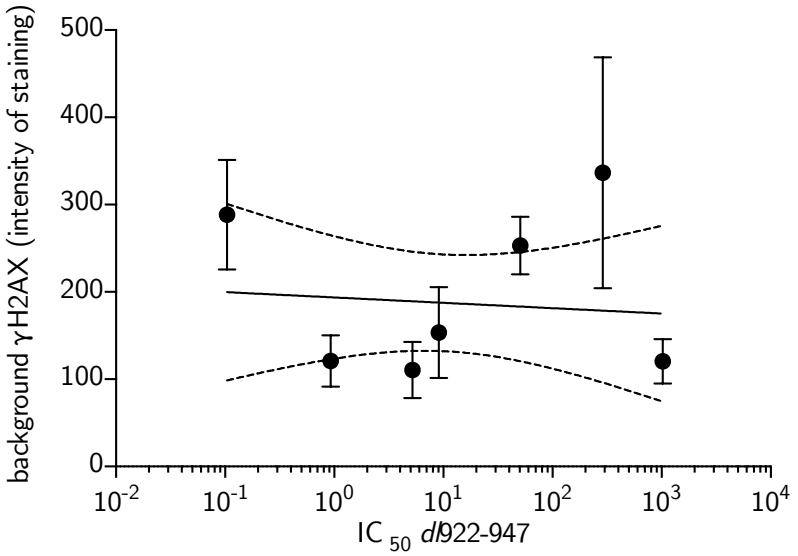

(b)

Figure 3.14: Background genomic damage and viral efficacy. Presence of γH2AX in untreated cells was detected in a panel of ovarian cancer cell lines by immunofluorescence. Images were captured on a Zeiss 510 confocal microscope and quantification of staining was assessed using ImageJ software. **(a)** Bars represent intensity of staining +/- S.E.M for each cell line. **(b)** Points represent the IC_{50} of each cell line plotted against background intensity of γH2AX +/- S.E.M. Solid line shows linear regression. No association seen.

3.2.9 *Genomic damage following infection with a non-replicating virus*

To assess whether viral replication is required for the induction of genomic DNA damage, γH2AX was assessed by immunofluorescence in TOV21G cells following infection with *dl*922-947 or the non-replicating viral vector (AdLm-X) (Figure 3.15a). The intensity of γH2AX staining, quantified in at least 50 cells, did not increase following infection with a non-replicating virus (Figure 3.15b). These results show that the presence of virus alone does not generate a DDR but adenoviral replication is required for inducing cellular DNA damage.

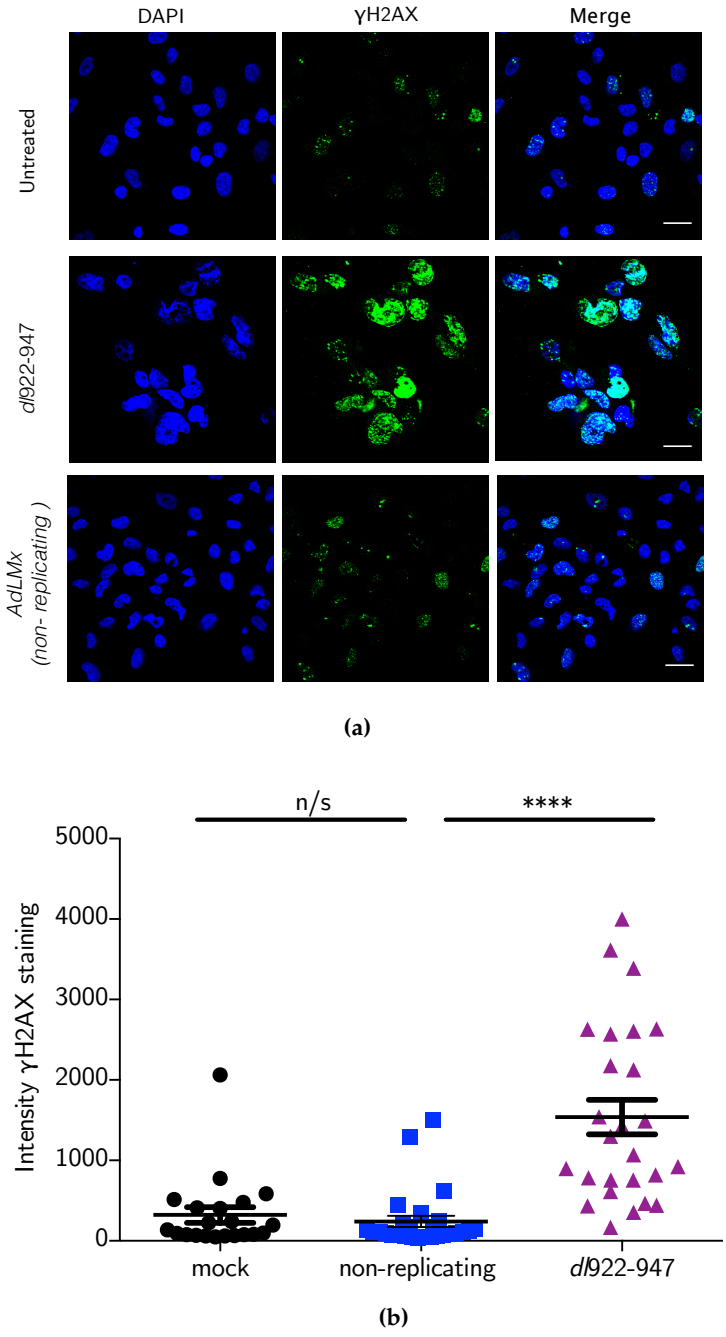

Figure 3.15: DNA damage following infection with a non-replicating virus. **(a)** Presence of γH2AX by immunofluorescence, 48 hours following infection with AdLMx (non-replicating adenovirus) *or* *dl*922-947 (MOI 7.5) in TOV21G cells. Scale bar = 20 μm. **(b)** γH2AX intensity was quantified in at least 30 cells. n/s: no significant difference between mock infected and cells infected with AdLMx, significant difference seen between γH2AX intensity of cells infected with AdLMx and *dl*922-947 **** $p < 0.0001$, 2 tailed t-test.

3.2.10 *Genomic damage following infection with E1A wild type virus*

Results from early in this chapter (Figure 3.1b) demonstrate that *dl*922-947 is more potent than the E1A wild-type adenovirus, *dl309*. To assess whether genomic damage varies between *dl*922-947 and *dl309*, TOV21G and IGROV1 cells were infected with *dl*922-947 or *dl309* at MOI 7.5 and fixed at 16, 24 and 48 hours post infection. γH2AX staining was assessed by immunofluorescence and quantified using ImageJ. Results revealed that in the highly sensitive TOV21G cells, there was significantly more γH2AX staining at both 16 and 24 hours post infection with *dl*922-947. At 48 hours this difference was lost (Figure 3.16a). The less sensitive IGROV1 cells did not show a difference in DNA damage between the two viruses at 16 hours but there was significantly more damage with *dl*922-947 at both 24 and 48 hours (Figure 3.16b). These results demonstrate that infection with the E1A deleted adenoviral vector, *dl*922-947, results in more DNA damage compared to the E1A wild-type virus. This is consistent with *dl*922-947 being more potent in ovarian cancer cells. The explanation for the loss of a difference at the late time points in the TOV21G cells could be due to cell death in these highly sensitive cells. Alternatively, due to the strength of the γH2AX signal, saturation had occurred and therefore further increases could not be detected.

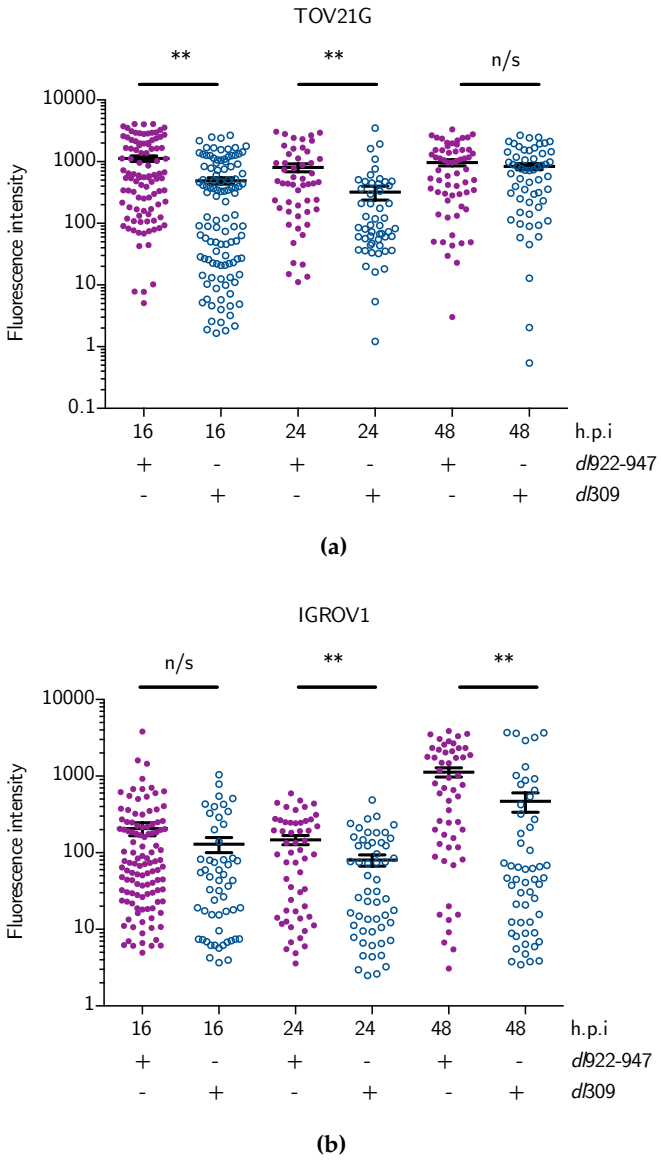

Figure 3.16: DNA damage following infection with E1A wild type virus and *dl*922-947. Presence of γH2AX by immunofluorescence, 16, 24 and 48 hours following infection with *dl309* (E1A wild-type adenovirus) *or* *dl*922-947 (both infected at MOI 7.5) in TOV21G cells **(a)** and IGROV1 cells **(b)**. γH2AX intensity was quantified in at least 50 cells. Significantly higher γH2AX intensity in the *dl*922-947 infected TOV21G cells compared to *dl309* infected cells at 16 and 24 hours post infection was observered. ** $p < 0.002$, 2 tailed t-test. Significantly higher γH2AX intensity in the *dl*922-947 infected IGROV1 cells compared to *dl309* infected cells at 24 and 48 hours post infection ** $p < 0.01$ 2-tailed t test. n/s: no significant difference between *dl*922-947 and *dl309* infected cells.

3.2.11 *DNA damage induced by chemotherapeutics and sensitivity to dl922-947*

To assess whether the correlation between DNA damage induced by *dl*922-947 and sensitivity to the virus reflects intrinsic cellular susceptibility to DNA damage as opposed to specific adenovirus-induced damage, γH2AX staining was assessed following treatment with other DNA damaging agents that result in DSBs. A panel of ovarian cancer cell lines was treated with hydroxyurea (2 mM for 24 hours) or etoposide (100 μM for 1 hour) and γH2AX was assessed by immunofluorescence. Although there appeared to be a trend of an association between the damage induced by hydroxyurea and etoposide and virus cytotoxicity, this did not reach statistical significance (Figure 3.17b and Figure 3.17a). There was also no correlation between the damage induced by PARP inhibitor (10 μM for 24 hours) and sensitivity to *dl*922-947 (Figure 3.17c). These experiments do, however, need to be repeated with the addition of further cell lines and this may reveal an association between DNA damage induced by certain DNA damaging agents. In addition, these agents induce DNA damage in different ways; etoposide causes DNA strands to break by inhibiting topoisomerase II (Hande, 1998). Hydroxyurea results in stalled replication forks that collapse to DSB (Petermann et al., 2010). In contrast, PARP inhibitors prevent single strand break repair by inhibiting the PARP1 enzyme. To induce double stand DNA damage PARP inhibitors rely on progression of the cell through the cell cycle and double strand breaks occur at the replication forks (Davar et al., 2012; Bryant et al., 2005; Farmer et al., 2005). In contrast to these types of DSBs, the DNA damage induced by *dl*922-947 is likely to be a result of viral replication and aberrant cell cycle progression. This may explain why sensitivity to *dl*922-947 does not correlate with DNA damage induced by chemotherapy agents.

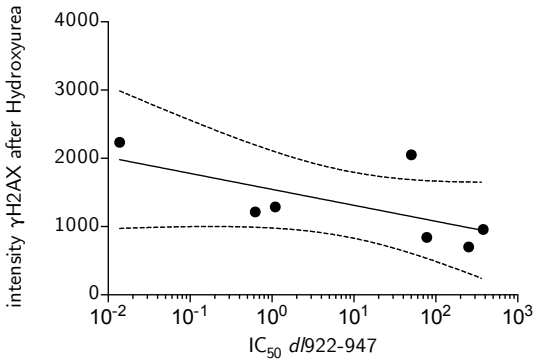

(a)

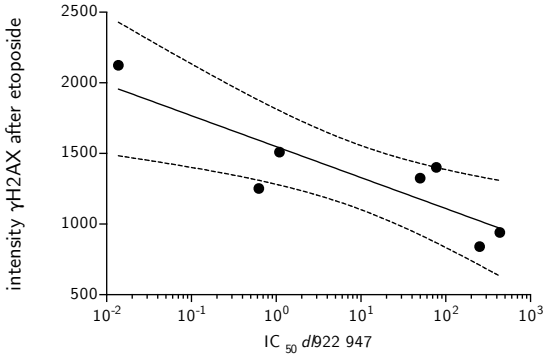

(b)

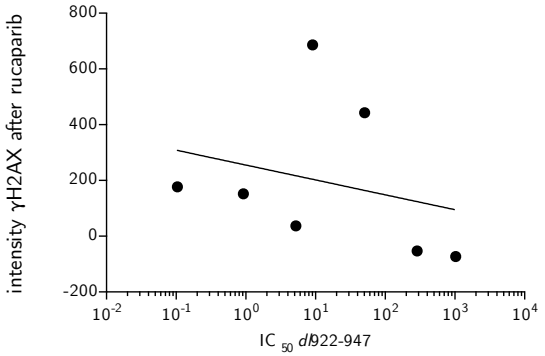

(c)

Figure 3.17: Correlation between adenovirus efficacy and DNA damage induced by chemotherapy agents. Ovarian cancer cells (TOV21G, IGROV1, OVCAR4, SKOV3ip1, PEO_4, PEO_1, $SKOV_3$) were treated with etoposide (100 μM for 1 hour) **(a)**, hydroxyurea (2 mM for 24 hour) **(b),** or the PARP inhibitor, rucaparib (10mM for 24 hour) **(c).** DSBs were assessed by γH2AX immunofluorescence and the intensity of γH2AX staining was correlated with cellular sensitivity to *dl*922-947 (IC_{50}). Each point represents a cell line, Solid black line shows the linear regression, dotted line represents 95% C.I. No correlation found between DNA damage induced by etoposide, hydroxyurea or PARP inhibitor and viral cytotoxicity.

3.3 DISCUSSION

These data show that ovarian cancer cells have a wide range of sensitivity to the E1A-CR2 mutant adenovirus, *dl*922-947 and that *dl*922-947 is more potent than an E1A wild-type virus. In this chapter, I have sought to determine the role of the cell cycle and DNA damage in determining the cytotoxicity of *dl*922-947.

Infectivity is an important determinant of cell sensitivity to virus. However, even following iso-infection, there still remain significant differences in sensitivity to *dl*922-947. The explanation for this difference remains to be identified but these data suggest that the DDR pathways of the cells may be critical.

Once adenovirus has entered the host cell, its priority is to optimize the host cell for replication of the viral genome. The virus drives the cell into an S phase-like state thereby creating an intracellular environment needed for viral replication (Flint and Shenk, 1989). The results presented here, together with previously published data, reveal that following infection with *dl*922-947 abnormal replication of cellular DNA occurs (Ingemarsdotter et al., 2015; Connell et al., 2011). There is also a stark contrast between sensitive and insensitive ovarian cancer cells, with sensitive cells readily accumulating DNA of more than 4N content but little change to the cell cycle occurs in the more resistant cells. A correlation exists between cytotoxicity of *dl*922-947 and populations with more than 4N DNA content. This suggests that cell cycle deregulation following infection may be important in determining sensitivity.

Why cells abnormally replicate their DNA following infection with *dl*922-947 is not fully understood. Similar results have been shown following infection with E1A wild-type virus. E1A expressing cells accumulate in the S and G2/M phases of the cell cycle (Howe and Bayley, 1992; Grand et al., 1998) and abnormal re-replication occurs in late S phase (Singhal et al., 2013). E1A expression is critical to viral

replication; it is the first viral gene to be expressed and expression depends entirely on host factors. Previous results have shown that expression of E1A following infection with *dl*922-947 correlates with cytotoxicity (Flak et al., 2010; Ingemarsdotter et al., 2015). To date, most research looking at cell cycle and adenovirus has focused on the CR2 region of E1A and its ability to drive the cell into S phase through its interaction with pRB (Nevins, 1992; Nemajerova et al., 2008). Much less is known, however, about the nature of the cellular DNA that replicates in these virally infected cells.

Since *dl*922-947 has a deletion in E1A-CR2, there are therefore regions in the viral DNA that are responsible for driving the abnormal replication seen following adenoviral infection. *dl*922-947 and other adenoviral vectors have been shown to over-ride multiple cell cycle checkpoints in tumour cells to allow the virus to drive quiescent cells into S phase, resulting in mitotic catastrophe (Connell et al., 2008; Cherubini et al., 2006). It has also been demonstrated that inhibition of the cell cycle CHK1 promotes over-replication in cells resistant to *dl*922-947 (Connell et al., 2011). An interaction between cell cycle checkpoints and adenovirus is clearly important in driving the cell through the cell cycle but whether this alone can explain the abnormal re-replication seen in sensitive cells remains to be determined. One study suggests that E1A induces changes in the dynamics of the replication pattern, with increased replicon length, fork velocity and inter-origin distance and fewer replication origins (Singhal et al., 2013). The molecular explanation for these changes has yet to be identified but it appears that adenovirus may have a direct effect on host cell replication kinetics highlighting the complexity of the interaction between virus and host cell. Further investigation into this abnormal replication may offer opportunities for ways of potentiating oncolytic adenoviral cytotoxicity.

Unscheduled DNA synthesis induces accumulation of DNA lesions (Saleh-Gohari et al., 2005; Baird et al., 2008; Machida and Dutta, 2005).

The aberrant replication pattern seen following adenoviral infection and *dl*922-947 has been shown to lead to replication stress and activation of the DDR pathways (Singhal et al., 2013; Connell et al., 2011). Upon recognition of DSBs, H2AX, a variant of histone H2A, is rapidly phosphorylated by phosphatidylinositol 3-kinase (PI3K)-elated kinases: ATM, ATR and DNA-PK (Ward and Chen, 2001; Park et al., 2003; Burma et al., 2001). This signal is then amplified through recruitment of other signal factors (Paull et al., 2000; Rogakou et al., 1998). γH2AX is an early marker of DSB formation and was assessed by cell cycle flow and immunofluorescence following infection with *dl*922-947. The data show that the extent of γH2AX induced by *dl*922-947 correlates with viral efficacy, and that the damage occurs specifically in cells with DNA content of 4N or greater. This suggests that dsDNA damage in infected cells may result from abnormal replication and replication stress.

The assessment of γH2AX by immunofluorescence demonstrated a much closer correlation between γH2AX compared to flow cytometry. Immunofluorescence is a very sensitive marker for measuring γH2AX (Löbrich et al., 2010) as each separate cell is able to be visualised and measured, and this may explain the difference in the degree of correlation between γH2AX measured by immunofluorescence and flow cytometry. Nevertheless both techniques show that there is clearly greater γH2AX in cells sensitive to *dl*922-947 compared to those resistant to virus suggesting that the degree of DSB is important in determining viral efficacy. Since infection with a non-replicating virus did not induce γH2AX the results show that phosphorylation of H2AX is a result of viral replication.

This staining pattern for γH2AX is, however, pan-nuclear rather than as discrete foci. The exact explanation for this pattern of staining is unclear. It is however, consistent with previously published data (Nichols et al., 2009). Patterns of γH2AX staining have also been shown to vary throughout the cell cycle with pan-nuclear staining

seen in uninfected M-phase cells (Hernández et al., 2013). Pan-nuclear staining is also associated with apoptosis (Podhorecka et al., 2010). Co-staining infected cells with cell phase specific markers (eg cyclin A for S-phase, CENP-F for G2) may shed some further light on the pattern of staining and cell cycle. Nichols et al. (2009) suggest that since γH2AX staining occurs throughout the nucleus it is distinct from H2AX phosphorylation at double strand breaks. It is suggested that it represents a response to viral replication and improper recruitment of repair factors. Although the exact significance of this pan-nuclear staining following viral infection is unknown, the presence of γH2AX may represent a signal to the cell to activate downstream pathways of the DDR and my results clearly demonstrate that increased γH2AX staining occurs in cells more sensitive to *dl*922-947.

To establish whether cells sensitive to virus are also more sensitive to double strand DNA damage induced by other agents, γH2AX staining was quantified following treatment with etoposide, hydroxyurea and rucaparib. The data show DSB damage induced by etoposide, hydroxyurea and PARP inhibitor does not correlate with viral sensitivity. All three of these agents induce damage in different ways. Etoposide inhibits topoisomerase II (which aids in DNA unwinding), prevents re-ligation of the DNA and in doing so causes DNA strands to break and the damage is repaired by both HR and NHEJ (Hande, 1998). Hydroxyurea depletes the cells of deoxynucleotide triphosphates (dNTPs), which initially results in stalled replication forks that, after prolonged treatment, collapse to DSB (Petermann et al., 2010). These DSBs are ultimately repaired by HR (Petermann et al., 2010). The PARP family of enzymes are crucial to the repair of single strand breaks (SSBs) via the base excision repair pathway (Hoeijmakers, 2001). PARP inhibitors cause the cell to be flooded with unprepared endogenously produced SSBs which, when encountered by a replication fork, cause fork collapse and the formation of DSBs (Bryant et al., 2005; Farmer et al., 2005; Davar et al., 2012). These

results suggest that *dl*922-947 induces genomic damage in a novel way that appears to rely on viral replication and aberrant cell cycle progression. Further investigation is therefore required with further cell lines and further types of DNA damaging agents to determine whether sensitivity to *dl*922-947 can be explained by innate cellular susceptibility to certain types of DNA damage.

Many unanswered questions remain. Firstly, what is the exact mechanism of cell death following viral infection? Work from our group has shown that that *dl*922-947 induces a novel mechanism of cell death independent of classical apoptosis (Baird et al., 2008). The results presented here show that DNA and cell cycle appear to be important in cytotoxicity following *dl*922-947 infection but the mechanism by which they result in, or contribute to, cell death is currently not known. The DDR response and cell cycle are closely interlinked and it remains to be determined which factor is driving cell death.

It is also not clear whether phosphorylation of H2AX is a result of abnormal cellular DNA replication and replication stress, a result of DSBs by an alternative mechanism driven by the virus or whether the virus itself is activating a DDR without actually causing DNA DSBs. Alternatively does the γH2AX just present a form of apoptotic or dying cell? If, however, the presence of viral replication is driving phosphorylation of H2AX, then is up regulation of the DDR required by the virus for replication? The next chapter attempts to investigate this question further by looking at the role of DNA repair proteins in viral replication.

4

HOMOLOGOUS RECOMBINATION AND VIRAL CYTOTOXICITY

4.1 INTRODUCTION

Results from Chapter 3 show that *dl*922-947 has considerable activity in ovarian cancer but the sensitivity of ovarian cancer cells to *dl*922-947 varies considerably, even between cells with similar infectivity. Results also revealed that infection with *dl*922-947 induces a DNA damage response by the phosphorylation of H2AX and that viral sensitivity closely correlates with the extent of DNA damage. In this chapter I investigate the role of cellular DNA repair in determining viral efficacy.

Understanding the role of the DNA repair pathways in novel treatments is particularly important for HGSOC where approximately 15% patients have germline mutations in BRCA1 or BRCA2 — key components of the HR DNA repair pathway. In addition, data from the Cancer Genome Atlas consortium (TCGA) inferred that HR defects may be present in 50% HGSOC, through a variety of additional mechanisms including somatic BRCA1/2 mutation and epigenetic loss of BRCA1 expression (TGCA, 2011). This distinction between HR competent and HR incompetent tumours has significant clinical relevance. Many studies have shown that patients with HR incompetent, BRCA mutant cancers present at a significantly younger age (Synowiec et al., 2016; Alsop et al., 2012) and have significantly improved survival compared to non BRCA mutant tumours (Boyd et al., 2000; Bolton et al., 2012). Importantly, BRCA mutant cancers are more likely to respond to platinum chemotherapy, currently the main treat-

ment for ovarian cancer (Tan et al., 2008; Gorodnova et al., 2015) and secondary mutations that result in gain of function of BRCA1 and BRCA2 restoring the function of HR are associated with platinum resistance (Sakai et al., 2008). There is also great interest in the use of PARP inhibitors in HR defective HGSOC (reviewed in (Wiggans et al., 2015)). Conversely, there are, however, few therapeutic targets available for HR competent tumours, which have a poorer prognosis and are less likely to respond to platinum-based chemotherapy (Mukhopadhyay et al., 2012). There is a critical clinical need to find strategies for these patients.

The interplay between viral infection and the host cell DNA damage response is complex. Among the challenges to the host cell is the viral DNA genome, which is viewed by the cell as DNA damage and results in activation of the DNA damage response (Weitzman and Ornelles, 2005; Carson et al., 2003). In order for adenoviruses to replicate efficiently, they need to circumvent the cellular DNA damage response and they achieve this through a series of mechanisms encoded by the E4 region of the virus. Although the inhibition of the NHEJ pathway is well documented, the role of the HR pathway in Ad5 infection has been less well investigated in adenoviral biology.

Given that the HR pathway is so important in ovarian cancer, this chapter focuses on key components of the pathway in determining viral efficacy.

4.2 RESULTS

4.2.1 *Adenovirus cytotoxicity is greater in HR competent ovarian cancer cells*

The results from the previous chapter suggest that a cell's susceptibility to DNA damage following viral infection may determine overall oncolytic viral efficacy. I therefore hypothesised that the correlation

between cellular susceptibility to DNA double strand break damage and virus efficacy might reflect the cell's ability to repair DSBs. There are two main pathways by which cells repair DSB, HR and NHEJ. Since HR pathway is important in ovarian cancer and it has been well documented that NHEJ is inhibited following adenoviral infection (Weitzman and Ornelles, 2005), I have therefore focused on the role of the HR pathway in determining efficacy of oncolytic adenovirus.

To investigate the link between HR function and viral cytotoxicity I initially used the PE01/ PE04 cell pair. These cells originate from the same ovarian cancer patient. PE01 are BRCA2-deficient ovarian cancer cells derived from ascites of a patient with poorly differentiated ovarian cancer at the time of first relapse and cisplatin sensitivity. PE04 cells were derived from the same patient at the time of platinum resistance and have a secondary BRCA2 mutation with restoration of the open reading frame and are thus BRCA2 functional and HR competent (Sakai et al., 2009). I first confirmed the function of the HR pathway in these cells using a previously described assay of HR (Mukhopadhyay et al., 2010). This assay quantifies RAD51 foci following treatment with the PARP inhibitor rucaparib. RAD51 plays a crucial role in HR: it mediates the search for the homologous DNA sequence and, once the homologous sequence is found, RAD51 filaments facilitate the invasion of the ssDNA overhang into the homologous double-stranded DNA (dsDNA) sequence (Karpenshif and Bernstein, 2012). Once RAD51 filaments are formed, the cell is committed to perform homology-mediated repair to correct the damaged DNA template (Holthausen et al., 2010). Cells with competent HR pathways have been shown to at least double the number of RAD51 foci following treatment with rucaparib whereas cells that do not increase RAD51 foci following rucaparib treatment are deemed HR defective (Mukhopadhyay et al., 2010).

I confirmed that PE04 cells increased RAD51 foci following PARP inhibitor treatment and thus demonstrate functional HR, whilst PE01

are HR defective (Figure 4.1a and Figure 4.1b). In keeping with this, I also confirmed that BRCA2 mutant PE01 are more sensitive than BRCA2 proficient PE04 to both cisplatin (Figure 4.2b) and the PARP inhibitor, rucaparib (Figure 4.2a).

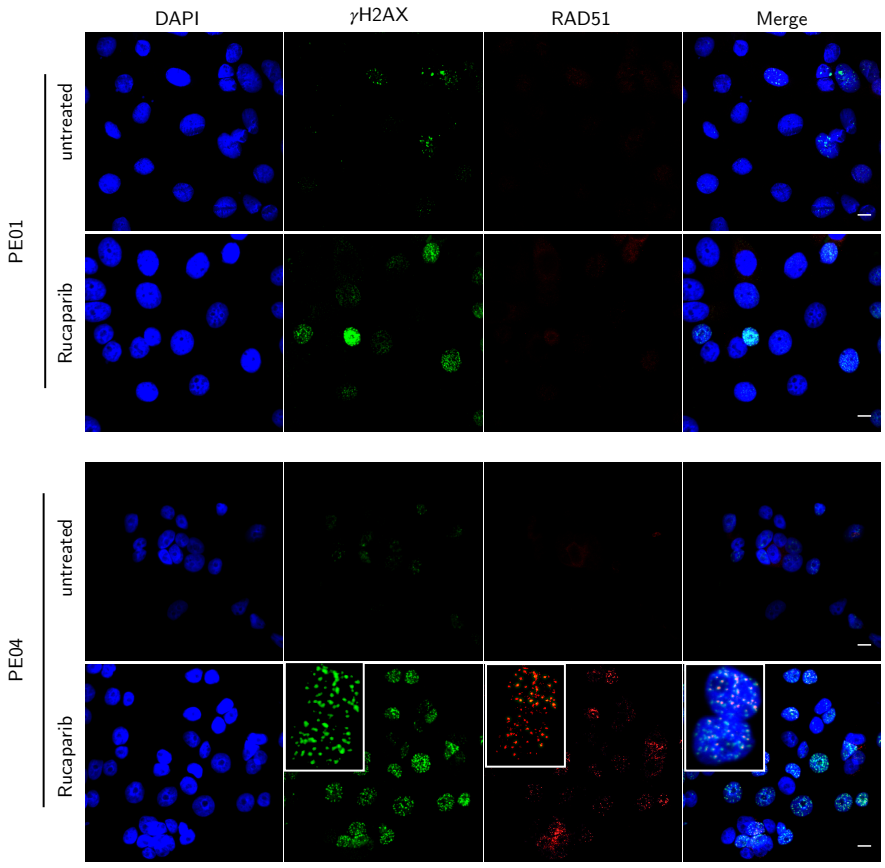

(a)

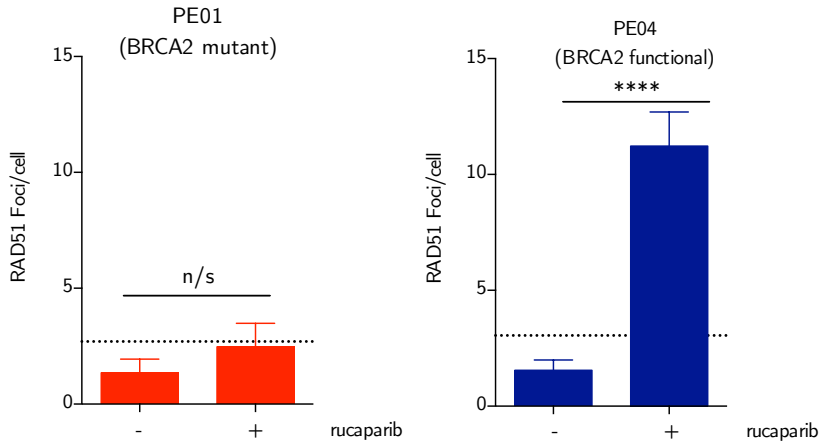

(b)

Figure 4.1: HR competence assessed in PE01 and PE04 cells. **(a)** Cells were treated with rucaparib (10 μM, 24 hours), permeabilized, fixed in 4% PFA, and stained for RAD51 and γH2AX. Representative immunofluorescence image shown. Scale bar = 10 μm. **(b)** RAD51 foci were counted in at least 30 nuclei per treatment condition. Bars show mean (+/- s.d.) number RAD51 foci per cell. Dotted line, 2 $\times$ number foci untreated cells.

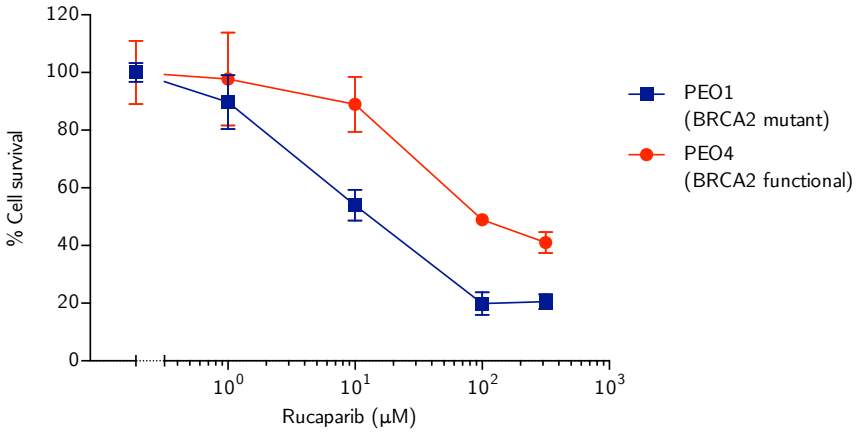

(a)

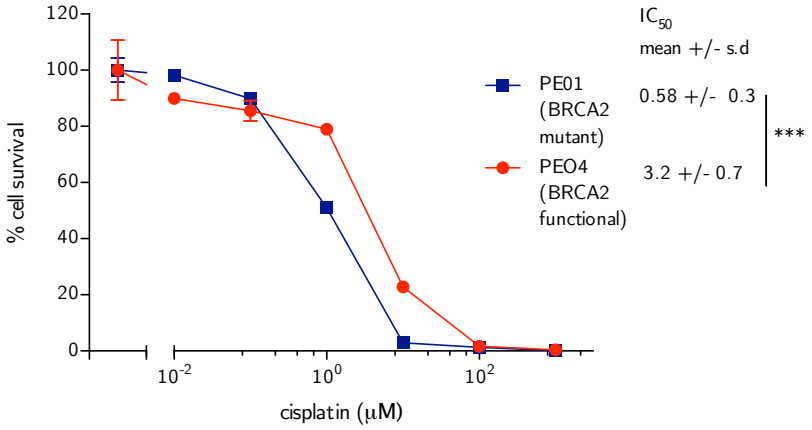

(b)

Figure 4.2: Cisplatin and rucaparib dose response curves. 1×10^4 PE01 and PE04 cells were treated with rucaparib **(a)** and cisplatin **(b)** in triplicate. Cell survival was measured 72 hours later by MTT (cisplatin) or 96 hours later by sulphorhodamine B (rucaparib) assay. Results presented as percentage cell survival compared to untreated cells (mean +/- s.d. n = 3) *** p = 0.005.

Unexpectedly, despite the fact that the PE01 cells are unable to repair dsDNA breaks, I found PE04 to be significantly more sensitive to cytotoxicity induced by the E1A CR2 deleted Ad5 virus *dl*922-947 (Figure 4.3a) as well as to *dl309* virus (E1A wild-type) (Figure 4.3b) and wild-type Ad5 virus (Figure 4.3c). This increased sensitivity to adenovirus in cells with functional HR pathways appears to be ade-

novirus type 5 specific as there was no difference in sensitivity between the BRCA2 mutant and BRCA2 functional cells lines to Ad11 and Ad35 (both group B viruses) (Figure 4.4).

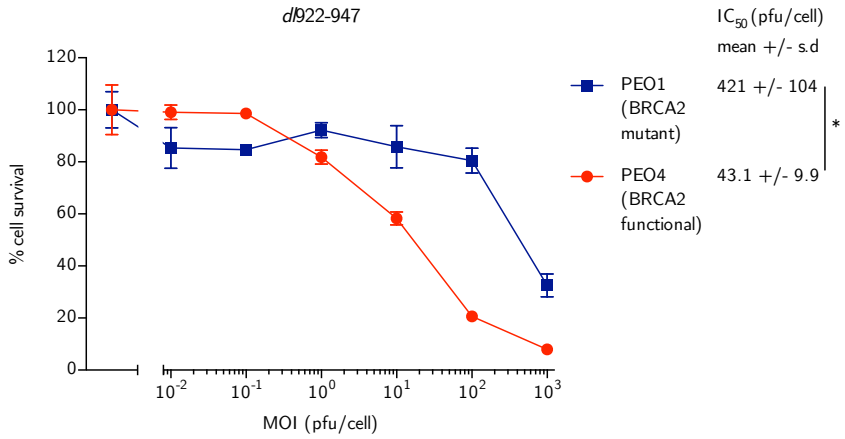

(a)

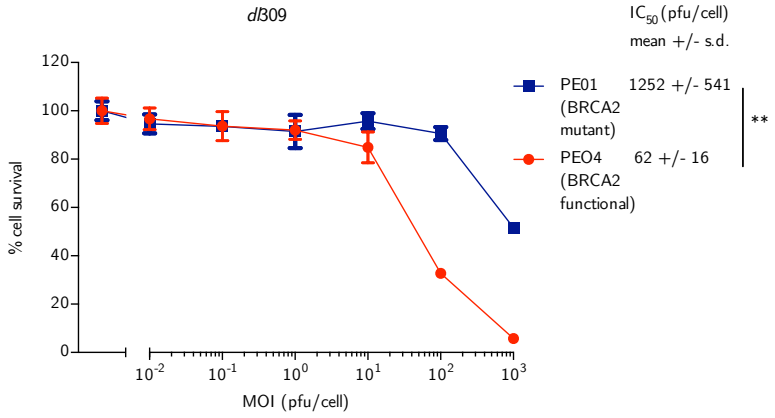

(b)

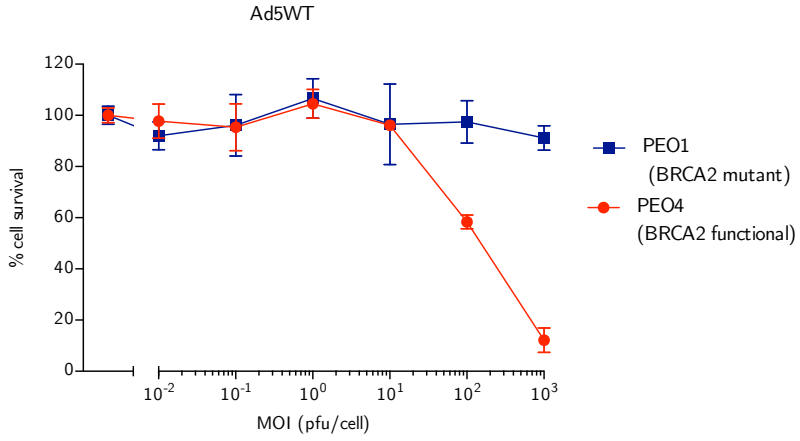

(c)

Figure 4.3: Sensitivity of PE01 and PE04 cells to adenovirus type 5. 1×10^4 cells were treated with increasing concentrations (MOI 0.01 – 1000) of *dl*922-947 **(a)**, *dl*309 **(b)** and wild-type Ad5 (**c**), cell survival was assessed by MTT assay 120 hours post infection. Results presented as percentage cell survival compared to mock infected cells (mean +/- s.d. n = 3), * p = 0.01, ** p = 0.0091. 2 tailed t-test.

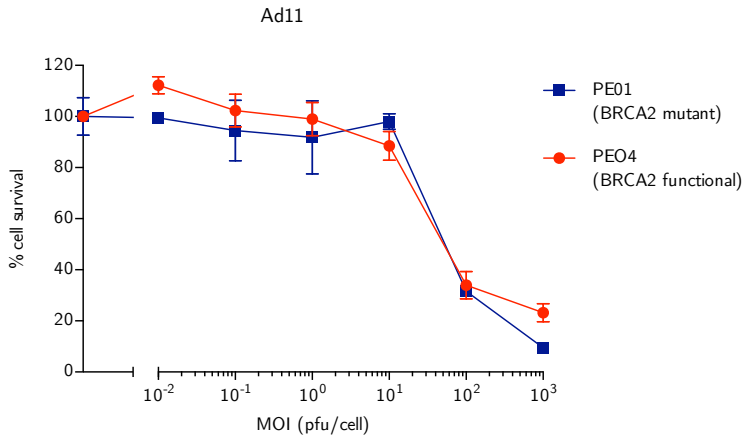

(a)

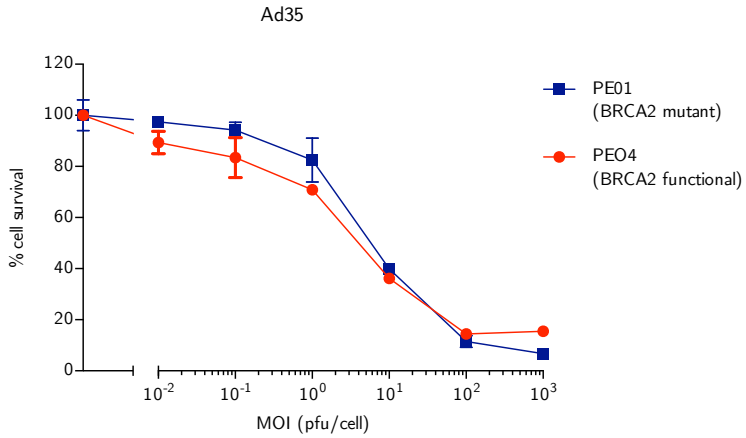

(b)

Figure 4.4: Sensitivity of PE01 and PE04 cells to group B adenovirus. $1x10^4$ cells were treated with increasing concentrations (MOI 0.01 – 1000) of Ad11 **(a)** or Ad35 **(a)**, cell survival was assessed by MTT assay 120 hours post infection. Results presented as percentage cell survival compared to mock infected cells (experiments performed by Suzanne Dowson).

4.2.2 *HR competence and viral efficacy in a panel of ovarian cancer cell lines*

To further assess whether HR function influences viral effiacy, HR function was assessed in a panel of ovarian cancer cell lines using the assay described above. Using this assay TOV21G, OVCAR4, UWB1.289

+BRCA1, COV318, PE04 and SKOV3 cells were defined as HR competent. In contrast, SKOV3ip1, UWB, IGROV1, PE01 and OVSAHO cells were defined as HR incompetent (Figure 4.5). Of the HR incompetent cells, PE01 and OVSAHO have a known BRCA2 mutation (Domcke et al., 2013; Sakai et al., 2009), UWB1.289 has a BRCA1 mutation (DelloRusso et al., 2007) and IGROV1 has a mutation both in BRCA1 and BRCA2 (Domcke et al., 2013).

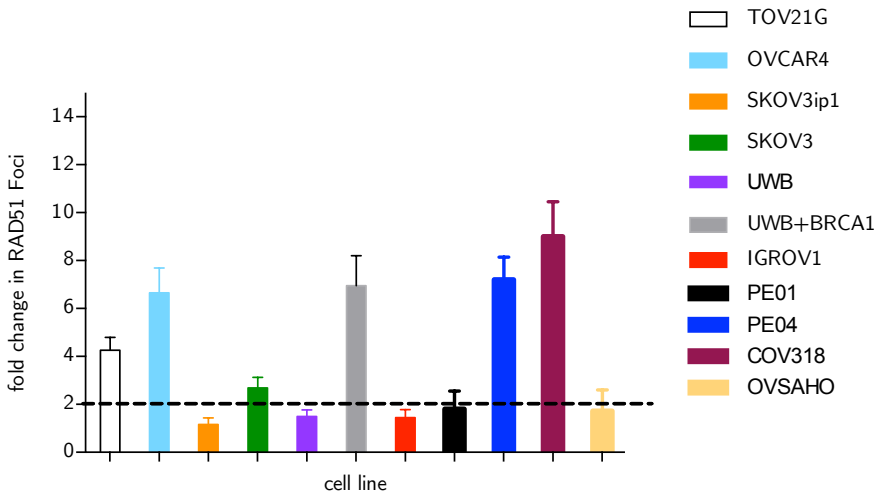

Figure 4.5: HR compentence of a panel of ovarian cancer cell lines. A panel of ovarian cancer cells (TOV21G, OVCAR4, COV318, UWB1.289, UWB1.289 +BRCA1, PE01, PE04, SKOV3ip1, SKOV3, IGROV1 and OVSAHO) were treated with rucaparib (10 μM, 24 hours), permeabilized, fixed in 4% PFA, and stained for RAD51. RAD51 foci were counted in at least 30 nuclei per treatment condition. Bars show fold change of RAD51 foci following treatment with rucaparib (+/- S.E.M.) number RAD51 foci per cell. Dotted line, 2 fold increase of RAD51 foci following rucaparib treatment. Results show that TOV21G, OVCAR4, COV318, UWB1.289+BRCA1, PE04, SKOV3 are HR compent and PE01, OVSAHO, UWB and SKOV3ip1 are HR incompetent.

To assess whether HR competence influences viral effiacy, HR competence was plotted against the IC_{50} to *dl*922-947 (Figure 4.6). Although the differences are not significant, the results follow the same

pattern seen in the PE01 and PE04 cells, that HR competent cells are more sensitive to adenoviral effiacy. This suggests that the HR pathway may be important in determining sensitivity to virus.

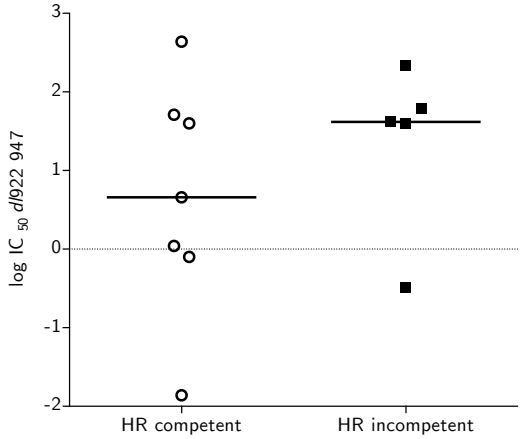

Figure 4.6: Association between IC_{50} *dl*922-947 and HR competence. Sensitivity to *dl*922-947 was assessed in a panel of cell lines, the IC_{50} was calculated and plotted against HR competence as assessed by Figure 4.5. Results suggest a trend that HR competent cells are more sensitive to *dl*922-947 but this was not significant. Solid line represents median value.

4.2.3 *Viral infectivity and cytotoxicity in a matched HR competent and incompetent cell line*

To investigate the differences in adenovirus sensitivity between the BRCA2 deficient and proficient PE01 and PE04 cells, respectively, I next assessed viral infectivity using an Ad5 GFP virus (E1 deleted Ad5 vector encoding GFP under the CMV immediate early promotor). Results revealed that the PE04 cells were 10 times more infectable with Ad5 vectors than the PE01 cells (Figure 4.7a). To determine whether this difference in infectability could explain the different in viral efficacy, I determined the dose of virus that achieved equal infection between the PE01 and PE04 cells (the iso-infective dose) (MOI 6 PE04, MOI 60 PE01 or MOI 10 PE04, MOI 100 PE01) (Figure 4.7b).

Even at iso-infection MOI, PE04 cells remained significantly more sensitive to both *dl*922-947, (Figure 4.8a) and *dl*309 (Figure 4.8b). This confirms the results in the previous chapter that infectivity is not the only determinant of viral cytotoxicity.

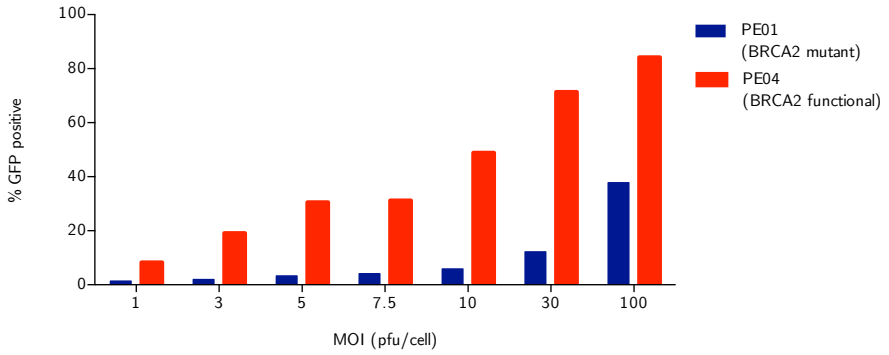

(a)

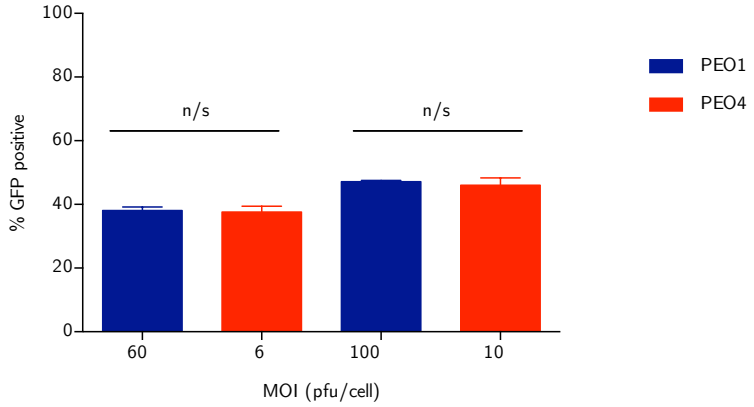

(b)

Figure 4.7: Viral infectivity in an HR competent and incompetent cell pair. **(a)** PE01 and PE04 cells were infected with Ad5 CMV-GFP with increasing doses of virus. Infectivity was assessed by GFP positivity 24hours later by flow cytometry. **(b)** Equal infection between PE01 and PE04 cells was achieved at MOI 60 (PE01) and MOI 6 (PE04) or MOI 100 (PE01) and 10 (PE04). PE01 and PE04 cells were infected in triplicate with Ad CMV-GFP at MOI 60 and 100 (PE01) and MOI 6 and 10 (PE04). Infectivity was assessed by GFP positivity 24 hours later by flow cytometry. Bars represent mean percentage of GFP positive cells +/- s.d, n = 3. n/s: no significant difference in GFP positivity between the cell lines.

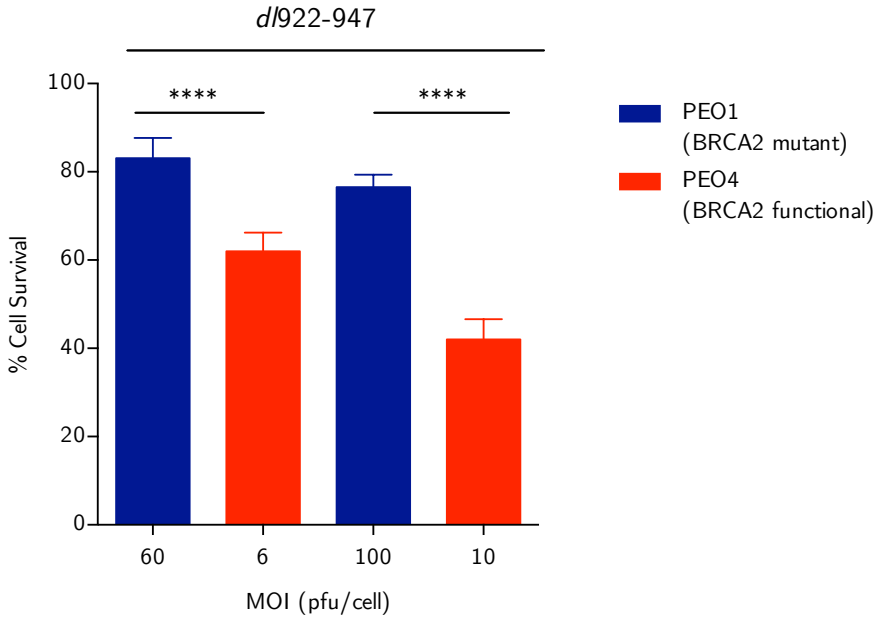

(a)

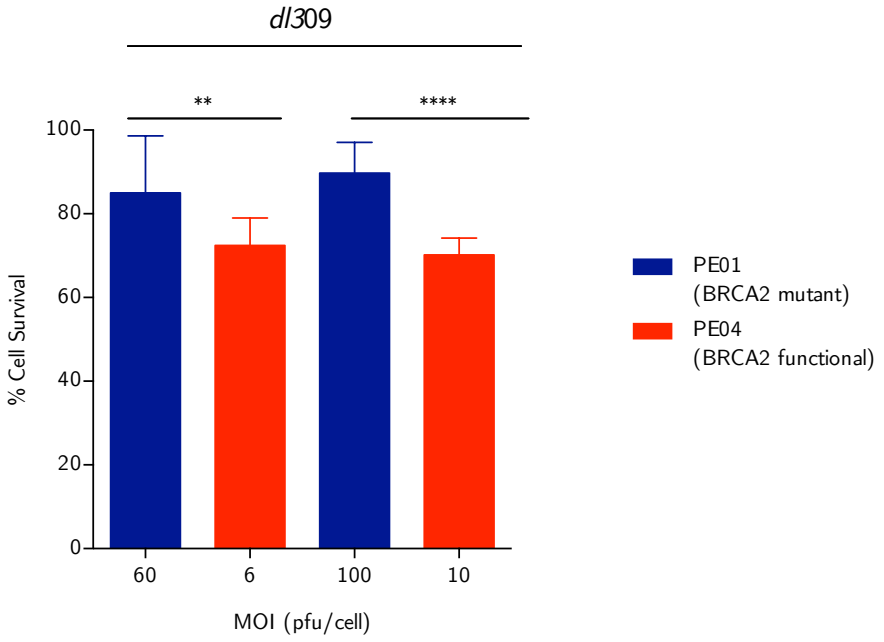

(b)

Figure 4.8: Viral cytotoxicity in an HR competent and incompetent cell line following iso-infection. 1×10^4 cells were infected with *dl*922-947 **(a)** or *dl309* **(b)** at the iso-infective dose (MOI 10 or 6 for PE04 and MOI 100 and 60 for PE01) and cell survival assessed by MTT 144 hours later (mean +/- s.d. n = 3, **** p< 0.0001, ** p =0.0086; 2 tailed t-test).

4.2.4 *Viral lifecycle in the matched HR competent and incompetent cell lines*

Following the observation that the HR competent cell line are more sensitive to viral cell death, I next investigated aspects of viral lifecycle in these cell lines. Viral replication was assessed using a $TCID_{50}$ assay, this revealed no significant difference in the number of infectious virions generated following iso-infection at 24, 48 and 72 hours (Figure 4.9). Viral protein expression was assessed by immunoblot. There was comparable early (E1A) and late (Ad5, structural proteins) viral protein expression in iso-infected cells (Figure 4.10a and Figure 4.10b).

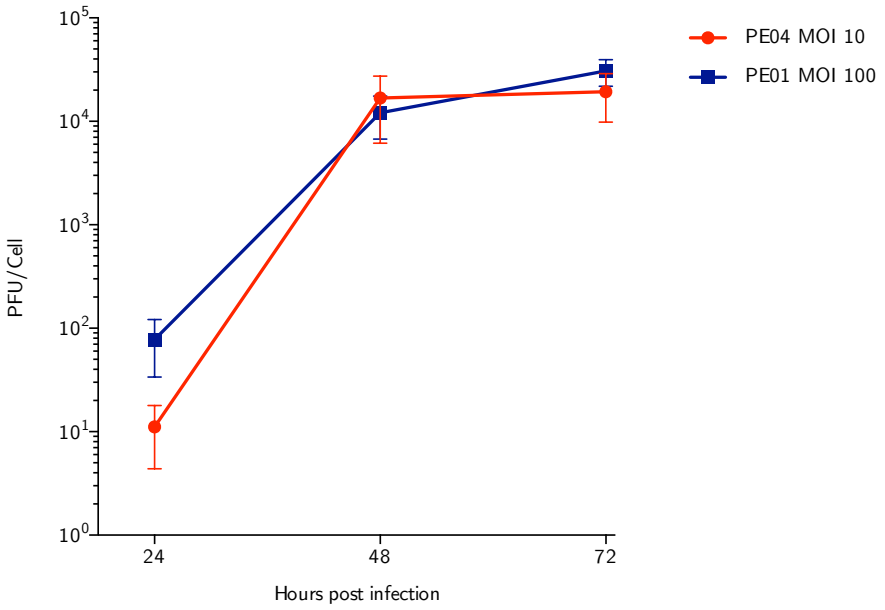

Figure 4.9: Viral replication in an HR competent and incompetent cell line. PE01 and PE04 cells were infected with *dl*922-947 MOI 100 (PE01) or 10 (PE04) for up to 72 hours. Virus replication was assessed by $TCID_{50}$. No significant difference was seen between the 2 cell lines, 2-tailed t-test.

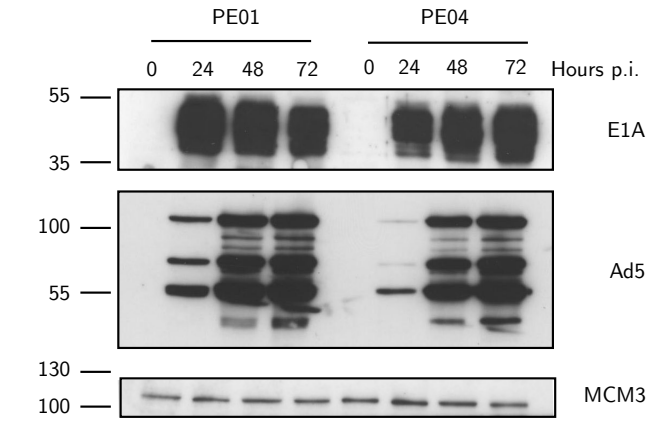

(a)

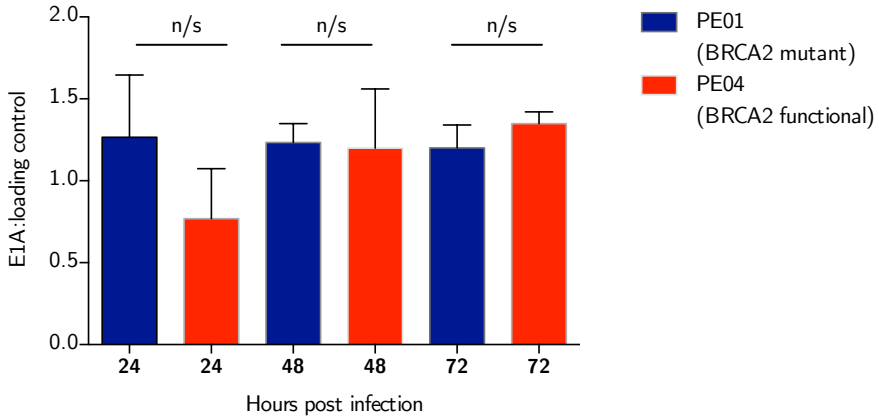

(b)

Figure 4.10: Protein expression in an HR competent and incompetent cell line. **(a)** PE01 and PE04 cells were infected with *dl*922-947 MOI 100 (PE01) or 10 (PE04). Protein was harvested up to 72 hours post-infection. Expression of E1A and adenovirus 5 structural proteins was assessed by immunoblot, MCM3 was used as a loading control. **(b)** Quantification of E1A immunoblots following 24, 48 and 72 hours following infection with *dl*922-947 in PE01 and PE04 cells. n/s: no significant difference in E1A protein expression between the PE01 and PE04 cells at each time point, 2 tailed t-test. n = 3.

Quantitative PCR indicated that there was more viral DNA generated in PE04 at 72hours (Figure 4.11). This was confirmed by Southern blotting as shown in Figure 4.12. In addition, Southern blotting

also revealed no obvious abnormalities in viral DNA processing, and specifically no obvious concatemers in either cell line (Figure 4.12). This suggests that the viral DNA is processed correctly despite differences in the DNA repair function of the host cell.

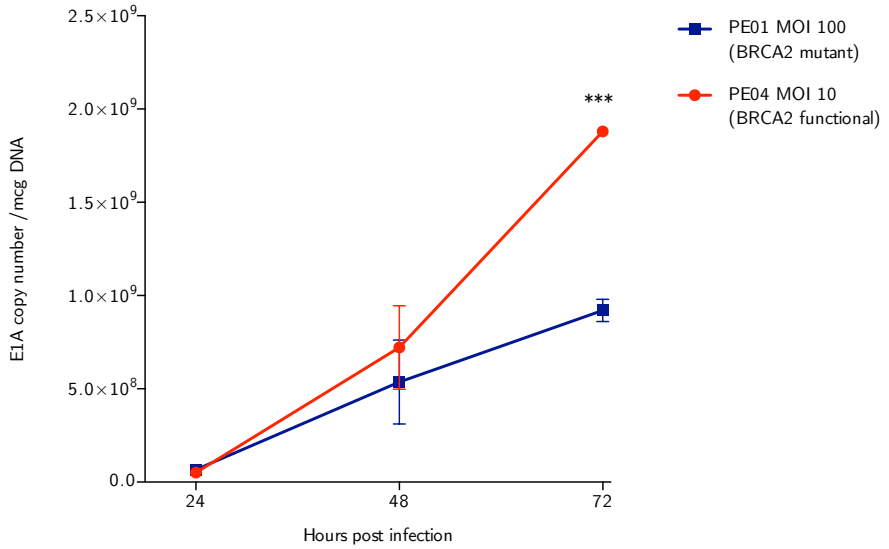

Figure 4.11: Assessment of viral DNA in an HR competent and incompetent cell line. PE01 and PE04 cells were infected with *dl*922-947 MOI 100 (PE01) or 10 (PE04) for up to 72 hours. Virus DNA assessed by quantitative PCR ***: $p < 0.001$, 2 tailed t-test.

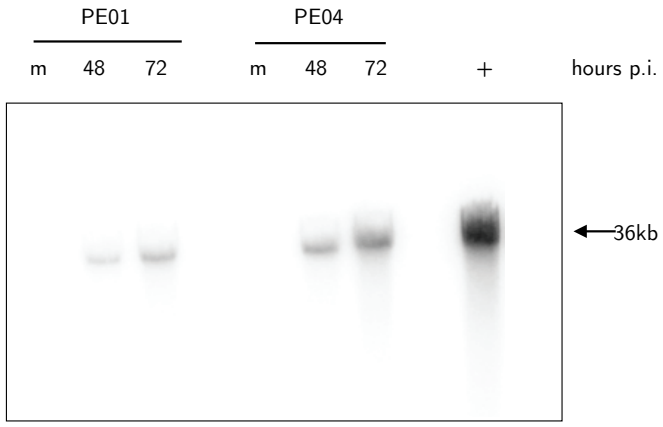

Figure 4.12: Assessment of viral DNA in an HR competent and incompetent cell line. PE01 and PE04 cells were infected with *dl*922-947 MOI 100 (PE01) or 10 (PE04) at 48 and 72h. DNA was extracted and subjected to neutral pulsed-field gel electrophoresis, probed with HRP-labelled adenovirus type 5 probe. 100 ng purified *dl*922-947 DNA was run as positive control (+). Experiment performed with Atsushi Shibata.

4.2.5 *DNA damage and cell cycle in PE01 and PE04 cells*

Chapter 3 showed that viral efficacy closely correlated with cell cycle changes and DNA damage (Section 3.2.3 and Section 3.2.5). I therefore went on to investigate whether the difference in sensitivity to Ad5 vectors between HR proficient and deficient cells was due to their differential accumulation of DNA damage following viral infection. DNA damage and cell cycle was assessed by flow cytometry using propidium iodide (PI) and co-staining with γH2AX in both mock infected cells and 48 hours following infection with *dl*922-947 at the iso-infective dose. Examples of the cell cycle profiles and distribution of γH2AX staining is shown in Figure 4.13.

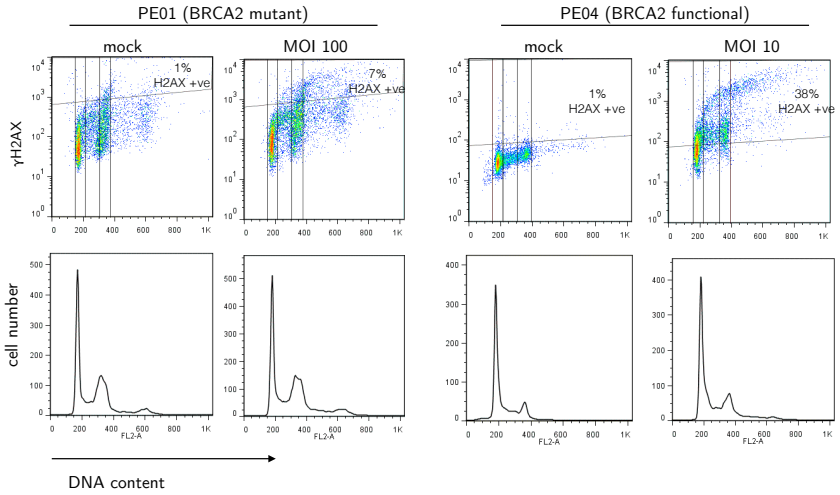

Figure 4.13: DNA damage and cell cycle in a matched HR competent and incompetent cell pair. PE01 and PE04 cells were harvested 48 hours following infection with *dl*922-947 (MOI 100 and 10 respectively) or mock infection, fixed in 70% cold ethanol, incubated with an anti-γH2AX antibody, counter-stained with PI and analysed by flow cytometry. Representative images shown, percentage of γH2AX increase was compared to mock infected cells.

As previously observed (Cooke et al., 2010), and in keeping with their BRCA2 mutation, the PE01 cells are genomically unstable and demonstrated a greater basal level of DNA damage and a higher proportion of cells with >4N DNA contents on flow cytometry (Figure 4.14a and Figure 4.14b). However, following iso-infection the more sensitive PE04 cells showed a greater increase in the proportion of cells with >4N (Figure 4.15a) and a greater amount of DNA damage compared to the PE01 cells (Figure 4.15a). This was consistent with the results from my previous chapter (Section 3.2.6 and Section 3.2.7) showing that virus-induced DNA damage correlates with sensitivity and also in keeping with previous data (Connell et al., 2011; Ingemarsdotter et al., 2015).

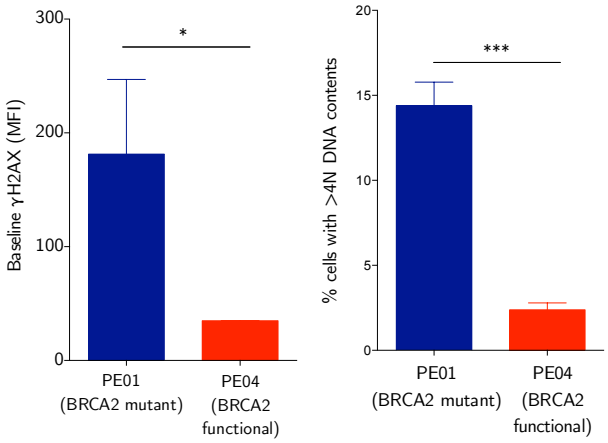

(a) **(b)**

Figure 4.14: Cell cycle and DNA damage in PE01 and PE04 cells at baseline. **(a)** γH2AX staining (quantified by mean fluorescence intensity) Significantly greater baseline γH2AX staining in the PE01 cells * p = 0.02, 2 tailed t-test. **(b)** Amount of cells with more than 4N DNA content in untreated PE01 and PE04 cells. Significantly higher proportion of PE01 cells with more than 4N DNA content at baseline, *** p = 0.0001, 2 tailed t-test. Bars represent mean +/- s.d, n = 3.

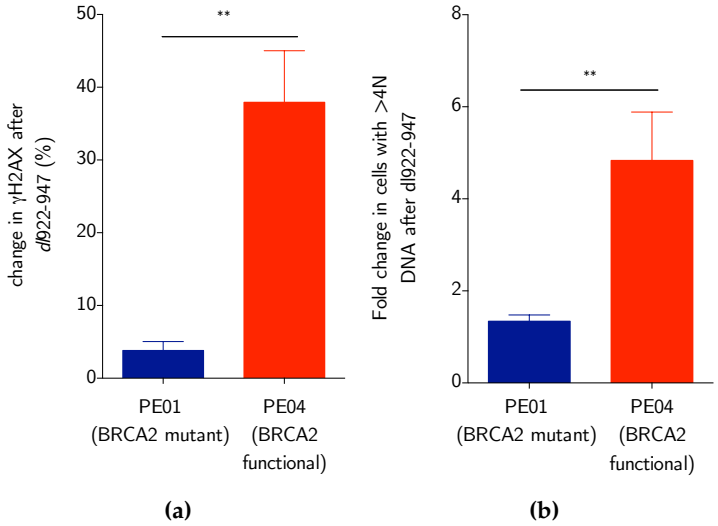

Figure 4.15: DNA damage and cell cycle following iso-infection with *dl*922-947. **(a)** Increase in γH2AX-positive cells following *dl*922-947 (MOI 100 for PE01 MOI 10 for PE04). ** p = 0.0012. **(b)** cells with more than 4N DNA following iso-infection. ** p = 0.0046, 2 tailed t-test.

4.2.6 *The addition of PARP inhibitor does not increase cytotoxicity to dl922-947*

PARP inhibitors, such as rucaparib and olaparib are increasingly being used clinically for patients with BRCA mutant ovarian cancer (Lee et al., 2013). The most well documented role of Poly(ADP-ribose) polymerase 1 (PARP1) is its essential role in the base excision repair (BER) pathway that repairs single strand breaks (SSBs) (Lieber, 2010). It is thought that PARP inhibition results in the accumulation of SSBs that are converted to DSBs at replication forks. These DSBs are unable to be repaired in HR incompetent cells, resulting in cell death whereas cells with competent HR pathways are unaffected by PARP (Yap et al., 2011). I therefore hypothesed that treatment with PARP inhibitors might increase the cytotoxicity of *dl*922-947 since the SSBs

generated by PARP inhibition would be rapidly converted to DSBs due to cell cycle progression as a result of *dl*922-947 infection.

To investigate this, a range of ovarian cancer cell lines were infected with *dl*922-947 at increasing concentrations and 24 hours following infection rucaparib was added (at a range of concentrations). In all the cell lines tested (both HR competent and defective) there was no effect of the addition of PARP inhibitor on viral dose response (Figure 4.16). Specifically PARP inhibitor did not sensitise the cells to viral cytotoxicity.

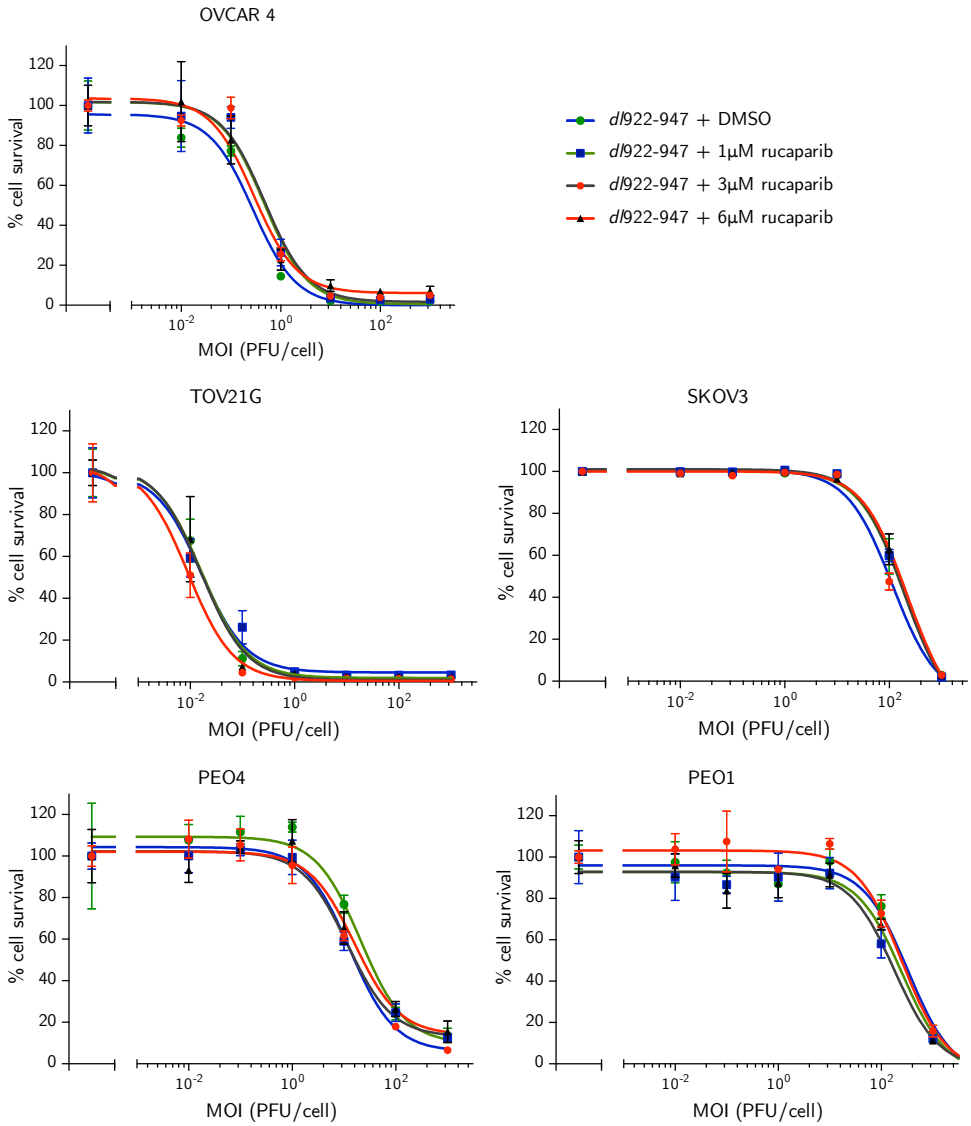

Figure 4.16: PARP inhibitor does not increase cytotoxicity to *dl*922-947. 1×10^4 HR competent cells (TOV21G, PE04, SKOV3, TOV21G) and an HR defective cells (PE01) were plated in 24 well plates and 24 hours later infected with increasing concentrations of *dl*922-947 (MOI 0.01 – 1000). 24 hours later rucaparib was added to all wells at a concentration of 0, 1, 3 and 6 μM. Cell survival assesssed 120 hours following rucaparib treatment by MTT assay. Results presented as cell survival compared to mock infected or normalised to rucaparib alone treated cells (mean +/- s.d, n = 3).

4.2.7 *MRE11 is degraded following infection with dl922-947*

Adenovirus has been shown to block aspects of the cellular DNA repair response. The MRN complex (MRE11, RAD50, NBS1) is a major target following Ad5 infection and MRE11 has been shown to be degraded following infection (Stracker et al., 2002). To investigate whether *dl*922-947 produces a similar reduction, MRE11 was assessed by immunoblot following infection with *dl*922-947. Consistent with previous observations, MRE11 is reduced in both the PE01 and PE04 cells (Figure 4.17). In addition there was no significant difference between the degree of degradation of MRE11 in the PE01 and PE04 cells following viral iso-infection. This indicates that differences in MRE11 degradation between cell lines does not explain the differences in sensitivity between the HR competent and incompetent cell line.

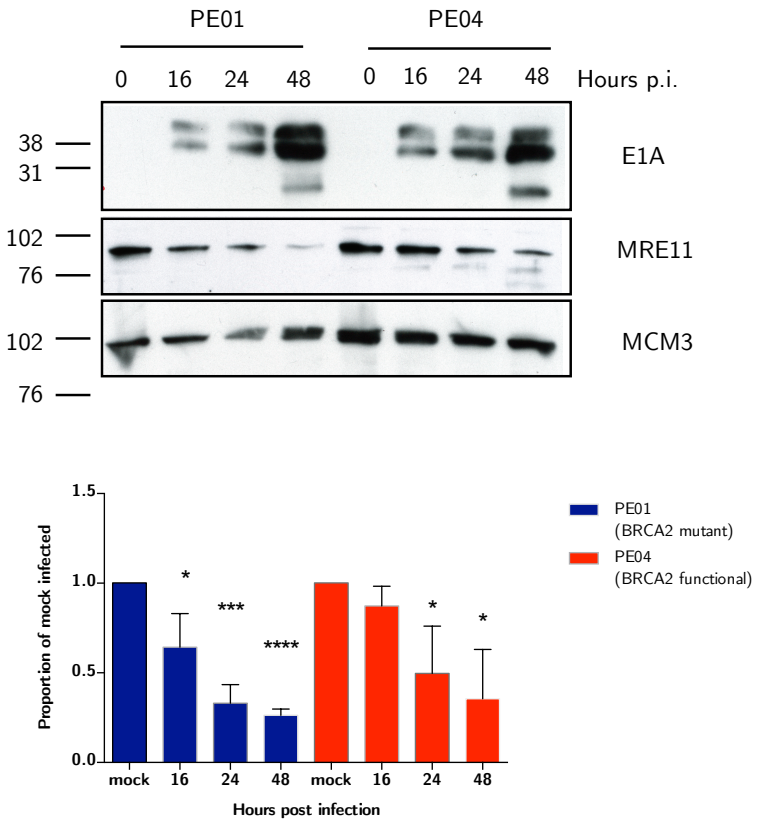

Figure 4.17: MRE11 is degraded following infection with *dl*922-947. PE01 and PE04 cells were harvested at 16, 24 and 48hours following infection with *dl*922-947 (MOI 100 and 10 respectively). Expression of E1A and MRE11 was detected by immunoblot. MCM3 was used as a loading control. Representative blot shown. Graph shows decrease of MRE11 following infection with *dl*922-947. Densitometry of bands was assessed using ImageJ, normalised to loading control and presented as proportion of mock infected cells, n = 3. (PE01: * p = 0.03, *** p = 0.004, **** p <0.0001, PE04: * p = 0.3; 2 tailed t-test results compared to mock infected MRE11). No significant difference in reduction of MRE11 was seen between the two cell lines, 2 tailed t-test.

4.2.8 *Inhibiting NHEJ has no effect on viral cytotoxicity in both the HR competent and incompetent cell lines*

Adenovirus has also been shown to inhibit NHEJ through mechanisms that include proteosomal degradation of DNA Ligase IV (Baker et al., 2007) and the viral proteins, E4-34kDa and E4-11kDa both bind and inactivate DNA PK, which is an essential kinase for NHEJ (Boyer et al., 1999a). I therefore hypothesised that the HR defective cell line may have up-regulation of NHEJ to compensate for lack of the HR pathway to repair DSBs: and in turn, this up regulation could affect viral cytotoxicity. To investigate this, NHEJ was inhibited using the DNA-PKcs inhibitor, Nu7026 (Nutley et al., 2005). There was no difference in sensitivity to the DNA-PK inhibitor between the PE01 and PE04 cells suggesting that there are no significant differences in the reliance on NHEJ function between these cell lines (Figure 4.18). This is consistent with previous findings which show that BRCA2 mutant cells show no increase in NHEJ (Xia et al., 2001). In addition, Nu7026 had no significant effect on viral cytotoxicity (Figure 4.19). Taken together, these results suggest that differences in NHEJ function cannot explain the difference in viral cytotoxicity between the BRCA2 competent and incompetent cell pair.

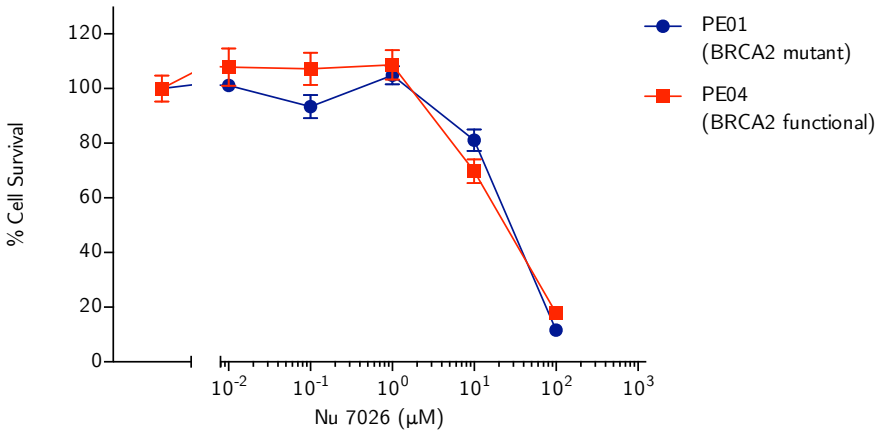

Figure 4.18: Sensitivity of BRCA2 deficient and proficient cells to DNA PK inhibitor. 2500 PE01 and PE04 cells were plated in a 96 well plate and treated with increasing concentrations of Nu7026. Cell survival was assessed by Cell Titer glo assay 120 hours post treatment. Results presented as percentage cell survival compared to untreated cells (mean +/- s.d. n = 3).

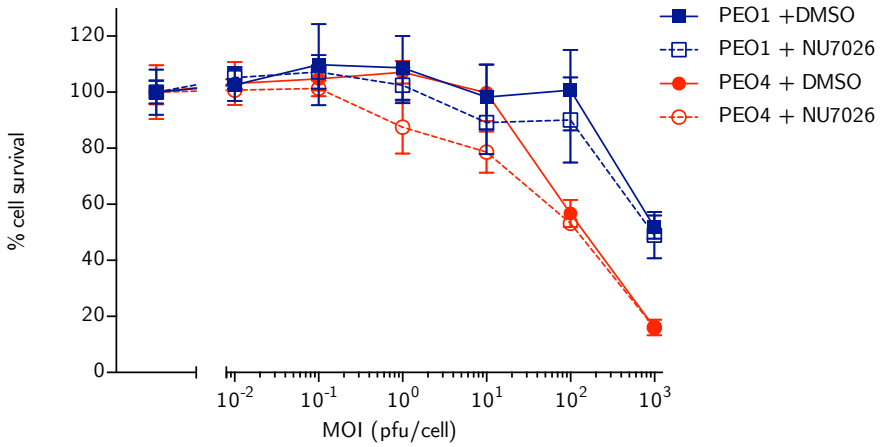

Figure 4.19: Effect of inhibition of DNA PK to viral cytotoxicity. 2500 PE01 and PE04 cells were plated in 96 well plate and infected with increasing concentrations *dl*922-947. 24 hours later 10 μM of Nu7026 was added and survival was assessed by cell titer glo assay 120 hours post infection. Results presented as percentage cell survival normalised to either mock infected cells or cells treated with Nu7026 alone (mean +/- s.d. n = 3).

4.2.9 *RAD51 is maintained at early time points following viral infection*

As dicussed earlier, RAD51 is a crucial downstream protein involved in HR repair, it is re-localised within the nucleus in response to DNA damage and catalyzes repair by HR by invading the homologous DNA strand (Baumann and West, 1998). Interestingly, despite degradation of MRE11, expression of RAD51 was maintained at 48 hours in both the PE01 and PE04 cells. RAD51 protein was, however, reduced at later time points (Figure 4.20). RAD51 has a short half life (around 5 hours) (Zhu et al., 2013) and since adenoviral infection results in the inhibition of cellular protein synthesis in later stages of infection (Huang and Schneider, 1991), this reduction in RAD51 may be be the result of reduced mRNA translation rather than protein degradation.

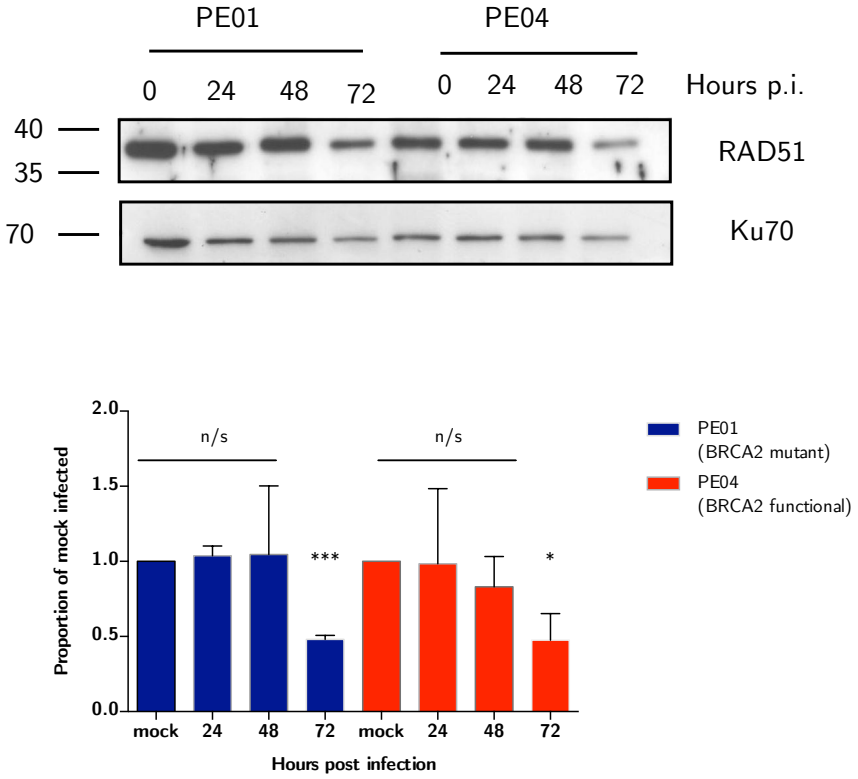

Figure 4.20: RAD51 is maintained at early time-points following infection with *dl*922-947. PE01 and PE04 cells were harvested following infection with *dl*922-947 (MOI 100 and 10 respectively). Expression of RAD51 was detected by immunoblot. Ku70 was used as a loading control. Representative blot shown. Graph shows RAD51 expression following infection with *dl*922-947. Densitometry of bands was assessed using ImageJ, normalised to loading control and presented as proportion of mock infected cells, n = 3. * p =0.01, **** p < 0.0001, 2 tailed t-test results compared to mock infected RAD51.

4.2.10 *BRCA2 co-localises with viral replication centres*

Adenoviral replication takes place within the nucleus of the cell in regions known as viral replication centers (VRC). These VRCs can be visualised by confocal microscopy using an antibody directed against the adenoviral protein, E2 DNA binding protein (E2 DBP) (Reich

et al., 1983). To assess whether core HR proteins may play a role in viral replication I analysed co-localisation between BRCA2 and E2 DBP in virus infected cells. There was clear co-localisation between BRCA2 and E2 DBP in the PE04 cells shown in Figure 4.21a. As expected no BRCA2 was observed in the PE01 (Figure 4.21b).

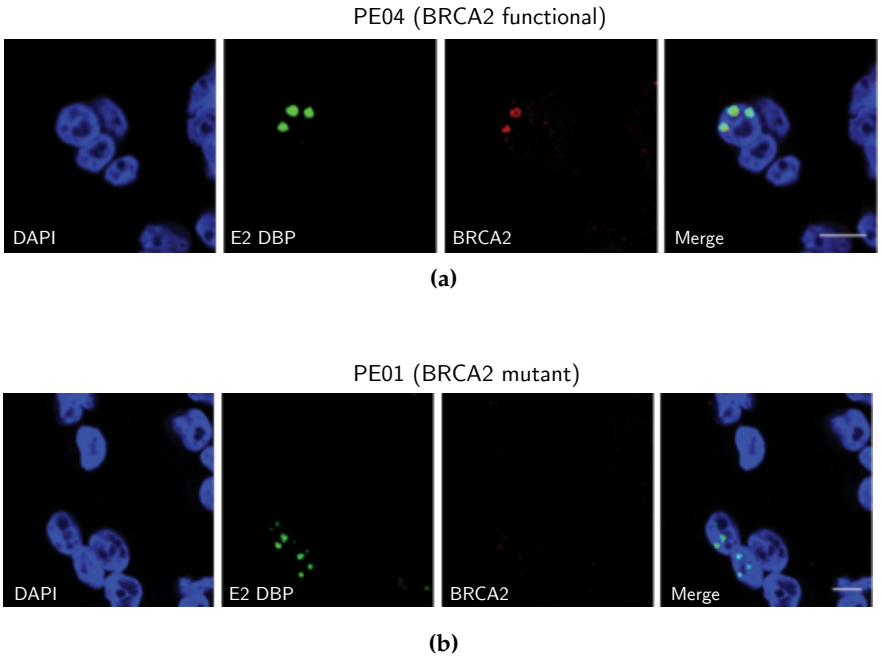

Figure 4.21: BRCA2 co-localises with viral replication centres. PE01 and PE04 cells were fixed in 4% PFA following infection with *dl*922-947 (MOI 300 and 30, respectively). Expression of adenovirus E2 DNA binding protein and BRCA2 was assessed by confocal microscopy in PE04 (a) and PE01 (b) cells. Scale bar = 10 μm.

TOV21G and HeLa cells are two further cell lines that demonstrate HR competence (Figure 4.22). Following infection with *dl*922-947 co-localisation was also seen between BRCA2 and VRCs in both the TOV21G (Figure 4.23a) and HeLa (Figure 4.23b) cells. These results imply that in cells with functional BRCA2, BRCA2 is recruited to VRCs .

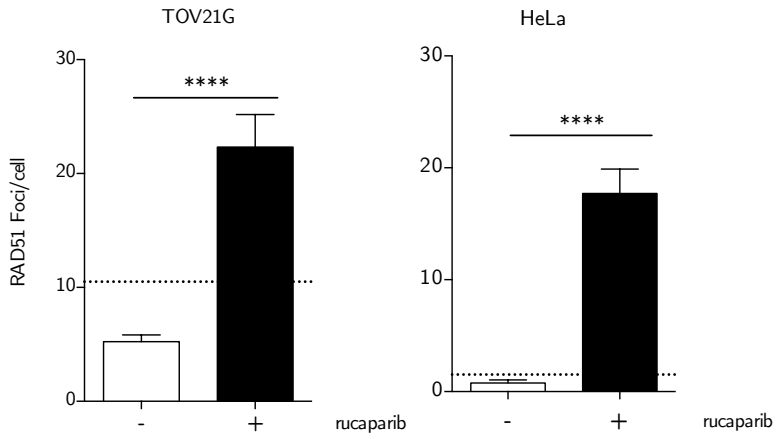

Figure 4.22: Assessment of HR function in TOV21G and HeLa cells. Cells were treated with rucaparib (10μM, 24 hours), permeabilised, fixed in 4% PFA, and stained for RAD51. RAD51 foci were counted in at least 30 nuclei per treatment condition. Bars show mean (+/- s.d.) number RAD51 foci per cell. Dotted line, 2 × number of foci in untreated cells. TOV21G and HeLa cells double their RAD51 foci following rucaparib treatment and are thus HR competent.

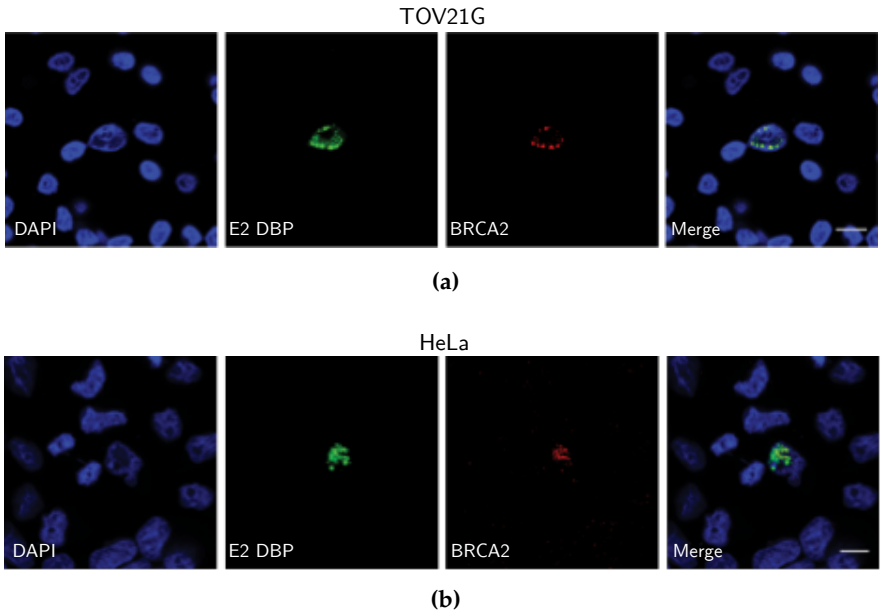

Figure 4.23: BRCA2 co-localises with viral replication centres. TOV21G **(a)** and HeLa **(a)** cells were fixed in 4% PFA following infection with *dl*922-947 (MOI 10). Expression of adenovirus E2 DNA binding protein and BRCA2 was visualised by confocal microscopy. Scale bar = 10 μm.

4.2.11 *BRCA2 influences adenovirus efficacy in HR competent cells*

To investigate whether BRCA2 function influences the response to *dl*922-947 in the HR competent cell lines, I depleted BRCA2 using siRNA. To quantify knockdown, western blotting of BRCA2 protein level was attempted. However, following multiple attempts using a variety of conditions, I was unable to achieve reliable and repeatable blots. BRCA2 knockdown following siRNA was therefore confirmed by quantitative RT-PCR (Figure 4.24).

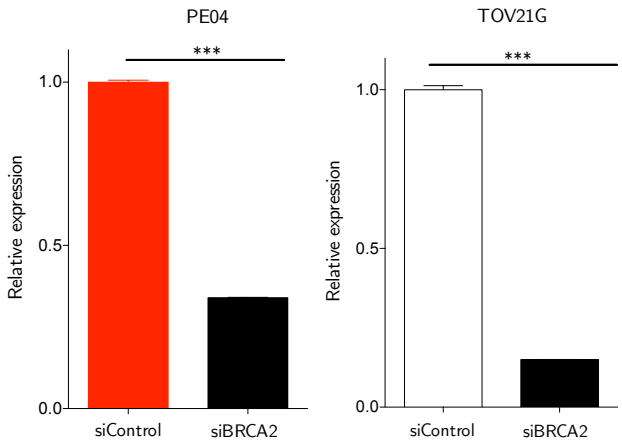

Figure 4.24: BRCA2 knockdown confirmed by quantative PCR. 48 hours following transfection of BRCA2 siRNA (SMART pool, Dharmacon) or control siRNA, cells were harvested in trizol, RNA extracted and quantative RT-PCR performed to quantify relative expression BRCA2 normalised to 18s. *** $p < 0.001$ 2 tailed t-test.

Following BRCA2 knockdown, I found a small but significant reduction in cytotoxicity following infection with *dl*922-947 in PE04 cells (Figure 4.25a). This was recapitulated in TOV21G and HeLa cells (Figure 4.25b) and (Figure 4.25c). Taken together, my data suggest that BRCA2 is recruited to VRC and augments viral cytotoxicity.

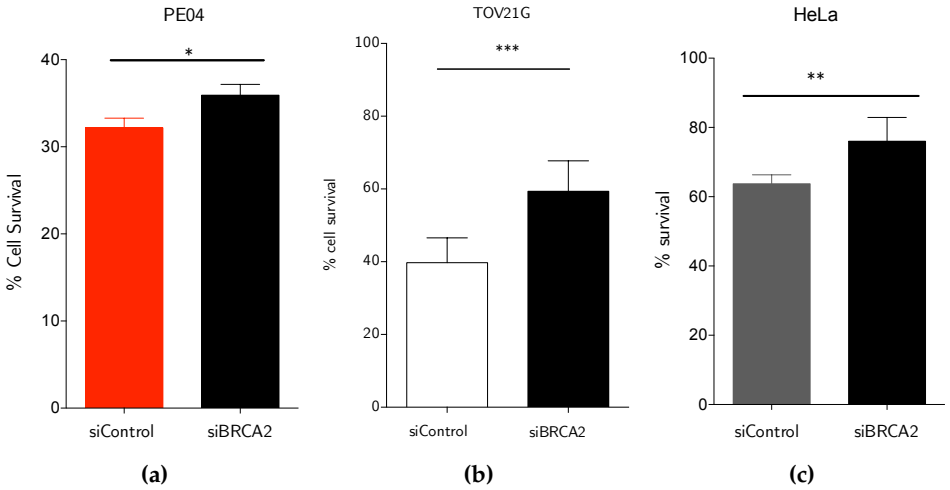

Figure 4.25: BRCA2 knockdown decreases adenovirus efficacy. 24h following siRNA-mediated BRCA2 knockdown, PE04 **(a)**, TOV21G **(b)** and HeLa **(c)** cells were infected with *dl*922-947 (MOI 30 for PE04, MOI 1 for TOV21G; MOI 8 for HeLa). Survival was assessed 96 hours post-infection by MTT assay; PE04: * p = 0.038. TOV21G: *** p = 0.007. HeLa: ** p = 0.0016 2 tailed t-test.

4.2.12 *RAD51 co-localises with VRC in HR competent and incompetent cells*

Following the finding that BRCA2 influenced viral cytotoxicity, I wanted to look at the role of another core HR protein, RAD51. Immunofluoresence revealed clear co-localisation between RAD51 and E2 DBP following infection with *dl*922-947 in PE04 cells (Figure 4.26a). This finding was confirmed in two other HR competent cells lines, TOV21G (Figure 4.26b) and HeLa (Figure 4.26c).

It is documented that, in BRCA2-deficient cells, RAD51 is unable to form foci at the site of DNA damage (Yang et al., 2011). However, to my surprise, I observed RAD51 foci co-localised with E2 DBP in PE01 cells (Figure 4.27), despite the absence of BRCA2. To further assess this, I looked at IGROV1 cells which are hypermutated and contain mutations in both BRCA1 and BRCA2 (Domcke et al., 2013). These

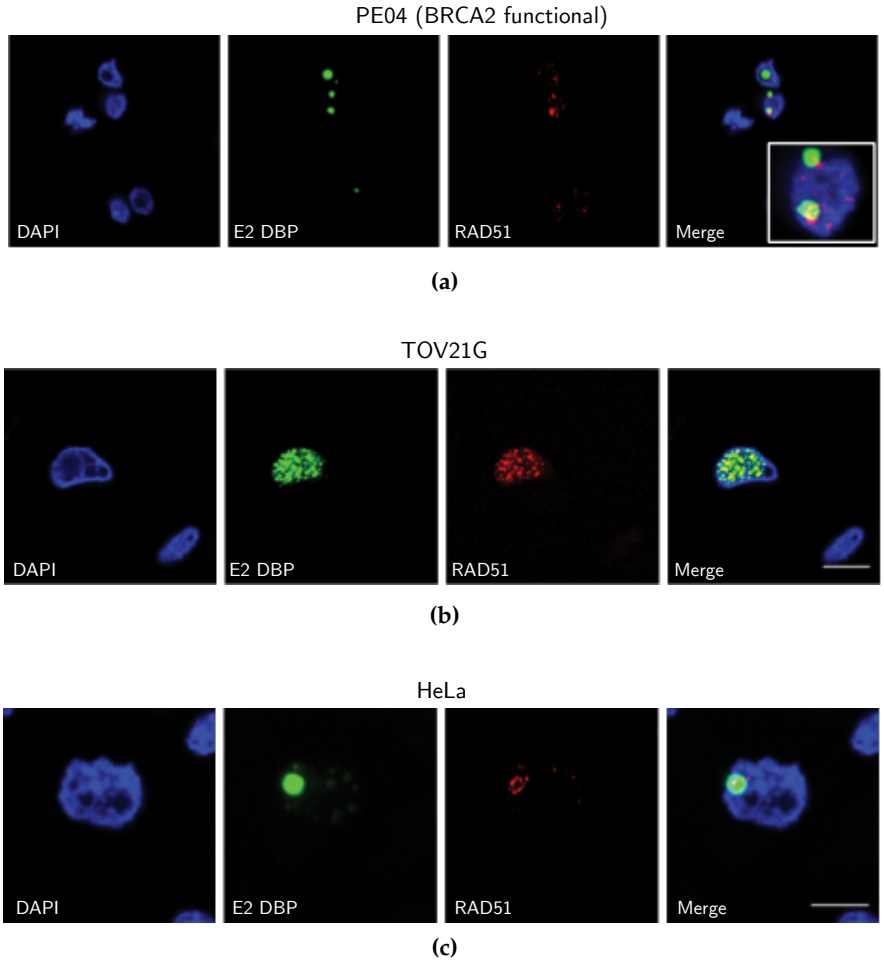

Figure 4.26: RAD51 co-localises with viral replication centres in HR competent cells. PE04 **(a)**, TOV21G **(b)**, and HeLa cells **(c)** were infected with *dl*922-947 (MOI30 for PE04, MOI 10 for HeLa and TOV21G). 24 hours following infection cells were fixed in 4% PFA. Expression of adenovirus E2 DNA binding protein and RAD51 was assessed by confocal microscopy. Scale bar = 10 μm.

cells were unable to form RAD51 foci following PARP inhibition (Figure 4.28a) and were therefore HR defective (Figure 4.28b). Consistent with the finding in PE01 cells, IGROV1 cells also revealed co-localisation between viral replication centres and RAD51 in infected cells (Figure 4.29).

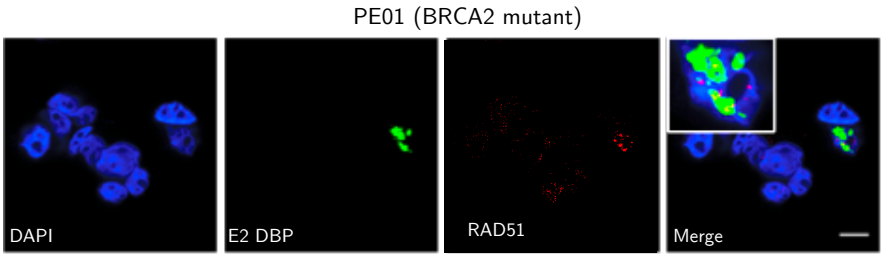

Figure 4.27: RAD51 co-localises with viral replication centres in the BRCA2 mutant, HR incompetent, PE01 cells. PE01 cells were infected with *dl*922-947 (MOI 300). 24 hours following infection, cells were fixed in 4% PFA. Expression of adenovirus E2 DNA binding protein and RAD51 was assessed by confocal microscopy. Scale bar = 10 μm.

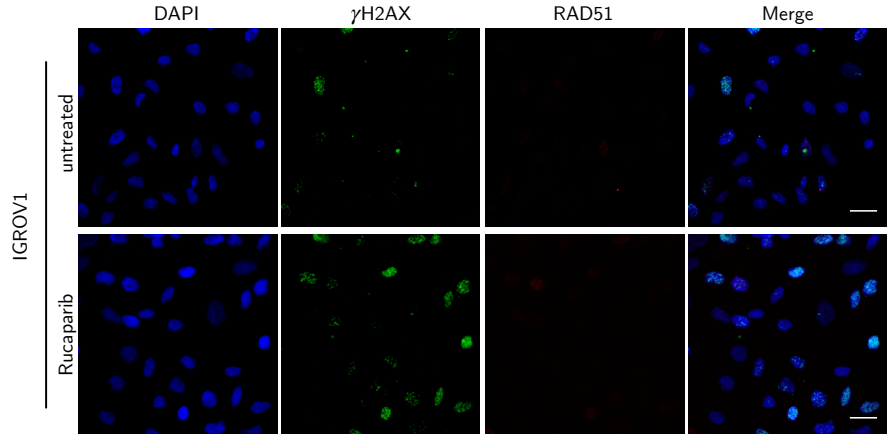

(a)

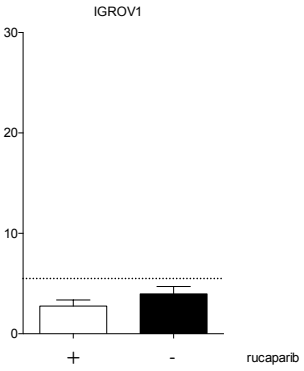

(b)

Figure 4.28: Assessment of HR function in IGROV1 cells. **(a)** 24 hours following treament with rucaparib, IGROV1 cells were permeabilised, fixed in 4% PFA and stained for RAD51 and γH2AX. Representative image shown. Scale bar = 10 μm.. (b) RAD51 foci were counted in at least 30 nuclei per condition. Bars shown mean (+/- s.d.). Dotted line, 2 × number of foci in untreated cells. No increased in RAD51 foci was seen following treatment with rucaparib.

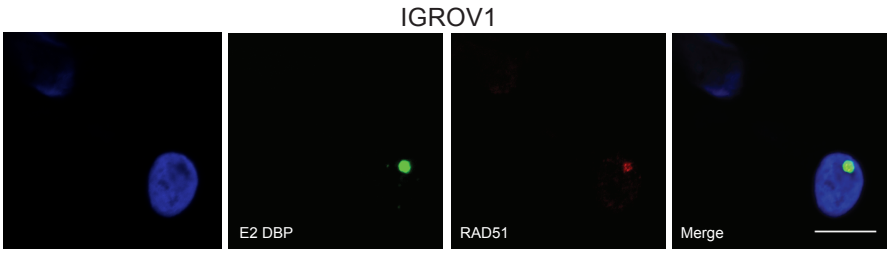

Figure 4.29: RAD51 co-localises with viral replication centres in the the HR incompetent, IGROV1 cell line. IGROV1 cells were infected with *dl*922-947 (MOI 10). 24 hours following infection cells were fixed in 4% PFA. Expression of adenovirus E2 DNA binding protein and RAD51 was assessed by confocal microscopy. Scale bar = 10 μm..

To further assess the interaction between RAD51 and E2 DBP, co-immunoprecipitation was performed in the TOV21G cells following infection with *dl*922-947. This suggested a direct interaction between RAD51 and E2 DBP 24 hours following infection (Figure 4.30).

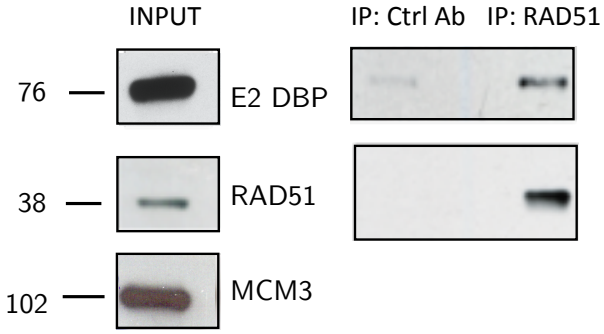

Figure 4.30: Co-immunoprecipitation of E2 DBP with RAD51. 24 hours following infection with *dl*922-947 (MOI 10), TOV21G cells were lysed and incubated with IP matrix beads conjugated to anti-RAD51 antibody (mouse, Santa Cruz, H-92) (IP:RAD51) or control antibody (IP:control). Proteins were then detected by immunoblotting, identifying E2 DBP binding to RAD51. Primary antibodies used for immunoblotting: rabbit anti-Ad5 E2 DBP and mouse anti-RAD51 (Abcam, ab213).

These data show that RAD51 can localise to viral replication centres and that this is independent of recruitment to DNA damage foci.

4.2.13 *RAD51 influences adenovirus efficacy in both HR competent and HR deficient cells.*

To investigate the requirement for RAD51 in viral cytotoxicity, I depleted RAD51 using two different siRNA constructs in both PE01 and PE04 cells and knockdown was confirmed by immunoblot (Figure 4.31).

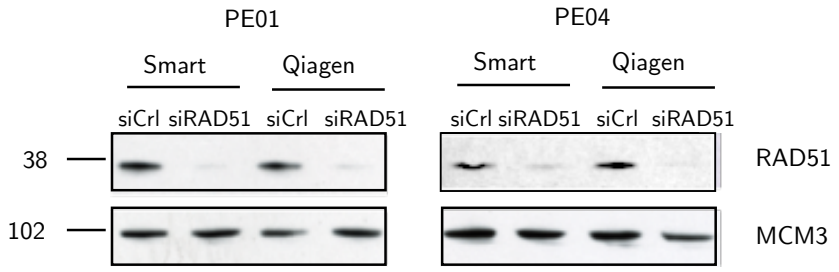

Figure 4.31: Immunoblot showing knockdown of RAD51 in both PE01 and PE04 cells using two different siRNA pools (SMART pool from Dharmacon and single siRAD51 from Qiagen). 48 hours following transfection with siRAD51 or siControl (siCrl), cells were harvested and lysed. Expression of RAD51 was detected by immunoblot; MCM3 was used as a loading control.

RAD51 depletion resulted in significant reductions in the efficacy of *dl*922-947 in both the HR competent PE04 cells (Figure 4.32a) and the BRCA2 mutant PE01 cells (Figure 4.32b). Depletion of RAD51 also caused significant reductions in the efficacy of the E1A wild-type adenoviral vector, *dl309*, in both the HR competent (Figure 4.33a) and HR incompetent cell lines (Figure 4.33b). These findings were recapitulated in HR competent HeLa and TOV21G cells (Figure 4.34a) and (Figure 4.34b) along with the HR defective IGROV1 cells (Figure 4.35).

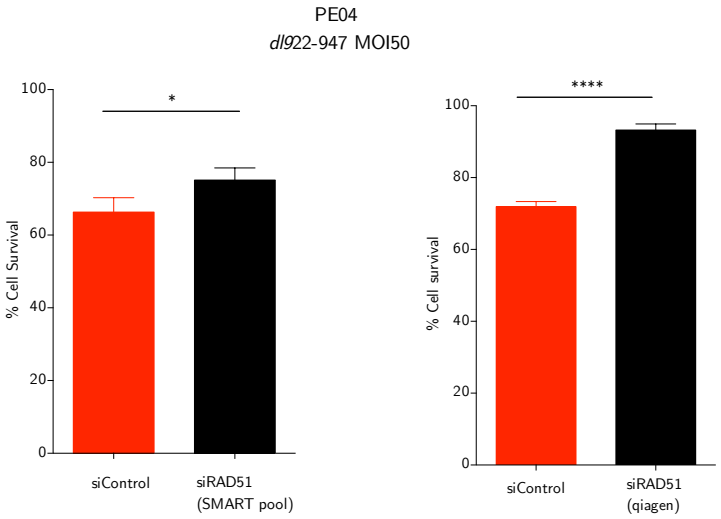

(a)

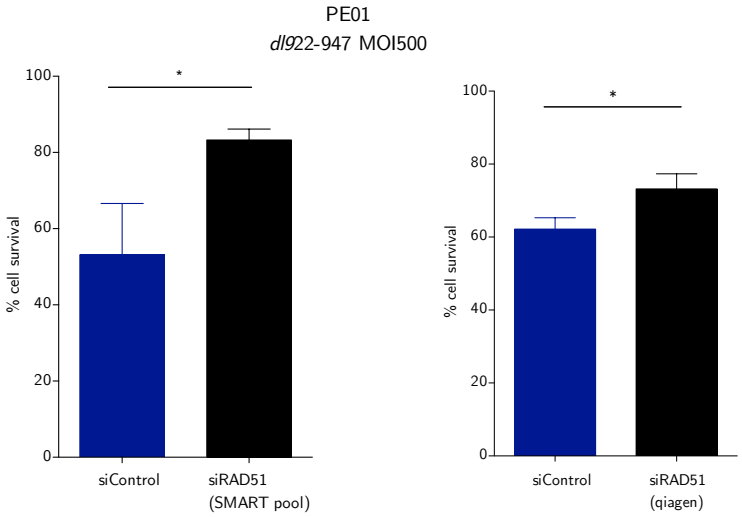

(b)

Figure 4.32: RAD51 siRNA reduces cytotoxicity to *dl*922-947 in HR competent and incompetent cell lines. 24 hours following siRNA-mediated RAD51 knockdown (left: SMART pool, right: qiagen) PE04 cells **(a)** and PE01 cells **(b)** were infected with *dl*922-947 (MOI 50 for PE04 and MOI 500 for PE01). Cell survival was assessed 96 hours after infection by the MTT assay. PE04: * p = 0.04, *** p = < 0.0001, PE01: * p = 0.02, 2 tailed t-test.

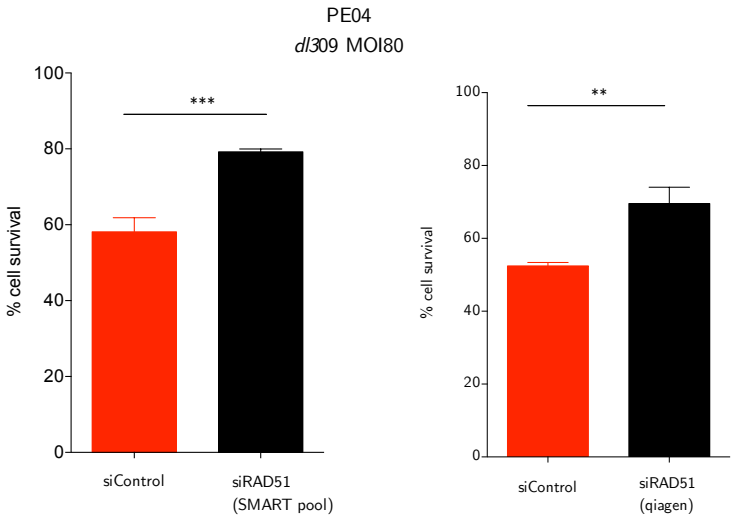

(a)

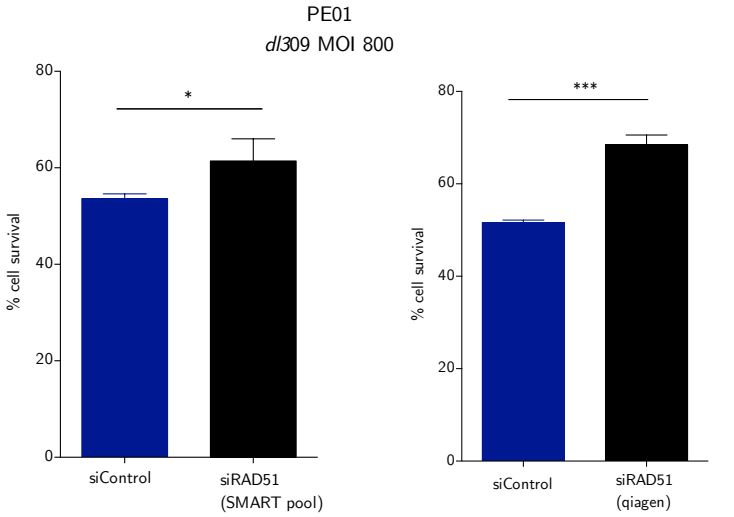

(b)

Figure 4.33: RAD51 siRNA reduces cytotoxicity to *dl309* in the HR competent and incompetent cell pair. 24 hours following siRNA-mediated RAD51 knockdown (left: SMART pool, right: Qiagen) PE04 **(a)** and PE01 **(b)** cells were infected with *dl309* (MOI 80 for PE04 and MOI 800 for PE01) survival was assessed 96 hours after infection by the MTT assay. PE04: *** p = 0.0007, *** p = 0.0028, PE01: * p = 0.045, *** p = 0.0002 2 tailed t-test.

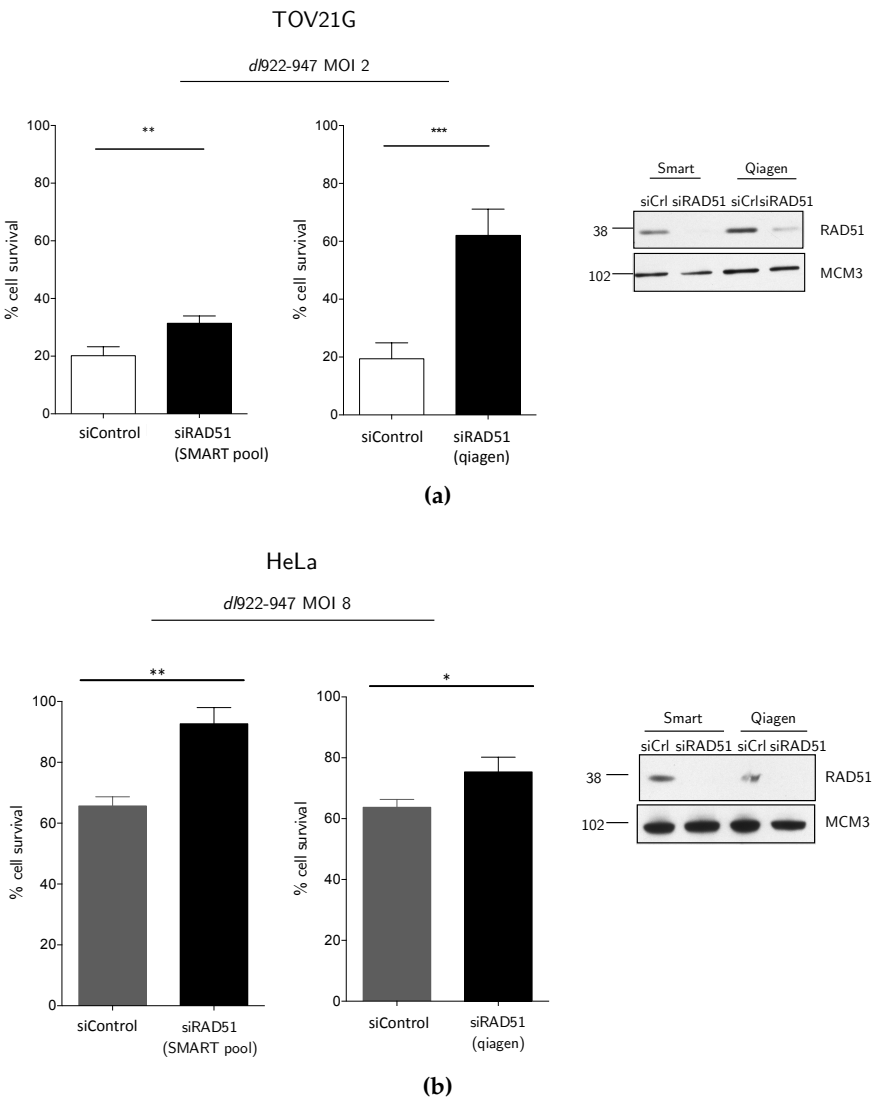

Figure 4.34: RAD51 knockdown reduces cytotoxicity in HR competent cell lines. 24 hours following siRNA-mediated RAD51 knockdown, TOV21G **(a)** and HeLa **(b)** cells were infected with *dl*922-947 (MOI 1 and 8 respectively). Cell survival was assessed 96 hours after infection by the MTT assay. To ensure knockdown was achieved, RAD51 knockdown was confirmed by immunoblot: 48 hours following transfection with siRAD51 or siControl (siCrl), cells were harvested and lysed. Expression of RAD51 was detected by immunoblot, MCM3 was used as a loading control. TOV21G: ** p = 0.0084, ***; p= < 0.0001. HeLa: ** p = 0.0016, *; p = 0.02, 2 tailed t-test.

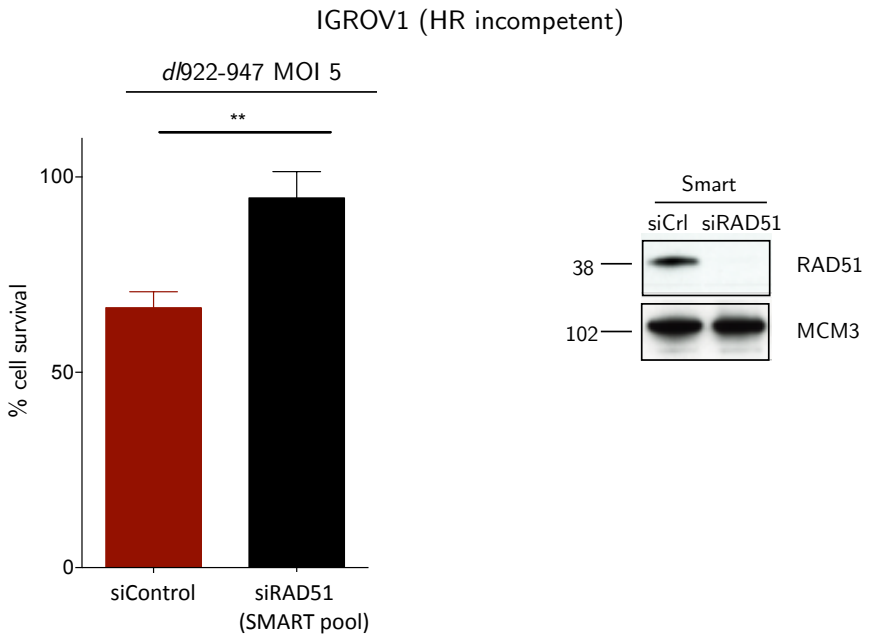

Figure 4.35: RAD51 knockdown reduces cytotoxicity in an incompetent cell line. 24 hours following siRNA-mediated RAD51 knockdown, IGROV1 cells were infected with *dl*922-947 (MOI 5). Cell survival was assessed 96 hours after infection by the MTT assay. To ensure knockdown was achieved, RAD51 knockdown was confirmed by immunoblot: 48 hours following transfection with siRAD51 or siControl (siCrl), cells were harvested and lysed. Expression of RAD51 was detected by immunoblot, MCM3 was used as a loading control. ** p = 0.0035 2 tailed t-test.

4.2.14 *RAD51 influences adenovirus replication in both HR competent and HR deficient cells.*

Investigation of the viral lifecycle of *dl*922-947 in the HR incompetent PE01 cell line and the HR competent PE04 cells revealed a significant increase in viral DNA in the more sensitive PE04 cells (Figure 4.11). To further assess whether the increase in viral replication is due to the presence of functional HR, viral DNA in infected cells was as-

sessed following depletion of RAD51. SiRNA-mediated knockdown of RAD51 resulted in reduced viral replication in both the HR competent PE04 cells (Figure 4.36a) and the HR competent TOV21G cells (Figure 4.36b). RAD51 depletion also resulted in reduced viral replication in the HR incompetent PE01 cells (Figure 4.36c). These results suggest that presence of RAD51, a key component of the HR pathway, results in more efficient viral replication.

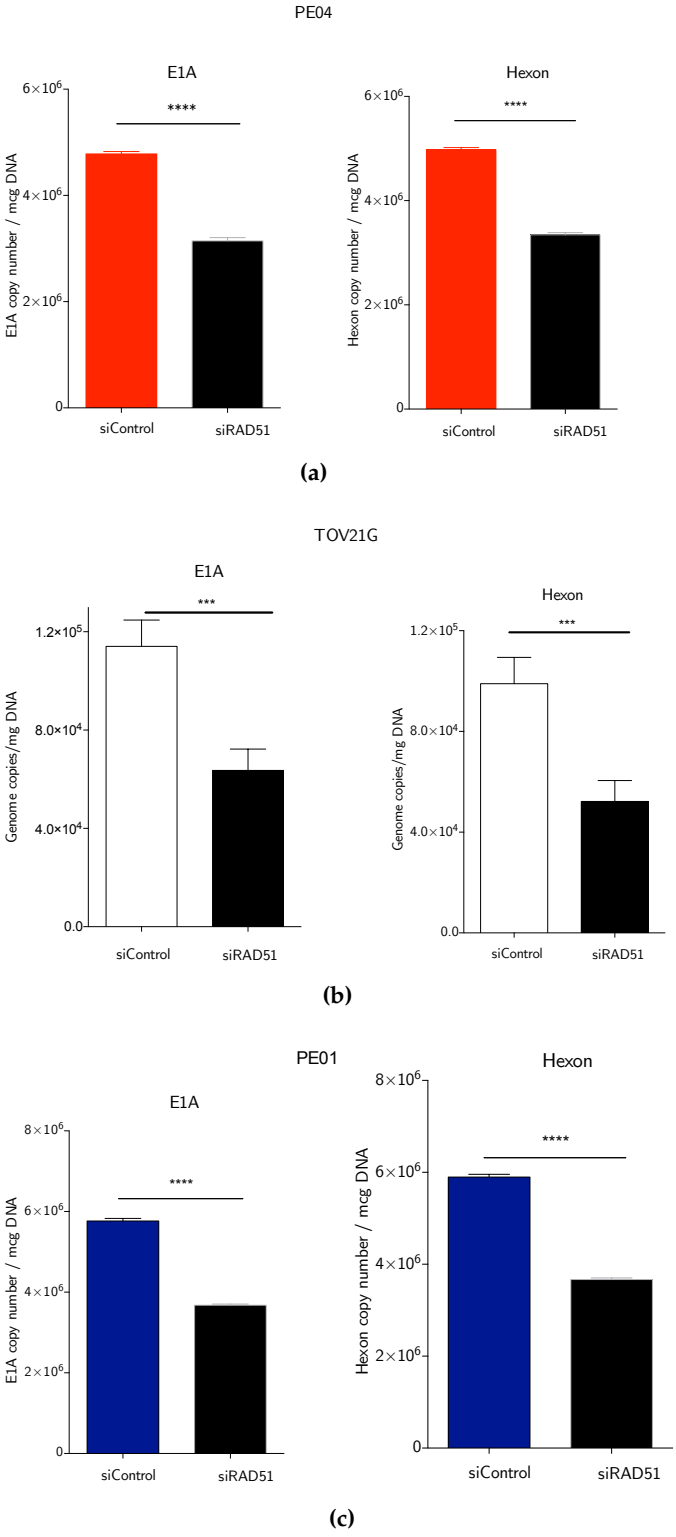

Figure 4.36: Viral replication is reduced following knockdown of RAD51. PE04 **(a)**, TOV21G **(b)** and PE01 **(c)** cells were infected with *dl*922-947 (MOI 100 for PE01 and MOI 10 for TOV21G and PE04). 24 hours after knockdown of RAD51 with SiRNA. Cells were harvested 48 hours later, DNA extracted and early and late viral proteins (E1A and Hexon) were assessed by quantitative PCR. **** p = < 0.0001, ***; p = < 0.0001, 2 tailed t-test.

4.2.15 *dl922-947 does not inhibit HR function in HR competent cell lines*

To assess whether adenovirus infection impaired the capacity of cells to repair DNA DSBs by HR, I first analysed RAD51 and γH2AX foci by confocal microscopy. In HR competent cells infected with *dl*922-947, RAD51 was able to localise, at least partially, to sites of DNA DSB damage, suggesting that HR function remains grossly intact following adenovirus infection (Figure 4.37). This functionality was further assessed using a fluorescence reporter assay , which incorporates a green fluorescence protein reporter (DR-GFP) as a repair substrate into the genome and assays non-crossover gene conversion events in response to DNA DSB damage (see Section 2.11 for full details). The HR competence of PE04 cells was again confirmed by this assay, with a significant increase in GFP events following expression of I-SceI compared to control plasmid, whereas PE01 showed no increase (Figure 4.38a). To investigate the effect of adenovirus infection on overall HR function, this assay was repeated 48 hours after infection with *dl*922-947 — results again showed that PE04, but not PE01, was able to repair I-SceI-induced DNA DSB damage using HR (Figure 4.38b). This implies that Ad5 infection does not functionally impair homology-mediated repair.

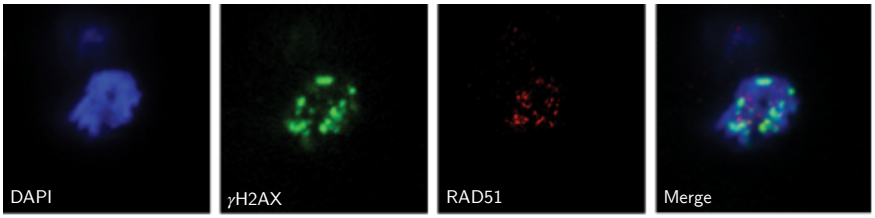

Figure 4.37: γH2AX and RAD51 foci following infection with *dl*922-947. PE04 cells were infected with *dl*922-947 (MOI 10). 24h post-infection, cells were fixed. Expression of γH2AX and RAD51 was assessed by confocal microscopy. Representative image shown.

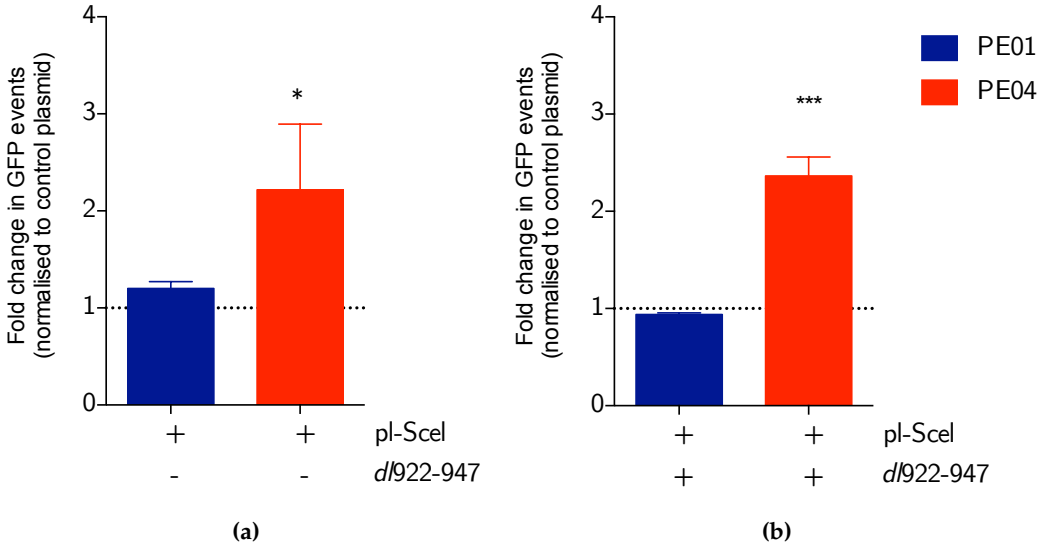

Figure 4.38: *dl*922-947 infection does not alter the function of HR. **(a)** PE01 and PE04 cells stably expressing DR-GFP plasmid were transfected with a plasmid encoding the rare cutting endonuclease (pI-SceI) or control plasmid. 24 hours thereafter, expression of GFP was assessed by flow cytometry. Data show fold change in GFP positive events following pI-SceI transfection relative to control plasmid (dotted line). Bars represent mean +/- s.d. * $p < 0.05$ compared to control plasmid transfection. No change in GFP events were seen in the PE01 cells following pI-SceI transfection confirming HR incompetence. In contrast, a 2 fold increase in GFP events was seen following pI-SceI transfection confirming their HR competence. **(b)** PE01 and PE04 cells stably expressing DR-GFP plasmid were infected with *dl*922-947 (MOI 50 and 500 respectively). 24 hours later, they were transfected with pI-SceI or control plasmid. 24 hours thereafter, expression of GFP was assessed by flow cytometry. The presence of *dl*922-947 did not change GFP events following plasmid trasnfection. Data again show fold change in GFP positive events following pI-SceI transfection relative to control plasmid (dotted line). Bars represent mean +/- s.d. ***: $p < 0.001$ compared to control plasmid transfection 2 tailed t-test.

As previously stated, loss of HR function makes cells sensitive to PARP inhibitor and cisplatin treatment. To further confirm that *dl*922-947 does not impair HR, PEo4 cells were treated with the PARP inhibitor rucaparib or cisplatin 24 hours following *dl*922-947 or mock infection: the presence of *dl*922-947 was unable to sensitize PEo4 cells to rucaparib (Figure 4.39a) or cisplatin (Figure 4.39b). This again implies that HR function remains intact following Ad5 infection.

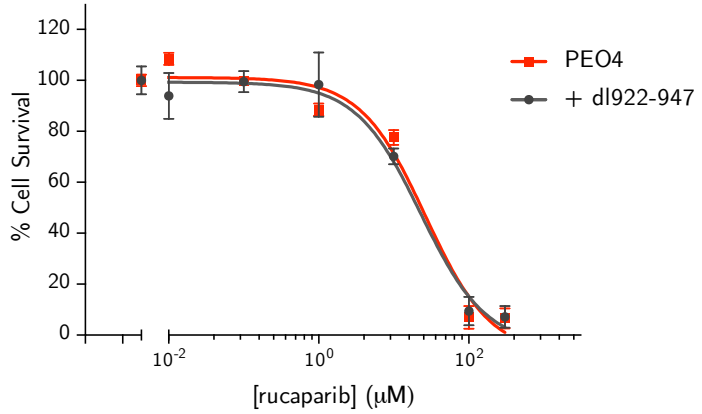

(a)

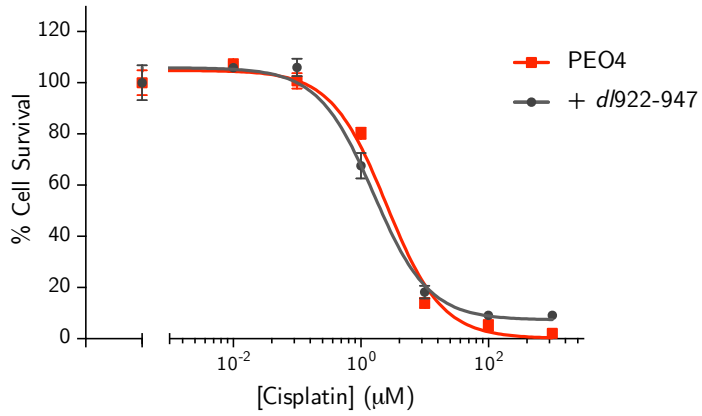

(b)

Figure 4.39: Adenovirus infection does not increase sensitivity to PARP inhibitor or cisplatin. PEo4 cells were infected with *dl*922-947 (MOI 50) and 24 hours later treated with rucaparib (0.01 – 300 μM) for 72h **(a)** or cisplatin (0.01-1000μM) for 72 hours **(b)** No change in the cells' sensitivity to PARP inhibitor or cisplatin was seen.

Together, these results indicate that Ad5 vectors do not inhibit HR function in infected cells — rather, components of the HR machinery localise to VRC and bind directly to E2 DBP. This interaction promotes viral DNA replication and increases overall cytotoxicity.

4.3 DISCUSSION

In this chapter I show that components of the HR pathway required for DNA DSB repair significantly influence the activity of Ad5 vectors. Using matched BRCA2 mutant and functional ovarian cancer cells, I show that the activity of both E1A wild-type (*dl309*) and E1A CR2-deleted (*dl*922-947) Ad5 viruses is greater in the presence of functional HR, with increased cytotoxicity and viral DNA replication. I have shown that BRCA2 co-localises with VRC within the nucleus. These results were recapitulated in other malignant cell lines, HeLa and TOV21G, that are BRCA2 wild-type and HR competent. I have also demonstrated that RAD51, a key partner of BRCA2, also influences Ad5 activity. Interestingly I also show that RAD51 influences adenovirus activity and locates to VRC in the absence of functional BRCA2.

Genomic analysis have shown that HR is vitally important in the biology of HGSOC (TGCA, 2011). Studies have shown a distinct clinical phenotype associated with HR proficient compared to HR deficient tumours. BRCA mutated ovarian cancer patients demonstrate superior response to platinum chemotherapy and longer platinum-free durations than wild-type BRCA ovarian cancer patients with BRCA2 mutation carriers having the best prognosis (Yang et al., 2011; Bolton et al., 2012). In contrast, tumours with intact HR are less likely to respond to platinum-based chemotherapy (Mukhopadhyay et al., 2012) and PARP inhibitors (Bryant et al., 2005) and in BRCA mutated cancers, secondary mutations that result in gain of function of BRCA1 or BRCA2 are associated with platinum resistance (Sakai et al., 2008;

Swisher et al., 2008). Thus, an understanding of the interaction between DDR pathways and any novel therapy, including oncolytic adenovirus therapy, is particularly important. Investigation of these pathways and in particular the HR pathway could aid patient selection for future clinical trials and open up opportunities to enhance the effiacy of treatments.

HR is one of two main mechanisms that repair highly toxic DNA DSBs. HR uses the undamaged sister chromatid to carry out high fidelity repair of predominantly replication-associated DSBs (Daley et al., 2013) and therefore can only function during S and G2 phases of the cell cycle when an intact sister chromatid can serve as a template for repair (Branzei and Foiani, 2008). Although this pathway repairs only a minor proportion of DSBs, it is important becauses it is high fidelity and crucial for the maintenance of genomic stability (Moynahan and Jasin, 2010). HR also deals with stalled and collapsed replication forks (Carr and Lambert, 2013; Petermann et al., 2010). HR is a complex process involving multiple proteins. RAD51 catalyses the defining step of HR: strand exchange, during which single stranded DNA invades homologous duplex DNA, displacing the identical strand of the duplex and forming a displacement loop (Sung, 1994; Baumann et al., 1996). BRCA2 is critical as it mediates the loading of RAD51 onto 3'-single strand DNA overhangs (created by CtIP ond MRE11 nuclease activity), creating a RAD51 nucleoprotein filament (Jensen et al., 2010). The nucleoprotein filament then catalyses the critical step of HR, strand invasion and homology search on the intact sister chromatid .

In contrast to HR, NHEJ represents the major DSB repair pathway in mammalian cells. NHEJ ligates DSBs with minimal end processing. It is not error free but it is active in all phases of the cell cycle, predominating in Go and G1 (Lieber, 2010; Branzei and Foiani, 2008). The core NHEJ proteins are Ku70, Ku80, DNA-dependent protein kinase catalytic subunit (DNA-PKcs), Artemis and DNA ligase

4. How cells choose between NHEJ and HR repair is a subject of intense interest. Clearly, cell cycle is a vital determinant, with NHEJ dominant in G1 (Delacôte and Lopez, 2008; Shrivastav et al., 2008). However, other factors play a part in pathway choice. For example, factors that inhibit resection such as the Ku heterodimer (Fattah et al., 2010) and 53BP1 (reviewed in Panier and Boulton, 2014) will favour NHEJ, whereas CtIP and Mre11 nuclease promote resection and therefore HR (Symington and Gautier, 2011). The complexity of DNA DSB damage is also a significant determinant of repair pathway choice. In S/G2 phase, data suggest that NHEJ initially attempts repair but if rapid end-joining does not occur, resection occurs promoting HR repair (Shibata et al., 2011). The repair of cellular DSBs is therefore a complex process that has many levels of control and its ultimate aim is to maintain integrity of the genome (Friedberg et al., 2006). Although results from this chapter and the previous one show that the DDR is clearly activated following infection with *dl*922-947 whether the repair pathways downstream of H2AX phosphorylation are able to repair DSB damage is currently not clear.

The interaction between adenoviral infection and the DDR is complex; in contrast to other forms of DNA damage, such as irradiation, where damage occurs almost instantaneously, viral infection represents a dynamic onslaught to the cell, which makes analysis challenging.

Activation of the cellular DDR could be deleterious to viral replication Ad5, therefore, inhibits DDR using a variety of mechanisms. A major target of the virus following Ad5 infection is the MRN complex (comprised of MRE11, RAD50 and NBS1) (Stracker et al., 2002). The MRN complex is inactivated by several mechanisms following Ad5 infection. E1B-55K together with E4orf6 form an E3 ubiquitin ligase complex with the cellular proteins Cul5, Rbx1 and elongins B and C and targets MRE11 for proteosomal degradation (Harada et al., 2002; Querido et al., 2001). A second mechanism is the mis-

localisation of the MRN components by E4-orf3 and E1B-55K from the nucleoplasm to nuclear tracks (Evans and Hearing, 2005) and cytoplasmic aggresomes (Araujo et al., 2005). This both sequesters the MRN complex away from the viral genomes and also results in MRE11 degradation. Consistent with these previous findings, I show that MRE11 expression diminishes following infection with *dl*922-947, in both HR competent and incompetent ovarian cancer cells. Infection by adenovirus also targets the NHEJ pathway by mechanisms such as proteasome-mediated degradation of DNA Ligase IV and inactivation of DNAPK (by viral E4-34kDa and E4-11kDa) (Baker et al., 2007; Boyer et al., 1999a). The results revealed that there is no difference in the NHEJ pathways between the BRCA2 WT and mutant cells. In addition, my Southern blot showed no concatemer formation in either PE04 or PE01 cells, suggesting that viral DNA can be processed correctly regardless of the state of cellular HR competence. The explanation of why the BRCA2 mutant cells are more resistant to viral infection is therefore not due to differences in the ability of the virus to inhibit factors such as MRE11 and the NHEJ pathway. Instead my results indicate that the virus requires functional HR for more efficient replication.

The relocation of other DDR proteins, including RPA32 (Stracker et al., 2005), ATR, ATRIP, RAD9, TOPBP1, RAD17 and hnRNPUL1 (Blackford et al., 2008; Carson et al., 2009, 2003), to VRC following Ad5 infection has been described previously by others. However, it has been unclear whether this relocalisation inhibits DNA damage repair function or whether it is required for viral replication (Turnell and Grand, 2012). In the case of BRCA2 and RAD51, my data suggest the latter, as loss of either protein reduces Ad5 replication. In addition, using three different techniques to assess HR function, my results suggest that the ability of cells to repair DNA DSB damage via HR is not inhibited following Ad5 infection. This reinforces the idea that

Ad5 utilises components of the HR pathway rather than degrading and inhibiting them as is the case with NHEJ.

Other DNA viruses have been shown to require components of the DNA repair pathways for efficient replication. ATM is required for optimal replication of SV40 (Sowd et al., 2013, 2014), Herpes simplex virus-1 (HSV-1) requires ATM and the MRN complex for virus replication (Lilley et al., 2005; Balasubramanian et al., 2010; Alekseev et al., 2014). Proteins involved in HR (RPA32, RAD51 and RAD52) have been shown to localise to EBV VRCs. It has been suggested that the HR proteins may be utilised by EBV to facilitate genome production as depletion of RPA32 and RAD51 inhibits viral DNA synthesis (Kudoh et al., 2009). It is possible that that one of the determining factors in the relationship of viruses to the DDR is the structure of viral DNA and how the DNA is replicated (Turnell and Grand, 2012).

The observation that adenoviral replication is more efficient in the presence of functional BRCA2 and RAD51 may be limited to Ad5 vectors as sensitivity to Ad11 and Ad35 does not vary between BRCA2 WT and mutant cells. Previous data has also demonstrated that substrates amongst the DDR proteins vary with different adenoviral serotypes. For example p53 and MRE11 are not degraded by group B and D viruses (Forrester et al., 2011; Cheng et al., 2011). Why different DNA viruses and different adenoviral serotypes have evolved different approaches to the DDR pathways remains to be understood. Nonetheless, there are features that are common to all DNA viruses. These viruses are able to override cell cycle checkpoints and drive cells into S phase to enable viral replication. Both data from this chapter and the previous one demonstrates the importance of this to viral efficacy. It is also clear that adenoviruses and other DNA viruses go to considerable lengths to manipulate components of the cellular DDR highlighting both the complexity of this interaction and also the importance of understanding this relationship in the development of more effective oncolytic viruses.

Several other key questions remain. First, how do cells retain the apparent capacity to repair DSB damage by HR following the proteasomal degradation of MRE11, which is critical for end-resection? Although MRE11 is clearly critical to end resection, other molecules, in particular CtIP and Exo1, can also fulfill this role (Makharashvili et al., 2014). It is therefore possible that other proteins substitute for the MRE11 end-resection function following Ad5 infection. Also, I show that degradation of MRE11 is not complete — thus, there may be a dosage effect whereby the remaining MRE11 retains sufficient end resection capacity following adenovirus infection. Nonetheless, whatever residual HR capacity remains following infection is still unable to repair virus-induced genomic DNA damage. This may result from both the cell cycle and DNA replication states induced by the virus. Adenovirus infection drives infected cells into an S phase-like state (Cherubini et al., 2006) but genomic DNA replication is clearly disorganised, which may prevent reliable generation of intact sister chromatids. Adenovirus infection overrides multiple cell cycle checkpoints, with appearance of multiple abnormal mitoses (Connell et al., 2008). Thus, cells may slip rapidly through S and G2 phases, thereby precluding HR repair. This re-emphasises the challenge of investigating cellular responses to adenovirus infection, where changes are dynamic and evolve over a period of 48 – 72 hours.

Further unanswered questions include, how do BRCA2 and RAD51 relocate to VRC and which adenovirus proteins drive the process? Also, what exactly is their function in viral replication? Following Ad infection, Ad5E4orf3 is responsible for re-localisation of PML bodies into cytoplasmic tracks (Carvalho et al., 1995; Doucas et al., 1996). It has been proposed that, during Ad infection, MRN complex is initially located to these tracts and then transported to aggresomes where it is degraded (Evans and Hearing, 2005; Araujo et al., 2005). Whether these tracks are also responsible for movement of cellular proteins like RAD51 into VRC is unknown. My immunoprecipitation

suggests a direct interaction between RAD51 and E2DBP. E2DBP is a multifunctional protein: it is involved in the initiation and elongation of viral DNA replication (De Jong and Van der Vliet, 1999) as well as the regulation of early RNA synthesis (Kitchingman, 1995). It is not known whether the interaction with BRCA2 or RAD51 could influence these functions resulting in more efficient viral DNA replication. Unfortunately my attempt at immunoblot and immunoprecipitation of BRCA2 were unsuccessful, so I do not know whether there is also a similar direct interaction with E2DBP. I also do not know whether other viral proteins associate with RAD51 and BRCA2.

Interestingly, the role of RAD51 in viral efficacy appears independent of its function in HR as knockdown of RAD51 in HR incompetent cell lines also reduces viral efficacy. My data, however, show that the presence of BRCA2 together with RAD51 results in more efficient viral replication. Adenovirus DNA replication generates a displaced single strand of parental DNA in addition to a duplex formed of a newly synthesised daughter strand plus the other parental strand, a structure that could resemble a replication fork. Previous work has shown that, although functional BRCA2 is necessary for RAD51 focus formation after exogenous damage, it is not required for the formation of S phase-associated RAD51 foci (Tarsounas et al., 2003). Both RAD51 and BRCA2 have recently been shown to protect newly replicated DNA strands at stalled replication forks from degradation (Hashimoto et al., 2010; Schlacher et al., 2011) and this role is independent of their function in HR. It is possible that adenovirus utilises this function of RAD51 and BRCA2 resulting in more accurate and efficient viral DNA replication, and that RAD51 can execute this role alone. Certainly, no BRCA2 homologue has been identified in lower eukaryotes, including *S.cerevisiae* in which RAD51 alone can resolve replication stress (Mozlin et al., 2008). Clearly, adenoviral replication and cytotoxicity can still occur in the absence of BRCA2 and RAD51,

suggesting that these proteins are supportive rather than critical to the adenoviral lifecycle.

In summary, this chapter shows for the first time that adenovirus type 5 re-localises components of the HR pathway to VRC and that viral replication is enhanced in the presence of functional HR. These data suggests that these viruses may have specific activity in poor prognosis ovarian cancers, those with platinum and PARP inhibitor resistance though intact HR function. Given the importance of HR in the biology of high grade serous ovarian cancer, an understanding of the interaction between HR and any novel therapy is particularly important in patient selection for clinical trials and identification of novel virus/drug combinations.

5

HIGH-THROUGHPUT DNA DAMAGE AND REPAIR SCREEN

5.1 INTRODUCTION

HGSOC is characterised by genomic instability and defects within the DNA damage repair pathways. Although these defects contribute to oncogenesis, exploiting these tumour specific defects also offers novel therapeutic targets (Helleday et al., 2008). Targeted therapy based on inhibiting the DDR offers the potential to tailor treatment to patients with tumours lacking specific DDR functions (O'Connor, 2015). The use of PARP inhibitors in HGSOC with defective HR illustrates the single agent activity of DDR inhibitors (Tutt et al., 2010). DDR inhibitors have the potential to augment the efficacy of other therapies such as chemotherapy or radiotherapy and this is being tested both in the preclinical and clinical setting (Curtin, 2012). In addition, chemotherapy resistance may be mediated through changes in the DDR pathways and therefore DDR inhibitors may play a role in reversal of treatment resistance (Curtin, 2012). This chapter investigates whether these concepts can be applied to oncolytic viral therapy and whether there are components of the DDR that can be targeted to enhance the efficacy of *dl*922-947.

Results from Chapter 3 show that the DDR is activated following oncolytic adenoviral infection and there is a close relationship between the degrees of DSB signaling by γH2AX and viral efficacy. Results from Chapter 4 show the importance of the DNA repair pathways and reveal that components of the HR pathway, RAD51 and BRCA2, are utilised in viral replication and that defects within the

this pathway may result in resistance to oncolytic adenovirus. Many other studies have shown that activation of the host DNA repair pathway could be deleterious to viral replication and therefore adenovirus has developed a number of strategies to inhibit these pathways (reviewed in Weitzman and Ornelles (2005)). This highlights the complexities of the interaction between adenovirus and the host cell but also raises the question of whether the DDR can be manipulated to enhance the efficacy of oncolytic virus. This chapter aims to identify components of the DNA damage repair pathway that are synthetically lethal with the oncolytic virus, *dl*922-947. This is achieved by using a high-throughput siRNA screen targeting DNA damage and repair genes.

5.2 RESULTS

5.2.1 *Experimental setup*

The Human DNA repair library Set V1.0 siRNA library (Qiagen, UK) targets 230 known and putative DNA repair proteins. Each gene in the library was targeted by two distinct siRNAs, with one siRNA per well of a 96 well plate. This siRNA library targets over 98% of all known DNA repair proteins. In particular it targets all the major components of BER (21 genes), MMR (11 genes), NER (28 genes), HR (19 genes) and NHEJ (28 genes) plus 15 DNA polymerases (Lord et al., 2008; Wood et al., 2005).

The first step was to identify appropriate cell lines to use in the siRNA screen. OVCAR4 and COV318 cells were chosen as they have been shown to have the characteristic features of HGSOC with copy number alterations and a *TP53* mutation (Domcke et al., 2013). OVCAR4 and COV318 cells both display similar sensitivity to the oncolytic virus *dl*922-947 (Figure 5.1) indicating that comparison of the results between the screens in the two cell lines would be possible.

Both cell lines were able to form RAD51 foci in response to DSB damage induced by rucaparib (Figure 5.2a) and fulfilled the criteria of competent HR by doubling RAD51 foci following rucaparib treatment (Figure 5.2b) (Mukhopadhyay et al., 2010). Consistent with this, these cells have also been shown to be BRCA1 and 2 wild-type (Domcke et al., 2013) and displayed resistance to the PARP inhibitor, rucaparib (Figure 5.3). As expected from a HGSOC cell line, both cell lines displayed sensitivity to cisplatin (IC_{50} OVCAR4 0.5 μM, IC_{50} COV318 2.9 μM) (Figure 5.1). These results indicated that OVCAR4 and COV318 cells would make a good model of HGSOC to use in a high throughput siRNA screen to identify genes that would enhance the efficacy of *dl*922-947.

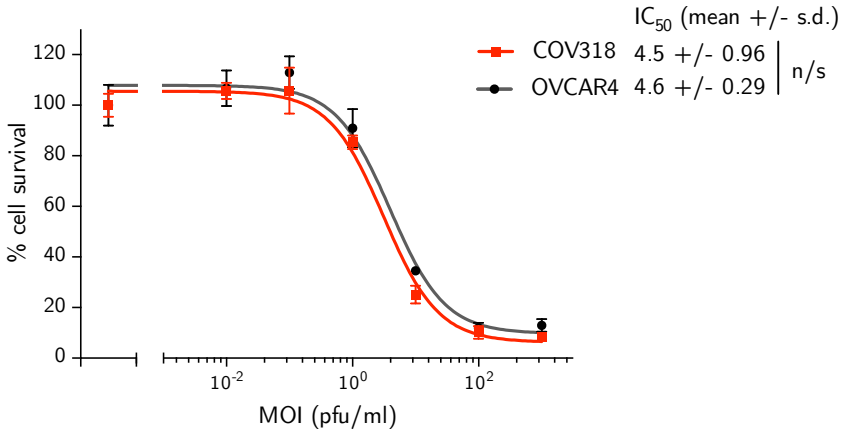

Figure 5.1: Sensitivity of OVCAR4 and COV318 cells to *dl*922-947. 2000 OVCAR4 and 4000 COV318 cells were treated with increasing concentrations of *dl*922-947, cell survival was assessed by Cell Titre glo 120 hours post infection. Results presented as percentage cell survival compared to mock infected cells (mean +/- s.d. n = 3), n/s: no significant difference between the IC_{50} results between the 2 cell lines.

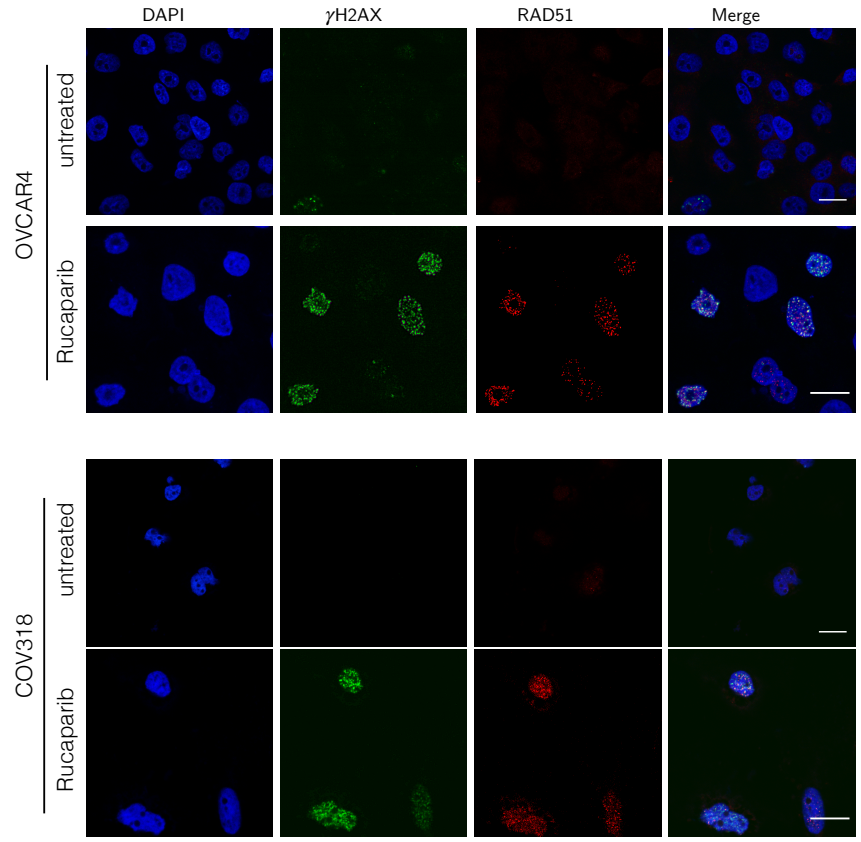

(a)

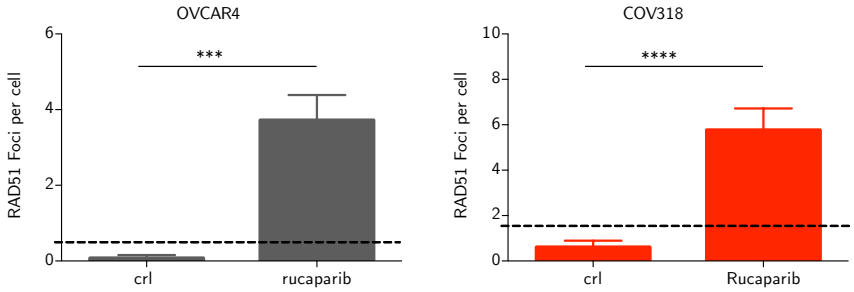

(b)

Figure 5.2: HR competence assessed in OVCAR4 and COV318 cells. **(a)** Cells were treated with rucaparib (10 μM, 24 hours), permeabilised, fixed in 4% PFA, and stained for RAD51 and γH2AX. Representative immunofluorescence image shown. Scale bar = 20 μm. **(b)** RAD51 foci were counted in at least 30 nuclei per treatment condition. Bars show mean (+/- s.d.) number RAD51 foci per cell. Dotted line, 2 $\times$ number foci untreated cells. *** p=0.001, ****p<0.0001, 2 tailed t-test

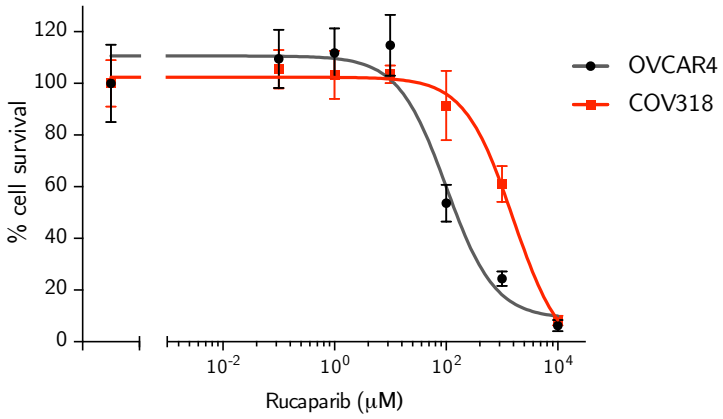

(a)

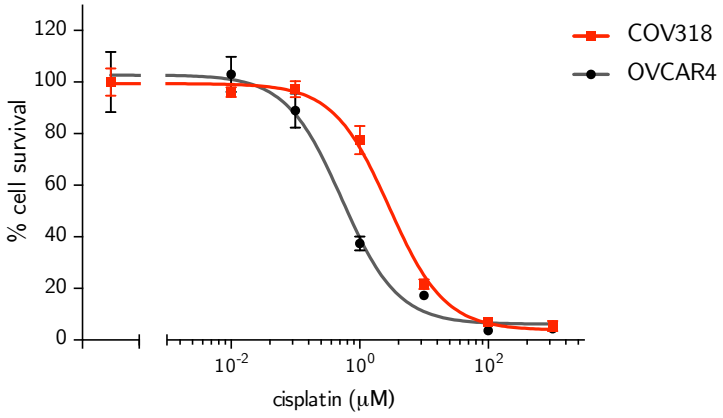

(b)

Figure 5.3: Sensitivity of OVCAR4 and COV318 cells to rucaparib **(a)** and cisplatin **(b)**. 2000 OVCAR4 and 4000 COV318 cells were treated with increasing concentrations of cisplatin or rucaparib in a 96 well plate, cell survival was assessed by Cell Titre glo 120 hours following treatment. Results presented as percentage cell survival compared to untreated cells +/- s.d.

5.2.2 *Optimisation experiments*

A series of optimisation experiments were performed to determine the optimal protocol to perform the siRNA screen. The aim was to identify conditions where the transfection reagent was minimally toxic but yielded efficient transfection. To do this a non-targeting control

siRNA (siCtrl) was used to assess toxicity and siRNA targeting PLK1 assessed transfection efficacy. PLK1 is a polo-like kinase implicated in mitosis and apoptosis; its silencing causes cell death in most cell lines (Liu and Erikson, 2003). From these validation experiments, the conditions that yielded the best results were with 2000 OVCAR4 cells and 4000 COV318 cells per well of a 96 well plate using RNAi max (invitrogen) as the transfection reagent (Figure 5.4).

Next, experiments were performed to identify the appropriate dose of virus to use in the screen. To see both increased efficacy and resistance to *dl*922-947 following siRNA I aimed to have around 60-70% cell death in cells treated with *dl*922-947. Following optimisation experiments, MOI5 was selected as the dose to proceed with (Figure 5.5).

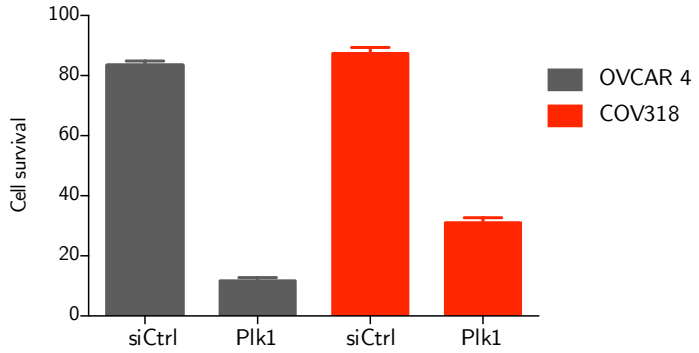

Figure 5.4: Optimisation of transfection reagents. 2000 OVCAR4 cells and 4000 COV318 cells were seeded in 96 well plates. 24 hours later the cells were transfected with RNAi MAX and 50 nM of control siRNA or siPLK1. The medium was changed after 6 hours. 120 hours following transfection cell survival was measured by Cell Titre glo. Data normalised to untransfected cells +/- s.d.

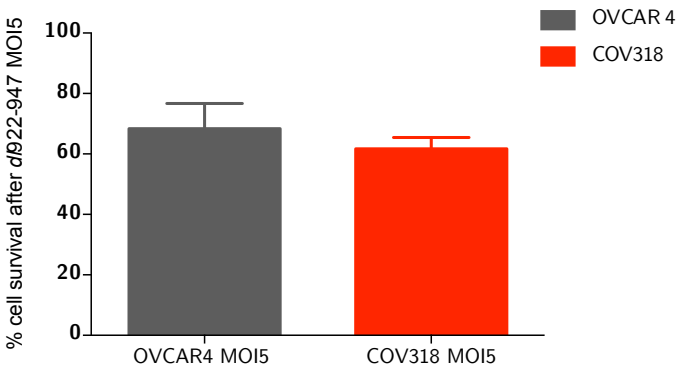

Figure 5.5: Optimisation of dose of virus. 2000 OVCAR4 cells and 4000 COV318 cells were seeded in 96 well plates. 24 hours later the cells were transfected with RNAi MAX and 50 nM of control siRNA. The medium was changed after 6 hours. 24 hours following transfection cells were infected with *dl*922-947 (MOI 5) or mock infected. 96 hours following infection cell survival was measured by Cell Titre glo. Bars represent survival compared to mock infected cells +/- s.d.

5.2.3 *DNA damage and repair screen*

OVCAR4 cells and COV318 cells were plated in 96 well plates (14 plates per cell line) and transfected the following day with the Human DNA repair library. SiCrl and siPLK1 were included on each plate for transfection controls. Medium was changed 6 hours later. 24 hours following transfection cells were infected with *dl*922-947 MOI 5. Cell viability was assessed 96 hours following infection by Cell Titre glo. For full details see materials and methods Section 2.12 and Figure 2.2.

Analysis of the results was performed by calculating Z scores. This is an established method for analysing the output from high throughput screens (Zhang et al., 1999a). Luminescence readings from each well were log transformed and normalised according to the median signal on each plate. These scores were then standardised by the use of a Z score statistic (the MAD score) to estimate variation in each screen. The Z score represents the magnitude of difference between

one siRNA compared to the rest of the screen. This is based on the assumption of a normal distribution of cell viability upon siRNA library transfection in a specific cell line. The screen was completed in duplicate and Z scores were calculated to show the effect of the siRNA in the mock infected wells, the cells infected with virus and a final ΔZ score showing the effect of virus (the difference between the mock and viral infected cells). Negative ΔZ scores represent genes synthetically lethal with *dl*922-947. Positive ΔZ scores represent genes that result in resistance to *dl*922-947 (ΔZ scores for all genes in the screen is shown in Section A.2).

Comparison of the screens revealed a close correlation between the duplicates suggesting good reproducibility (Figure 5.6). OVCAR4 cells show greater correlation between the two screens indicating the results from this cell line are probably more robust than the results from COV318 cells. This difference reflects the more efficient transfection seen in these cells. The final ΔZ score showing the effect due to virus effect was calculated and the duplicates of the screen were combined and are displayed in Figure 5.7a and Figure 5.7b. In addition Figure 5.8 shows the results presented as a waterfall plot. A robust significance or 'hit' threshold was defined as a ΔZ of -2 or less. This threshold is higlighted in figures Figure 5.7a, Figure 5.7b and Figure 5.8 by the red dotted line. Figure 5.8 also shows examples of genes that, when silenced, results in increased sensitivity (negative Z score) or resistance (positive Z score) to *dl*922-947 in both COV318 and OVCAR4 cells.

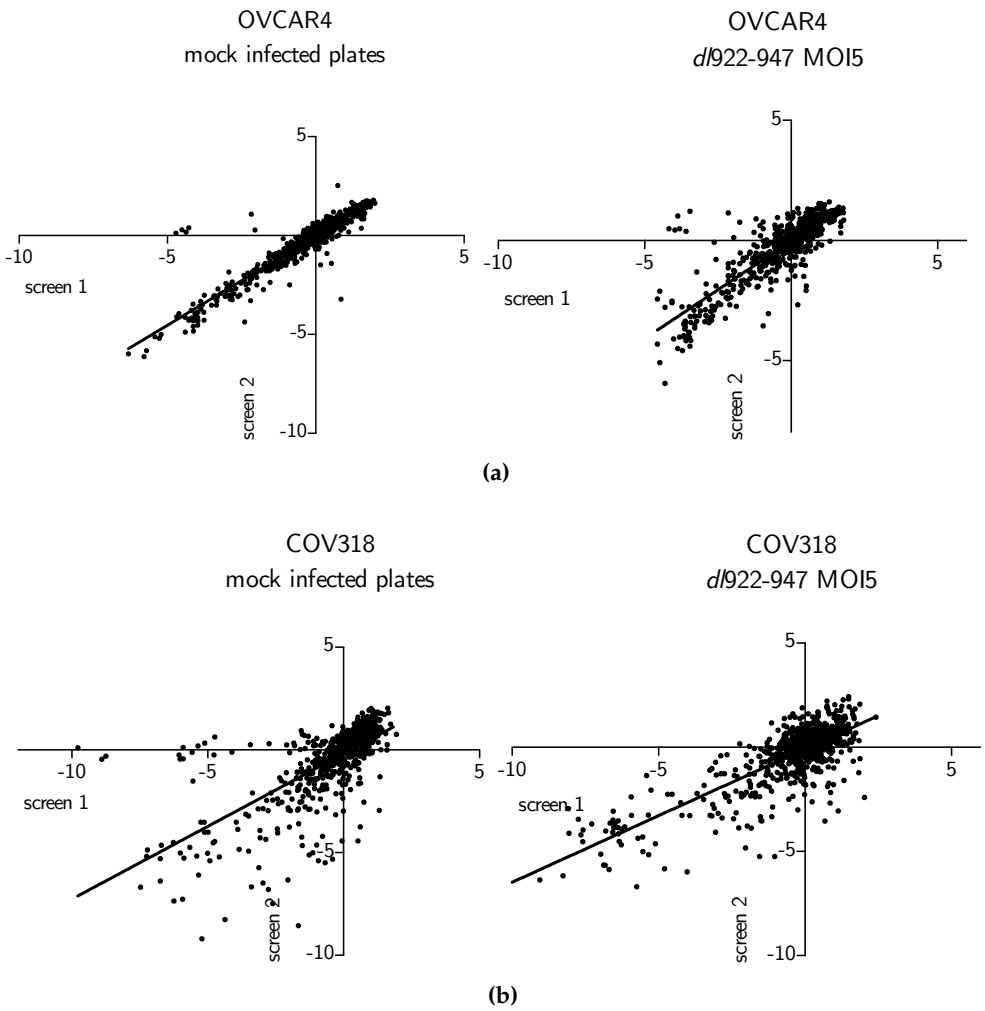

Figure 5.6: Reproducibility of HTS. Correlation of the effect of SiRNA on cell viability in mock infected cells and cells infected with *dl*922-947 (MOI 5) in the duplicate screens. **(a)** Correlation of Z score in OVCAR4 cells in mock infected cells (Spearman r = 0.92, p < 0.0001) and cells infected with *dl*922-947 (Spearman r = 0.81, p < . **(b)** Correlation of Z score in COV318 cells in mock infected cells (Spearman r = 0.72, p < 0.0001) and cells infected with *dl*922-947 (Spearman r = 0.65, p < 0.0001).

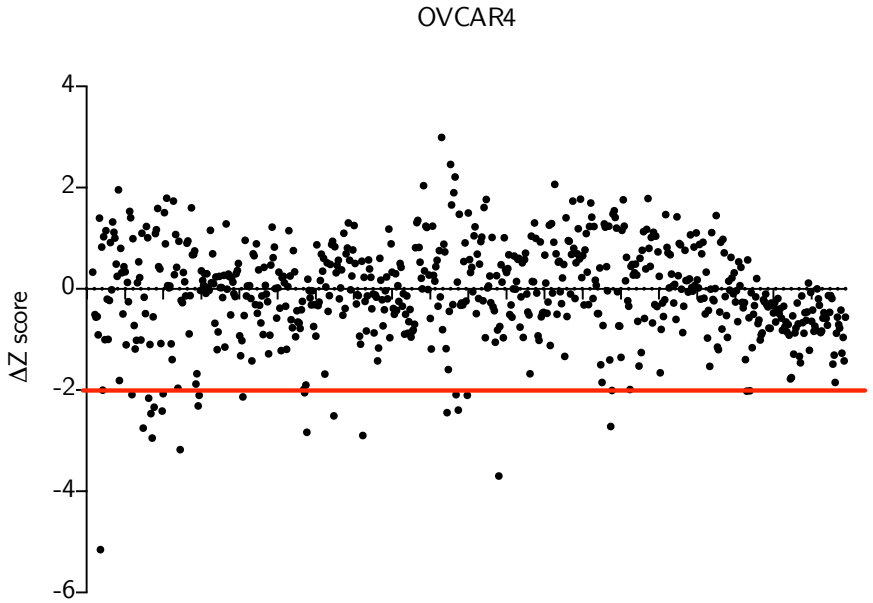

(a)

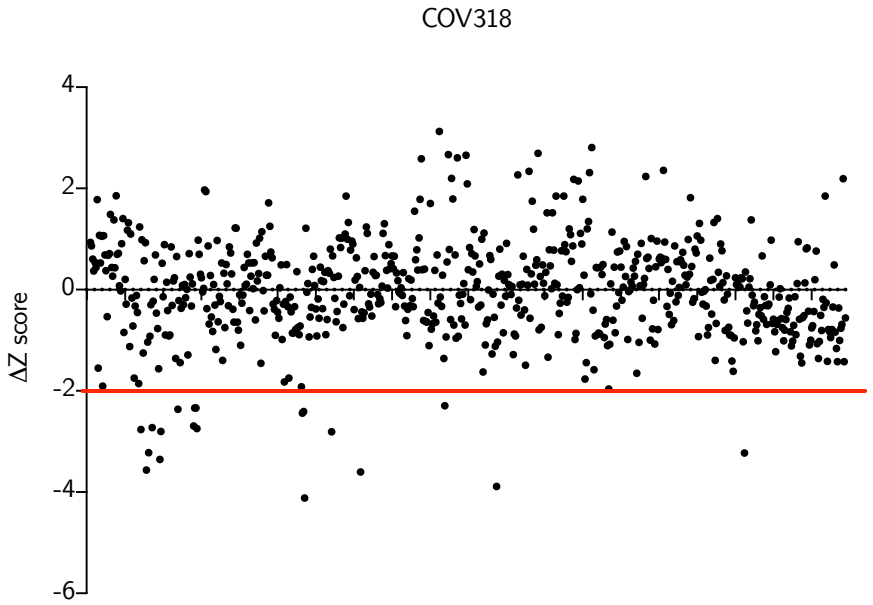

(b)

Figure 5.7: Scatter plot showing average ΔZ scores for virus effect in OVCAR4 cells **(a)** and COV318 **(b)**. ΔZ score of 0 = no change in cytotoxicity to virus; ΔZ score of > 0 = resistance to virus; ΔZ score < 0 increased sensitivity to virus. Red line indicates -2 average ΔZ score significance level.

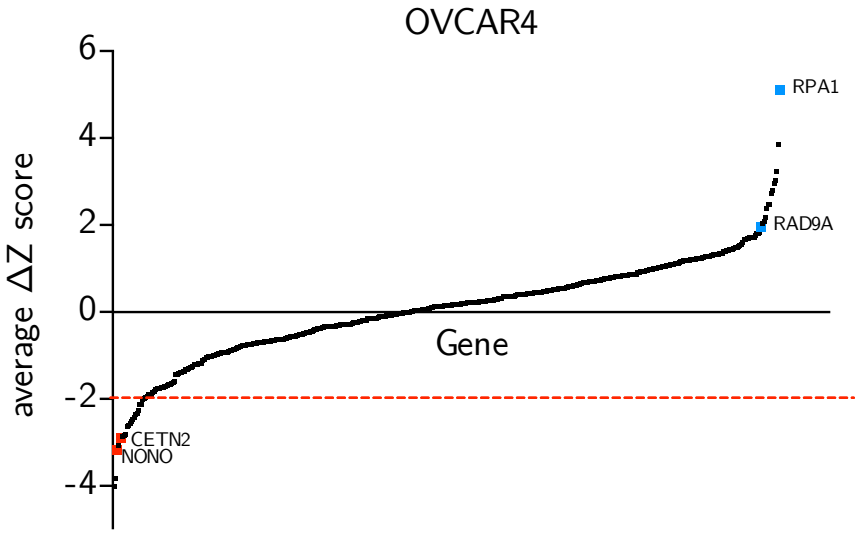

(a)

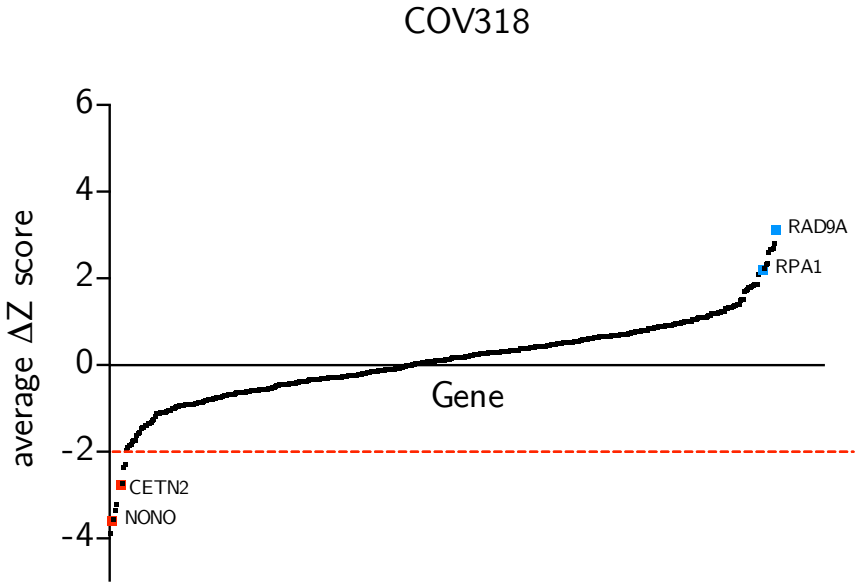

(b)

Figure 5.8: Waterfall plot of Scatter plot showing average ΔZ scores for virus effect in OVCAR4 cells **(a)** and COV318 **(b)**. Red line indicates -2 average ΔZ score significance level. Each point represents the average ΔZ score for each siRNA. Examples of genes that sensitised both OVCAR4 and COV318 cells to virus are shown in red, example of genes that resulted in resistance are shown in blue.

5.2.4 *Hits from screen that resulted in increased sensitivity to dl922-947*

Hits were identified based on a ΔZ score of -2. This identified 5 genes that sensitised both OVCAR4 and COV318 cells to *dl*922-947: *RBM4, CCT5, CETN2, MMP9, NONO, MBD1*. Figure 5.9 shows the ΔZ score for the effect of virus for the individual hits identified for the two siRNAs used in the screen (labelled siRNA1 and siRNA2). Although a good correlation between the effects of the siRNAs was seen in both the cell lines, the two individual siRNAs did not appear to have the same effect. This could be due to one siRNA giving more efficient knockdown or that the effect was due to off target effects of the siRNA. Further validation of these genes is therefore required.

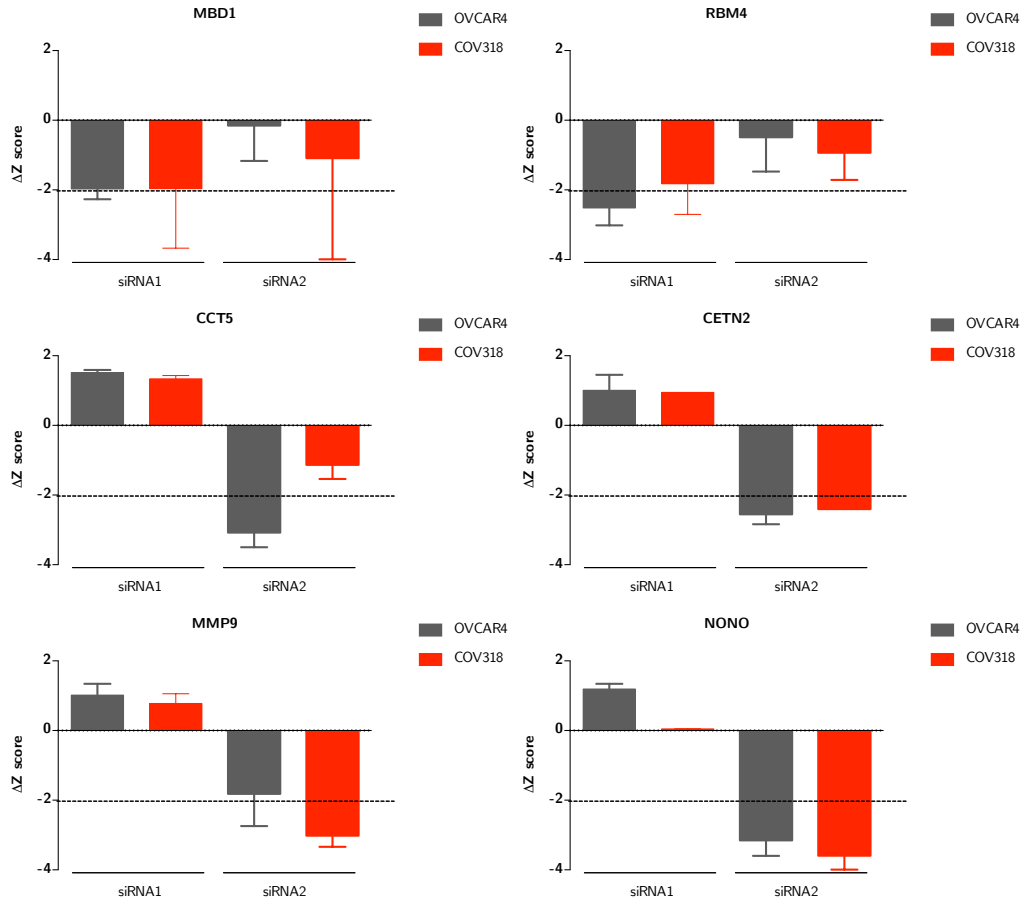

Figure 5.9: Genes selected from the high-throughput siRNA screen that resulted in sensitisation to *dl*922-947. Genes were selected from the screen if the ΔZ score reached -2. Graphs show the average ΔZ score for each siRNA in the OVCAR4 and COV318 cells. Dotted line represents -2 average ΔZ score significance level.

The genes identified as being potentially synthetically lethal with *dl*922-947 have diverse roles as summarised below:

NONO (non-POU domain containing, octamer-binding):

- ssDNA and RNA binding protein (Yang et al., 1993)
- Involved in transcriptional regulation and RNA splicing (Emili et al., 2002).
- Recruited to sites of DNA damage, promotes NHEJ, inhibits HR (Krietsch et al., 2012).

RBM4 (RNA Binding motif protein 4):

- RNA binding protein involved in processes such as alternative splicing of pre-mRNA (Lai et al., 2003) and translation regulation (Lin et al., 2007).
- Required for micro-RNA gene silencing and associates with members of the argonaute family (Lin and Tarn, 2009)

CCT5 (Chaperonin Containing TCP1, Subunit 5)

- Molecular chaperone that is a member of the chaperonin containing TCP1 complex (CCT). The complex folds various proteins, including actin and tubulin (Kubota et al., 1994).

CETN2 (centrin 2):

- The centrins are small calcium binding proteins that are ubiquitous centrosome components (Satisbury, 1995). Centrin 2 is required for centriole duplication and centrioles play a role in organising spindle pole morphology and in the completion of cytokinesis (Salisbury et al., 2002).
- CETN2 is required for efficient Nucleotide excision repair (NER) (Dantas et al., 2012). It stabilises the xeroderma pigmentosum group C responsible gene product (XPC) repair complex and stimulates NER (Araki et al., 2001).

MMP9 (Matrix metalloproteinase 9)

- The MMP family are zinc-dependent endopeptidases that have been shown to play a central role in many normal and pathological conditions including wound healing, angiogenesis, embryogenesis, arthritis and tumor metastasis (Nagase and Woessner, 1999) .
- has also been shown to interact with Ku at the cell membrane of highly invasive hematopoietic cells (Monferran et al., 2004)

MBD1 (Methyl-CpG binding domain protein 1):

- binds to methylated CpG islands and couples DNA methylation to transcriptional repression (Ng et al., 2000)
- has been implicated in gene regulation, chromatin formation and genome stability (Lopez-Serra et al., 2006)
- binds to mediator of DNA damage checkpoint protein 1 (MDC1), which is induced by radiation and regulates NBS1 activation in the presence of DNA damage (Xu et al., 2013).

5.2.5 *Screen hits that resulted in resistance to dl922-947*

I next identified the genes from the screen that showed positive ΔZ scores. This suggests inhibition of these genes results in resistance to *dl*922-947. Despite extensive optimisation of the screen, the virus dose of MOI5 did not result in as much cell death as predicted (less than 10% cell death in one screen) (Figure 5.10). This impacted the ability to see genes that would result in resistance to *dl*922-947. A positive ΔZ score of 1 was therefore used to identify genes that resulted in resistance to virus. Figure 5.11 shows the average ΔZ scores for the two different siRNAs in the OVCAR4 and the COV318 cell lines. Despite the technical difficulties, the screen showed that *RAD51* and *BRCA2* both resulted in positive Z scores, in agreement with the results from Chapter 4. Along with these important HR genes, further HR associated genes were identified - *RAD54L* (Tan et al., 2003), *RAD9A* (Lieberman, 2006) along with *BRCA1*. This adds strength to the results from the previous chapter, that viral replication may involve components of the HR pathway. Interestingly, knockdown of *RPA1* and *RPA3* also resulted resistance to virus (Figure 5.11). RPA is involved early in the repair of DSBs. Following end resection at DSBs, RPA binds to ssDNA prior to RAD51 and is involved in regulating HR repair (Maréchal and Zou, 2015).

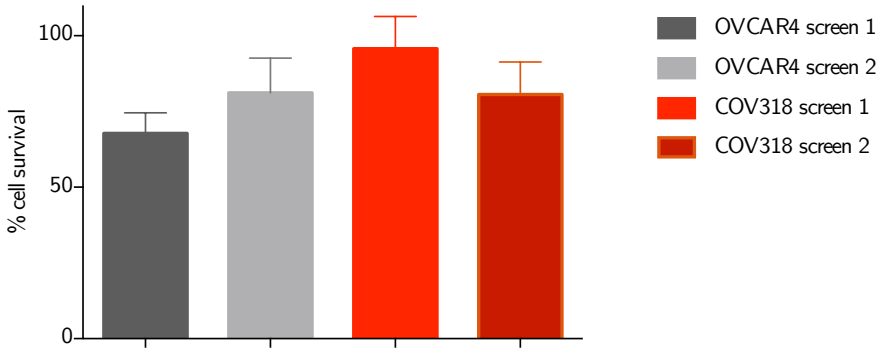

Figure 5.10: Cell survival following infection with *dl*922-947 in the siControl wells. The luminescence values from the siControl wells were analysed from the screen data to determine cell survival following MOI5. Bars represent average percentage cell survival +/- s.d. in siControl wells in all the plates of the screen.

Further genes identified that resulted in resistance to *dl*922-947 were *DDX48* (RNA helicase) and *NUP205* (nucleoporin 205kDa, subunit of the nuclear pore complex) (Figure 5.12). Nuclear pore complexes (NPCs) control transport of macromolecules between the nucleus and cytoplasm (Theerthagiri et al., 2010). NUP205 has recently been shown to be actively dephosphorylated by the Ad5-encoded protein E4orf4 and is required by Ad5 to regulate viral gene expression and efficient viral replication (Lu et al., 2014) (Figure 5.12).

These results may reveal important information about the interaction of oncolytic virus and the host cell and further investigation of these targets may shed further light on adenoviral biology.

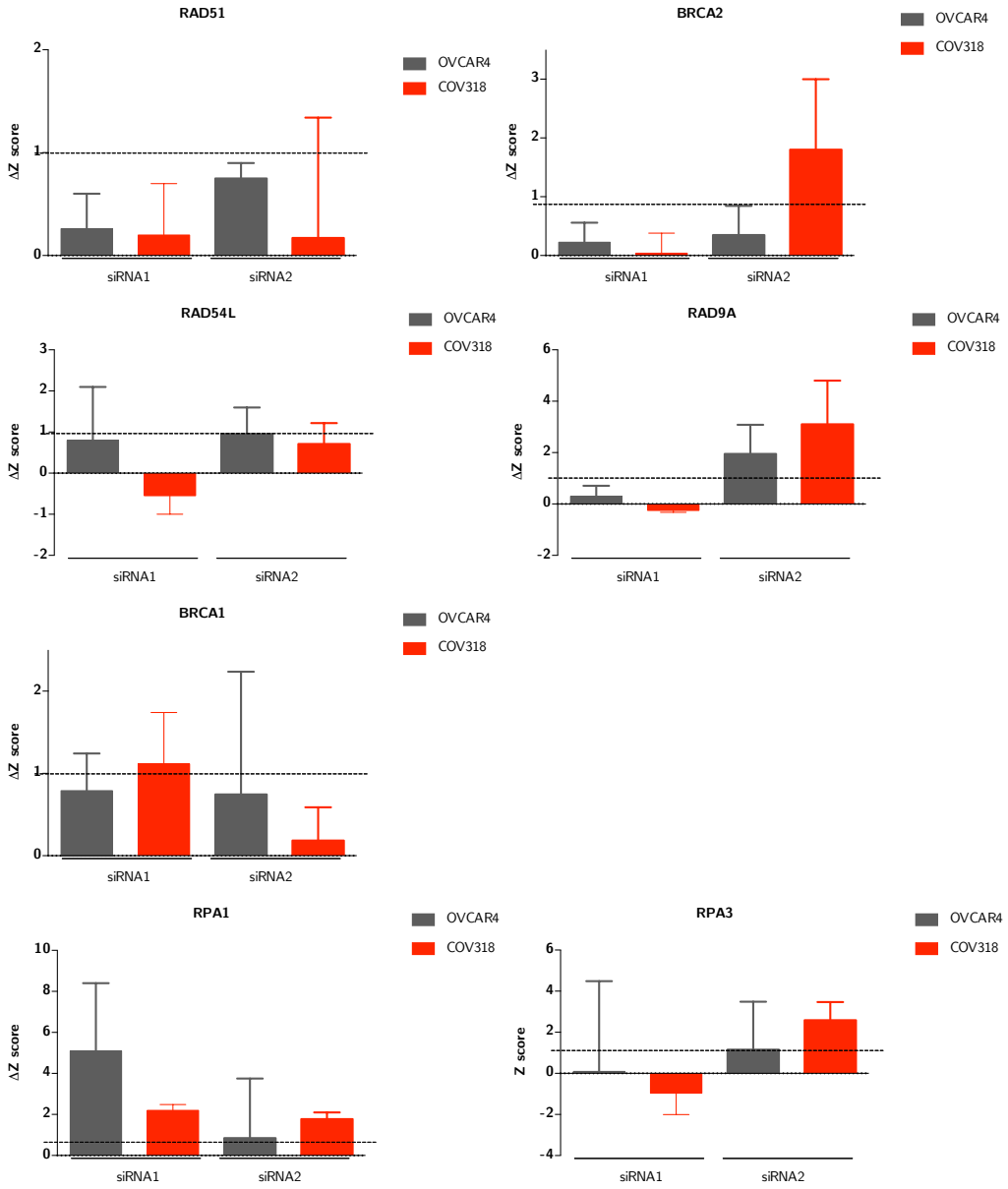

Figure 5.11: Genes selected from the high-throughput siRNA screen that resulted in resistance to *dl*922-947. HR related genes were selected from the screen if the ΔZ score reached 1. Graphs show the average ΔZ score for each siRNA in the OVCAR4 and COV318 cells. Dotted line represents 1 average ΔZ score significance level.

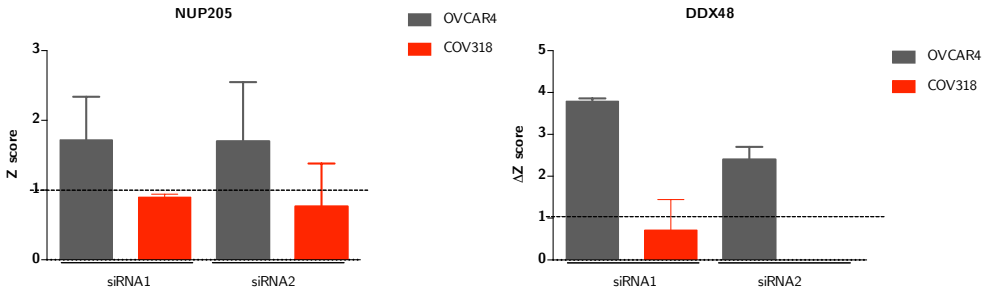

Figure 5.12: Genes selected from the high-throughput siRNA screen that resulted in resistance to *dl*922-947. HR related genes were selected from the screen if the ΔZ score reached 1. Graphs show the average z score for each siRNA in the OVCAR4 and COV318 cells. Dotted line represents 1 average Z score significance level.

5.2.6 *Validation of siRNA hits*

In addition to silencing a target gene, siRNAs potentially suppress the expression of a large number of other genes through off target effects. Therefore, I repeated the HTS assay separately with four individual siRNAs targeting each of the selected genes that sensitised to *dl*922-947 using a custom made 96 well plate from Qiagen. Successful validation of a 'hit' gene would be determined if at least 2 out of the 4 individual siRNAs sensitised to *dl*922-947 (Echeverri et al., 2006).

As shown in Figure 5.13a and Figure 5.13b none of the genes validated using this method. Despite the disappointing results, one of the siRNAs targeting NONO did result in significantly increased cytotoxicity with *dl*922-947 in both the OVCAR4 and the COV318 cells. Further experiments are therefore required to assess the significance of this finding.

There are a number of possible explanations for the lack of consitent positive findings with all the siRNAs. Firstly, it is possible the siRNAs were not achieving efficient knockdown with all of the siRNAs. Alternatively, the effects I saw in the screen were due to off target effects rather than silencing of the gene in question. In addition,

experiments using a 96 well plate to assess viral cell death following siRNA knockdown may not be the ideal format. In the experiments previously performed to look at viral efficacy following siRNA mediated knockdown, optimal results were achieved with a larger number of cells in a 24 well plate (for example: Figure 4.35 and Figure 4.34b). Further validation experiments are therefore required, with assessment of the degree of knockdown by immunoblot in parallel.

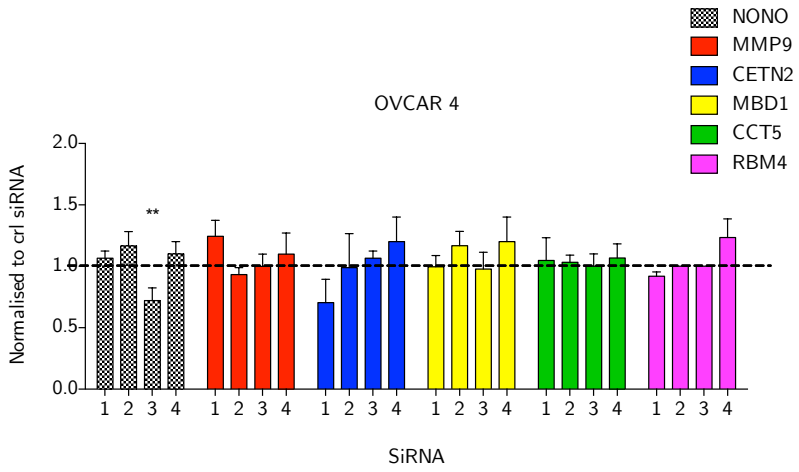

(a)

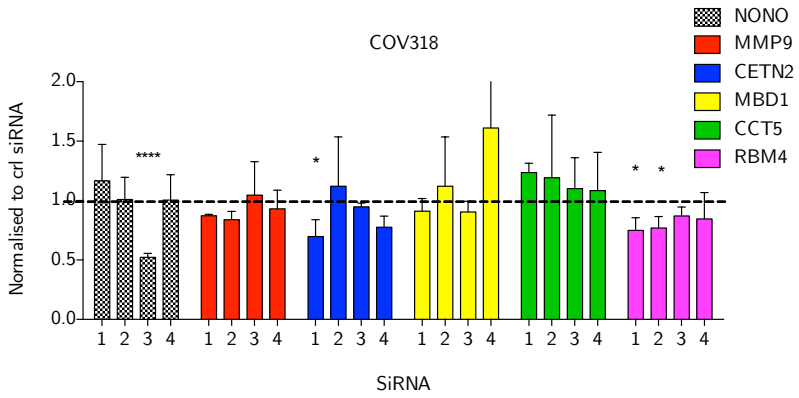

(b)

Figure 5.13: High-throughput screen validation. 2000 OVCAR4 **(a)** and 4000 COV318 **(b)** cells were plated on 96 well plates. 24 hours later cells were transfected with 4 siRNAs targeting each of the genes identified from the screen as 'hits' along with siControl. 24 hours thereafter cells were infected with *dl*922-947 MOI5 or mock infected. Cell viability was measured 96 hours following infection by Cell Titre glo. The bars represent the mean of 3 independent experiments +/- S.E.M. t-tests peformed to compare each individual siRNA to siControl in each cell line: ** $p = 0.0095$, **** $p < 0.0001$, * $p = 0.02$.

5.2.7 *Further validation of hits*

Despite the disappointing results, one of the siRNAs targeting NONO did result in significantly increased cytotoxicity with *dl*922-947 in both the OVCAR4 and the COV318 cells. To assess whether NONO is a novel target that is synthetically lethal with *dl*922-947, I performed further validation experiments. Following from the methods used in the previous chapter, where more reliable results were achieved using a larger number of cells, I repeated the experiment in a 24 well plate. I have also used a SMART pool targeted NONO instead of single siRNAs. Knockdown of NONO resulted in increased cytotoxicity to *dl*922-947 (at MOI 5, 10 and 20) in the OVCAR4 cells (Figure 5.14a). A similar trend was also seen in the COV318 cells although the effects were not as significant (Figure 5.14b). Immunoblot was performed to determine the degree of knockdown of NONO 48 hours following transfection of the siRNA (Figure 5.15). Complete knockdown was not achieved in either cell line. However, there appeared to be a greater degree of knockdown in the OVCAR4 cells compared to the COV318. This may explain why the cytotoxic effect in the COV318 cells was not as significant as in the OVCAR4 cells. These results suggest that NONO is a novel target that is synthetically lethal with *dl*922-947.

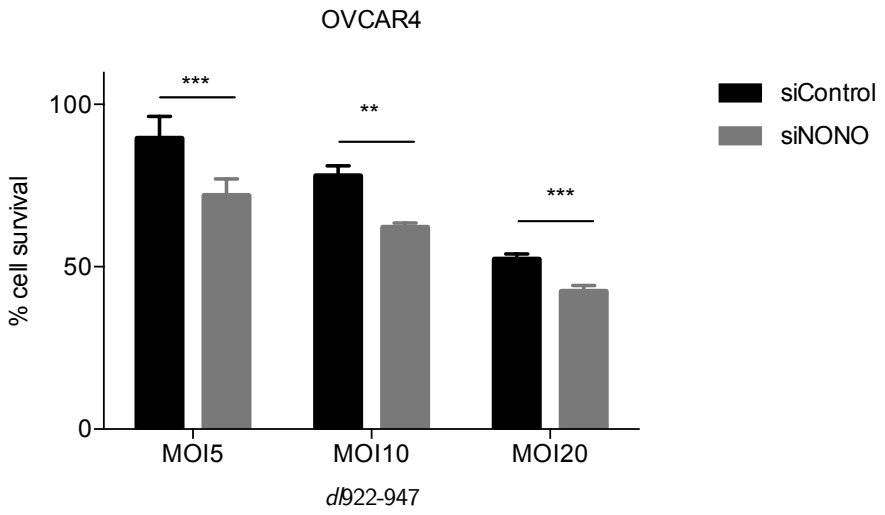

(a)

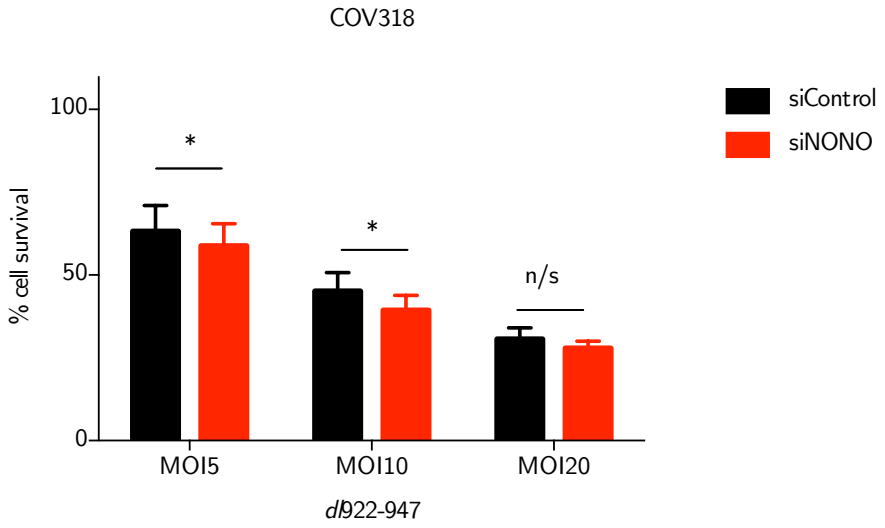

(b)

Figure 5.14: NONO siRNA increases cytotoxicity to *dl*922-947. 24 hours following siRNA-mediated NONO knockdown (using SMART pool) OVCAR4 cells **(a)** and COV318 cells **(b)** were infected with *dl*922-947 (MOI 5). Cell survival was assessed 96 hours after infection by the MTT assay. Bars represent cell survival compared to mock infected cells, (mean of 2 independent experiments +/- s.d.) OVCAR4: *** $p < 0.0007$, ** $p = 0.0047$ COV318: * $p < 0.04$, n/s no signnificant difference between siControl and siNONO, 2 tailed t-test.

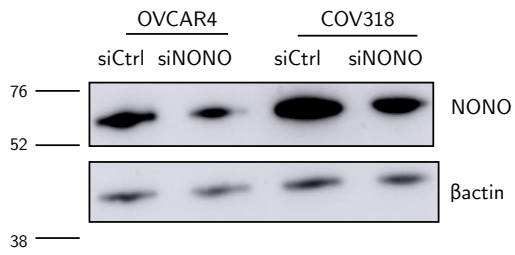

Figure 5.15: Immunoblot showing knockdown of NONO in both OVCAR4 and COV318 cells using SMART pool siNONO from Dharmacon. 48 hours following transfection with siNONO or siControl (siCrl), cells were harvested and lysed. Expression of NONO was detected by immunoblot, βactin was used as a loading control.

Further validation of this result is required. Initially I would like to repeat the above experiment again with the SMART pool but also use at least 2 single siRNAs in a 24 well plate format to confirm the result. Concurrently I would ensure knockdown was achieved at the protein level by immunoblot.

Once validation of the target is achieved, I would aim to assess the mechanism behind how the gene influences adenoviral biology. This would involve assessing aspects of viral lifecycle along with the cellular response following knockdown of the gene. Ideally these experiments would be repeated in further cell lines including both HR competent and incompetent cells.

5.3 DISCUSSION

This chapter demonstrates the use of a high-throughput siRNA screen targeting DNA repair proteins to identify targets that influence the efficacy of the oncolytic virus, *dl*922-947. Using this technique, over 200 genes have been assessed and the results indicate that the DNA binding protein, NONO, may be a novel target that enhances viral cytotoxicity.

High throughput siRNA screens offer a powerful tool for identifying previously unknown targets (Mohr and Perrimon, 2012; Campeau and Gobeil, 2011). However, as these results demonstrate, there are challenges when using this technique. Despite extensive optimisation experiments to identify cell number, transfection reagent and dose of virus, the results from the screen showed inconsistencies. Firstly the two siRNAs within the screen itself did not yield the same results. Then, using 4 different siRNAs to validate the possible hits, sensitisation to *dl*922-947 was not achieved with all the siRNAs used for each gene suggesting that the screen had identified false positive results. False positives (and false negatives) represent a major challenge in high throughput screening (Mohr and Perrimon, 2012). There may be a number of possible explanations for these results. The first is that the effect seen is due to an off target effect rather than knockdown of the gene in question. Off targets effects are a known problem with the use of siRNA (Birmingham et al., 2006). Alternatively, each of the siRNAs used resulted in different degrees of knockdown of the target genes with some being more effective than others. A limitation if the screen is that a single concentration of siRNA was used (50nM). At this concentration, some of the siRNAs might not be able to silence their genes effectively or they might be able to silence their genes but have significant off target effects. There also may be a dosage effect where a certain degree of knockdown is needed to influence viral efficacy but if more or less is achieved this effect is lost. Finally, it is also possible that the format of the experiment may not be optimal for seeing differences in cytotoxicity from virus following knockdown. Viral cell death is acutely sensitive to cell number. In a 96 well plate only 2000-4000 cells are plated per well. This small number of cells need to be both transfected and then infected with virus. Any small variation in cell number may have a significant impact on the end point of viral cytotoxicity.

This screen was only performed in two cell lines. Both OVCAR4 and COV318 have been shown to be representative of HGSOC, however they are also both BRCA1 and 2 wild type and HR functional. Since 50% of HGSOC shows defects within the HR pathway (TGCA, 2011) it would be important to repeat this screen in cells which are HR defective. In cells with loss of one repair pathway, there can be up-regulation or reliance on alternative repair pathways to compensate for the loss (Curtin, 2012). It is therefore possible that further targets may be identified that are synthetically lethal with *dl*922-947 in cells with defective HR.

Furthermore, this screen was only performed at one time-point. The cellular effects of *dl*922-947 are dynamic and evolve over a number of hours (Russell, 2000). The virus interacts with the host cell at all time-points throughout infection from cell entry to viral replication, assembly of new virions and culminating in cell death and release of mature virions (Berk, 2005; Flint and Shenk, 1989). Different cellular genes are required by adenovirus at various times during infection (Berk, 2005) and in addition the host cell mounts a complex antiviral response that evolves throughout infection (Weitzman and Ornelles, 2005). It is possible that assessing cell survival or aspects of viral life-cycle following knockdown of genes at different points following infection would reveal further genes that could influence efficacy to viral cell death. In addition, cell survival was assessed at 96 hours following infection to see maximal viral cytotoxicity. However, this was also 120 hours following knockdown by siRNA. Typically siRNA mediated knockdown are maximal at 48-72 hours (Holmes et al., 2010). In addition, the optimal timing of knockdown of each gene may vary (Perrimon and Mathey-Prevot, 2007). By 120 hours knockdown is likely to be lost (Mocellin and Provenzano, 2004) and therefore the effect on cytotoxicity may not be evident.

Statistical evaluation of the assay performance is a very critical step in high throughput screening data analysis. A number of data anal-

ysis methods have been developed to correct for plate to plate assay variability and systematic errors, and assess assay quality. The main assumption made when analysing this screen data is that the data is normally distributed. A log transformation was applied to the data to achieve more symmetrically distributed data around the mean as in a normal distribution (Goktug et al., 2013). Median and median absolute deviation (MAD) are then used as statistical parameters as opposed to mean and standard deviation, to diminish the effect of outliers on the final analysis results (Goktug et al., 2013; Chung et al., 2008). A Z score (the number of standard deviations from the mean) was then used to normalise data. This indicates the strength of each siRNA relative to the rest of the sample distribution. A limitation to the use of a Z score is that, due to the effect of outliers, weak hits may have been missed (Goktug et al., 2013). In order to correct systematic errors occurring in a plate-specific manner (for example, different cell-growth rates in each well due to evaporation issues that can be seen at the edges of plates) a plate-wise normalisation was also applied to the data (Zhang et al., 2008). Although a number of statistical tests are applied to screen data results, false positives and false negatives remain a recognised problem (Malo et al., 2010). Some researchers recommend alternative statistical tests including trimmed mean polish (Malo et al., 2010) and strictly standardized mean difference (SSMD) (Zhang and Heyse, 2009). As knowledge of the use of high-throughput siRNA screens increases it is likely that the statistical analysis will continue to be refined and optimised.

The hits identified from the screen have diverse roles within the cell including functions within the DDR. Following validation experiments NONO was identified as the most promising gene which displays synthetic lethality with *dl*922-947. Further investigation is required to validate its role in influencing cytotoxicity. NONO (non POU domain containing octamer binding protein) is a multifunctional protein and highly expressed in a variety of cell lines and

tissues (Passon et al., 2012). It has a well documented role in alternative splicing (Emili et al., 2002) and contributes to transcriptional regulation (Rosonina et al., 2005; Kaneko et al., 2007). In addition, it has been shown that a complex of SFPQ (Spicing factor proline/glutamine-Rich) and NONO cooperates with Ku protein at an early step of NHEJ, stimulating end joining activity (Udayakumar and Dynan, 2015). Attenuation of NONO protein expression delays the resolution of γH2AX foci after ionizing irradiation and leads to an accumulation of chromosomal aberrations (Li et al., 2009b). Recruitment of NONO to DNA damage sites has been shown to be completely dependent on PAR, generated by activated PARP1 (Krietsch et al., 2012). Furthermore, upon PAR-dependent recruitment, NONO stimulates NHEJ and represses HR *in vivo* (Krietsch et al., 2012).

NONO has been shown to be highly expressed in breast cancer tissues as compared with the adjacent normal tissues in human patients. It is proposed that through regulation of SREBP 1a (a master activator for genes involved in lipid biosynthesis), NONO supports the increased cellular demand of lipids for breast cancer growth (Zhu et al., 2015). A rearrangement between this gene and the transcription factor E3 gene has been observed in papillary renal cell carcinoma (Clark et al., 1997).

Further experiments are obviously required to investigate role of NONO in influencing cytotoxicity of cells to *dl*922-947. There is currently no published data on the role of NONO in adenoviral biology suggesting that these results may represent a novel finding. It may be that expression of NONO influences adenoviral replication through its ability to up-regulate NHEJ and down regulate HR. It is possible that knockdown of NONO results in stimulation of factors involved in the HR pathway which are subsequently required for viral replication (as shown in Chapter 4). NONO has been shown to play a role in regulating viral gene expression in Epstein Barr virus (EBV). NONO, together with SFPQ, associate with a non-coding RNA produced by

EBV which interacts with the host transcription factor paired box protein 5 (PAX5). This regulates both EBV gene regulation and lytic replication (Lee et al., 2016). These results raise the possibility of whether NONO also interacts with the non-coding viral associated (VA) RNAs in adenovirus.

Despite the limitations of this screen, the results are supportive of the data from Chapter 4. Knockdown of both RAD51 and BRCA2 resulted in resistance to *dl*922-947 along with other genes from the HR pathway, including RAD54L and BRCA1. In addition RPA1 and RPA3 produced similar results. RPA binds to ssDNA prior to RAD51 binding and is both a positive and negative regulator of RAD51 function. BRCA1, BRCA2 and RAD54L also play a role in regulating binding of RAD51 to ssDNA (Shrivastav et al., 2008; Tan et al., 2003; Cousineau et al., 2005). These results imply that it could be the regulation of RAD51 binding to ssDNA that influences viral cytotoxicity.

In summary, these results have identified novel targets that both increase efficacy of oncolytic adenovirus (NONO) and also those which result in resistance to the virus (e.g. RPA). These data illustrate the complex interaction between *dl*922-947 and the cellular DDR and further investigation of these genes may reveal new information regarding the interaction between adenovirus and the host cell. Since the DDR pathway is frequently mutated in ovarian cancer, these results could also lead to the identification of patients who would benefit from oncolytic adenoviral therapy. In addition, knowledge of the genes and pathways involved in determining oncolytic viral cytotoxicity may result in mechanisms to enhance the potency of these viruses and guide appropriate virus/drug or chemotherapy combinations.

Part IV

DISCUSSION

6

DISCUSSION

6.1 A BRIEF SUMMARY

Survival for women with ovarian cancer has changed little since the introduction of platinum based chemotherapy more than 30 years ago (Vaughan et al., 2011). Late stage and recurrent ovarian cancer has a poor prognosis, response to therapy beyond first line treatment is low and chemotherapy resistance represents a major challenge (Korkmaz et al., 2016). There is a need for new and more effective therapies.

Replication competent oncolytic viruses are a novel treatment for human malignancies. These viruses have been engineered such that they take advantage of cancer specific changes for preferential replication in tumour cells resulting in tumour cell death and release of mature virions that go on to infect neighbouring cells. The results presented here show that the E1A-CR2 deleted adenoviral vector, *dl*922-947, has considerable efficacy in ovarian cancer cell lines but sensitivity to viral cytotoxicity varies. This thesis has focused on the role of the DDR in determining the potency of oncolytic virus.

The results demonstrate the importance of both the cell cycle and the DDR. The degree of de-regulation of the cell cycle and the extent of DSB damage that occur following viral infection closely correlate with *dl*922-947 potency. The data reveal that viral replication and cytotoxicity are enhanced in the presence of functional HR pathways and that adenovirus relocalises key components of the HR pathway to VRC. Finally, through the use of a high throughput siRNA screen, additional components of the DDR pathways have been identified that both increased sensitivity to virus (e.g. NONO) and also promote re-

sistance (e.g. RPA). Together these results suggest that viral efficacy is determined, at least in part, by intrinsic properties of the tumour cell's DDR pathways.

Defects within the DDR pathways are common in human malignancies. HGSOC in particular is characterised by genomic instability and defects within the HR pathway. An understanding of the interaction between the DDR and any novel therapy is therefore vitally important for patient selection for clinical trials and identification of novel virus/drug combinations.

6.2 CONCLUSIONS AND FUTURE WORK

Ultimately, the aim of this work is to translate the findings to clinical trials and treatment of patients. Evidence for the clinical use of oncolytic adenoviral therapy has been provided by the E1B-55K deleted adenoviral vector, ONXY-015 (Larson et al., 2015). However, although ONYX 015 demonstrated safety, it did not show significant clinical efficacy as a single agent (Larson et al., 2015). To improve anti-tumour efficacy, ONXY 015 was the first oncolytic virus to be combined with chemotherapy in a clinical trial (Khuri et al., 2000). Local responses were achieved with direct injection of the virus when combined with cisplatin and 5-fluorouracil (5-FU) in patients with head and neck cancer (Khuri et al., 2000). H101 is similar to ONYX-015 and following successful clinical trials, has now been approved for use for treating advanced head and neck cancer in China (Yu and Fang, 2007). This illustrates that oncolytic viruses have the potential to be used as part of the standard treatment in the management of patients with cancer.

There are also a number of notable examples of other non-adenoviral oncolytics that have entered late-phase clinical trials. One of the most recent trials is a phase III trial of T-VEC (talimogene laherparepvec), an oncolytic herpes simplex virus expressing granulocyte-macrophage colony stimulating factor (GM-CSF) in melanoma. In this

trial, patients were randomised to either intralesional virus or subcutaneous GM-CSF. Overall response rates in the T-VEC arm were 26.4% compared to 5.7% in the GM-CSF arm with significantly higher durable responses in the T-VEC arm (16.3% vs 2.1%) (Andtbacka et al., 2015). Vaccinia and reovirus are also promising potential therapies. JX594 is an oncolytic vaccinia virus, also engineered to express GM-CSF. It has shown efficacy when administered intratumourally to patients with unresectable hepatocellular carcinoma with an objective response seen in 3 of 10 evaluable patients (Park et al., 2008). A further phase II dose finding trial has demonstrated that overall survival is related to dose (14.1 months in the high dose group vs 6.7 months) (Heo et al., 2013). A phase II study of an engineered pox virus, PROSTVAC-VF, with GMCSF, given to men with castration-resistant prostate cancer, has shown an 8 month survival benefit when compared to controls (21.1 months vs 16.6 months) (Kantoff et al., 2010).

The above examples show that oncolytic viruses show promise but there remains a considerable disparity between the efficacy of oncolytic virus seen in preclinical work compared with success in clinical trials. For viral therapy to move forward, the reasons behind the difficulty in translating in vitro results into a clinical setting need to be addressed. Some of the key challenges in studying oncolytic viruses are outlined below.

6.2.1 *The mechanism of cell death*

There are many unanswered questions regarding the mechanism of action of oncolytic adenovirus, not least the mode of death that is induced. Oncolytic viruses can kill infected cancer cells in many ways, ranging from direct cell lysis through to a variety of cytotoxic immune mediated mechanisms (Russell et al., 2012). The conventional concepts of cell death such as apoptosis, necrosis or autophagy do

not appear to explain the mechanism of cell death (Baird et al., 2008). This may be partially explained by the fact that oncolytic viruses, including adenovirus, take over and deregulate multiple cellular pathways including control of the molecular cell death machinery of the infected cell. This allows the virus to fully exploit the host cell for preferential replication of its own genome and assembly of new viral particles. If the mechanism of oncolysis can be identified, then it may be possible for it to be manipulated for therapeutic gain.

The data presented here show that the greater the amount of DNA damage induced by the virus, the greater the cell death. It remains to be determined whether the DNA damage is causing cell death or whether it is just a marker of dying cells. If it is the former, then promoting DSBs in the context of viral infection could increase cytotoxicity. Data to support this come from preclinical studies showing the synergistic activity of combining the administration of ionising radiation (IR) and oncolytic adenovirus (Lamfers et al., 2002; Bieler et al., 2008; Passaro et al., 2013; Zhang et al., 2003b). However, results suggest that the interaction between IR and viral cytotoxicity is more complex than simply the generation of DSBs. Enhanced viral replication following IR has been reported in some studies (Lamfers et al., 2002; Geoerger et al., 2003) but not all (reviewed in (Touchefeu et al., 2011)). The results presented in this thesis show that over-replication of genomic DNA correlates with viral potency. If the mechanism for inducing DNA damage also causes cell cycle arrest, then this could influence the efficacy of the oncolytic virus. In support of this hypothesis, previous results have also shown that irradiation timing is crucial for an effect. In a preclinical study of anaplastic thyroid carcinoma (ATC) synergistic effects were only seen when ATC cells were irradiated 24h prior to infection with *dl*922-947. This observation was attributed to changes in the cell cycle following IR that produced an optimal environment for viral replication (Passaro et al., 2013). It is not possible to uncouple the cell cycle changes from the DDR and

this demonstrates one of the challenges in assessing the specific role of DNA damage in viral efficacy.

In addition, to maximise oncolytic viral potency you need to maximise viral replication within the cells. It is possible that increasing DSBs may cause cell death prior to optimal viral replication and limit the amount of infectious virions produced from the cell. This could in turn reduce viral cytotoxicity. Results from my thesis show the importance of the DNA repair pathways for enhanced viral replication. If the mechanism of inducing additional cellular damage also influences the pathways that are involved in viral replication, this could also have a negative impact on viral cytotoxicity.

The exploitation of the DDR to increase viral efficacy is clearly complex and inter-linked with the cell cycle. A greater understanding of the mechanism behind virally induced DSBs is needed to fully exploit the potential to increase DSBs in the context of viral infection.

6.2.2 *Identification of biomarkers*

The key to any successful therapy is targeting the right treatment to the right patient. Development of predictive biomarkers are becoming increasingly important tools in drug development and clinical research (de Gramont et al., 2015). Results have revealed the importance of the DDR in determining cytotoxicity to *dl*922-947 and identified functional HR pathways as being a possible biomarker. This raises the question of how these tumours with competent HR pathways can be identified. The assay used within this thesis identified HR competent tumours by their ability to produce RAD51 foci in response to PARP inhibitor treatment. This functional assay has been used successfully in ovarian cancer clinical samples (Mukhopadhyay et al., 2010), and a similar strategy using IR to induce DNA damage has been assessed in breast cancer samples (Naipal et al., 2014). There are, however, difficulties in translating this functional assay into clini-

cal practice. One of the challenges for this assay is the requirement of the cell/tissue to be cultured and have dividing cells that go through S phase. This is necessary since HR only functions in S phase, and the generation of DSBs following PARP inhibitor treatment requires the cell to encounter a SSB at a replication fork that will only occur if the cell is cycling. Whether a form of this assay can be translated into routine clinical practice remains to be determined. Further strategies that have been developed to identify HR defective tumours from HR competent tumours include assessment of genomic scars (reviewed in (Watkins et al., 2014)), the use of gene expression profiles ((Konstantinopoulos et al., 2010) and next generation sequencing (Pennington et al., 2014). The main challenge is to select a method that is robust, simple and reproducible for routine clinical practice (De Picciotto et al., 2016).

Although components of the HR pathway are important in determining the potency of *dl*922-947, viral replication and cytotoxicity can still occur even in cells with mutations within the HR pathway suggesting that other factors are involved. Previous work has identified basal p21 expression as an important factor in identifying cells sensitive to adenovirus cytotoxicity and correlates with expression of E1A (Flak et al., 2010). It is postulated that high levels of p21 prior to adenoviral infection produces a cellular environment that promotes viral replication and this is thought to be through its interaction with cyclin D. Adenovirus interacts with a huge array of cellular components and deregulates multiple pathways within the host cell. In addition, viral infection is a dynamic process that evolves over many hours. This is in contrast to other therapies like chemotherapy and irradiation where damage occurs almost instantaneously and yet even with many chemotherapy agents, predictive biomarkers are yet to be found. These complexities surrounding viral infection question whether it is possible to identify a single biomarker that could predict which tumours are most likely to respond.

6.2.3 *The role of the immune system*

Investigating oncolytic viruses is further complicated by the complex interaction with the immune system. On one hand, the ability of viruses to induce a host antiviral immune response may also result in clearance of the virus through neutralising antibodies and/or cytotoxic T-cell-mediated immune responses thus hindering their effectiveness (reviewed in (Ferguson et al., 2012)). These antiviral immune responses are also responsible for the dose limiting toxicities of oncolytic viral therapy (Reid et al., 2002). On the other hand, it has also become apparent that the immune response triggered by oncolytic viruses is a critical component of their anti-tumour effect (Melcher et al., 2011). Following oncolytic viral cell death, tumour cells release tumour associated antigens (TAAs) and potentially novel cancer antigens (neo-antigens). They also release pathogen-associated molecular patterns (PAMPs) and danger-associated molecular pattern signals (DAMPs) and cytokines. Together these factors can promote an adaptive immune response that has potential to modify the immune suppressive nature of the tumour microenvironment (Kaufman et al., 2015b) and mediate tumour regression at distant sites that are not exposed to the virus (Kaufman et al., 2015b; Mastrangelo and Lattime, 2002; Cerullo et al., 2010). Data presented in this thesis are from experiments performed using cell culture only, and it is clear that to assess the relevance of these findings fully, in vivo experiments are needed within an immune competent model.

6.3 POTENTIAL FUTURE DIRECTIONS

6.3.1 *Development of experimental models*

The role of the immune microenvironment in HGSOC and the importance of the immune system in the efficacy of oncolytic adenovirus highlight the need for better experimental models. It is important to perform experiments in culture conditions that more closely resemble the tumour microenvironment (Bowtell et al., 2015). This could include 3D matrices and co-culture of malignant cells with fibroblasts and immune cells (Bowtell et al., 2015). There is also a need for an accurate and representative murine models of human ovarian cancer (Vaughan et al., 2011). Recent research has demonstrated the inadequacy of commonly used cell lines as models for HGSOC (Domcke et al., 2013). Primary cells obtained directly from patients may better represent HGSOC and ideally the findings from this thesis should be reproduced in these cells.

There is clearly a need for preclinical assessment of adenoviral gene therapy within the context of an immune competent host. Unfortunately, this is challenging because murine cells do not support productive replication of human adenovirus (Young et al., 2012). Previous work has shown that, although murine cells can be infected with human adenovirus, there is failure of adenovirus protein synthesis, especially late structural proteins. This can be partially overcome by the in trans expression of L4-100K (a non-structural late viral protein) suggesting that murine models that support human adenovirus replication could potentially be generated (Young et al., 2012). Further work investigating this is needed. Syrian hamsters are partially permissive to human adenovirus (Thomas et al., 2006) and therefore could be a useful alternative, although there are few Syrian hamster experimental tools (e.g. antibodies, transgenic models), which makes analysis challenging.

Evaluating the immune response and tumour microenvironment in response to oncolytic adenovirus may lead to increased understanding of the factors that result in optimal viral efficacy whilst minimising toxicity.

6.3.2 *Extending findings to other viruses and DNA repair pathways*

This thesis has shown the importance of the DDR and HR pathway in the potency of group C Ad5 vectors. I have demonstrated that the presence of factors of the HR pathway, RAD51 and BRCA2, result in increased viral replication and both proteins are found in VRCs suggesting they may have a direct role in viral replication. RAD51 binds to ssDNA and BRCA2 stabilises this interaction. The results from HTS identified a number of other factors that resulted in resistance to virus and many of these also interact with ssDNA (e.g.RPA) or regulate the binding of RAD51 with ssDNA (e.g.RAD54L). This suggests that it may be the ability of these proteins to bind, and stabilise, ssDNA that the virus utilises to promote viral replication. Adenoviruses have a unique mechanism of replicating their DNA: only one strand is replicated at a time, and replication generates a displaced single strand of parental DNA in addition to a duplex formed of a daughter strand plus the other parental strand. The displaced strand forms a circular structure that subsequently undergoes second strand synthesis (de Jong et al., 2003). It is possible that the role of these cellular HR proteins is to stabilise and protect the free viral ssDNA strand to prevent degradation.

There are a multitude of other viral vectors in clinical development including other adenoviral serotypes (reviewed in (Larson et al., 2015; Turnbull et al., 2015)). All viruses are obligate parasites and interact with the host cell but the mechanisms of viral lifecycle, especially the mechanism of viral replication, vary considerably. It is likely that the specific protein interactions will be very different and may depend on

the mechanism of viral replication (Turnell and Grand, 2012). Even different adenoviral serotypes vary in their interaction with host cell proteins (Forrester et al., 2011). It is therefore possible that the findings from this thesis are specific to group C adenovirus. One important question is whether these findings can be extended to other viral vectors. To fully investigate the clinical relevance of these findings, assessment of the DDR in determining the efficacy of other oncolytic viruses should be undertaken.

This thesis has focused on the HR pathway in HGSOC but many other hereditary and sporadic cancers are characterised by defects in DNA repair pathways. For example, MMR defects are seen in colorectal cancer (Cunningham et al., 2001) along with gastric cancer (Fleisher et al., 1999), endometrial cancer (Esteller et al., 1998) as well as ovarian cancer (Xiao et al., 2014). Defects within the BER pathway are found in germ cell tumours (Robertson et al., 2001). Loss of ERCC1, a component of the NER pathway, is seen in glioma (Chen et al., 2010) and lung cancer (Kiyohara and Yoshimasu, 2007). These are just a few examples of DDR defects found in human malignancies but the prevalence of these defects highlights the importance of assessing further components in the DDR in determining the potency of oncolytic viruses.

This thesis has investigated the pathways involved in repair of DNA DSBs. It is yet to be fully determined whether the repair of other DNA lesions could play a role in the lifecycle of oncolytic adenovirus. The results, however, show that the combination of *dl*922-947 and PARP inhibitor did not affect viral efficacy, implying that generation of SSBs may not influence viral cell death. In addition, the HTS did not identify factors involved in the MMR, BER or NER pathways suggesting that these pathways do not play a significant role in viral mediated cell death, under these experimental conditions. Further experiments with cell lines deficient and proficient in specific DNA damage repair pathways will assess this further.

6.3.3 *Combination treatment*

Oncolytic viruses have demonstrated tolerable safety profiles and there is potential for combining their treatment with other cancer agents to improve therapeutic response. Combination of oncolytic adenovirus with agents such as chemotherapy and radiotherapy has been studied in preclinical testing. For example, increased clinical efficacy has been seen with combinations of adenovirus and gemcitabine, cisplatin, temozolamide, irinotecan and paclitaxel (Bhattacharyya et al., 2011; Hallden and Portella, 2012; Bressy and Benihoud, 2014). The mechanism of action of these agents and their influence on the DDR and cell cycle needs to be carefully considered to optimise their potential. Understanding the basic biology of adenoviruses and the mechanism of sensitisation by chemotherapeutics and other therapies will assist in translating these preclinical studies to clinical trials.

The importance of the immune microenvironment in both HGSOC and the role of the immune system in the cytotoxicity of oncolytic viruses provides a strong rational for combining immune checkpoint inhibitors with oncolytic viruses (Turnbull et al., 2015). Evidence for the potential success of this strategy comes from preliminary analysis of a phase 1b clinical trial of T-VEC and ipilimumab, a monoclonal antibody against cytotoxic T lymphocyte antigen 4 (CTLA4) have reported response rates of 41% with a 24% complete response rate in patients with advanced melanoma (Puzanov et al., 2014). Since both of these agents interact with and manipulate the immune system, the potential immunbe mediated toxicity is a particular concern when investigating this combination. The results of further clinical trials are awaited.

Knowledge regarding the interaction of oncolytic virus and the DDR raises the possibility that components of the damage response pathways can be targeted to enhance viral efficacy. For example, inhibition of CHK1 has been shown to promote over-replication of ge-

nomic DNA and DNA damage following infection with *dl*922-947 which is associated with enhanced cytotoxicity both *in vitro* and *in vivo* (Connell et al., 2011). The development of new inhibitors of the DDR, and increased knowledge of defects within the DDR in tumours, may lead to further novel virus/drug combinations.

6.3.4 *Development of future clinical trials*

Oncolytic viruses are live viruses that proliferate upon clinical administration. There are important biosafety considerations due to the replication potential of these agents. Safe storage, preparation, handling and administration of the virus all need to be carefully considered (Kaufman et al., 2015b). One unique potential safety risk is the concern that an oncolytic virus might spread from the treated patient and mutate to regain its wild-type pathogenic potential (Russell et al., 2012). Virus shedding has been documented in urine or respiratory secretions (Liu et al., 2007), but oncolytic virus transmission to contacts and carers has not yet been seen (Russell et al., 2012). The potential of the theoretical risks of viral shedding depends on the nature of the virus, the comorbidity of the patient and the co morbidities of close contacts (for example immune compromised individuals).

Currently there are few data on correlating viral dose with in vivo replication (Kaufman et al., 2015b), therefore establishing the safe and effective dose can be challenging. In addition, since oncolytic viruses are removed by the immune system, many other factors need to be considered such as the presence of pre-existing neutralising antibodies and the competency of the patient's immune system at the time of oncolytic viral administration. These factors could affect both the safety and efficacy of the treatment (Kaufman et al., 2015b).

The route of administration of the virus also needs careful consideration. Many of the successful trials with oncolytic virus have used intratumoural injection (Turnbull et al., 2015). This is not pos-

sible with HGSOC where there may not be an accessible injectable target and the disease has often spread throughout the abdomen. Administration of the virus directly into the peritoneal cavity may offer the best solution. This was the route used in previous oncolytic viral trials in ovarian cancer including the original ONYX-015 trial (Vasey et al., 2002) as well as the trial of the infectivity enhanced Δ24-RGD adenovirus (Kimball et al., 2010). The current clinical trial of the oncolytic adenovirus ColoAd1 is also using intraperitoneal delivery (NCT02028117).

A question raised from oncolytic viral therapy trials is how response should be evaluated. It is now clear that immune therapies can result in pseudoprogressive changes (therapy mediated tumour swelling), which can transiently occur before a tumour regresses (Wolchok et al., 2009). Patterns of acute tumour enlargement followed by regression have been seen after intrahepatic injection of ONYX-015 in combination with 5-FU/leucovorin for hepatic colorectal metastasis in 11 out of 24 patients (Reid et al., 2002). Delayed responses were also seen in the trial of T-VEC, which were preceded by apparent tumour progression (Senzer et al., 2009). These data suggest that pseudoprogression may be a feature of oncolytic viral therapy and need to be taken into account when evaluating tumour responses (Larson et al., 2015)

To address some of these issues, future clinical trials should ideally include data on the pharmacodynamics of virus delivery. This should include immune responses to the virus, assessment of virus shedding and evidence for lack of viral replication in normal tissue (Kaufman et al., 2015b). Biopsies of tissue are needed at trial entry and ideally following virus administration to confirm intratumour viral replication and will give vital information on potential biomarkers. Careful design of clinical trials is vital to fully assess the potential of oncolytic viruses and guide future development of these agents.

6.4 CONCLUDING REMARKS

Resistance to therapies that are used to treat malignancy is a major problem, and novel approaches are therefore needed. The ability of oncolytic viruses to replicate along with their capacity to take over and deregulate multiple cellular pathways make them a unique therapeutic option. This thesis has demonstrated the importance of the cellular DDR in determining the efficacy of oncolytic adenovirus in ovarian cancer and suggests that, if this complex interaction between the host and the virus can be completely understood, the full capacity of oncolytic viruses could be realised. The distinct properties of oncolytic viruses have the potential to make up an important component in the strategy to tackle the complex, evolving nature of cancer.

Part V

APPENDIX

A

APPENDIX

A.1 PUBLICATIONS

DNA Damage and Repair

Molecular Cancer Research

RAD51 and BRCA2 Enhance Oncolytic Adenovirus Type 5 Activity in Ovarian Cancer

Laura A. Tookman[1], Ashley K. Browne[1], Claire M. Connell[1], Gemma Bridge[1], Carin K. Ingemarsdotter[1], Suzanne Dowson[2], Atsushi Shibata[3], Michelle Lockley[1], Sarah A. Martin[1], and Iain A. McNeish[1,2]

Abstract

Homologous recombination (HR) function is critically important in high-grade serous ovarian cancer (HGSOC). HGSOC with intact HR has a worse prognosis and is less likely to respond to platinum chemotherapy and PARP inhibitors. Oncolytic adenovirus, a novel therapy for human malignancies, stimulates a potent DNA damage response that influences overall antitumor activity. Here, the importance of HR was investigated by determining the efficacy of adenovirus type 5 (Ad5) vectors in ovarian cancer. Using matched *BRCA2*-mutant and wild-type HGSOC cells, it was demonstrated that intact HR function promotes viral DNA replication and augments overall efficacy, without influencing viral DNA processing. These data were confirmed in a wider panel of HR competent and defective ovarian cancer lines. Mechanistically, both BRCA2 and RAD51 localize to viral replication centers within the infected cell nucleus and that RAD51 localization occurs independently of BRCA2. In addition, a direct interaction was identified between RAD51 and adenovirus E2 DNA binding protein. Finally, using functional assays of HR competence, despite inducing degradation of MRE11, Ad5 infection does not alter cellular ability to repair DNA double-strand break damage via HR. These data reveal that Ad5 redistributes critical HR components to viral replication centers and enhances cytotoxicity.

Implications: Oncolytic adenoviral therapy may be most clinically relevant in tumors with intact HR function. *Mol Cancer Res; 14(1); 44–55. ©2015 AACR.*

Introduction

Aberrant DNA damage responses (DDR) are common in human malignancies (1). This is particularly true in high-grade serous ovarian cancer (HGSOC), where approximately 15% patients have germline mutations in *BRCA1* or *BRCA2* (2). Moreover, data from The Cancer Genome Atlas (TCGA) consortium inferred that homologous recombination (HR) defects may be present in 50% HGSOC, through a variety of additional mechanisms, including somatic *BRCA1/2* mutation and epigenetic loss of BRCA1 expression (3). A separate study, which used functional assays of HR competence in primary ascites cells from women with advanced HGSOC, strikingly concurred with TCGA, with 52% (26/50) showing HR deficiency (4). There is great interest in the use of poly-(ADP ribose) polymerase (PARP) inhibitors in HR-defective HGSOC (5), but there are few therapeutic targets available for HR-competent tumors, which have a poorer prognosis (6) and are less likely to respond to platinum-based chemotherapy (4).

Oncolytic adenoviruses are a potential novel therapy for ovarian and other human cancers. These viruses infect malignant cells, multiply selectively within them and cause cell death with release of mature virions that infect neighboring cells. An understanding of the complex interplay between the virus and host cells is vital to increase efficacy, develop biomarkers, and improve patient selection in clinical trials. E1A CR2-deleted Ad5 vectors, such as *dl*922-947 (7) and Δ24 (8), replicate selectively within cells with a defective Rb pathway, a frequent abnormality in many malignancies, including HGSOC (3). We have previously shown that *dl*922-947 has considerable activity in ovarian cancer and is more potent than E1A wild-type adenoviruses and the E1B-55K deletion-mutant *dl*1520 (9, 10). *dl*922-947 induces death via a necrosis-like mechanism (11), but the sensitivity of ovarian cancer cells to *dl*922-947 varies considerably, even between cells with similar infectivity (12).

Infection by many DNA viruses, including adenovirus, triggers a DDR, which viruses seek to circumvent through a series of mechanisms. A major target following adenovirus type 5 (Ad5) infection is the MRN complex (MRE11, RAD50, NBS1) and components of the non-homologous end-joining (NHEJ) pathway. Immediately following infection, before E1A is expressed, core protein VII protects the viral genome from recognition by MRN (13). As early proteins are expressed, MRN is inactivated by several mechanisms, including proteosomal degradation (14, 15) and mislocalization to PML-containing "nuclear tracks" (16, 17). Specific mechanisms that inhibit NHEJ include proteosomal degradation of DNA Ligase IV (18) and inactivation of DNA-dependent protein kinase (DNA-PK; ref. 19).

[1]Centre for Molecular Oncology, Barts Cancer Institute, Queen Mary University of London, London, United Kingdom. [2]Institute of Cancer Sciences, University of Glasgow, Glasgow, United Kingdom. [3]Advanced Scientific Research Leaders Development Unit, Gunma University, Maebashi, Gunma, Japan.

Note: Supplementary data for this article are available at Molecular Cancer Research Online (http://mcr.aacrjournals.org/).

Corresponding Author: Iain A. McNeish, Institute of Cancer Sciences, University of Glasgow, Wolfson Wohl Cancer Research Centre, Garscube Estate, Glasgow G61 1QH, UK. Phone: 44-141-330-3968; Fax: 44-141-330-4127; E-mail: Iain.mcneish@glasgow.ac.uk

doi: 10.1158/1541-7786.MCR-15-0188-T

©2015 American Association for Cancer Research.

AACR

Beyond the observation that the BLM helicase is also degraded following Ad5 infection (20), there has been little specific investigation into the role of components of the HR pathway in adenovirus biology. Previously, we showed that oncolytic adenovirus activity is associated with profound deregulation of cell-cycle checkpoints and cell-cycle progression (21), inducing cellular DNA damage, with subsequent activation of DDR pathways, including ATR-Chk1 (22). Here, we have investigated the relationship between homology-mediated DSB repair and oncolytic adenovirus activity in ovarian cancer further. Our data indicate for the first time that key HR components BRCA2 and RAD51 interact with viral DNA replication centers and promote both virus replication and cytotoxicity.

Materials and Methods

Cell lines, viruses, and chemotherapy

Cells were cultured in Dulbecco's modified Eagle medium (DMEM) or RPMI (both Sigma) supplemented with 10% heat-inactivated FBS (Biosera), 100 units/mL penicillin and 100 mg/mL streptomycin (PAA Laboratories). Cell lines were maintained at 37°C in a humidified atmosphere with 5% CO_2 and routinely passaged twice a week using 0.5% trypsin in PBS. All cell lines were routinely tested for *mycoplasma* and underwent 10-loci STR profiling to verify their authenticity, most recently in July 2014. SKOV3 and HeLa were obtained from Cancer Research UK Cell Services (Clare Hall, Hertfordshire, UK), TOV21G from Prof. F. Balkwill (Barts Cancer Institute, UK) and IGROV1 from NCI. PEO1 and PEO4 were kindly provided by Dr. Simon Langdon (University of Edinburgh, UK). Of these cell lines, IGROV1, PEO1, PEO4, and SKOV3 cells were maintained in RPMI, HeLa, and TOV21G cells in DMEM.

All viruses, including wild-type Ad5, Ad11 and Ad35, were originally obtained from Dr. Y. Wang (Barts Cancer Institute, UK). The Ad5 mutant *dl*922-947 is deleted in the region encoding amino acids 122 to 129 of E1A CR2. It also contains a 745-bp deletion in E3B (nt 30,005–30,750) that is substituted by a 642-bp non-coding DNA fragment (7). *dl*309 has the same E3B deletion as *dl*922-947 but is E1A wild-type. Ad GFP is deleted in E1 and E3B and has green fluorescent protein (GFP) in the E1 position under control of the cytomegalovirus (CMV) immediate early promoter.

Cisplatin (Accord Healthcare) was obtained for the chemotherapy pharmacy, St Bartholomew's Hospital, London. Rucaparib was provided by Clovis Oncology.

Cell survival assays

For adenovirus and cisplatin experiments, cell survival was measured using the MTT assay (23) using a Wallac1420 Multilabel reader (PerkinElmer Life and Analytical Sciences). A total of 10^4 cells were infected in 24-well plates in serum-free medium. Cell viability was measured after 120 hours. CellTitre Glo (Promega) and sulphorhodamine B assays were used in assays involving PARP inhibitors. For clonogenic assays, cells were infected in 24-well plates as above. Then, 72 hours after infection, cells were trypsinized and 100 to 200 cells were plated onto 6-well plates in triplicate. Colonies were stained with Crystal Violet 10 days thereafter and counted.

Virus infectivity assay

Cells (5×10^5) were infected with Ad GFP. GFP fluorescence was assessed 24 hours after infection on a FACSCaliber (Becton Dickinson). All conditions were repeated in triplicate and analyzed using FlowJo software.

Viral replication assays: $TCID_{50}$ and quantitative PCR

Cells (2×10^5) were infected with *dl*922-947 in serum-free medium and re-fed 2 hours later with serum containing medium. Up to 72 hours after infection, cells were harvested in 0.1 mol/L Tris pH 8.0 and subjected to 3 rounds of freeze/thawing (liquid N_2/37°C); all time points were harvested in triplicate. The supernatant was titred on JH293 cells.

Cells (2×10^5) were harvested at 24 to 72 hours following infection, washed twice in ice-cold PBS, and scrapped into 500 μL PBS. Extraction of viral DNA was performed using the QIAmp DNA Blood Mini Kit (Qiagen). Real-time PCR was performed using ABI Prism7500. Oligonucleotides and probes were as follows:

E1A: sense: 5′-CCACCTACCCTTCACGAACTG; antisense: 5′-GCCTCCTCGTTGGGATCTTC; probe: ATGATTTAGACGT GACGGCC
Hexon: sense: 5′-GGTGGCCATTACCTTTGACTCT; antisense: 5′-GGGTAAGCAGGCGGTCATT; probe: 5′-CTGTCAGCTGGCCTGG

PCR conditions were as follows: 50°C for 2 minutes, 95°C for 10 minutes, followed by 40 cycles of 95°C for 15 seconds, and 60°C for 60 seconds. A standard curve using 10^3 to 10^9 *dl*922-947 genomes was used for quantification.

Reverse transcriptase PCR

For analysis of BRCA2 expression, 1 μg DNase-treated RNA was reverse transcribed using the Applied Biosystems High Capacity cDNA Reverse Transcription Kit (Life Technologies). The following primers and probes were used to assess BRCA2 transcription. BRCA2-sense 1: 5′-CAGAAGCCCTTTGAGAGTGGA; BRCA2-antisense 1: 5′-TGAGACCATTCACAGGCCAA; BRCA2 probe 1: 5′-(6FAM)CCAAGGAAGTTGTACCGTC(TAM); BRCA2-sense 2: 5′-CCACAGCCAGGCAGTCTGTAT; BRCA2-antisense 2: 5′-AGAACACGCAGAGGGAACTTG BRCA2 probe 2: 5′-(6FAM)CCACTCTGCCTCGAAT(TAM). Data were normalized to 18S.

Immunoblotting

Protein lysates were electrophoresed on precast gels (Invitrogen) and transferred onto nitrocellulose membranes (GE Healthcare) by semi-dry blotting. Antibody binding was visualized using enhanced chemiluminescence (GE Healthcare). Antibodies were obtained as follows: E1A (mouse, Becton Dickinson 554155), Ad5 (goat, Abcam Ab36851), RAD51 (rabbit, Santa-Cruz sc-8348), mcm3 (rabbit, Abcam ab36851), Ku70 (goat, Santa-Cruz, sc-1486), and (rabbit, Cell Signaling, 4895). All HRP-conjugated secondary antibodies were obtained from Dako.

Southern blotting

Cells (10^6) plated and infected with *dl*922-947 (MOI 10 for PEO4, MOI 100 for PEO1 cells). Forty-eight and 72 hours later, cells were trysinized and washed in TBS. Extraction of DNA was performed using the QIAmp DNA Blood Mini Kit (Qiagen). DNA concentration was measured using Nanodrop ND-1000 spectrophotometer and 10 μg genomic DNA was electrophoresed on a 1% agarose gel. The gel was soaked in 200 mL 0.2 mol/L HCl for 10 minutes, washed and then soaked in alkaline transfer buffer (0.4 mol/L NaOH, 1 mol/L NaCl). DNA was transferred onto a Hybond N^+ membrane (GE Healthcare Life Sciences) by

conventional capillary transfer over 48 hours. Probe Labeling against viral DNA, hybridization, and detection was performed using the Amersham ECL Direct Nucleic Acid Labeling and Detection systems.

Flow cytometry

For cell-cycle analyses, cells were trypsinized, washed twice in ice-cold PBS, and fixed in ice-cold 100% ethanol. Cells were then washed with PBS and resuspended in 200 μL propidium iodide (PI) and 100 μg/mL RNase A (MP Biomedicals). For γH2AX analysis, cells were harvested, washed, and fixed in ice-cold 70% ethanol. After incubation with primary anti-γH2AX mAb or IgG control, cells were washed and then incubated with FITC-conjugated anti-mouse secondary antibody (Invitrogen) for 1 hour in the dark and analyzed using a FACSCaliber flow cytometer. Results analyzed using FlowJo software.

Immunofluorescence and coimmunoprecipitation

Cells were seeded on poly-L-lysine–coated coverslips and treated with rucaparib (10 μmol/L for 24 hours) or *dl*922-947 for up to 48 hours. Following treatment, medium was aspirated and 0.04% Triton (Sigma) in PBS added for 1 minute. Cells were then fixed in 3% paraformaldehyde and 2% sucrose for 10 minutes. The cells were stained with anti-γH2AX antibody (Millipore) or a rabbit anti-Ad5 E2-DNA binding protein (E2-DBP, a kind gift of Dr. David Ornelles, Wake Forest Medical Center, NC) and costained with anti-RAD51 or anti-BRCA2 antibody for 45 minutes at 37°C. Following incubation for 45 minutes at 37°C with secondary antibodies, cells were costained with DAPI. Coverslips were mounted on slides and images captured using a Zeiss 510 or 710 confocal microscope and foci were counted using ImageJ software.

TOV21G cells (2×10^6) were infected with *dl*922-947 (MOI 10) and lysed 24 hours later in 800 μL RIPA lysis buffer (with complete protease inhibitors, Roche). Sepharose beads (35 μL; Santa Cruz) were incubated with anti-RAD51 antibody (Santa Cruz, H-92, sc8349) or control antibody (anti-HA, Sigma H6908) for 1 hour at 4°C. Lysates were then incubated with the IP matrix beads for 1 hour at room temperature and washed with RIPA lysis buffer. SDS loading buffer was added, samples boiled, and proteins detected by Western blot as described earlier. Primary antibodies used were rabbit anti-Ad5 E2 DBP and anti-RAD51 (Abcam, ab213).

siRNA

Small-interference RNA (siRNA) targeted against BRCA2 and RAD51 were obtained from either Dharmacon (siGENOME SMARTpool; GE Life Sciences) or Qiagen. A nontargeting (NT) pool of siRNA was also used (Qiagen). All cell lines were transfected using lipofectamine 2000 (Invitrogen), apart from IGROV1 cells where DharmaFECT1 (Dharmacon) was used. A final concentration of 10 nmol/L RAD51 siRNA and 30 nmol/L or 50 nmol/L (depending on the cell line) BRCA2 siRNA was used. Twenty-four hours following transfection, cells were infected with *dl*922-947 or *dl*309. Cell survival was assessed 120 hours later by the MTT assay. Cell survival following siRNA was compared with the scrambled control. All experiments were repeated using a second siRNA (Qiagen) at a concentration of 50 nmol/L.

HR reporter assay

Full details of the assay are reported elsewhere (24). Briefly, pDR-GFP (a gift from Maria Jasin; Addgene plasmid 26475; ref. 25) contains two differently mutated GFP genes orientated as direct repeats and separated by a puromycin resistance gene. One of the GFP constructs, SceGFP, is mutated to contain the recognition site for the rare-cutting endonuclease I-SceI; as a result, exposure to I-SceI will induce a unique double-strand break. The I-SceI site is incorporated at a BcgI restriction site by substituting 11 bp of wild-type GFP sequence with those of the I-SceI recognition site. These substituted base pairs also supply two in-frame stop codons, which terminate translation and inactivate the protein. Downstream of the SceGFP gene is an 812-bp internal GFP fragment termed iGFP. Homologous sequences in the two mutated GFP genes are separated by 3.7 kb. When I-SceI–induced DSB occurs, iGFP sequence can act a donor strand to allow homology-mediated repair and generation of a functional GFP open reading frame—this in turn can be detected by flow cytometry.

PEO1 and PEO4 cells were transfected with pDR-GFP using FugeneHD. Following puromycin selection, 10^6 cells were plated and 24 hours later transfected with either 1 μg pI-SceI or pCAAGs (negative empty vector control). Twenty-four hours later, cells were infected with *dl*922-947 (MOI 50 for PEO4 cells MOI 500 for PEO1 cells). Twenty-four hours thereafter, cells were analyzed for GFP events using a FACSCaliber. Events (100,000) were recorded and results analyzed using FlowJo software.

Results

Adenovirus cytotoxicity is greater in HR-competent ovarian cancer cells

To investigate the link between cellular HR function and adenovirus activity, we first utilized the PEO1/PEO4 cell pair (26). These cells originate from the same ovarian cancer patient: PEO1 was derived at the time of first, platinum-sensitive relapse and contains a deleterious *BRCA2* mutation; PEO4 was derived at subsequent relapse, when platinum resistance had developed, and contains a secondary *BRCA2* mutation that restores the open reading frame (27). Using a previously described assay of HR competence, based upon formation of RAD51 foci in response to DSB damage (28), we confirmed that PEO4 cells demonstrate functional HR, while PEO1 are HR defective (Fig. 1A and Supplementary Fig. S1). We also confirmed that BRCA2-mutant PEO1 are more sensitive than BRCA2 wild-type PEO4 to both cisplatin and the PARP inhibitor rucaparib (Supplementary Fig. S2).

We found PEO4 to be significantly more sensitive to cytotoxicity induced by the E1A CR2-deleted Ad5 vector *dl*922-947 (Fig. 1B) as well as Ad5 WT and *dl*309 (E1A wild-type; Fig. 1C). PEO4 were slightly more infectable with Ad5 vectors than PEO1 (data not shown). However, even when MOI was adjusted to ensure equal levels of infection (hereafter called iso-infection), PEO4 remained significantly more sensitive to both *dl*922-947 and *dl*309 (Fig. 1D). This increased sensitivity in PEO4 was confirmed by the clonogenic assay (Supplementary Fig. S3). By immunoblot, there was comparable early (E1A) and late viral protein expression in iso-infected cells (Fig. 1E). Assessing viral replication, there was no significant difference in the number of infectious virions generated following iso-infection (Fig. 1F). However, quantitative PCR indicated that there was more viral DNA generated in PEO4 (Fig. 1G), which was

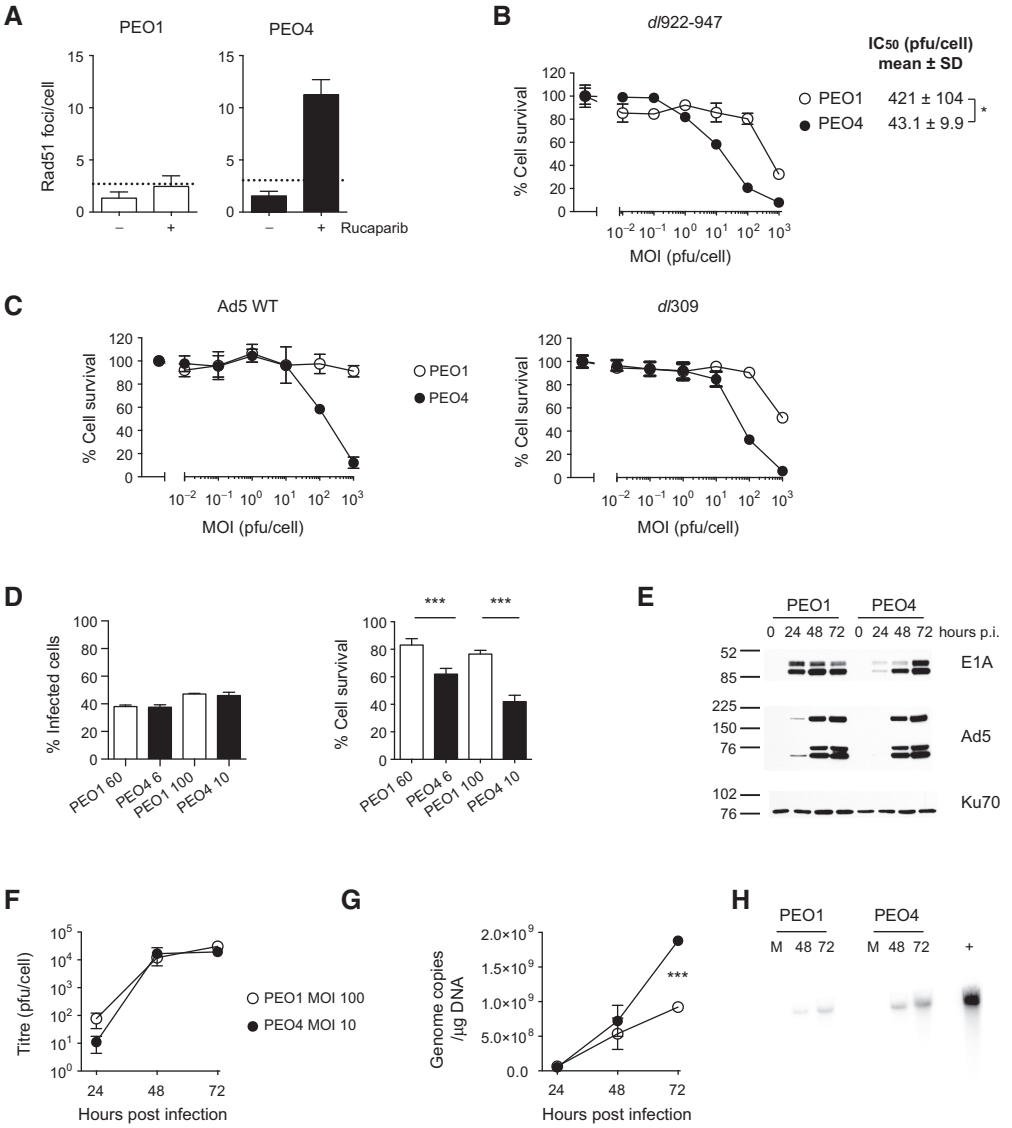

Figure 1.

Greater efficacy and viral DNA replication in HR-competent than HR-defective ovarian cancer cells. A, competence of HR was assessed in PEO1 and PEO4 cells. Cells were treated with rucaparib (10 µmol/L, 24 hours), permeabilized, fixed in 4% PFA, and stained for RAD51 and γH2AX. RAD51 foci were counted in at least 30 nuclei per treatment condition. Bars, mean (±SD) number of RAD51 foci per cell. Dotted line, 2× number of foci in untreated cells. B, 10^4 PEO1 and PEO4 cells were infected in triplicate with *dl*922-947. Cell survival was measured 120 hours after infection by the MTT assay. Mean ± SD IC_{50} for four experiments are shown: *, $P = 0.011$. C, 10^4 PEO1 and PEO4 cells were infected in triplicate with Ad5 WT (left) or *dl*309 (right) (MOI 0.001–1000 pfu/cell). Cell survival was measured 120 hours after infection by the MTT assay. D, PEO1 and PEO4 cells were infected with Ad CMV-GFP (left) at MOI 60 and 100 (PEO1) and 6 and 10 (PEO4). GFP positivity was assessed 24 hours after infection by flow cytometry. PEO1 and PEO4 cells were also infected with *dl*922-947 (right) at MOI 60 and 100 (PEO1) and 6 and 10 (PEO4). Cell survival was assessed 120 hours after infection by the MTT assay. Data, mean ±SD; $n = 3$. ***, $P < 0.001$. E, PEO1 and PEO4 cells were infected with *dl*922-947 MOI 100 (PEO1) or 10 (PEO4). Protein was harvested up to 72 hours after infection. Expression of E1A and adenovirus 5 structural proteins was assessed by immunoblot. E1A band density was assessed from three separate exposures: 24, 48, and 72 hours; mean (±SD). E1A:KU70 ratio was 1.3 ± 0.2, 1.4 ± 0.1, and 1.4 ± 0.2 for PEO1, and 0.7 ± 0.4, 1.2 ± 0.3, and 1.6 ± 0.2 for PEO4. F and G, PEO1 and PEO4 cells were infected with *dl*922-947 MOI 100 (PEO1) or 10 (PEO4) for up to 72 hours. Virus replication was assessed by TCID50 (1F) or quantitative PCR (1G). ***, $P < 0.001$. H, PEO1 and PEO4 cells were infected with *dl*922-947 MOI 100 (PEO1) or 10 (PEO4) for up to 72 hours. DNA was extracted and subjected to neutral pulsed-field gel electrophoresis, probed with HRP-labeled adenovirus type 5 probe. 100 ng purified *dl*922-947 DNA was run as a positive control (+).

confirmed by Southern blotting (Fig. 1H). There were no obvious abnormalities in viral DNA processing on the Southern blot, and specifically no obvious concatemers in either cell line (Fig. 1H and Supplementary Fig. S4 for long exposure). The increased sensitivity appeared to be Ad5 specific, as there was no difference between PEO1 and PEO4 in sensitivity to the group B adenoviruses Ad11 and Ad35 (Supplementary Fig. S5).

Adenovirus DNA replication triggers the DDR and interacts with core HR machinery

We first investigated whether the difference in sensitivity to Ad5 vectors between HR-proficient and HR-deficient cells was reflected in their accumulation of DNA damage. In keeping with their germline *BRCA2* mutation and genomic instability (29), uninfected PEO1 cells demonstrated greater basal levels of DNA damage (γH2AX positivity) and a higher proportion of the cells with >4N DNA content on flow cytometry than PEO4 (Fig. 2A and Supplementary Figs. S1 and S6). However, following iso-infection with *dl*922-947, there were significantly greater increases in both γH2AX positivity and >4N DNA in PEO4 (Fig. 2A), consistent with our previous observations that virus-induced DNA damage correlates with sensitivity (22, 30).

Inhibition of NHEJ using the DNA-PKcs inhibitor NU7026 had no effect on cytotoxicity (data not shown), and, as previously noted (14), there was a reduction in expression of MRE11 following *dl*922-947 infection in both PEO1 and PEO4 (Fig. 2B), and the reduction was similar in both cell lines. However, expression of RAD51 did not diminish following infection in either PEO1 or PEO4 (Fig. 2C). By confocal microscopy, BRCA2 expression was maintained in PEO4 following *dl*922-947 infection. Interestingly, there was clear colocalization between BRCA2 and viral replication centers (VRC), as indicated by expression of viral E2 DNA binding protein (E2 DBP; Fig. 2D). Furthermore, we also saw clear colocalization between RAD51 and E2 DBP in PEO4 (Fig. 2E). It is widely known that, in BRCA2-deficient cells, RAD51 is unable to form foci at the site of DNA damage (Supplementary Fig. S1; ref. 28). However, to our surprise, we observed RAD51 foci colocalized with E2 DBP in PEO1 cells, despite the absence of BRCA2 (Fig. 2E). These findings were confirmed in two other lines that demonstrated HR competence, TOV21G, and HeLa (Fig. 3A), as well as in IGROV1 cells, which are hypermutated and contain mutations in both *BRCA1* and *BRCA2* (ref. 31; http://cancer.sanger.ac.uk/cell_lines) and were HR defective in our assay (Fig. 3A). In both HR-competent lines, there was colocalization between viral replication centers and BRCA2 (Fig. 3B; Supplementary Fig. S7), while all three lines, regardless of HR status, showed RAD51 foci associated with E2 DBP (Fig. 3C). Coimmunoprecipitation suggested a direct interaction between RAD51 and E2 DBP following Ad5 infection in TOV21G cells (Fig. 3D). Thus, for the first time, these data show that RAD51 and BRCA2 can localize to viral replication centers and that this is independent of recruitment to DNA damage foci.

RAD51 and BRCA2 influence adenovirus efficacy in both HR-competent and HR-deficient cells

To investigate the requirement for RAD51 in viral replication and cytotoxicity, we depleted RAD51 using two different siRNA constructs in both PEO1 and PEO4 cells (Fig. 4A). RAD51 depletion caused significant reductions in efficacy of *dl*922-947 in both cell lines (Fig. 4B and Supplementary Fig. S8), and also reduced viral replication (Fig. 4C). Again, these findings were recapitulated in HR-competent HeLa and TOV21G cells, with reductions in both viral cytotoxicity (both *dl*922-947 and *dl*309) and replication (Fig. 4D and E; Supplementary Fig. S9) upon RAD51 silencing, as well as by clonogenic assay in PEO1 and PEO4 cells (Supplementary Fig. S10). Moreover, we were able to confirm this finding in HR-defective IGROV1 cells (Fig. 4F). We also found a small but significant reduction in cytotoxicity following BRCA2 knockdown in PEO4 (Fig. 5A), which was recapitulated in TOV21G and HeLa cells (Fig. 5B and C). Taken together, our data suggest that recruitment of RAD51 and BRCA2 to VRC augments viral replication and cytotoxicity, and is independent of its role in the response to DNA damage.

***dl*922-947 does not inhibit HR function in HR-competent cell lines**

To assess whether adenovirus infection impaired the capacity of cells to repair DNA double-strand break damage by HR, we first used confocal microscopy. In HR-competent cells infected with *dl*922-947, RAD51 was able to localize, at least partially, to sites of DNA DSB damage, suggesting that HR function remains grossly intact following adenovirus infection (Fig. 6A). This functionality was further assessed using a fluorescence reporter assay, which incorporates a green fluorescence protein reporter (DR-GFP) as a repair substrate into the genome and assays non-crossover gene conversion events in response to DNA DSB damage (see Materials and Methods for full assay details). The HR competence of PEO4 cells was again confirmed by this assay, with a significant increase in GFP events following expression of I-SceI compared with control plasmid, whereas PEO1 showed no increase (Fig. 6B). RAD51 knockdown abolished any increase GFP events in PEO4 (Supplementary Fig. S11). To investigate the effect of adenovirus infection on overall HR function, this assay was repeated 48 hours after infection with *dl*922-947, results again showed that PEO4, but not PEO1, was able to repair I-SceI–induced DNA DSB damage using HR (Fig. 6C). This implies that Ad5 infection does not functionally impair homology-mediated repair. To confirm this, PEO4 cells were treated with the PARP inhibitor rucaparib 24 hours following *dl*922-947 or mock infection: the presence of *dl*922-947 was unable to sensitize PEO4 cells to rucaparib (Fig. 6D), again indicating that HR function remains intact following Ad5 infection.

Together, these results indicate that Ad5 vectors do not inhibit HR function in infected cells—rather, components of the HR machinery localize to VRC and bind directly to E2 DBP. This interaction promotes viral DNA replication and increases overall cytotoxicity.

Discussion

In this article, we show for the first time that components of the HR pathway of DNA double-strand break repair significantly influence the activity of Ad5 vectors. Using matched *BRCA2*-mutant and wild-type ovarian cancer cells, we show that the activity of both E1A wild-type (Ad5 WT and *dl*309) and E1A CR2-deleted (*dl*922-947) Ad5 viruses is greater in the presence of functional BRCA2, with increased cytotoxicity and viral DNA replication, and that BRCA2 colocalizes with VRC within the nucleus. These results were recapitulated in other malignant cell lines, HeLa and TOV21G, that are *BRCA2* wild-type and HR competent. Moreover, we were able to demonstrate that RAD51, a key partner of BRCA2, also influences Ad5 activity. Strikingly, we

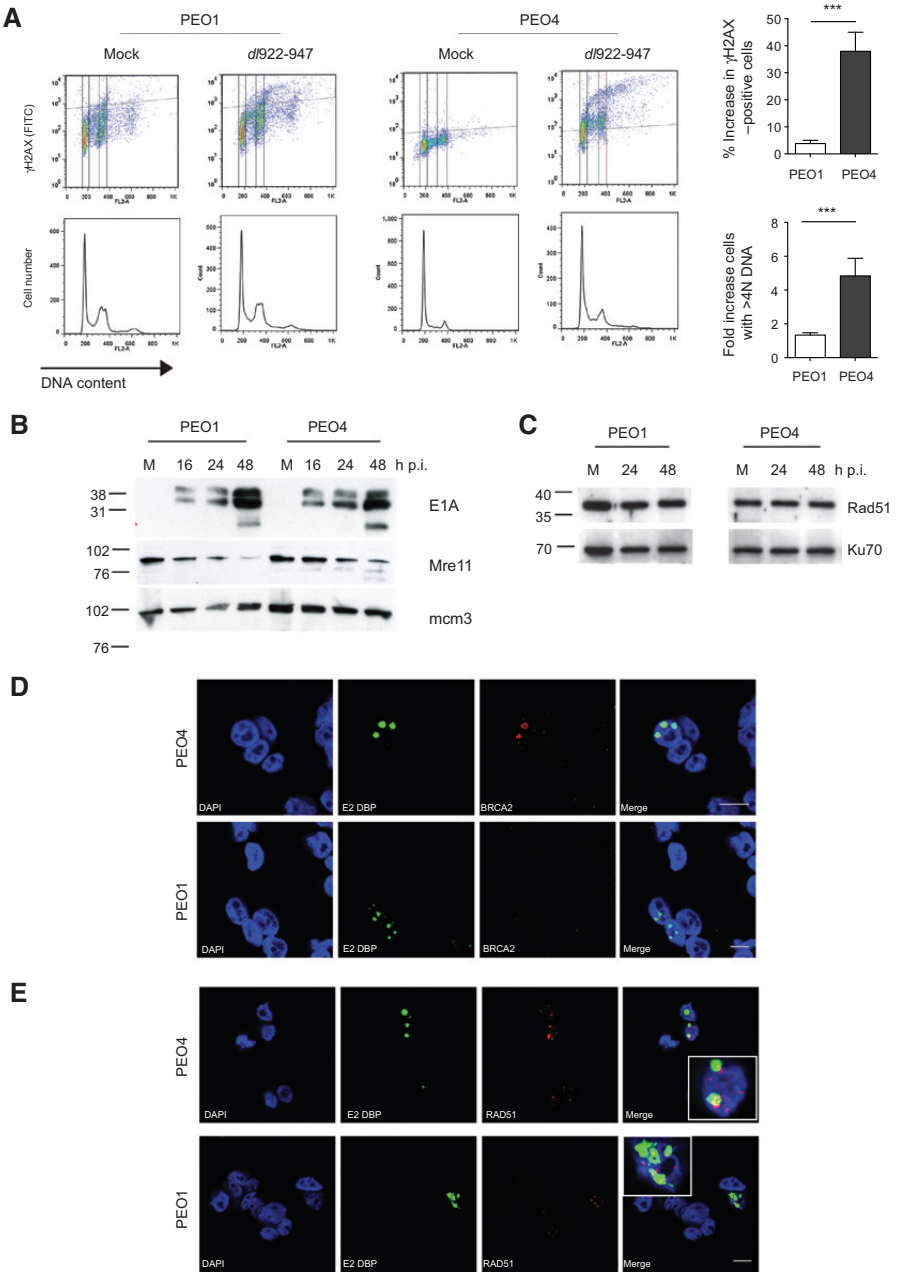

Figure 2.
*dl*922-947 replication induces genomic DNA damage; RAD51 and BRCA2 colocalize with sites of adenovirus replication. A, PEO1 and PEO4 cells were harvested 48 hours following infection with *dl*922-947 (MOI 100 and 10, respectively) or mock infection, fixed in 70% cold ethanol, incubated with an anti-γH2AX Ab, counterstained with PI, and analyzed by flow cytometry (left). Increase in γH2AX-positive cells and cells with >4N DNA are plotted (right); bars, mean ±SD; $n = 3$. ***, $P < 0.001$. B and C, PEO1 and PEO4 cells were harvested following infection with *dl*922-947 (MOI 100 and 10, respectively). Expression of E1A, MRE11 (B), and RAD51 (C) was detected by immunoblot. D and E, PEO1 and PEO4 cells were fixed in 4% PFA following infection with *dl*922-947 (MOI 300 and 30, respectively). Expression of adenovirus E2 DNA binding protein, BRCA2 (D), and RAD51 (E) was assessed by confocal microscopy.

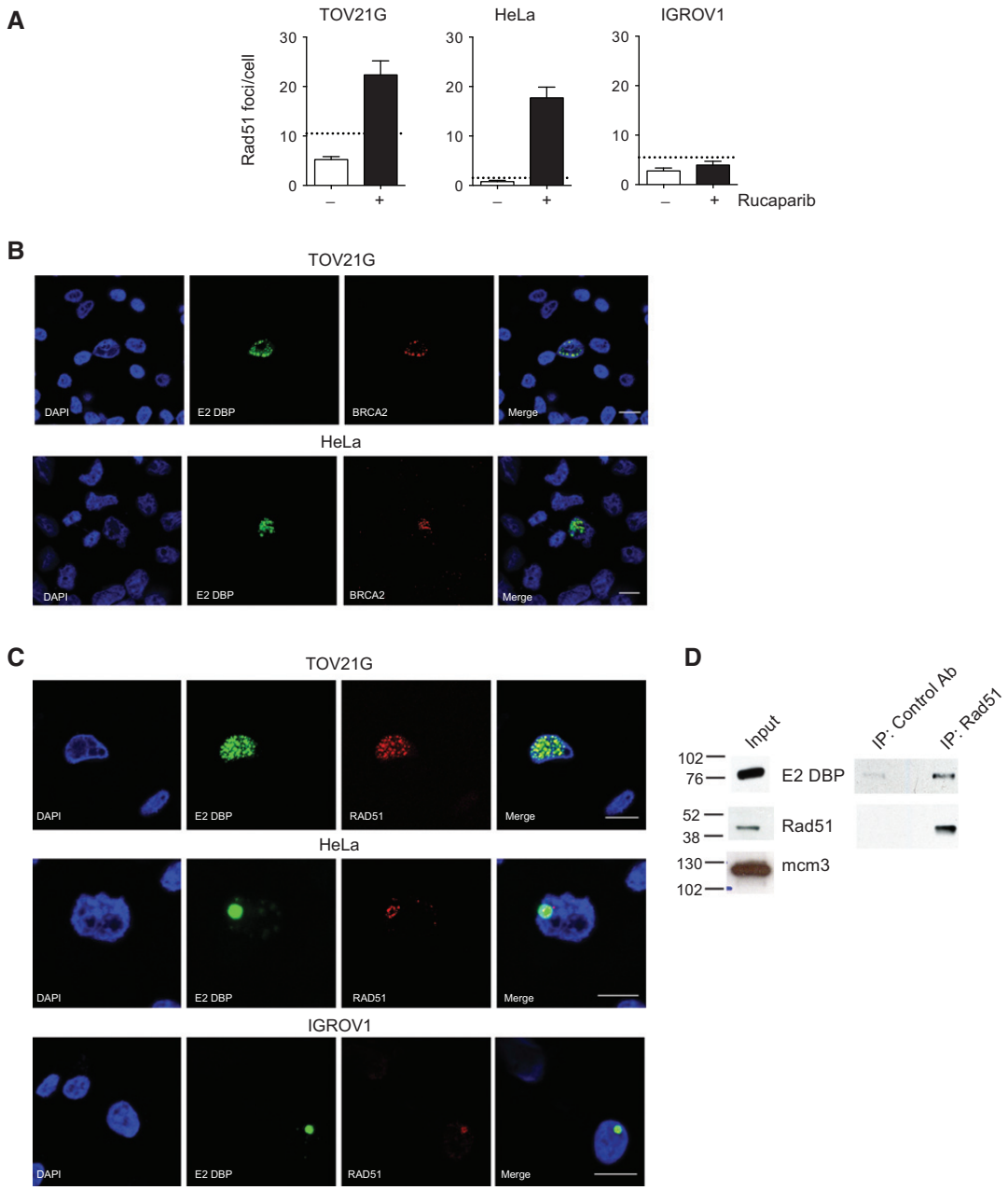

Figure 3.
RAD51 and BRCA2 colocalize with sites of adenovirus replication in multiple malignant cell lines. A, HR competence was assessed in TOV21G, HeLa, and IGROV1 cells as for Fig. 1A. Bars, mean (±SD) number of RAD51 foci per cell. Dotted line, 2× number of foci in untreated cells. TOV21G and HeLa demonstrate HR competence, while IGROV1 are HR defective. B and C, cells were fixed in 4% PFA following infection with *d*/922-947 (MOI 10). Expression of adenovirus E2 DNA binding protein, BRCA2 (B), and RAD51 (C) was assessed by confocal microscopy. D, RAD51 was immunoprecipitated from TOV21G infected with *d*/922-947 (MOI 10), and the presence of E2 DNA binding protein was detected by immunoblotting.

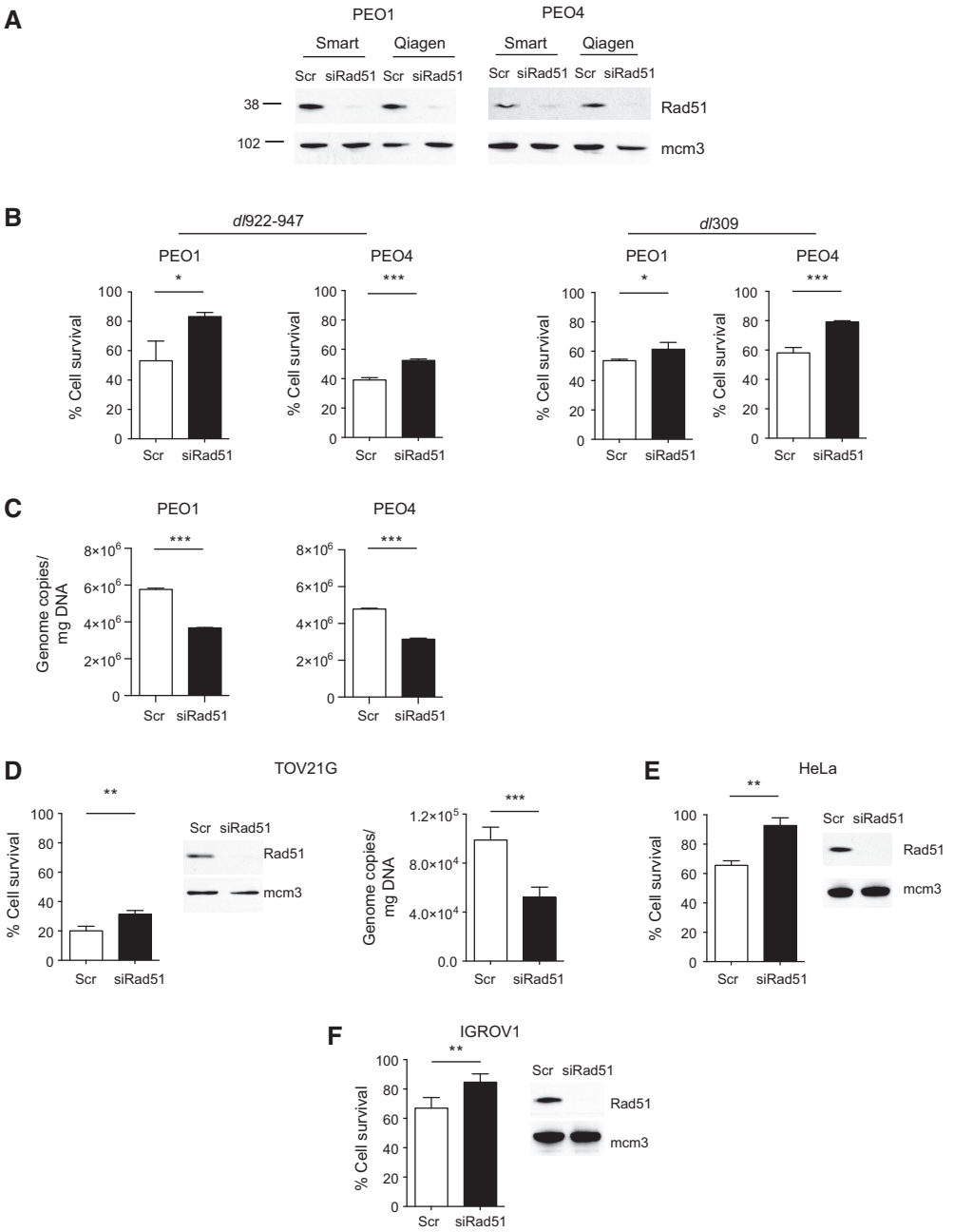

Figure 4.
RAD51 knockdown decreases adenovirus efficacy and replication. A, using two different siRNA pools, RAD51 was knocked down in both PEO1 and PEO4 cells. B and C, 24 hours following siRNA-mediated RAD51 knockdown, PEO1 (MOI 300) and PEO4 cells (MOI 30) were infected with *dl*922-947 (left) and *dl*309 (right, MOI 500 and 50). Survival was assessed 96 hours after infection by the MTT assay (B). Viral replication was also assessed 48 hours after infection by quantitative PCR (C). *, $P < 0.05$; ***, $P < 0.001$. D–F, 24 hours following siRNA-mediated RAD51 knockdown, TOV21G (D), HeLa (E), and IGROV1 (F) cells were infected with *dl*922-947 (MOI 1, 8, and 5 respectively). Survival was assessed 96 hours after infection by the MTT assay. RAD51 knockdown was confirmed by immunoblot. Viral replication was also assessed in TOV21G 48 hours after infection. **, $P < 0.01$; ***, $P < 0.001$.

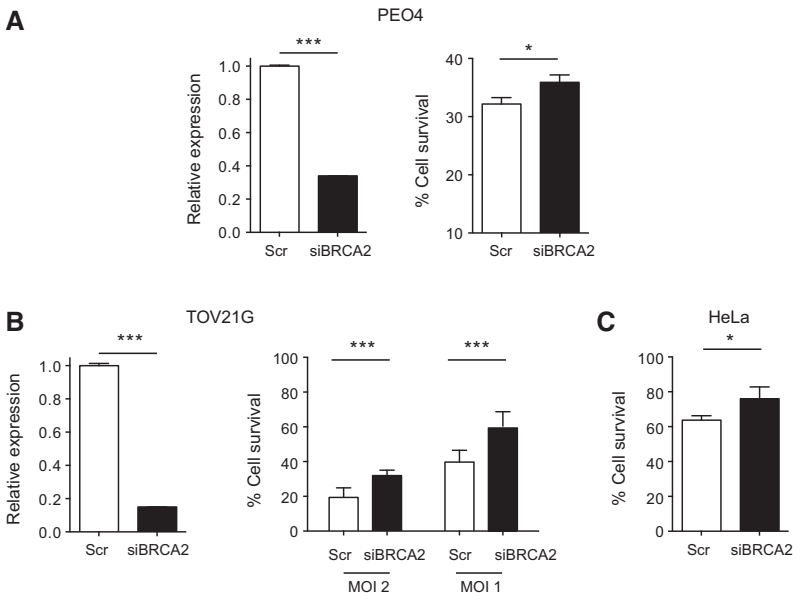

Figure 5.
BRCA2 knockdown also decreases adenovirus efficacy and replication. A, 24 hours following siRNA-mediated BRCA2 knockdown, PEO4 cells were infected with *dl*922-947 (MOI 30). Survival was assessed 96 hours after infection by the MTT assay. BRCA2 knockdown was confirmed by quantitative RT-PCR, normalized to 18S RNA. *, $P < 0.05$; ***, $P < 0.001$. B and C, 24 hours following siRNA-mediated BRCA2 knockdown, TOV21G (B) and HeLa (C) cells were infected with *dl*922-947 (MOI 1 and 2 for TOV21G; MOI 8 for HeLa). Survival was assessed 96 hours after infection by the MTT assay. BRCA2 knockdown was confirmed by quantitative RT-PCR in TOV21G cells, normalized to 18S RNA. *, $P < 0.05$; ***, $P < 0.001$.

show that RAD51 influences adenovirus activity and locates to VRC in the absence of functional BRCA2.

HR is vitally important in the biology of HGSOC. Tumors with intact HR are less likely to respond to platinum-based chemotherapy (4) and have a worse overall prognosis (6). HR is a complex process involving multiple proteins. However, BRCA2 is particularly important, as it mediates the loading of RAD51 onto 3′-single-stranded DNA overhangs (created by MRE11 nuclease activity), creating a RAD51 nucleoprotein filament. The nucleoprotein filament then catalyzes the critical step of HR, namely strand invasion and homology search on the sister chromatid.

The interaction between adenoviral infection and the DDR is complex; in contrast to other forms of DNA damage, such as irradiation, where damage occurs almost instantaneously, viral infection represents a dynamic onslaught to the cell, which makes analysis challenging. However, the DDR is clearly activated following viral infection—here and previously (22), we show robust phosphorylation of H2AX following infection with *dl*922-947 and other Ad5 viruses, which others have also observed (32). We have also shown that Ad5 infection activates replication-dependent ATR/Chk1 signaling (22). Ad5 inhibits DDR using a variety of mechanisms, prime among which is proteasome-mediated degradation of key cellular proteins, including MRE11 and DNA Ligase IV. Degradation is largely orchestrated by E1B55K and E4orf6, in concert with cellular proteins Cul5, Rbx1, and elongins B and C (15, 33), while infection with E4-deleted viruses results in concatemer formation (34). Consistent with these previous findings, we show here that MRE11 expression diminishes following Ad5 infection in ovarian cancer cells, regardless of their HR competence, and that inhibition of DNA-PK has no effect on overall cytotoxicity in both HR-competent and HR-defective cells. In addition, our Southern blot showed no concatemer formation in either PEO4 or PEO1 cells, suggesting that viral DNA can be processed correctly regardless of the state of cellular HR competence.

The relocation of other DDR proteins, including RPA32 (35), ATR, ATRIP, Rad9, TOPBP1, Rad17, and hnRNPUL1 (36–38), to VRC following Ad5 infection has been described previously. However, it has been unclear whether this relocalization inhibits DNA damage repair function or whether it is required for viral replication (reviewed in 39)—in the case of BRCA2 and RAD51, our data suggest the latter, as loss of either protein reduces Ad5 replication. In addition, using three different techniques to assess HR function, our results suggest that the ability of cells to repair DNA DSB damage via HR is not inhibited following Ad5 infection. This reinforces the idea that Ad5 utilizes components of the HR pathway rather than degrading and inhibiting them, as is the case with NHEJ.

Several key questions remain. First, how do cells retain the apparent capacity to repair DSB damage by HR following the proteasomal degradation of MRE11, which is critical for end resection? Although MRE11 is clearly critical to end resection, other molecules, in particular CtIP and Exo1, can also fulfill this role (40, 41). Thus, it is possible that other proteins substitute for the MRE11 end-resection function following Ad5 infection. Also, degradation of MRE11 is not complete (see Fig. 2B and ref. 42); thus, there may be a dosage effect whereby the remaining MRE11 retains sufficient end-resection capacity following adenovirus infection. Nonetheless, whatever residual HR capacity remains following infection is still unable to repair virus-induced genomic DNA damage. This may result from both the cell-cycle and DNA replication states induced by the virus. Adenovirus infection drives infected cells into an S phase–like state, with endoreduplication of genomic DNA (43). However, genomic DNA replication is clearly disorganized, which may preclude reliable generation of intact sister chromatids. In addition, adenovirus infection causes override of multiple cell-cycle checkpoints, with

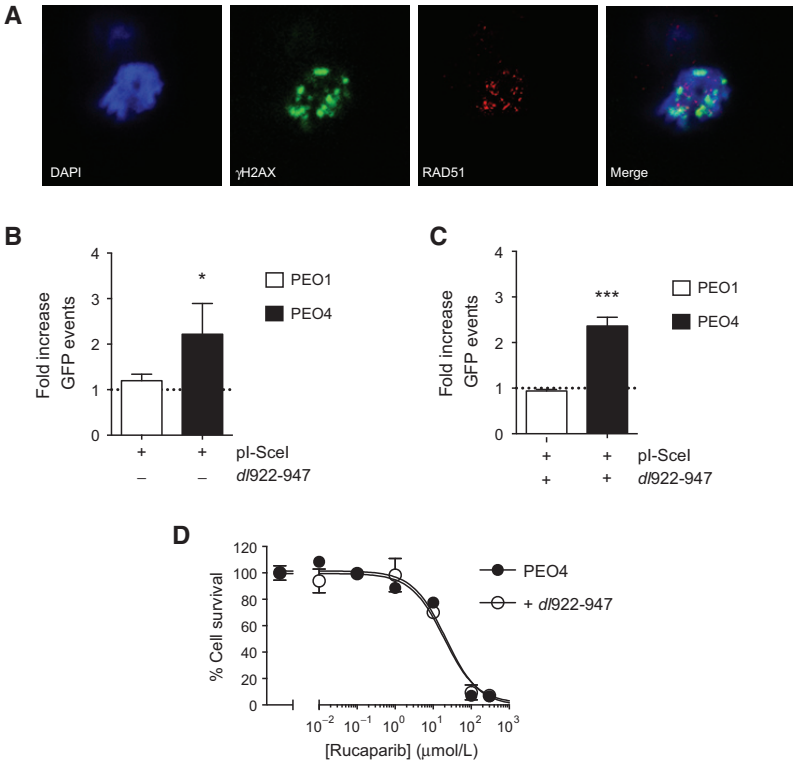

Figure 6.
Adenovirus infection does not inhibit homology-mediated DNA repair. A, PEO4 cells were infected with *dl*922-957 (MOI 10). 24 hours after infection, cells were fixed. Expression of γH2AX and RAD51 was assessed by confocal microscopy. B, PEO1 and PEO4 cells stably expressing DR-GFP plasmid were transfected with a plasmid encoding the rare cutting endonuclease (pI-SceI) or control plasmid. 24 hours thereafter, expression of GFP was assessed by flow cytometry. Data show fold change in GFP-positive events following pI-SceI transfection relative to control plasmid (dotted line). Bars, mean ±SD. *, $P < 0.05$ compared with control plasmid transfection. C, PEO1 and PEO4 cells stably expressing DR-GFP plasmid were infected with *dl*922-947 (MOI 50 and 500, respectively). 24 hours later, they were transfected with pI-SceI or control plasmid. 24 hours thereafter, expression of GFP was assessed by flow cytometry. Data again show fold change in GFP-positive events following pI-SceI transfection relative to control plasmid (dotted line). Bars, mean ±SD. ***, $P < 0.001$ compared with control plasmid transfection. D, PEO4 cells were infected with *dl*922-947 MOI 50 and 24 hours later treated with rucaparib (0.01–300 μmol/L) for 72 hours.

appearance of multiple abnormal mitoses (21). Thus, cells may slip rapidly through S and G_2 phases, thereby precluding HR repair. This reemphasizes the challenge of investigating cellular responses to adenovirus infection, where changes are dynamic and evolve over a period of 48 to 72 hours.

A second key question is how do BRCA2 and RAD51 relocate to VRC and which adenovirus proteins drive the process? And indeed what is their precise function within these VRC? Ad5E4orf3 is responsible for relocalization of PML protein into cytoplasmic tracks, but whether it is also responsible for movement of cellular proteins into VRC is unknown. Our immunoprecipitation suggested a direct interaction between RAD51 and E2DBP; our attempts at immunoblot and immunoprecipitation of BRCA2 were unsuccessful, so we do not know whether there is also a similar direct interaction with E2DBP. Certainly, the RAD51 role in viral efficacy appears independent of its function in HR as knockdown in HR-incompetent cell lines also reduces viral efficacy. Our data, however, show that the presence of BRCA2 together with RAD51 results in more efficient viral replication. Adenovirus DNA replication generates a displaced single strand of parental DNA in addition to a duplex formed of a newly synthesized daughter strand plus the other parental strand, a structure that could resemble a replication fork. Both RAD51 and BRCA2 have recently been shown to protect newly replicated DNA strands at stalled replication forks from degradation (44, 45) and this role is independent of their function in HR. It is possible that adenovirus utilizes this function of RAD51 and BRCA2 resulting in more accurate and efficient viral DNA replication, and that RAD51 can execute this role alone. Certainly, no BRCA2 homolog has been identified in lower eukaryotes, including *Saccharomyces cerevisiae*, in which Rad51 alone can resolve replication stress. Clearly adenoviral replication and cytotoxicity can still occur in the absence of BRCA2 and RAD51, suggesting that these proteins are supportive rather than critical to the adenoviral lifecycle.

Third, why are there differences between adenovirus species in this effect? Here, we show that sensitivity to Ad11 and Ad35 does not vary between BRCA2 WT and mutant cells, and previous data demonstrate that DDR proteins vary in their targeting by different adenoviral serotypes (42). Nonetheless, it is clear that interaction with DDR machinery is a widespread phenomenon in DNA virus infection. ATM is required for optimal replication of SV40 (46) and HSV-1 requires ATM and the MRN complex for virus replication (47), while proteins involved in HR have been shown to localize to EBV VRCs (48).

In summary, we show for the first time that adenovirus type 5 relocalizes components of the HR pathway to VRC and that viral replication is enhanced in the presence of functional HR. We have recently shown that oncolytic adenoviruses may be more effective in ovarian cancers with paclitaxel resistance (30). Data here show that these viruses may also have specific activity in another group

of poor prognosis ovarian cancers, namely those with platinum and PARP inhibitor resistance through intact HR function. Given the importance of HR in the biology of HGSOC, an understanding of the interaction between HR and any novel therapy is particularly important in patient selection for clinical trials and identification of novel virus/drug combinations.

Disclosure of Potential Conflicts of Interest

No potential conflicts of interest were disclosed.

Authors' Contributions

Conception and design: L.A. Tookman, C.M. Connell, I.A. McNeish
Development of methodology: L.A. Tookman, I.A. McNeish
Acquisition of data (provided animals, acquired and managed patients, provided facilities, etc.): L.A. Tookman, A.K. Browne, C.K. Ingemarsdotter, S. Dowson, A. Shibata, I.A. McNeish, G. Bridge
Analysis and interpretation of data (e.g., statistical analysis, biostatistics, computational analysis): L.A. Tookman, S. Dowson, M. Lockley, S.A. Martin, I.A. McNeish
Writing, review, and/or revision of the manuscript: L.A. Tookman, C.M. Connell, C.K. Ingemarsdotter, S. Dowson, A. Shibata, M. Lockley, S.A. Martin, I.A. McNeish, G. Bridge
Administrative, technical, or material support (i.e., reporting or organizing data, constructing databases): A.K. Browne, S. Dowson
Study supervision: S.A. Martin, I.A. McNeish

Acknowledgments

The authors thank Linda Hammond and Guglielmo Rosignoli for technical assistance with microscopy and flow cytometry respectively.

Grant Support

This work was funded by the Medical Research Council, grant references G1002009 (to L.A. Tookman) and G0601891 (to I.A. McNeish).

The costs of publication of this article were defrayed in part by the payment of page charges. This article must therefore be hereby marked *advertisement* in accordance with 18 U.S.C. Section 1734 solely to indicate this fact.

Received April 27, 2015; revised September 15, 2015; accepted September 30, 2015; published OnlineFirst October 9, 2015.

References

1. Alexandrov LB, Nik-Zainal S, Wedge DC, Aparicio SA, Behjati S, Biankin AV, et al. Signatures of mutational processes in human cancer. Nature 2013;500:415–21.
2. Alsop K, Fereday S, Meldrum C, Defazio A, Emmanuel C, George J, et al. BRCA mutation frequency and patterns of treatment response in BRCA mutation-positive women with ovarian cancer: a report from the Australian Ovarian Cancer Study Group. J Clin Oncol 2012;30:2654–63.
3. TCGA. Integrated genomic analyses of ovarian carcinoma. Nature 2011; 474:609–15.
4. Mukhopadhyay A, Plummer ER, Elattar A, Soohoo S, Uzir B, Quinn JE, et al. Clinicopathological features of homologous recombination-deficient epithelial ovarian cancers: sensitivity to PARP inhibitors, platinum, and survival. Cancer Res 2012;72:5675–82.
5. McNeish I, Coleman RL, Oza A, Konecny G, O'Malley DM, Kichenadasse G, et al. Updated results of Ariel2, a phase 2 open-label study to identify ovarian cancer patients likely to respond to rucaparib. Int J Gynecol Cancer 2014;24:323–4.
6. Bolton KL, Chenevix-Trench G, Goh C, Sadetzki S, Ramus SJ, Karlan BY, et al. Association between BRCA1 and BRCA2 mutations and survival in women with invasive epithelial ovarian cancer. JAMA 2012;307:382–90.
7. Heise C, Hermiston T, Johnson L, Brooks G, Sampson-Johannes A, Williams A, et al. An adenovirus E1A mutant that demonstrates potent and selective systemic anti-tumoral efficacy. Nature Med 2000;6:1134–9.
8. Fueyo J, Gomez-Manzano C, Alemany R, Lee P, McDonnell T, Mitlianga P, et al. A mutant oncolytic adenovirus targeting the Rb pathway produces anti-glioma effect *in vivo*. Oncogene 2000;19:2–12.
9. Lockley M, Fernandez M, Wang Y, Li NF, Conroy SE, Lemoine NR, et al. Activity of the adenoviral E1A deletion mutant dl922-947 in ovarian cancer: comparison with adenovirus wild-type, bioluminescence monitoring and intraperitoneal delivery in icodextrin. Cancer Res 2006;66:989–98.
10. Leyton J, Lockley M, Aerts JL, Baird SK, Aboagye EO, Lemoine NR, et al. Quantifying the activity of adenoviral E1A CR2 deletion mutants using renilla luciferase bioluminescence and 3′-Deoxy-3′-[18F]Fluorothymidine positron emission tomography imaging. Cancer Res 2006;66:9178–85.
11. Baird SK, Aerts JL, Eddaoudi A, Lockley M, Lemoine NR, McNeish IA. Oncolytic adenoviral mutants induce a novel mode of programmed cell death in ovarian cancer. Oncogene 2008;27:3081–90.
12. Flak MB, Connell CM, Chelala C, Archibald K, Salako MA, Pirlo KJ, et al. p21 promotes oncolytic adenoviral activity in ovarian cancer and is a potential biomarker. Mol Cancer 2010;9:175.
13. Karen KA, Hearing P. Adenovirus core protein VII protects the viral genome from a DNA damage response at early times after infection. J Virol 2011; 85:4135–42.
14. Karen KF, Hoey PJ, Young CS, Hearing P. Temporal regulation of the Mre11-Rad50-Nbs1 complex during adenovirus infection. J Virol 2009;83: 4565–73.
15. Harada JN, Shevchenko A, Pallas DC, Berk AJ. Analysis of the adenovirus E1B-55K-anchored proteome reveals its link to ubiquitination machinery. J Virol 2002;76:9194–206.
16. Araujo FD, Stracker TH, Carson CT, Lee DV, Weitzman MD. Adenovirus type 5 E4orf3 protein targets the Mre11 complex to cytoplasmic aggresomes. J Virol 2005;79:11382–91.
17. Evans JD, Hearing P. Relocalization of the Mre11-Rad50-Nbs1 complex by the adenovirus E4 ORF3 protein is required for viral replication. J Virol 2005;79:6207–15.
18. Baker A, Rohleder KJ, Hanakahi LA, Ketner G. Adenovirus E4 34k and E1b 55k oncoproteins target host DNA ligase IV for proteasomal degradation. J Virol 2007;81:7034–40.
19. Boyer J, Rohleder K, Ketner G. Adenovirus E4 34k and E4 11k inhibit double strand break repair and are physically associated with the cellular DNA-dependent protein kinase. Virology 1999;263: 307–12.
20. Orazio NI, Naeger CM, Karlseder J, Weitzman MD. The adenovirus E1b55K/E4orf6 complex induces degradation of the Bloom helicase during infection. J Virol 2011;85:1887–92.
21. Connell CM, Wheatley SP, McNeish IA. Nuclear survivin abrogates multiple cell cycle checkpoints and enhances viral oncolysis. Cancer Res 2008;69:7923–31.
22. Connell CM, Shibata A, Tookman LA, Archibald KM, Flak MB, Pirlo KJ, et al. Genomic DNA damage and ATR-Chk1 signaling determine oncolytic adenoviral efficacy in human ovarian cancer cells. J Clin Invest 2011;121: 1283–97.
23. Mosmann T. Rapid colorimetric assay for cellular growth and survival: application to proliferation and cytotoxicity assays. J Immunol Methods 1983;65:55–63.
24. Plessis D, Sale JE. Monitoring I-SceI-induced double-strand break repair in DT40 cells. Methods Mol Biol 2012;920:371–7.
25. Pierce AJ, Johnson RD, Thompson LH, Jasin M. XRCC3 promotes homology-directed repair of DNA damage in mammalian cells. Genes Dev 1999;13:2633–8.
26. Langdon SP, Lawrie SS, Hay FG, Hawkes MM, McDonald A, Hayward IP, et al. Characterization and properties of nine human ovarian adenocarcinoma cell lines. Cancer Res 1988;48:6166–72.
27. Sakai W, Swisher EM, Jacquemont C, Chandramohan KV, Couch FJ, Langdon SP, et al. Functional restoration of BRCA2 protein by secondary BRCA2 mutations in BRCA2-mutated ovarian carcinoma. Cancer Res 2009;69:6381–6.
28. Mukhopadhyay A, Elattar A, Cerbinskaite A, Wilkinson SJ, Drew Y, Kyle S, et al. Development of a functional assay for homologous recombination status in primary cultures of epithelial ovarian tumor and correlation with sensitivity to poly(ADP-ribose) polymerase inhibitors. Clin Cancer Res 2010;16:2344–51.

29. Cooke SL, Ng CK, Melnyk N, Garcia MJ, Hardcastle T, Temple J, et al. Genomic analysis of genetic heterogeneity and evolution in high-grade serous ovarian carcinoma. Oncogene 2010;29:4905–13.
30. Ingemarsdotter CK, Tookman LA, Browne A, Pirlo K, Cutts R, Chelela C, et al. Paclitaxel resistance increases oncolytic adenovirus efficacy via upregulated CAR expression and dysfunctional cell cycle control. Mol Oncol 2015;9:791–805.
31. Domcke S, Sinha R, Levine DA, Sander C, Schultz N. Evaluating cell lines as tumour models by comparison of genomic profiles. Nat Commun 2013;4:2126.
32. Nichols GJ, Schaack J, Ornelles DA. Widespread phosphorylation of histone H2AX by species C adenovirus infection requires viral DNA replication. J Virol 2009;83:5987–98.
33. Querido E, Blanchette P, Yan Q, Kamura T, Morrison M, Boivin D, et al. Degradation of p53 by adenovirus E4orf6 and E1B55K proteins occurs via a novel mechanism involving a Cullin-containing complex. Genes Dev 2001;15:3104–17.
34. Weiden MD, Ginsberg HS. Deletion of the E4 region of the genome produces adenovirus DNA concatemers. Proc Natl Acad Sci U S A 1994;91:153–7.
35. Stracker TH, Lee DV, Carson CT, Araujo FD, Ornelles DA, Weitzman MD. Serotype-specific reorganization of the Mre11 complex by adenoviral E4orf3 proteins. J Virol 2005;79:6664–73.
36. Blackford AN, Bruton RK, Dirlik O, Stewart GS, Taylor AM, Dobner T, et al. A role for E1B-AP5 in ATR signaling pathways during adenovirus infection. J Virol 2008;82:7640–52.
37. Carson CT, Schwartz RA, Stracker TH, Lilley CE, Lee DV, Weitzman MD. The Mre11 complex is required for ATM activation and the G2/M checkpoint. EMBO J 2003;22:6610–20.
38. Carson CT, Orazio NI, Lee DV, Suh J, Bekker-Jensen S, Araujo FD, et al. Mislocalization of the MRN complex prevents ATR signaling during adenovirus infection. EMBO J 2009;28:652–62.
39. Turnell AS, Grand RJ. DNA viruses and the cellular DNA-damage response. J Gen Virol 2012;93:2076–97.
40. Gravel S, Chapman JR, Magill C, Jackson SP. DNA helicases Sgs1 and BLM promote DNA double-strand break resection. Genes Dev 2008;22:2767–72.
41. Makharashvili N, Tubbs AT, Yang SH, Wang H, Barton O, Zhou Y, et al. Catalytic and noncatalytic roles of the CtIP endonuclease in double-strand break end resection. Mol Cell 2014;54:1022–33.
42. Forrester NA, Sedgwick GG, Thomas A, Blackford AN, Speiseder T, Dobner T, et al. Serotype-specific inactivation of the cellular DNA damage response during adenovirus infection. J Virol 2011;85:2201–11.
43. Cherubini G, Petouchoff T, Grossi M, Piersanti S, Cundari E, Saggio I. E1B55K-deleted adenovirus (ONYX-015) overrides G1/S and G2/M checkpoints and causes mitotic catastrophe and endoreduplication in p53-proficient normal cells. Cell Cycle 2006;5:2244–52.
44. Hashimoto Y, Ray Chaudhuri A, Lopes M, Costanzo V. Rad51 protects nascent DNA from Mre11-dependent degradation and promotes continuous DNA synthesis. Nat Struct Mol Biol 2010;17:1305–11.
45. Schlacher K, Christ N, Siaud N, Egashira A, Wu H, Jasin M. Double-strand break repair-independent role for BRCA2 in blocking stalled replication fork degradation by MRE11. Cell 2011;145:529–42.
46. Sowd GA, Mody D, Eggold J, Cortez D, Friedman KL, Fanning E. SV40 utilizes ATM kinase activity to prevent non-homologous end joining of broken viral DNA replication products. PLoS Pathog 2014;10:e1004536.
47. Lilley CE, Carson CT, Muotri AR, Gage FH, Weitzman MD. DNA repair proteins affect the lifecycle of herpes simplex virus 1. Proc Natl Acad Sci U S A 2005;102:5844–9.
48. Kudoh A, Iwahori S, Sato Y, Nakayama S, Isomura H, Murata T, et al. Homologous recombinational repair factors are recruited and loaded onto the viral DNA genome in Epstein–Barr virus replication compartments. J Virol 2009;83:6641–51.

Research article

Genomic DNA damage and ATR-Chk1 signaling determine oncolytic adenoviral efficacy in human ovarian cancer cells

Claire M. Connell,[1,2] Atsushi Shibata,[2] Laura A. Tookman,[1] Kyra M. Archibald,[1] Magdalena B. Flak,[1] Katrina J. Pirlo,[1] Michelle Lockley,[1] Sally P. Wheatley,[2] and Iain A. McNeish[1]

[1]Centre for Molecular Oncology and Imaging, Barts Cancer Institute, Queen Mary University of London, London, United Kingdom.
[2]Genome Damage and Stability Centre, University of Sussex, Brighton, United Kingdom.

Oncolytic adenoviruses replicate selectively within and lyse malignant cells. As such, they are being developed as anticancer therapeutics. However, the sensitivity of ovarian cancers to adenovirus cytotoxicity varies greatly, even in cells of similar infectivity. Using both the adenovirus E1A-CR2 deletion mutant *dl*922-947 and WT adenovirus serotype 5 in a panel of human ovarian cancer cell lines that cover a 3-log range of sensitivity, we observed profound overreplication of genomic DNA only in highly sensitive cell lines. This was associated with the presence of extensive genomic DNA damage. Inhibition of ataxia telangiectasia and Rad3-related checkpoint kinase 1 (ATR-Chk1), but not ataxia telangiectasia mutated (ATM), promoted genomic DNA damage and overreplication in resistant and partially sensitive cells. This was accompanied by increased adenovirus cytotoxicity both in vitro and in vivo in tumor-bearing mice. We also demonstrated that Cdc25A was upregulated in highly sensitive ovarian cancer cell lines after adenovirus infection and was stabilized after loss of Chk1 activity. Knockdown of Cdc25A inhibited virus-induced DNA damage in highly sensitive cells and blocked the effects of Chk1 inhibition in resistant cells. Finally, inhibition of Chk1 decreased homologous recombination repair of virus-induced genomic DNA double-strand breaks. Thus, virus-induced host cell DNA damage signaling and repair are key determinants of oncolytic adenoviral activity, and promoting unscheduled DNA synthesis and/or impeding homologous recombination repair could potentiate the effects of oncolytic adenoviruses in the treatment of ovarian cancer.

Introduction

Oncolytic viruses multiply selectively within infected cancer cells and cause death, with the release of mature viruses that infect neighboring cells. The adenovirus deletion mutant *dl*922-947 contains a 24-bp deletion (amino acids 122–129) in the E1A-CR2 region, which binds to E2F-pRb complexes, thereby dissociating E2F to drive cells into an S phase–like state, allowing transactivation of genes necessary for viral DNA replication (1). We have previously shown that *dl*922-947 has considerable activity in ovarian cancer and is more potent than E1A WT adenoviruses and the E1B-55K mutant *dl*1520 (Onyx-015, H101) (2, 3). *dl*922-947 replicates selectively in cells with abnormalities of the Rb pathway and consequent G_1/S checkpoint, defects seen in over 90% of human cancers (4). Multiple different Rb pathway abnormalities have been described in ovarian cancer (5, 6), and, even in ovarian cancer cells that are readily infected with adenovirus serotype 5 (Ad5) vectors, there is huge variability in sensitivity to *dl*922-947–mediated cell death. In addition, the mechanisms by which oncolytic adenoviruses induce cell death in cancer cells remain unclear (7).

We recently showed that early expression of E1A correlated well with cell sensitivity to *dl*922-947 (8). Upon infection, E1A is the first adenoviral protein to be expressed and is required for the efficient transcription of other viral early genes (9) as well as the disruption of pRb-E2F complexes (1). We have previously shown that *dl*922-947 activity is also associated with deregulation of multiple cell cycle checkpoints, which accelerates cell cycle progression and enhances efficacy (10).

However, one consequence of such deregulated cell cycle progression is unscheduled replication of cellular DNA, which will activate the DNA damage signaling pathways whose function is to preserve the integrity of the cellular genome (11). Two key kinases are central to DNA damage responses, ataxia telangiectasia mutated (ATM) and ataxia telangiectasia and Rad3-related (ATR). ATM is classically activated by double-strand breaks (DSBs), whereas ATR can be activated by a wide variety of DNA events, including replication-associated DNA damage, resected DSB ends, and nucleotide excision repair. When activated, both trigger a series of signaling events and activate downstream cellular proteins, such as the checkpoint kinases 1 and 2 (Chk1 and Chk2). Both ATM and ATR can be activated by adenovirus infection (12, 13). However, the virus can evade some DNA damage responses: for example, E4orf3 causes immobilization of the MRN complex, which can inhibit ATR signaling (14), while MRE11 is degraded in response to the activity of the E1B55K/E4orf6 complex (15), which blocks signaling downstream of ATM. Nonetheless, infected cells still demonstrate some evidence of DNA damage signaling in the form of H2AX phosphorylation (13, 16).

We sought to explore the link between genomic DNA replication, DNA damage responses, and the overall efficacy of oncolytic adenoviruses in ovarian cancer. Our findings suggest that host cell DNA damage responses induced by aberrant genomic DNA replication strongly influence the potency of adenoviruses. Highly sensitive cells displayed profound overreplication of genomic DNA with

Authorship note: Claire M. Connell and Atsushi Shibata contributed equally to this work.

Conflict of interest: The authors have declared that no conflict of interest exists.

Citation for this article: *J Clin Invest.* 2011;121(4):1283–1297. doi:10.1172/JCI43976.

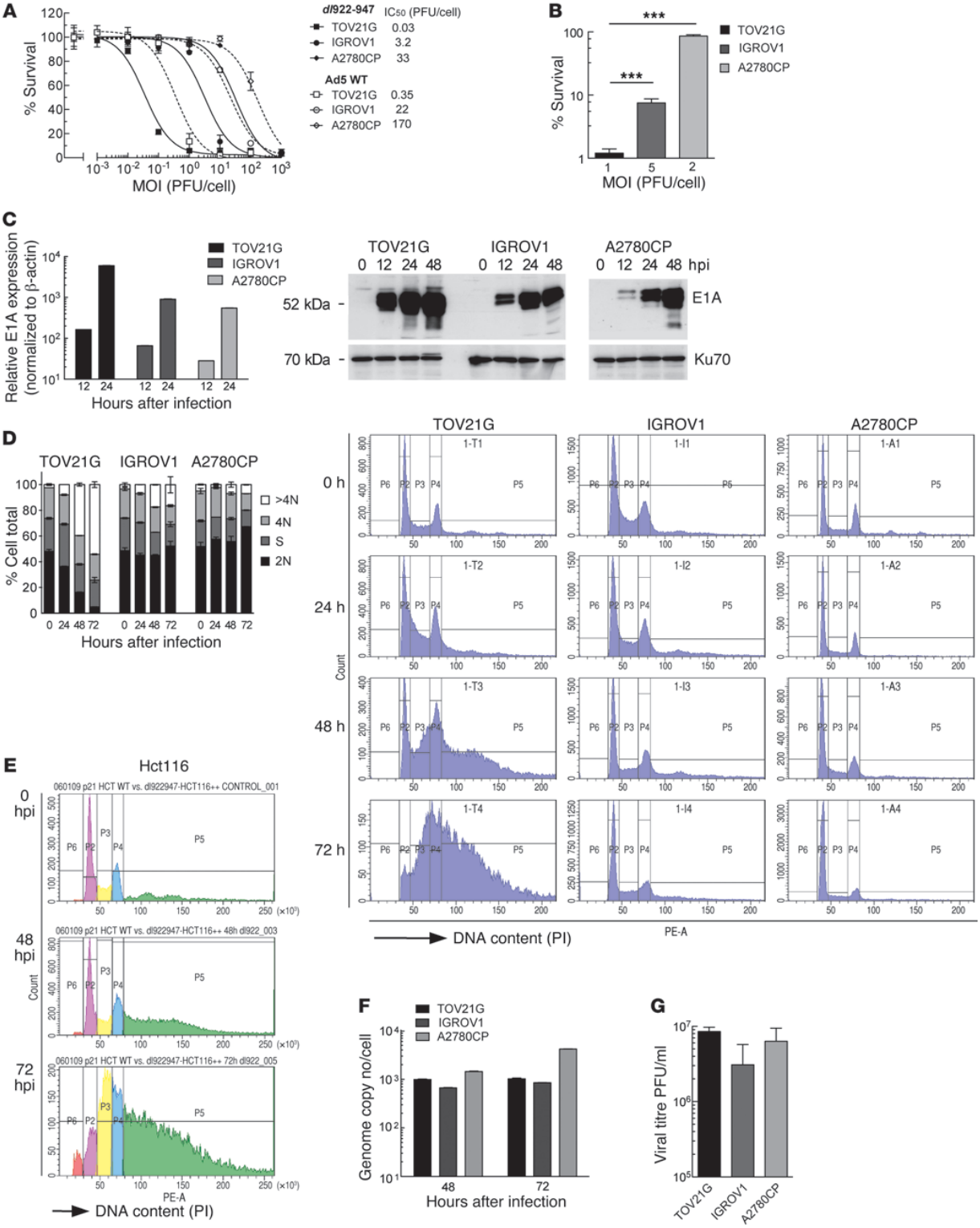
A
% Survival
MOI (PFU/cell)
dl922-947 IC50 (PFU/cell)
TOV21G 0.03
IGROV1 3.2
A2780CP 33
Ad5 WT
TOV21G 0.35
IGROV1 22
A2780CP 170
B
% Survival
MOI (PFU/cell)
TOV21G
IGROV1
A2780CP
***
***
C
Relative E1A expression (normalized to β-actin)
Hours after infection
TOV21G
IGROV1
A2780CP
0 12 24 48 hpi
52 kDa
70 kDa
E1A
Ku70
D
% Cell total
Hours after infection
>4N
4N
S
2N
0 h
24 h
48 h
72 h
Count
DNA content (PI)
PE-A
E
Hct116
0 hpi
48 hpi
72 hpi
DNA content (PI)
F
Genome copy no/cell
Hours after infection
G
Viral titre PFU/ml

Figure 1
Positive correlation between virus sensitivity and overreplication phenotype after *dl*922-947 infection in ovarian cancer cell lines. (**A**) Cell survival in TOV21G, IGROV1, and A2780CP cells was assessed by MTT assay 120 hpi with *dl*922-947 and Ad5 WT. (**B**) Survival of TOV21G, IGROV1, and A2780CP cells 120 hpi with *dl*922-947 at MOIs that permit 50% cell infectivity (MOI 1, 5, and 2 PFU/cell, respectively; data not shown). ***$P < 0.001$. (**C**) Expression of E1A was assessed by quantitative RT-PCR and immunoblot after infection with *dl*922-947 (MOI 7.5). Transcription is normalized to β-actin and presented relative to that of uninfected cells. Error bars (representing SD) are plotted on all data points but may be too small to be visible. (**D**) TOV21G, IGROV1, and A2780CP cells were harvested up to 72 hpi with *dl*922-947 (MOI 7.5), fixed in 70% cold ethanol, stained with PI, and analyzed by flow cytometry. >4N, cells with more than 4 N DNA content; 4N, cells with 4 N DNA content; S, cells in S phase; 2N, cells with 2 N DNA content. (**E**) Hct116 cells were harvested up to 72 hpi with *dl*922-947 (MOI 7.5), fixed in 70% cold ethanol, stained with PI, and analyzed by flow cytometry. IC_{50} for Hct116 cells 120 hpi with *dl*922-947 is approximately 0.04 PFU/cell (data not shown). (**F** and **G**) Replication of *dl*922-947 was assessed in TOV21G, IGROV1, and A2780CP cells after infection with *dl*922-947 (MOI 7.5) by quantitative PCR (**E**) 48 and 72 hpi and (**F**) by $TCID_{50}$ 72 hpi.

associated DNA damage and downstream signaling after infection with *dl*922-947. Moreover, inhibition of the ATR-Chk1 pathway increased genomic DNA overreplication and damage by preventing Chk1-mediated degradation of the Cdc25A phosphatase. Furthermore, Chk1 inhibition increased the number of DSBs, the most cytotoxic form of DNA damage, by preventing homologous recombination (HR) and increased sensitivity to *dl*922-947 activity both in vitro and in vivo. Similar results were observed after WT adenovirus infection, demonstrating that our findings are not specific to E1A-CR2 deletion mutants. Importantly, inhibition of the ATR-Chk1 pathway augmented sensitivity to adenovirus in cancer cells without affecting nonmalignant cells. As clinical trials of E1A-CR2–deleted adenoviruses have commenced (17), a better understanding of cellular responses to virus infection is vital and would open up the prospect of increased anticancer activity in patients.

Results

Adenovirus-induced cytotoxicity is associated with overreplication of cellular DNA in sensitive cells. The sensitivity of cancer cell lines to the oncolytic adenovirus *dl*922-947 varies considerably, even in cells with similar infectivity (8). TOV21G, IGROV1, and A2780CP are 3 ovarian cancer cell lines that cover a range of sensitivities, with IC_{50} values varying over 3 log scales (Figure 1A). The same wide range of sensitivity was seen with E1A WT adenoviruses (Figure 1A and Supplemental Figure 1A; supplemental material available online with this article; doi:10.1172/JCI43976DS1), although the WT viruses were consistently less potent in cancer cells than *dl*922-947, as seen before (3). The wide variation of sensitivity was not caused by differences in infectivity, as there were profound differences in cell survival at MOI that permitted 50% cells to be infected (Figure 1B). *E1A* is the first adenovirus gene to be expressed (18). As before, we found that early E1A transcription and protein expression correlated with cellular sensitivity to adenovirus (Figure 1C).

Cell cycle analysis revealed a stark contrast between the profiles of sensitive and insensitive cells after infection. TOV21G cells readily accumulated DNA contents of more than 4 N after *dl*922-947 infection; by 72 hours, the proportion of TOV21G cells with a DNA content of more than 4 N exceeded 50%. In IGROV1 cells, of intermediate sensitivity, the proportion reached 16.3% but only reached 7.0% in insensitive A2780CP cells, with little change throughout the course of infection (Figure 1D). Analysis of Hct116, another highly sensitive cancer line (*dl*922-947 $IC_{50} \approx$ 0.04 PFU/cell; data not shown), yielded similar cell cycle profiles to those of TOV21G cells, with a DNA content of more than 4 N of 58% by 72 hours after infection (hpi) (Figure 1E), while another resistant line, SKOV3ip1, generated profiles very similar to those of A2780CP cells (data not shown). Ad5 WT infection caused overreplication in TOV21G cells, although the proportion of cells with more than 4 N DNA was lower, reaching 34% 72 hpi (Supplemental Figure 1B). Thus, the effects seen with *dl*922-947 are not unique to ovarian cancer cells or to E1A-CR2 adenoviral deletion mutants, but they are greater than those seen with WT virus. The quantity of viral DNA generated in A2780CP cells was at least as great as that in the more sensitive TOV21G and IGROV1 cell lines (Figure 1F), indicating that the overreplication phenotype does not represent viral DNA but is a consequence of cellular DNA replication, consistent with previous reports (19, 20). In addition, the differential sensitivity amongst the cell lines was uncoupled from infectious virion production, with no significant difference in the number of virions produced in the 3 cell lines (Figure 1G). Adenovirus-induced cytotoxicity therefore appears not to depend upon the extent of virion production.

Oncolytic adenovirus cytotoxicity is associated extensive genomic DNA damage. Aberrant initiation of cellular DNA replication induces the accumulation of replication-associated DNA lesions (11, 21). To assess the extent of such DNA damage, cells were harvested up to 72 hpi with *dl*922-947, and phosphorylation of H2AX (ser 139; γH2AX) was analyzed immunocytochemically by flow cytometry with propidium iodide (PI) counterstaining to define cell cycle phase (22). Mock-infected cells displayed little γH2AX. In contrast, a huge increase in γH2AX was detectable in sensitive TOV21G cells after infection, and this increase occurred specifically in S and G_2/M cells and cells with more than 4 N DNA content (Figure 2A), indicating that DNA damage occurred after replication; at 48 hpi, over 90% of the overreplicated cells were γH2AX positive, compared with less than 10% γH2AX positivity in the G_1 population. Even in the insensitive A2780CP cells, in which there was minimal overreplication, the large majority of γH2AX positivity was seen in the S, G_2/M, and more than 4 N DNA content populations; by 48 hpi, only 7.9% cells were overreplicated, but 83% of these were γH2AX positive, whereas 60% of cells remained in G_1 phase, of which only 1% were γH2AX positive (Figure 2A).

It is known that expression of E1A can induce chromosomal aberrations (23). To assess the relationship between E1A expression and γH2AX, cells were infected with *dl*922-947 or a nonreplicating E1-deleted Ad5 vector, and the intensity of γH2AX and E1A within individual cells was assessed by immunofluorescence (IF) intensity over 48 hours (Figure 2, B and C). Infection with the nonreplicating vector induced no increase in γH2AX (data not shown). After *dl*922-947 infection, E1A and γH2AX increased in both sensitive and insensitive cell lines over time, and there was a strong positive correlation between the 2 across both cell lines ($r^2 = 0.879$, Pearson $r = 0.937$, $P = 0.0006$; Supplemental Figure 2A). However, the increases in both E1A and γH2AX were significantly greater in TOV21G cells than in A2780CP cells (Figure 2C and Supplemental Figure 2B). In addition, we identified a positive correlation between γH2AX and BrdU signals ($r^2 = 0.692$, Pearson

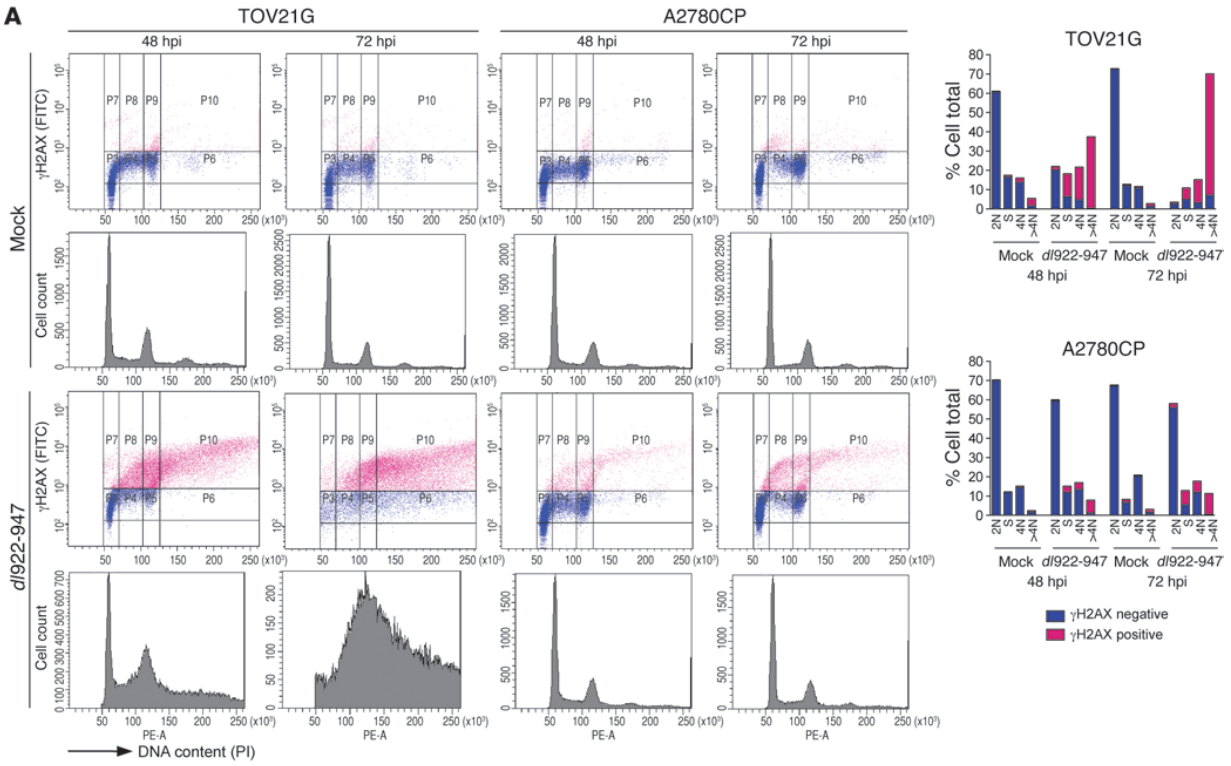
A
TOV21G
A2780CP
48 hpi
72 hpi
Mock
dl922-947
γH2AX (FITC)
Cell count
DNA content (PI)
PE-A
P7 P8 P9 P10
P3 P4 P5 P6
% Cell total
2N S 4N >4N
Mock dl922-947 Mock dl922-947
γH2AX negative
γH2AX positive

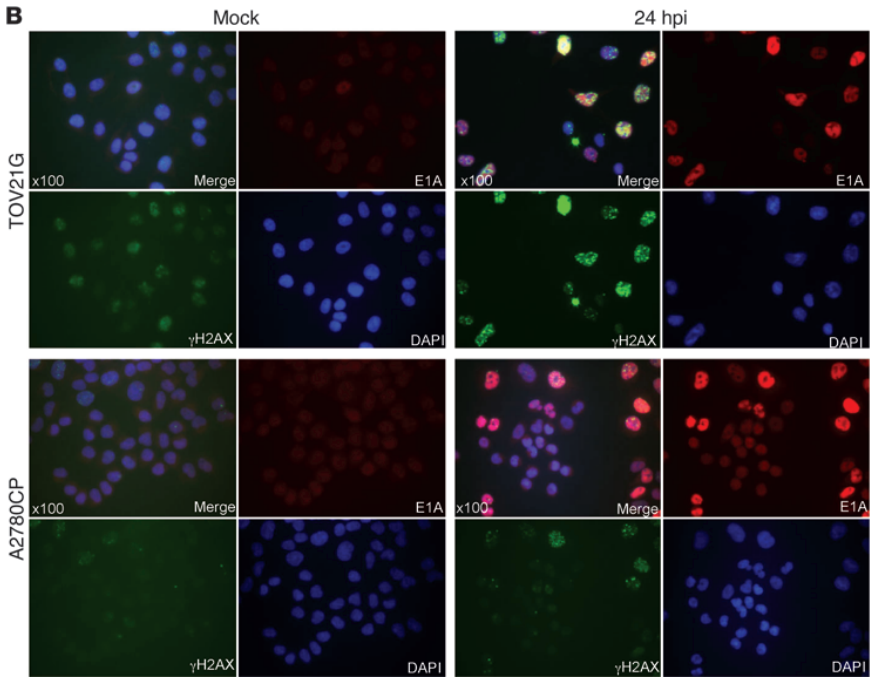
B
Mock
24 hpi
TOV21G
A2780CP
x100
Merge
E1A
γH2AX
DAPI

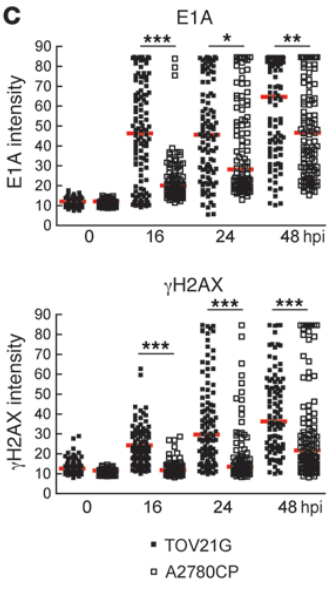
C
E1A
γH2AX
E1A intensity
γH2AX intensity
0 16 24 48 hpi
TOV21G
A2780CP

Figure 2
*dl*922-947 infection induces genomic DNA damage. (**A**) TOV21G and A2780CP cells were harvested after infection with *dl*922-947 (MOI 7.5), fixed in 70% cold ethanol, incubated with an anti-γH2AX antibody, counterstained with PI, and analyzed by flow cytometry. (**B** and **C**) TOV21G and A2780CP cells were fixed after infection with *dl*922-947 (MOI 7.5), stained for expression of E1A and γH2AX, counterstained with DAPI, and imaged. (**B**) Fluorescence intensity was assessed in more than 100 cells per condition using ImageJ software. Original magnification, ×100. (**C**) Each point represents a single cell, and each red bar represents the median. $^{*}P < 0.05$, $^{**}P < 0.01$, $^{***}P < 0.0001$; Mann-Whitney test.

$r = 0.832$, $P < 0.0001$, Supplemental Figure 3). BrdU-positive cells showed a pan-nuclear signal, distinct from virus replication centers, which are seen at discrete sites within the nucleus (24), supporting the association of γH2AX with genomic DNA replication. γH2AX was also detected in TOV21G cells after infection with E1A WT adenovirus, although the damage occurred more slowly than that with *dl*922-947 (Supplemental Figure 4).

Since significantly greater H2AX phosphorylation was observed in S and G_2/M cells and cells with more than 4 N DNA content, we investigated whether virus infection produced DSBs during genomic DNA replication. To analyze genomic DSBs, DNA from TOV21G and A2780CP cells was extracted up to 48 hpi, subjected to neutral pulsed-field gel electrophoresis (PFGE), and then labeled with anti-genomic DNA and anti-adenovirus type 5 DNA probes. X-irradiation (20 Gy) and TNF-related apoptosis-inducing ligand (TRAIL) (250 ng/ml) were used as positive controls for DSB and apoptotic DNA damage, respectively. *dl*922-947 induced genomic DSB damage in TOV21G cells, as indicated by the migration of genomic DNA out of the well (Figure 3A). DNA damage was initiated 24 hpi but greatly increased at 48 hpi. The intensive damage signal at approximately 50 kb is likely to represent apoptotic DNA fragmentation (25) rather than adenoviral DNA, as there is a large increase in this signal between 24 and 48 hpi in TOV21G cells but little increase in adenovirus DNA. Thus, there were different kinetics of genomic DNA damage and viral replication, which verified that infection with *dl*922-947 induces DNA damage in sensitive cells. In contrast, the resistant A2780CP cells had no genomic DNA damage compared with mock-infected controls, despite containing demonstrable adenoviral DNA. These results suggest strongly that cellular sensitivity to *dl*922-947 positively correlates with overreplication of genomic DNA and associated DNA damage.

H2AX can be phosphorylated by ATR at replication collapse (26). To investigate whether overreplication could induce ATR to activate Chk1, phosphorylation of Chk1 was examined after infection with *dl*922-947 (Figure 3B). In highly sensitive TOV21G cells, Chk1 was activated earlier than in either of the other 2 cell lines, confirming that there is functional downstream signaling in response to virus-induced genomic DNA overreplication and damage. Some later phosphorylation was seen in both IGROV1 and A2780CP cells, in keeping with the lower levels of overreplication and H2AX phosphorylation in these cells.

Chk1 inhibition augments dl922-947–induced overreplication and genomic DNA damage. To assess whether manipulation of the ATR-Chk1 pathway could influence the efficacy of adenoviruses in insensitive ovarian cancers, A2780CP cells were infected in the presence of the Chk1 inhibitor UCN-01 (7-hydroxystaurosporine; ref. 27). First, cells were harvested for cell cycle analysis up to 72 hpi. Virus or UCN-01 alone exerted no effect upon cell cycle profile, but the combination of *dl*922-947 with UCN-01 resulted in dose-dependent overreplication, leading

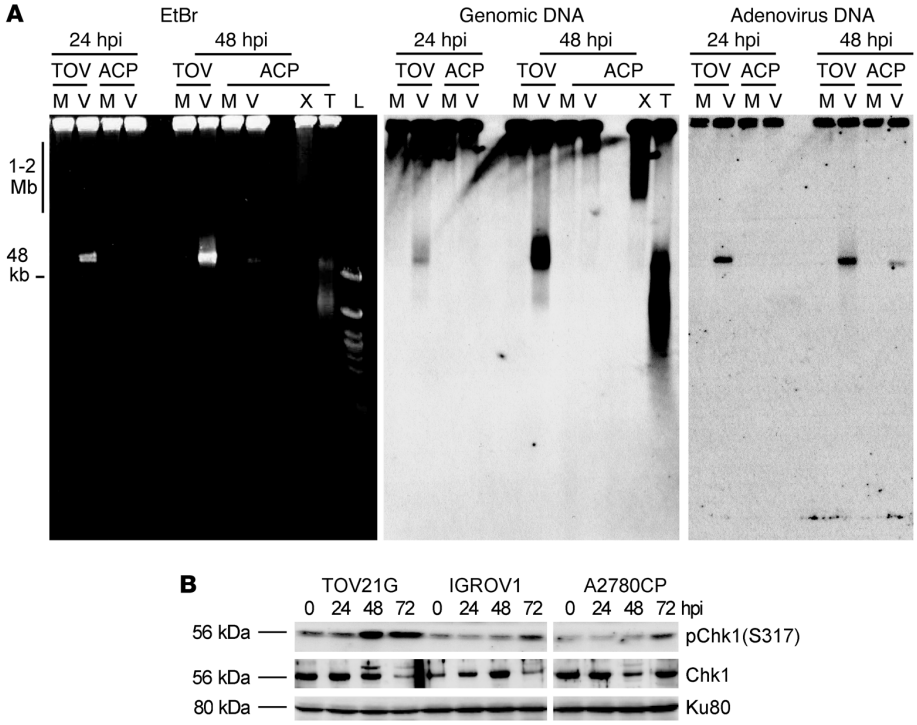

Figure 3
*dl*922-947–induced genomic DNA damage causes Chk1 phosphorylation. (**A**) TOV21G and A2780CP cells were infected with *dl*922-947 (MOI 7.5) for up to 48 hours. A2780CP cells were also treated with x-irradiation (20 Gy, 30 minutes) or TRAIL (250 ng/ml, 3 hours). DNA was extracted and subjected to neutral PFGE, stained with ethidium bromide (EtBr), and then probed with HRP-labeled genomic DNA or adenovirus type 5 probe. TOV, TOV21G; ACP, A2780CP; M, mock; V, *dl*922-947 infection; X, x-irradiation; T, TRAIL; L, Ladders. (**B**) Phosphorylation of Chk1 in TOV21G, IGROV1, and A2780CP cells infected with *dl*922-947 (MOI 7.5) for up to 72 hours was assessed by immunoblot.

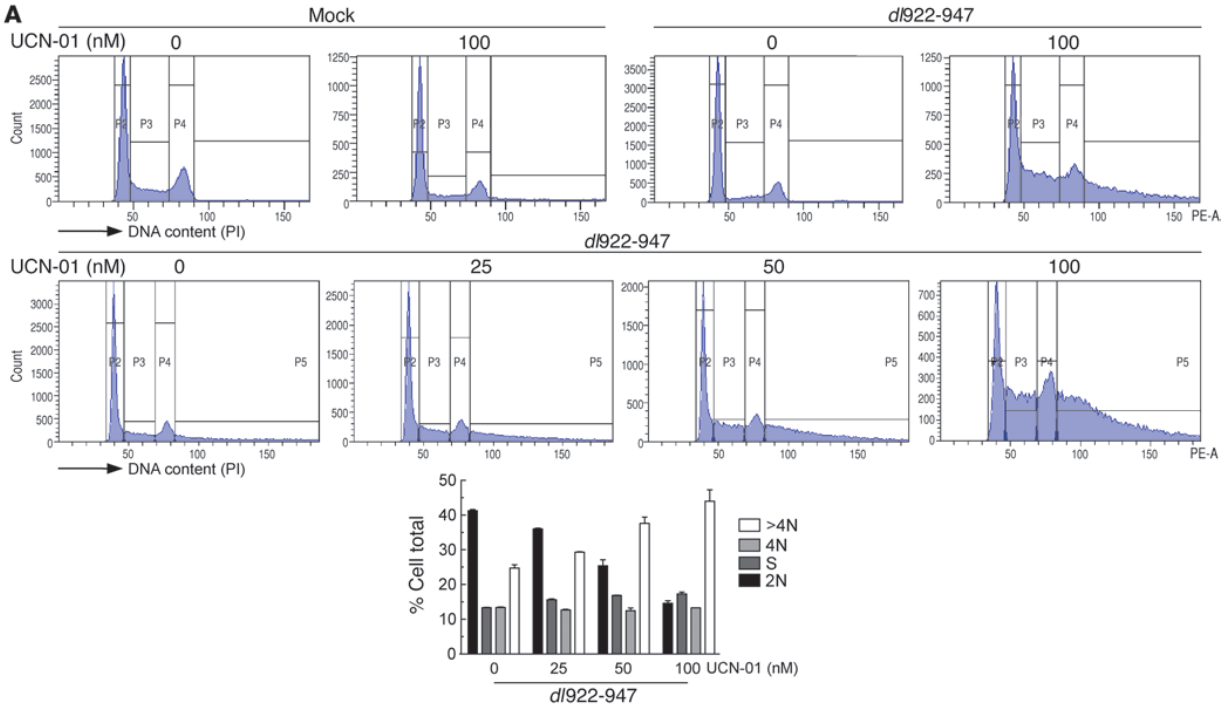

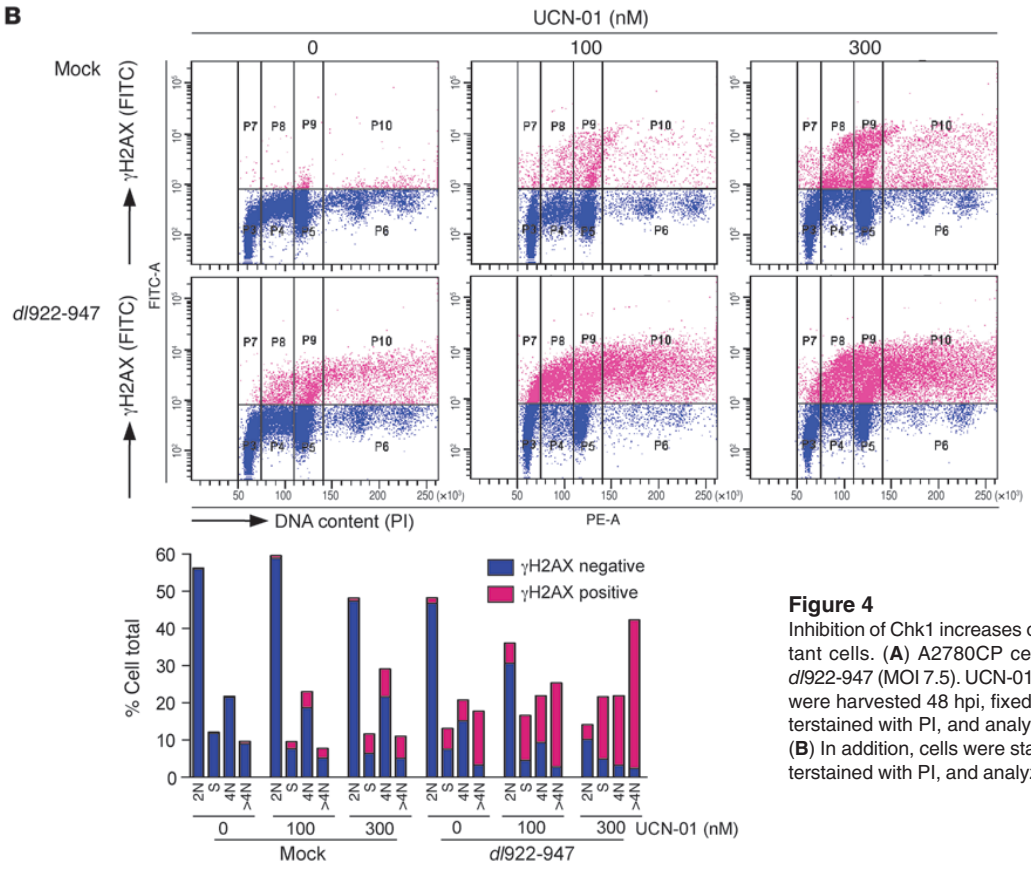

Figure 4
Inhibition of Chk1 increases overreplication in resistant cells. (**A**) A2780CP cells were infected with *dl*922-947 (MOI 7.5). UCN-01 was added 6 hpi. Cells were harvested 48 hpi, fixed in cold ethanol, counterstained with PI, and analyzed by flow cytometry. (**B**) In addition, cells were stained for γH2AX, counterstained with PI, and analyzed by flow cytometry.

to greater accumulation of cells with more than 4 N DNA content (Figure 4A). This UCN-01 effect was also seen with intermediate-sensitivity IGROV1 cells, indicating that these effects are not cell-type specific (Supplemental Figure 5). Similarly, inhibition of ATR-Chk1 signaling by siRNA-mediated knockdown of ATR induced a small but significant increase in overreplication (Supplemental Figure 6). UCN-01 also greatly enhanced γH2AX, as detected by flow cytometry (Figure 4B). Furthermore, the increase in γH2AX was most marked in S/G_2 and overreplicated cells; treatment of cells with UCN-01 alone in the absence of virus infection had no effect upon the proportion of overreplicated cells. However, the combination of *dl*922-947 and 300 nM UCN-01 increased the proportion of overreplicated cells from 11% (UCN-01 alone) and 17% (*dl*922-947 alone) to 42.3% (combination), with over 89% of the cells with more than 4 N DNA content being γH2AX positive. By comparison, under 10% of G_1 phase cells were γH2AX positive, despite receiving the same treatment. Importantly, UCN-01 did not induce overreplication in primary human fibroblast cells after infection with either *dl*922-947 or Ad5 WT, implying that the effects of Chk1 inhibition on viral function are specific to malignant cells (Supplemental Figure 7).

IF analysis of γH2AX and E1A intensity in A2780CP cells after infection with *dl*922-947 indicated that 300 nM UCN-01 slightly increased the median intensity of E1A per cell from 11.5 to 15.6 relative fluorescence units (RFU) (Figure 5A; $P = 0.02$) but induced a greater proportional increase in γH2AX: there was no difference in the median intensity of γH2AX staining after UCN-01 and *dl*922-947 given individually (9.9 and 9.5 RFU, respectively), but the combination caused a highly significant increase to 35.7 RFU ($P < 0.0001$). Thus, inhibition of Chk1 augmented the accumulation of γH2AX following E1A expression, an effect that was also seen in IGROV cells (data not shown). To confirm that this effect was Chk1 specific, IGROV1 cells were transfected with siRNA to Chk1 prior to infection with *dl*922-947. IF demonstrated a significant increase in γH2AX formation compared with that in control cells 24 hpi at 2 MOIs (Figure 5B).

To analyze directly the effect of Chk1 inhibition and associated overreplication upon genomic DNA damage, DNA was extracted from A2780CP cells after infection and subjected to neutral PFGE. Treatment with UCN-01 or *dl*922-947 alone induced modest DNA damage, but the combination of UCN-01 and *dl*922-947 induced large numbers of genomic DSBs in a UCN-01 concentration–dependent manner (Figure 5C). Labeling with an adenovirus DNA probe confirmed that, as in Figure 3A, the large band at approximately 50 kb seen in the genomic DNA blot does not correspond to adenoviral DNA, despite the similar size, and also that UCN-01 treatment does not compromise viral DNA replication.

Chk1 inhibition decreases HR repair in dl922-947–treated cells. Replication-associated DNA breaks are preferentially repaired via the HR pathway (28). In response to such breaks, activated Chk1 is responsible for recruitment of Rad51, which in turn catalyses the homology search and DNA strand exchange functions that are central to HR (reviewed in ref. 29). To examine how Chk1 inhibition alters HR repair after *dl*922-947 infection, we quantified Rad51 focus formation by IF in A2780CP cells. *dl*922-947 infection alone caused a significant increase in the number of Rad51-positive cells, but there was a significant and dose-dependent reduction in Rad51 positivity in the presence of UCN-01 (Figure 6). Collectively, the results in Figures 4–6 demonstrate that inhibition of Chk1 increases overreplication with extensive DNA damage and prevention of HR pathway activation.

Chk1 inhibition augments adenovirus activity in vitro and in vivo. The overreplication and genomic DNA damage effects induced by UCN-01 caused a dose-dependent increase in cytotoxicity of both *dl*922-947 and Ad5 WT in both A2780CP and IGROV1 cells (Figure 7A and data not shown). In addition, UCN-01 did not impede the production of intracellular infectious virions and caused an increase in virus release, possibly due to increased cell death and lysis (Figure 7B). siRNA-mediated Chk1 knockdown was highly toxic, such that it was not possible to maintain cells alive for the duration of a cytotoxicity assay. However, to demonstrate further that the effects were specific to Chk1, both A2780CP and IGROV1 cells were infected with *dl*922-947 or Ad5 WT in the presence of the Chk1 inhibitor PF-00477736 (30). Sensitivity to both viruses was increased in both cell lines (Figure 7C).

To investigate whether these effects translated into increased antitumor activity in vivo, female nude mice bearing size-matched subcutaneous IGROV1 tumors received a single intratumoral injection of *dl*922-947 (10^{10} particles), with or without a single dose of UCN-01 (7.5 mg/kg) i.p. 24 hours later. Tumors were harvested 48 hours after virus. Greater E1A was detected in tumors from mice treated with *dl*922-947 and UCN-01 compared with those treated with *dl*922-947 and vehicle (Figure 7D). Mice bearing established IGROV1-luciferase i.p. xenografts were then treated with *dl*922-947 and UCN-01 alone and in combination. UCN-01 and *dl*922-947 given individually caused tumor stasis, as monitored by bioluminescence imaging, whereas combination treatment caused significant tumor regression, which was sustained until the end of the experiment (Figure 7E). In A2780CP xenografts, UCN-01 and *dl*922-947 alone had no therapeutic effect, whereas the combination again caused regression, although this was temporary (data not shown).

Cdc25A is a key regulator of adenovirus cytotoxicity. To understand how Chk1 inhibition can promote overreplication, increase DNA damage, and augment viral activity, we investigated the Chk1 target Cdc25A. Cdc25A is a target of E1A transactivation during adenovirus infection and promotes E1A-induced S phase entry (31). Deregulated Cdc25A phosphatase activity is sufficient to induce unscheduled genomic DNA replication through activation of cyclin-dependent kinases (32, 33). During an unperturbed interphase, Cdc25A is subject to basal physiological turnover, which is accelerated in response to genotoxic damage (34), mediated by the ATR-Chk1 pathway (35, 36). To investigate a possible link between Chk1, Cdc25A, and cellular sensitivity, Cdc25A expression was assessed after infection with *dl*922-947. As with E1A, virus-induced Cdc25A expression was greater in TOV21G cells than in the insensitive cells (Figure 8A), which resulted predominantly from increased transcription (Supplemental Figure 8A). An increase in transcription was observed in both IGROV1 and A2780CP cells at higher MOIs (Supplemental Figure 8B), suggesting a possible threshold effect. A2780CP cells were then infected with *dl*922-947 for 48 hours in the presence and absence of UCN-01. Cdc25A was degraded via a ubiquitin-proteasome-dependent pathway, and the combination of *dl*922-947 and the proteasome inhibitor MG132 caused a very marked increase in Cdc25A levels (Figure 8B), indicating that Cdc25A is targeted for proteasome-dependent degradation in insensitive A2780CP cells after *dl*922-947 infection. Chk1 inhibition with UCN-01 stabilized Cdc25A, with a very marked increases in γH2AX (Figure 8B). There was also an increase in E1A (Figure 8C), which complemented the IF and overreplication data (Figures 4 and 5) and the immunohistochemistry from IGROV1 tumors (Figure 7D) and substantiated Chk1 as a mediator of

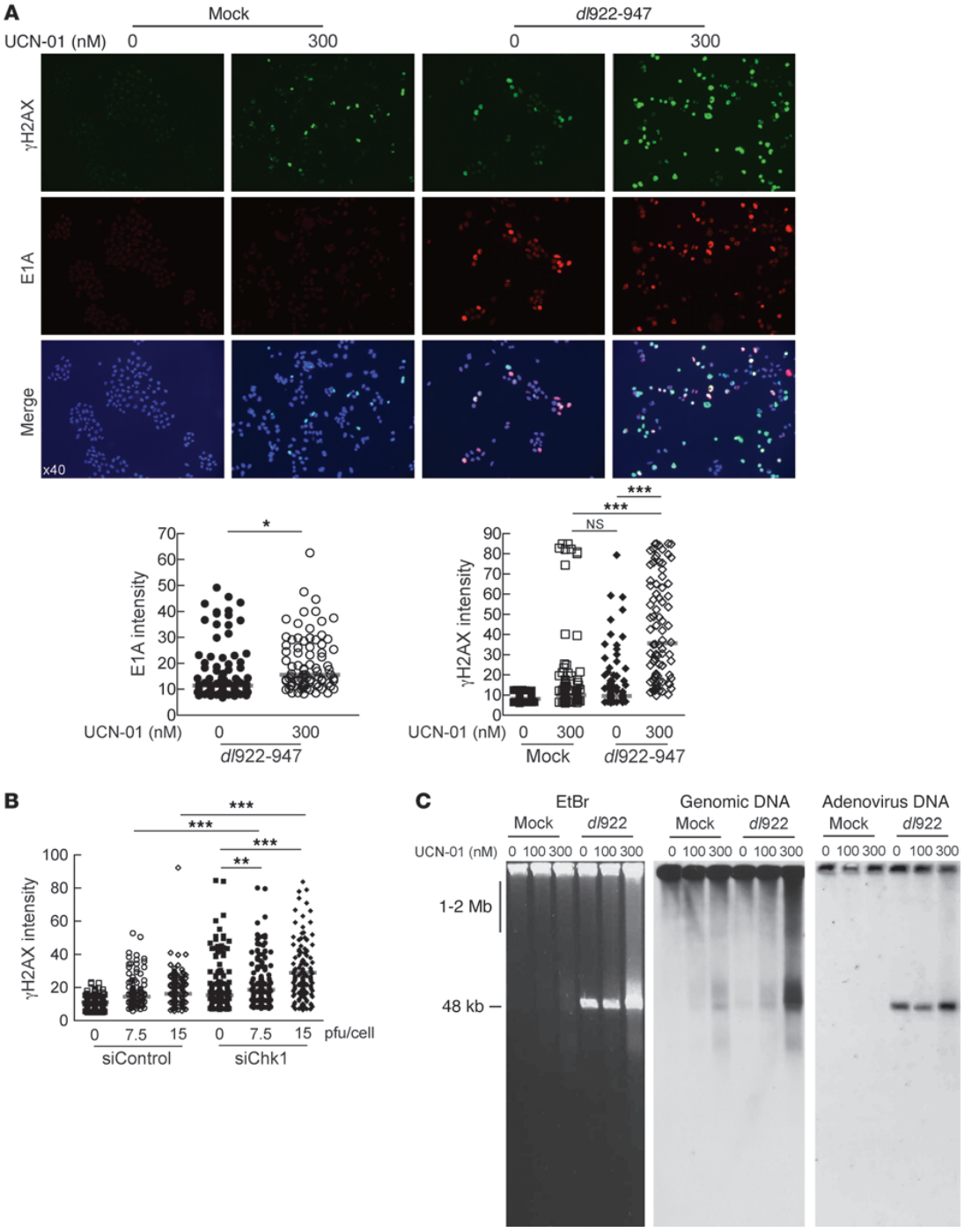

Figure 5

Loss of Chk1 activity increases genomic DNA damage. (**A**) A2780CP cells were infected with *dl*922-947 (MOI 7.5) and treated with UCN-01 6 hours later. 48 hpi, cells were fixed, stained for expression of E1A and γH2AX, counterstained with DAPI, and imaged. Fluorescence intensity was assessed in more than 100 cells per condition using ImageJ software. Each point represents a single cell, and each red bar represents the median. Original magnification, ×40. $^{*}P < 0.05$, $^{***}P < 0.0001$; Mann-Whitney test. (**B**) IGROV1 cells were transfected with Chk1 (siChk1) or scrambled control siRNA (siControl) oligonucleotides 24 hours prior to infection with *dl*922-947 (MOI 7.5 and 15). Cells were fixed 24 hours thereafter, stained for expression of γH2AX, and counterstained with DAPI. Fluorescence intensity was assessed as before. $^{**}P < 0.01$, $^{***}P < 0.0001$; Mann-Whitney test. (**C**) A2780CP cells were infected with *dl*922-947 (MOI 7.5) for 48 hours, with or without treatment with UCN-01. DNA was extracted and subjected to neutral PFGE and probed with HRP-labeled genomic DNA or adenovirus type 5 probe.

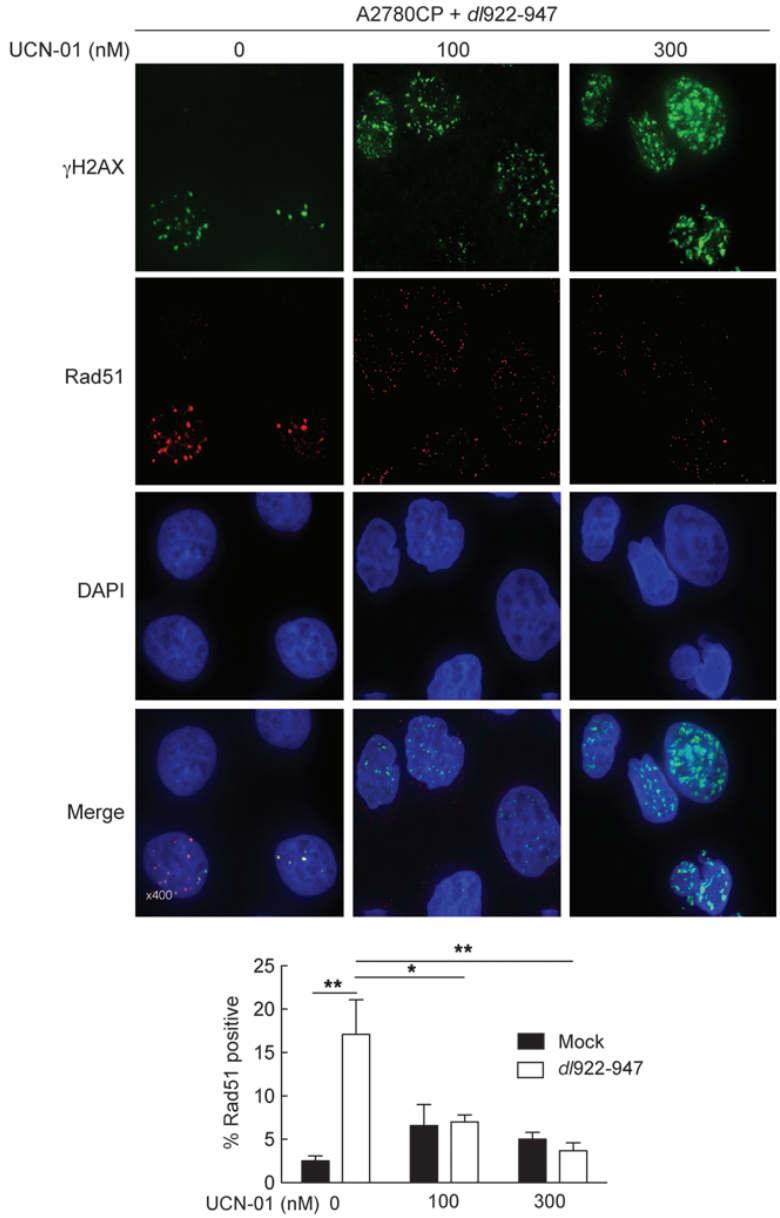

Figure 6
UCN-01 reduces HR DNA repair. A2780CP cells were infected with *dl*922-947 (MOI 7.5) and treated with UCN-01 6 hours later. 48 hpi, cells were fixed, stained for expression of γH2AX and Rad51, counterstained with DAPI, and imaged. Original magnification, ×400. The numbers of Rad51-positive (>10 foci) nuclei in 10 fields of view were counted. $^{*}P < 0.05$, $^{**}P < 0.01$.

Cdc25A degradation. The increase in Cdc25A with UCN-01 did not result from increased transcription (data not shown), confirming that Cdc25A stabilization occurs posttranscriptionally. MG132 did not increase virus-induced H2AX phosphorylation, because adenovirus function depends critically upon proteasomal degradation of key cellular proteins, including p53 (37).

siRNA-mediated ATR knockdown was also able to stabilize Cdc25A after *dl*922-947 infection (Figure 8D), in contrast to the ATM inhibitor 2-morpholin-4-yl-6-thianthren-1-yl-pyran-4-one (data not shown), confirming the involvement of the ATR-Chk1 pathway. Finally, overexpression of Cdc25A significantly increased virus cytotoxicity in both A2780CP cells (Figure 8E) and IGROV1 cells (data not shown), with increased γH2AX formation (Figure 8E). Conversely, Cdc25A knockdown reduced virus-induced DNA damage in TOV21G cells (Figure 8F) and also reversed both the DNA damage and overreplication seen in A2780CP cells treated with UCN-01 after virus infection (Figure 8G). These results substantiate Cdc25A as an important mediator of virus-induced DNA damage and as a key target for Chk1 activity after infection.

Overall, we propose a model whereby the sensitizing effects of Chk1 inhibition upon adenovirus-induced cell death in cancer cells are compound (Figure 9). These include (a) prevention of Chk1-mediated degradation of Cdc25A, which promotes unscheduled DNA synthesis with consequent induction of DNA damage, and (b) inhibition of Chk1-mediated recruitment of Rad51 to DSBs, which impairs HR repair. Together, these effects expedite the accumulation of cytotoxic lesions and cell death after infection.

Discussion

The mode of adenovirus-induced cell death has remained obscure (7) and thereby difficult to manipulate for therapeutic gain. Unscheduled DNA synthesis induces the accumulation of replication-associated DNA lesions (11, 21, 38), and our data support a correlation between adenovirus-induced genomic DNA overreplication and cytotoxicity in ovarian cancer. We demonstrate that the E1A-CR2 mutant adenovirus *dl*922-947 induced massive accumulation of genomic DNA damage, specifically in cell lines sensitive to adenovirus-induced cell death. Similar DNA damage was also induced in sensitive cells by the WT adenovirus, although this occurred more slowly. The damage, in the form of DSBs, occurred predominantly and specifically in replicating cells and was most prominent in those cells harboring a more than 4 N DNA content, consistent with DNA damage being dependent upon aberrant overreplication of genomic DNA. As a consequence, DSBs were less abundant in resistant cells, in which there was minimal overreplication after infection.

Sensitive cells support greater transcription of E1A in the first hours after infection. Similarly, sensitive cells permit transcription of Cdc25A early after infection, which promotes G_1/S transition by dephosphorylating, and thereby activating, cyclin A- and cyclin E-cdk2 kinases, which are the rate limiting factors for firing of DNA replication origins. Transactivation of Cdc25A

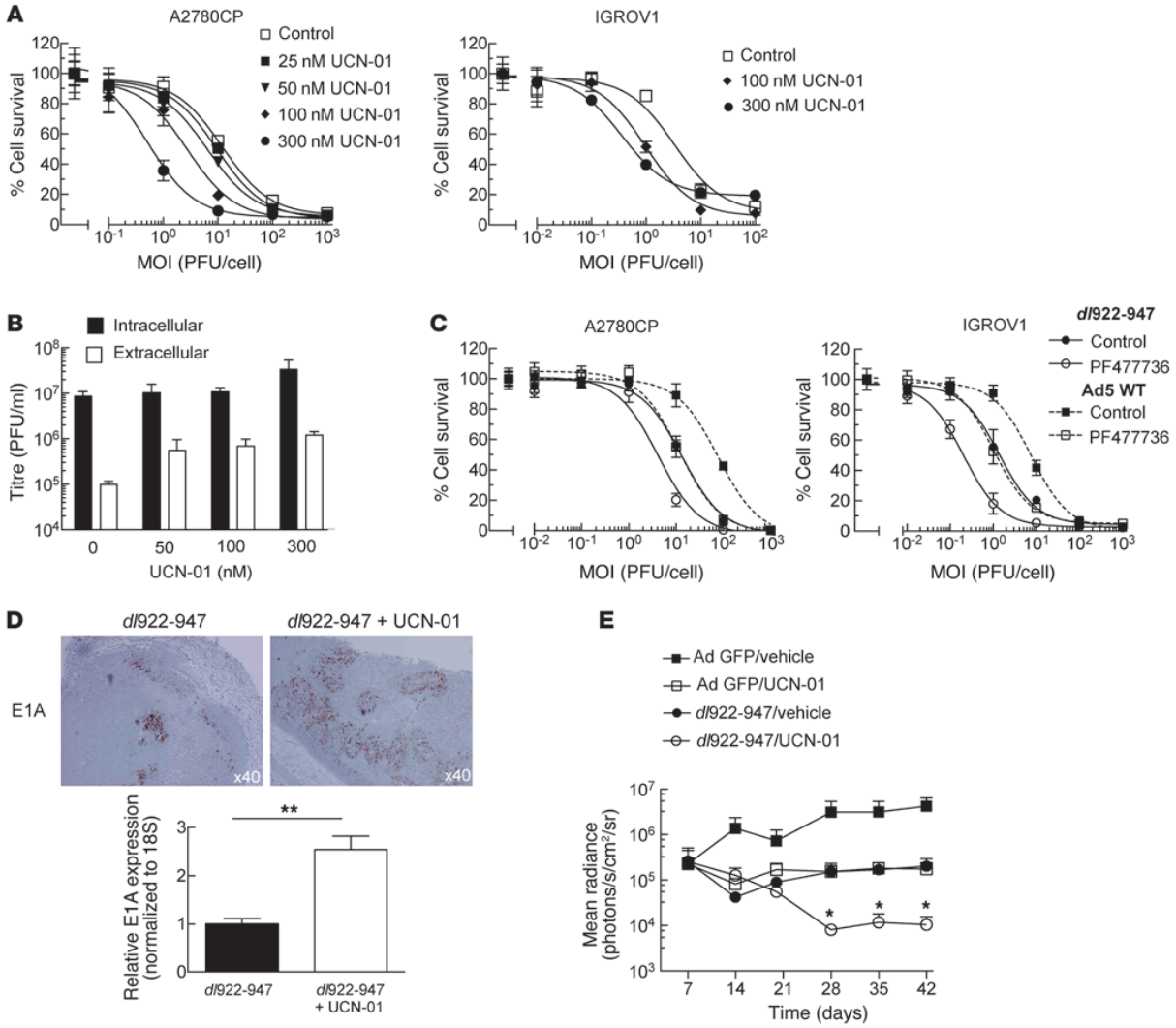

Figure 7

UCN-01 increases *dl*922-947 activity in vitro and in vivo. (**A**) A2780CP and IGROV1 cells were infected with *dl*922-947. UCN-01 was added 6 hpi. Cell survival was assessed 120 hpi. (**B**) A2780CP cells were harvested 72 hours after *dl*922-947 (MOI 7.5) infection and treatment with UCN-01. Titers of intracellular and extracellular adenovirus were assessed by $TCID_{50}$. (**C**) A2780CP and IGROV1 cells were infected with *dl*922-947 or Ad5 WT. PF477736 (360 nM for A2780CP, 120 nM for IGROV1) was added 6 hpi. Cell survival was assessed 120 hpi. (**D**) *dl*922-947 (10^{10} particles) was injected into subcutaneous IGROV1 xenografts on the flank of athymic *nu*/*nu* female mice. 24 hpi, mice received a single i.p. dose of UCN-01 (7.5 mg/kg) or vehicle (20% icodextrin). Mice were killed 24 hours thereafter. Expression of E1A was assessed by immunohistochemistry (top). RNA was extracted from snap frozen tumors, and E1A expression was assessed by qRT-PCR (bottom). Expression was normalized to that of 18S RNA and plotted relative to mice that received *dl*922-947 and vehicle. Original magnification, ×40. $^{**}P < 0.01$. (**E**) 5×10^6 IGROV1-luciferase cells were injected i.p. into athymic *nu*/*nu* female mice. On day 9, mice were randomly allocated to receive i.p. *dl*922-947 or control adenovirus (5×10^9 particles/day on days 9, 10, 15, and 16), with or without i.p. UCN-01 (5 mg/kg on days 11, 12, 17, and 18). Tumor burden was assessed using bioluminescence imaging. Bars represent SEM; $n = 5$/group. $^{*}P < 0.05$, for 1-tailed comparison of *dl*922-947/UCN-01 versus both adenovirus GFP/UCN-01 and *dl*922-947/vehicle.

through 2 functional E2F-binding sites (E2F-A and E2F-C) within the Cdc25A promoter is essential for efficient induction of S phase by E2F1 and pRb family members (39). Cdc25A also promotes E1A-mediated S phase entry and DNA synthesis following after with adenovirus (31). Previously, it was reported that E1A expression was not responsible for γH2AX formation in HeLa cells after adenovirus infection: widespread γH2AX was seen only after infection with WT virus and not a nonreplicating pTP-deleted virus. In these experiments, E1A expression was seen with both viruses but at greater levels with the WT virus (16). However, we found a good correlation between E1A expression and appearance of γH2AX across cell lines. Our data suggest that

there may be a threshold effect, whereby E1A expression must reach a threshold level to induce sufficient Cdc25A to promote genomic DNA overreplication (31). Thus, rapid genomic overreplication and DNA damage are seen in TOV21G cells but at much lower levels in resistant and partially sensitive cells and only once E1A expression reaches a level sufficient to transactivate Cdc25A or after infection at much greater MOI.

Inhibition of ATR-Chk1-Cdc25A pathway augments dl922-947 cytotoxicity via 2 mechanisms

In our model (Figure 9), we suggest that Chk1 inhibition increases virus cytotoxicity via 2 separate mechanisms.

Increase in overreplication via Cdc25A stabilization. Cdc25A is subject to proteasome-dependent degradation mediated by the ATR-Chk1 pathway. This acts to modulate the pro-replicative activity of cyclin E-cdk2 during an unperturbed cell cycle (35). Replication-associated DNA damage intensifies ATR-Chk1 signaling, which accelerates Cdc25A degradation to enact S phase checkpoint control (35, 40). As a consequence, downregulation of either ATR or Chk1 activity results in accumulation of Cdc25A and deregulated DNA synthesis (40). The increase in overreplication was less marked with ATR knockdown than with UCN-01–mediated Chk1 inhibition, which may simply reflect difficulty in achieving complete knockdown. We failed to detect accumulation of Cdc25A in uninfected cells after either ATR siRNA (data not shown) or Chk1 inhibition with UCN-01 (Figure 8C) but did so only with *dl*922-947 infection. The increased Cdc25A levels seen with Chk1 inhibition in infected cells were achieved despite no increase in Cdc25A transcription but were still sufficient to promote overreplication. The overreplication promoted the formation and accumulation of genotoxic DNA lesions to sensitize these otherwise resistant cells to *dl*922-947–induced cell death. Further evidence for a role for Cdc25A was provided by overexpression, which increased DNA damage and cytotoxicity in A2780CP cells, while, conversely, Cdc25A knockdown not only reduced virus-induced DNA damage in TOV21G cells but also reversed the overreplication promoted by UCN-01 in A2780CP cells. One question is how TOV21G cells can maintain Cdc25A expression (Figure 8A) in the presence of active phospho-Chk1 (Figure 3B). The levels of Cdc25A after infection will reflect the balance between virus-induced expression and Chk1-mediated degradation. In TOV21G cells, E1A levels were sufficient to overcome the effects of Chk1 — indeed, Chk1 inhibition in TOV21G cells increased their overreplication even further (data not shown).

Augmentation of DNA damage by preventing HR repair. There is evidence that adenovirus infection can inhibit certain forms of DNA damage repair: the E1B55K/E4orf6 complex promotes the degradation of DNA ligase IV, which is vital to the process of nonhomologous end-joining (41). However, replication-associated DSBs are preferentially repaired by HR, in which Rad51 is a key mediator (reviewed in ref. 29). Phosphorylation of Rad51 by Chk1 promotes the chromatin association of Rad51 and is required for efficient HR repair and survival after replication stress-induced DNA damage (36). Interestingly, we detected Rad51 foci as well as γH2AX signal after infection with *dl*922-947, indicating that *dl*922-947–induced DSBs activate both DNA damage and DNA repair signaling. We demonstrate that inhibition of Chk1 activity with UCN-01 reduced the formation of Rad51 foci after infection, implying that UCN-01 also impacts on adenovirus-induced signaling to ATR-Chk1-Rad51–directed HR repair.

Our data also suggest strongly that cell sensitivity to virus-induced cytotoxicity is not a direct function of intracellular virion load: the number of viral genomes and functional virions was similar in all 3 cell lines examined here, despite their widely differing sensitivity to virus cytotoxicity. Moreover, UCN-01 treatment increased cell death without any substantial increase in the number of intracellular virions.

The factors that determine cellular sensitivity to adenovirus-mediated cytotoxicity are likely to be legion. We have recently demonstrated that expression of p21 in ovarian cancer is a marker for a host cell environment conducive to the expression of E1A (8). *E1A* is the first viral gene to be expressed after infection, and its expression correlates with cellular sensitivity. The data presented here indicate that the cellular environment can also impact on events downstream of E1A expression and, furthermore, can be instrumental in the ultimate fate of a cell. In addition, the ease of virus spread between infected cells will contribute to overall cell sensitivity. Spread relies both upon release of virus from initially infected cells as well as upon subsequent infection of neighboring cells. Although adenovirus release is largely lytic, we have recently shown that a nonlytic mechanism may exist, dependent upon stabilized microtubules (42). The in vitro experiments described here lasted for 5 days at most, which allowed approximately 2–3 rounds of replication (43). It will therefore be important to investigate the patterns of DNA damage and cytotoxicity in ovarian cancer cells after infection at a lower MOI, which will demand multiple rounds of replication and release.

Two major questions remain. First, why are the changes greater after *dl*922-947 infection compared with those after WT adenovirus infection? *dl*922-947 has greater cytotoxicity than Ad5 WT in a variety of cancer models (2, 3), which has been demonstrated again here. However, the molecular origin of this increased activity is uncertain. The data presented here indicate that the superior activity of *dl*922-947 mirrors the increased DNA damage and overreplication. The 24-bp deletion within E1A-CR2 region in *dl*922-947 greatly reduces binding to host cell p107, pRb, and cyclin A (1), effects that correlate with reinitiation of DNA synthesis and host cell overreplication (44) as well as induction of cdk1 activity (45). Thus, the superior potency of *dl*922-947 may be caused by uncoordinated host cell DNA replication, with consequent activation of DNA damage responses. Second, what is the role of HR competence in repairing virus-induced genomic DNA damage? There is much interest in the role of HR incompetence as a predictor of ovarian cancer responsiveness to PARP inhibition (38, 46, 47). Our data would suggest that HR incompetence would predispose cells to adenovirus-induced cell death, while inhibiting HR in HR-proficient cells could convey sensitivity to otherwise resistant cells. We are currently exploring both questions further.

In summary, our data demonstrate that mechanisms to promote unscheduled DNA synthesis and/or impede HR repair will potentiate the accumulation of cytotoxic lesions and increase death induced by the oncolytic adenovirus *dl*922-947. As UCN-01 has already shown itself to be safe in patients with advanced ovarian cancer (48), combination trials with oncolytic viruses should be explored.

Methods

Cell culture, adenoviruses, and cell viability assays. All cells were maintained at 37°C with 5% CO_2, in Dulbecco's modified Eagle's medium supplemented with 10% FCS, penicillin/streptomycin, and fungizone. *dl*922-947 is an adenovirus type 5 mutant containing a 24-bp deletion in E1A-CR2, which is also deleted in E3B. *dl*309 is identical to *dl*922-947 apart from a WT E1A region. Control

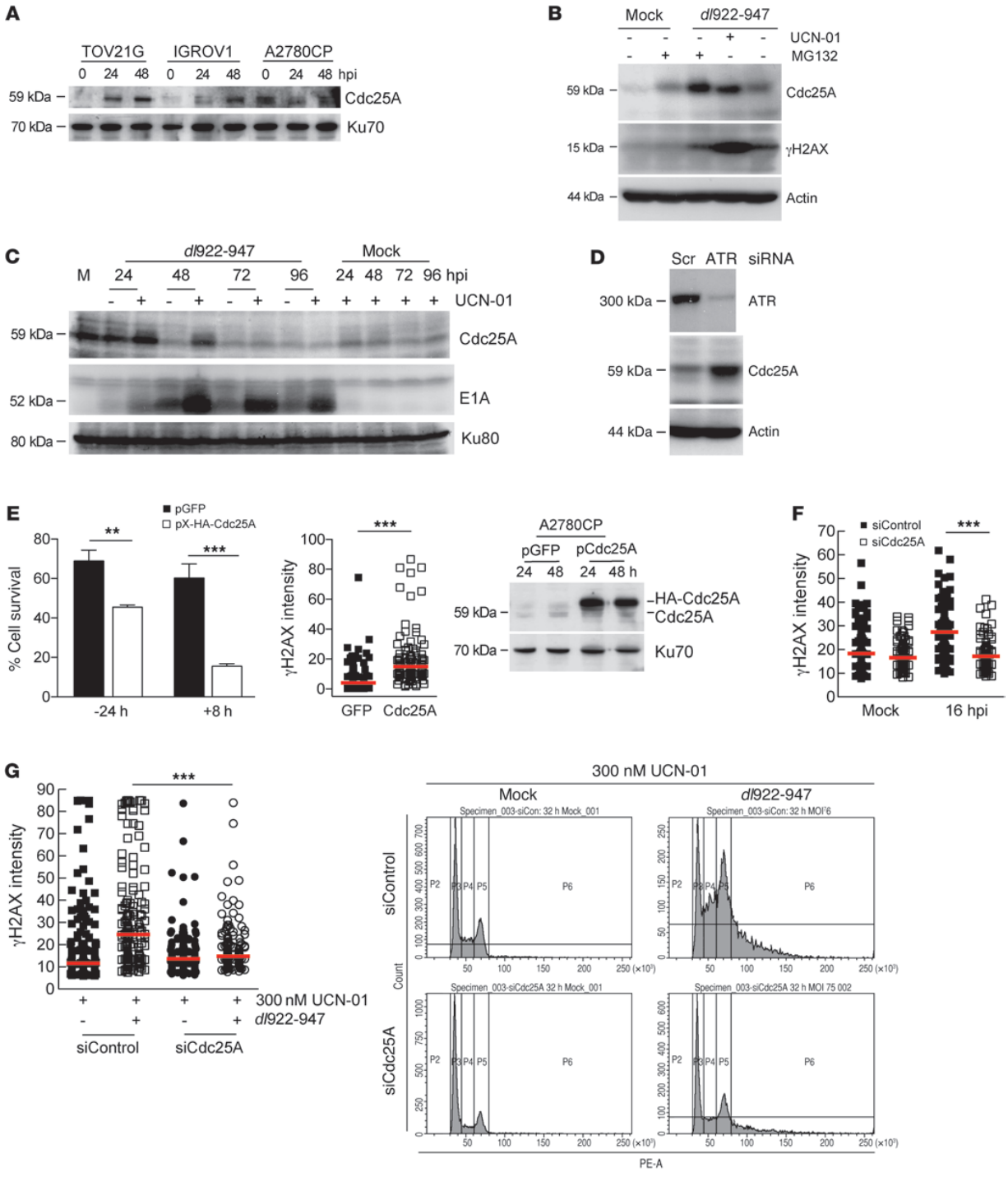
A
TOV21G
IGROV1
A2780CP
0 24 48 0 24 48 0 24 48 hpi
59 kDa
Cdc25A
70 kDa
Ku70
B
Mock
dl922-947
UCN-01
MG132
59 kDa
Cdc25A
15 kDa
γH2AX
44 kDa
Actin
C
dl922-947
Mock
M 24 48 72 96 24 48 72 96 hpi
UCN-01
59 kDa
Cdc25A
52 kDa
E1A
80 kDa
Ku80
D
Scr ATR siRNA
300 kDa
ATR
59 kDa
Cdc25A
44 kDa
Actin
E
pGFP
pX-HA-Cdc25A
% Cell survival
-24 h
+8 h
γH2AX intensity
GFP Cdc25A
A2780CP
pGFP pCdc25A
24 48 24 48 h
59 kDa
HA-Cdc25A
Cdc25A
70 kDa
Ku70
F
siControl
siCdc25A
γH2AX intensity
Mock
16 hpi
G
γH2AX intensity
300 nM UCN-01
dl922-947
siControl
siCdc25A
300 nM UCN-01
Mock
dl922-947
siControl
siCdc25A
Count
PE-A

Figure 8
Cdc25A is a key regulator of adenovirus cytotoxicity. (**A**) Cdc25A expression was assessed by immunoblot after *dl*922-947 infection (MOI 7.5). (**B** and **C**) A2780CP cells infected with *dl*922-947 were treated with UCN-01 (300 nM) or MG132 (10 μM) and harvested 48 hpi. (**B**) Cdc25A and γH2AX expression 24 hpi and (**C**) E1A expression up to 96 hpi were assessed by immunoblot. (**D**) 24 hours after transfection with ATR-specific siRNA or scrambled control (Scr), A2780CP cells were infected with *dl*922-947 (MOI 7.5). ATR and Cdc25A expression was assessed by immunoblot 72 hpi. (**E**) A2780CP cells were transfected with pX-HA-Cdc25A or pGFP 24 hours before (–24 hours) or 8 hours after (+8 hours) infection with *dl*922-947 MOI 100. Cell survival was assessed 96 hpi (left). $^{**}P < 0.01$, $^{***}P < 0.001$. γH2AX expression was also assessed in cells infected with *dl*922-947 and transfected 8 hours later with pX-HA-Cdc25A (middle). Red bars represent median. $^{***}P < 0.0001$; Mann-Whitney test. Expression of HA-tagged Cdc25A was confirmed by Cdc25A immunoblot (right). (**F**) TOV21G cells were transfected with Cdc25A-specific siRNA or scrambled control, infected with *dl*922-947 (MOI 7.5 and 15) later and stained for γH2AX expression 16 hours thereafter. Red bars represent median. $^{***}P < 0.0001$; Mann-Whitney test. (**G**) A2780CP cells were transfected with Cdc25A-specific siRNA or scrambled control 24 hours prior to infection with *dl*922-947 (MOI 7.5). Cells were additionally treated with UCN-01 6 hpi and fixed 24 hpi. γH2AX expression (left) and flow cytometry (right) were performed as before. Red bars represent median. $^{***}P < 0.0001$; Mann-Whitney test.

viruses adenovirus CMV GFP and adenovirus LM-X are both E1-deleted nonreplicating vectors as previously described (49). For viability assays, 2×10^4 cells were infected in serum-free medium at MOI 0.001–1,000 PFU/cell. After 2 hours, cells were refed with medium containing 5% FCS. Cell viability was assayed by MTT assay using a Victor3 Plate Reader (Perkin Elmer). All viability assays were done in triplicate, and experiments were repeated at least twice. For siRNA experiments, cells were transfected with ON-TARGETplus SMARTpool siRNAs or scrambled siRNA control (Dharmacon) using DharmaFECT1. Virus infection took place 24 hours after knockdown. Cells were exposed to 5 Gy X-irradiation using an Hs-X-Ray System (A.G.O. Installations Ltd.). ATM inhibitor 2-morpholin-4-yl-6-thianthren-1-yl-pyran-4-one was obtained from Calbiochem. The plasmid pX-HA-cdc25a was donated by Ingrid Hoffman (German Cancer Research Center, Heidelberg, Germany) (33), and pGFP was obtained from Invitrogen. Plasmids (1 μg) were transfected into cells in 24-well plates using FuGene (Roche).

Quantitative PCR and $TCID_{50}$ assays. Real-time PCR was performed on an ABI Prism 7700 (Applied Biosystems). Oligonucleotides and probes for E1A and β-actin are as follows: E1A, sense primer, 5′-CCACCTACCCTTCACGAACTG; anti-sense primer, 5′-GCCTCCTCGTTGGGATCTTC; probe, ATGATTTAGACGTGACGGCC; and β-actin, sense primer, 5′-GCCAGCTCACCATGGATGAT; anti-sense primer, 5′-CACCTCCCCTGTGTGGACTT; probe, AGGCGGACTATGACTTAGTTGCGTACACCCT.

Those for 18S RNA and Cdc25A were purchased from Applied Biosystems (reference numbers 4310893E and Hs00947998_m1, respectively). PCR conditions were as follows: 50°C for 2 minutes and 95°C for 10 minutes, followed by 40 cycles of 95°C for 15 seconds and 60°C for 60 seconds. Where stated, a standard curve using 10^3–10^9 *dl*922-947 genomes was used for quantification.

Figure 9
Proposed mechanism for role of DNA damage and Chk1 inhibition in *dl*922-947 cytotoxicity. (i) Inhibition of Chk1-mediated degradation of Cdc25A promotes unscheduled DNA synthesis, with consequent induction of DNA damage. (ii) Inhibition of Chk1 activity prevents recruitment of Rad51 to DSBs, which impairs HR repair. These mechanisms expedite the accumulation of cytotoxic lesions and ensuing cell death after infection.

For tissue culture infectious dose 50% ($TCID_{50}$) assays, 10^5 cells were infected at MOI 7.5 PFU/cell. Cells were harvested into 0.5 ml 0.1 M Tris, pH 8.0, and subjected to 3 rounds of freeze/thawing (liquid N_2/37°C), after which they were centrifuged. The supernatant was titered on JH293 cells by serial dilution. To assay viral release from infected cells, culture medium was removed from cells every 24 hours and titered separately on JH293 cells.

Immunoblotting and IF. Protein lysates were electrophoresed on SDS-polyacrylamide gels and transferred onto nitrocellulose membranes by semidry blotting. Antibody binding was visualized using enhanced chemiluminescence (GE Healthcare). Antibodies used were anti-E1A, anti-Cdc25A, anti-ATR, anti-Actin, and anti-Ku70 (all Santa Cruz Biotechnology Inc.); anti-γH2AX (Upstate Biotechnology); anti-Ser 317 phospho-Chk1 (Cell Signaling Technology); anti-PARP (Serotec); and anti-Ku-80 (gifted from the lab of Penny Jeggo, University of Sussex). For IF, cells were grown on poly-L-lysine–coated coverslips, infected with *dl*922-947 (MOI 7.5), and fixed with 5% formaldehyde. Cells were permeabilized with 0.15% Triton X-100, and primary antibody binding was visualized with Texas Red– or Fluorescein-conjugated secondary antibodies (Vector Laboratories). For Rad51 staining, cells were preextracted with 0.15% Triton X-100 and fixed with 5% formaldehyde. Coverslips were mounted in DAPI-containing Vectashield and imaged using either a Zeiss Axioplan2 or a Zeiss Axiovert 200M fluorescence microscope with a ×4 or ×10 objective lens and a digital camera (OrcaER, Hamamatsu) and Delta Vision Spectris software, with a ×100 objective lens for Rad51 foci (Applied Precision). Images taken at ×40 magnification were processed using Simple PCI software, and signal intensity per nucleus was analyzed using NIH ImageJ (http://rsbweb.nih.gov/ij/).

Flow cytometry. For cell cycle analyses, cells were trypsinized, washed twice in ice-cold PBS, and fixed in 70% ethanol. Cells were then washed with PBS and resuspended in 200 μl trypsinized PI and 100 μg/ml RNase A (MP Biomedicals). For γH2AX analysis, cells were harvested, washed, and fixed in ice-cold 70% ethanol. After incubation with primary anti-γH2AX mAb and FITC-conjugated anti-mouse secondary antibody for 20 minutes each at 37°C in the dark, cells were counterstained with PI. Cells were analyzed using a Fluorescence Activated Cell Sorter (FACSCanto, BD Biosciences), with FACS Diva software.

PFGE. Cells were infected with *dl*922-947 (MOI 7.5), with or without treatment with UCN-01. After trypsinization, cells were washed twice with PBS and were embedded in 0.75% low melting agarose gel plug (SeaPlaque agarose, Cambrex Bioproducts) at a concentration of 0.75×10^5 cells/plug. Plugs were then placed in buffer containing 20 mg/ml proteinase K, 0.5 M EDTA, and 1% sarkosyl (pH 9.0) and incubated at 50°C for 24 hours in the dark. Plugs were washed with 50 mM EDTA at room temperature for 1 hour and stored at 4°C in the same buffer. PFGE was carried out a CHEF Mapper (Bio-Rad), with a cooling module (Model 1000 Mini Chiller, Bio-Rad) in

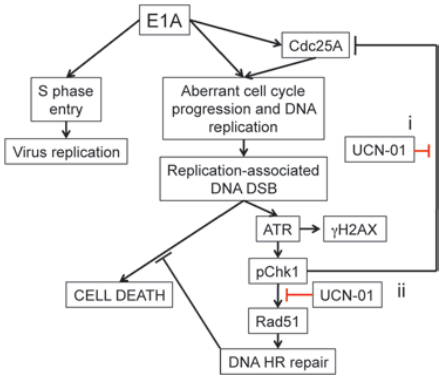

1% agarose gel (Pulsed Field Certified Agarose, Bio-Rad) in 0.5 × TBE. The forward voltage gradient was 5.4 V/cm for 5 to 60 seconds, and the reverse voltage gradient was 3.6 V/cm for 5 to 60 seconds, for a total of 20 hours at 14°C. After PFGE, gels were stained with ethidium bromide and photographed under UV transillumination. Southern blot hybridization was carried out using standard procedures with HRP-conjugated genomic DNA or adenovirus type probes.

In vivo analyses and immunohistochemistry. Experiments were performed under suitable United Kingdom Home Office personal and project license authority. All animal studies were also reviewed and approved by the ethical review board of the Biological Services Unit, Queen Mary University of London.

For analysis of E1A expression, 5×10^6 IGROV1 cells were inoculated subcutaneously onto the flank of female *nu/nu* mice on day 1. Once tumors reached approximately 250 mm^3, *dl*922-947 or vehicle was injected intratumorally (single injection, 1×10^{10} particles in 50 μl PBS). A single dose of i.p. UCN-01 or vehicle (7.5 mg/kg in 20% icodextrin) was administered 24 hours later. Mice were killed 24 hours thereafter. Tumors were excised and fixed in 10% formal-buffered saline (n = 2 per group) or snap frozen in dry ice (n = 3 per group). Fixed tumors were transferred to ice-cold 70% ethanol after 24 hours, and 4-μm sections were cut and processed. E1A expression was detected using a rabbit anti-Ad2 E1A antibody (Santa Cruz Biotechnology Inc.). Total RNA was extracted from snap-frozen tumors using TRIzol. After DNAse digestion (Qiagen), 1 μg total RNA was reverse transcribed using random hexonucleotide primers (First-Strand Synthesis Kit, Roche) and analyzed by quantitative PCR. For assessment of antitumor efficacy, 5×10^6 IGROV1-luciferase or A2780CP-luciferase cells were inoculated i.p. into female *nu/nu* mice on day 1. In IGROV1 experiments, *dl*922-947 or control adenovirus CMV-GFP (5×10^9 particles in 400 μl 20% icodextrin) were injected i.p. on days 9, 10, 15, and 16. UCN-01 (5 mg/kg) or vehicle (20% icodextrin) were administered i.p. on days 11, 12, 17, and 18. For A2780CP experiments, virus was administered on days 9, 11, 15, and 17, and UCN-01/vehicle were administered on days 10, 12, 16, and 18. Mice were injected i.p. with 125 mg/kg D-luciferin (Calliper Life Sciences) and then anesthetized (2% isoflurane by inhalation). Five minutes later, while still under anesthetic, they were placed in a light-tight chamber on a warmed stage (37°C), and light emission from a defined region of interest on the ventral aspect was imaged on a Xenogen IVIS Imaging System 100 (Alameda). Data were analyzed using Living Image software (also Xenogen) and are presented as mean radiance (photons/s/cm^2/steradian [photons/s/cm^2/sr]).

Statistics. All statistical analyses were generated with GraphPad Prism 5.00. All analyses are unpaired, 2-tailed Student's *t*-test unless otherwise stated. All experiments were performed in triplicate and error bars represent SD unless otherwise stated. *P* values of less than 0.05 were considered significant.

Acknowledgments

This work is supported by the Medical Research Council (grant reference G0601891). We would like to thank Mohammed Ikram for assistance with immunohistochemistry and Ingrid Hoffman (German Cancer Research Center, Heidelberg, Germany), who donated the plasmid pX-HA-Cdc25A.

Received for publication November 22, 2010, and accepted in revised form January 12, 2011.

Address correspondence to: Iain A. McNeish, Centre for Molecular Oncology and Imaging, John Vane Science Centre, Charterhouse Square, London, EC1M 6BQ, United Kingdom. Phone: 44.20.7882.3840; Fax: 44.20.7882.3884; E-mail: i.a.mcneish@qmul.ac.uk.

Sally P. Wheatley's present address is: School of Biomedical Sciences, University of Nottingham, Nottingham, United Kingdom.

1. Fattaey AR, Harlow E, Helin K. Independent regions of adenovirus E1A are required for binding to and dissociation of E2F-protein complexes. *Mol Cell Biol*. 1993;13(12):7267–7277.
2. Heise C, et al. An adenovirus E1A mutant that demonstrates potent and selective systemic antitumoral efficacy. *Nat Med*. 2000;6(10):1134–1139.
3. Lockley M, et al. Activity of the adenoviral E1A deletion mutant dl922-947 in ovarian cancer: comparison with adenovirus wild-type, bioluminescence monitoring and intraperitoneal delivery in icodextrin. *Cancer Res*. 2006;66(2):989–998.
4. Sherr CJ, McCormick F. The RB and p53 pathways in cancer. *Cancer Cell*. 2002;2(2):103–112.
5. D'Andrilli G, Kumar C, Scambia G, Giordano A. Cell cycle genes in ovarian cancer: steps toward earlier diagnosis and novel therapies. *Clin Cancer Res*. 2004;10(24):8132–8141.
6. Yaginuma Y, et al. Analysis of the Rb gene and cyclin-dependent kinase 4 inhibitor genes (p16INK4 and p15INK4B) in human ovarian carcinoma cell lines. *Exp Cell Res*. 1997;233(2):233–239.
7. Baird SK, Aerts JL, Eddaoudi A, Lockley M, Lemoine NR, McNeish IA. Oncolytic adenoviral mutants induce a novel mode of programmed cell death in ovarian cancer. *Oncogene*. 2008;27(22):3081–3090.
8. Flak MB, et al. p21 promotes oncolytic adenoviral activity in ovarian cancer and is a potential biomarker. *Mol Cancer*. 2010;9:175.
9. Jones N, Shenk T. An adenovirus type 5 early gene function regulates expression of other early viral genes. *Proc Natl Acad Sci U S A*. 1979;76(8):3665–3669.
10. Connell CM, Wheatley SP, McNeish IA. Nuclear survivin abrogates multiple cell cycle checkpoints and enhances viral oncolysis. *Cancer Res*. 2008;69(19):7923–7931.
11. Saleh-Gohari N, Bryant HE, Schultz N, Parker KM, Cassel TN, Helleday T. Spontaneous homologous recombination is induced by collapsed replication forks that are caused by endogenous DNA single-strand breaks. *Mol Cell Biol*. 2005;25(16):7158–7169.
12. Cherubini G, Petouchoff T, Grossi M, Piersanti S, Cundari E, Saggio I. E1B55K-deleted adenovirus (ONYX-015) overrides G1/S and G2/M checkpoints and causes mitotic catastrophe and endoreduplication in p53-proficient normal cells. *Cell Cycle*. 2006;5(19):2244–2252.
13. Blackford AN, et al. A role for E1B-AP5 in ATR signaling pathways during adenovirus infection. *J Virol*. 2008;82(15):7640–7652.
14. Carson CT, et al. Mislocalization of the MRN complex prevents ATR signaling during adenovirus infection. *Embo J*. 2009;28(6):652–662.
15. Karen KF, Hoey PJ, Young CS, Hearing P. Temporal regulation of the Mre11-Rad50-Nbs1 complex during adenovirus infection. *J Virol*. 2009;83(9):4565–4573.
16. Nichols GJ, Schaack J, Ornelles DA. Widespread phosphorylation of histone H2AX by species C adenovirus infection requires viral DNA replication. *J Virol*. 2009;83(12):5987–5998.
17. Kimball KJ, et al. A phase I study of a tropism-modified conditionally replicative adenovirus for recurrent malignant gynecologic diseases. *Clin Cancer Res*. 2010;16(21):5277–5287.
18. Hearing P, Shenk T. The adenovirus type 5 E1A enhancer contains two functionally distinct domains: one is specific for E1A and the other modulates all early units in *cis*. *Cell*. 1986;45(2):229–236.
19. Murray JD, Braithwaite AW, Taylor IW, Bellett AJ. Adenovirus-induced alterations of the cell growth cycle: effects of mutations in early regions E2A and E2B. *J Virol*. 1982;44(3):1072–1075.
20. Braithwaite AW, Murray JD, Bellett AJ. Alterations to controls of cellular DNA synthesis by adenovirus infection. *J Virol*. 1981;39(2):331–340.
21. Machida YJ, Dutta A. Cellular checkpoint mechanisms monitoring proper initiation of DNA replication. *J Biol Chem*. 2005;280(8):6253–6256.
22. Huang X, Darzynkiewicz Z. Cytometric assessment of histone H2AX phosphorylation: a reporter of DNA damage. *Methods Mol Biol*. 2006;314:73–80.
23. Caporossi D, Bacchetti S. Definition of adenovirus type 5 functions involved in the induction of chromosomal aberrations in human cells. *J Gen Virol*. 1990;71(pt 4):801–808.
24. Ornelles DA, Shenk T. Localization of the adenovirus early region 1B 55-kilodalton protein during lytic infection: association with nuclear viral inclusions requires the early region 4 34-kilodalton protein. *J Virol*. 1991;65(1):424–429.
25. Susin SA, et al. Molecular characterization of mitochondrial apoptosis-inducing factor. *Nature*. 1999;397(6718):441–446.
26. Ward IM, Chen J. Histone H2AX is phosphorylated in an ATR-dependent manner in response to replicational stress. *J Biol Chem*. 2001;276(51):47759–47762.
27. Zhao B, et al. Structural basis for Chk1 inhibition by UCN-01. *J Biol Chem*. 2002;277(48):46609–46615.
28. Arnaudeau C, Lundin C, Helleday T. DNA double-strand breaks associated with replication forks are predominantly repaired by homologous recombination involving an exchange mechanism in mammalian cells. *J Mol Biol*. 2001;307(5):1235–1245.
29. Li X, Heyer WD. Homologous recombination in DNA repair and DNA damage tolerance. *Cell Res*. 2008;18(1):99–113.
30. Blasina A, et al. Breaching the DNA damage checkpoint via PF-00477736, a novel small-molecule inhibitor of checkpoint kinase 1. *Mol Cancer Ther*. 2008;7(8):2394–2404.
31. Spitkovsky D, Jansen-Durr P, Karsenti E, Hoffman I.

S-phase induction by adenovirus E1A requires activation of cdc25a tyrosine phosphatase. *Oncogene*. 1996;12(12):2549–2554.
32. Molinari M, Mercurio C, Dominguez J, Goubin F, Draetta GF. Human Cdc25 A inactivation in response to S phase inhibition and its role in preventing premature mitosis. *EMBO Rep*. 2000; 1(1):71–79.
33. Blomberg I, Hoffmann I. Ectopic expression of Cdc25A accelerates the G(1)/S transition and leads to premature activation of cyclin E- and cyclin A-dependent kinases. *Mol Cell Biol*. 1999;19(9):6183–6194.
34. Mailand N, et al. Rapid destruction of human Cdc25A in response to DNA damage. *Science*. 2000;288(5470):1425–1429.
35. Sorensen CS, Syljuasen RG, Lukas J, Bartek J. ATR, Claspin and the Rad9-Rad1-Hus1 complex regulate Chk1 and Cdc25A in the absence of DNA damage. *Cell Cycle*. 2004;3(7):941–945.
36. Sorensen CS, et al. The cell-cycle checkpoint kinase Chk1 is required for mammalian homologous recombination repair. *Nat Cell Biol*. 2005;7(2):195–201.
37. Harada JN, Shevchenko A, Pallas DC, Berk AJ. Analysis of the adenovirus E1B-55K-anchored proteome reveals its link to ubiquitination machinery. *J Virol*. 2002;76(18):9194–9206.
38. Bryant HE, et al. Specific killing of BRCA2-deficient tumours with inhibitors of poly(ADP-ribose) polymerase. *Nature*. 2005;434(7035):913–917.
39. Katich SC, Zerfass-Thome K, Hoffmann I. Regulation of the Cdc25A gene by the human papillomavirus Type 16 E7 oncogene. *Oncogene*. 2001; 20(5):543–550.
40. Sorensen CS, et al. Chk1 regulates the S phase checkpoint by coupling the physiological turnover and ionizing radiation-induced accelerated proteolysis of Cdc25A. *Cancer Cell*. 2003;3(3):247–258.
41. Baker A, Rohleder KJ, Hanakahi LA, Ketner G. Adenovirus E4 34k and E1b 55k oncoproteins target host DNA ligase IV for proteasomal degradation. *J Virol*. 2007;81(13):7034–7040.
42. Ingemarsdotter CK, Baird SK, Connell CM, Oberg D, Hallden G, McNeish IA. Low-dose paclitaxel synergizes with oncolytic adenoviruses via mitotic slippage and apoptosis in ovarian cancer. *Oncogene*. 2010;29(45):6051–6063.
43. Shenk T. Adenoviridae: the viruses and their replication. In: Knipe DM, Howley PM, eds. *Fields Virology*. 4th ed. Philadelphia, Pennsylvania, USA: Lippincott, Williams and Wilkins; 2001:2265–2300.
44. Howe JA, Bayley ST. Effects of Ad5 E1A mutant viruses on the cell cycle in relation to the binding of cellular proteins including the retinoblastoma protein and cyclin A. *Virology*. 1992;186(1):15–24.
45. Wang HG, Draetta G, Moran E. E1A induces phosphorylation of the retinoblastoma protein independently of direct physical association between the E1A and retinoblastoma products. *Mol Cell Biol*. 1991;11(8):4253–4265.
46. Farmer H, et al. Targeting the DNA repair defect in BRCA mutant cells as a therapeutic strategy. *Nature*. 2005;434(7035):917–921.
47. Fong PC, et al. Poly(ADP)-Ribose Polymerase Inhibition: Frequent Durable Responses in BRCA Carrier Ovarian Cancer Correlating With Platinum-Free Interval. *J Clin Oncol*. 2010;28(15):2512–2519.
48. Hotte SJ, et al. Phase I trial of UCN-01 in combination with topotecan in patients with advanced solid cancers: a Princess Margaret Hospital Phase II Consortium study. *Ann Oncol*. 2006;17(2):334–340.
49. McNeish IA, Tenev T, Bell S, Marani M, Vassaux G, Lemoine N. Herpes simplex virus thymidine kinase/ganciclovir-induced cell death is enhanced by co-expression of caspase-3 in ovarian carcinoma cells. *Cancer Gene Ther*. 2001;8(4):308–319.

A.2 RESULTS FROM SCREEN

	OVCAR4 screen 1	OVCAR4 screen 2	COV318 screen 1	COV318 screen 2
Gene	ΔZ score	ΔZ score	ΔZ score	ΔZ score
AHCY	0.71	0.91	1.39	0.75
AHCY	-0.92	-4.72	0.34	0.72
ADPRT	1.32	0.91	0.96	1.15
ADPRT	-2.42	-0.44	-2.26	-1.56
ADPRTL2	0.71	1.35	1.18	0.96
ADPRTL2	-2.72	-1.26	0.52	0.84
APEX2	-0.42	-2.32	0.42	0.33
APEX2	-0.80	-1.14	-1.75	0.68
ATR	-0.35	0.79	0.32	1.04
ATR	-2.08	-1.12	0.35	1.07
ARMET	1.28	0.80	1.13	1.84
ARMET	1.53	1.35	-0.01	0.89
BLM	-0.01	1.49	0.01	0.52
BLM	0.47	-0.17	1.61	1.14
BRCA2	0.46	-0.08	0.28	0.58
BRCA2	0.71	0.00	-0.19	3.91
C18orf37	-2.98	-2.93	2.09	-0.69
C18orf37	0.11	1.36	1.19	0.25
CANX	-1.07	0.44	-0.04	0.19
CANX	-1.26	-0.23	0.72	-0.77
CARM1	-2.69	-0.72	0.22	1.60
CARM1	-0.92	-1.00	1.14	1.67
CCNH	-0.58	-1.15	-0.63	-1.06
CCNH	-0.77	-0.44	-0.29	0.69
CCT4	-0.91	-0.60	-0.66	0.10
CCT4	2.56	2.22	1.52	0.84
CCT5	1.44	1.60	1.44	1.21
CCT5	-3.47	-2.65	-0.72	-1.52
CDK7	0.23	1.04	1.26	0.93
CDK7	0.89	-0.45	0.66	-0.99
CKN1	-1.29	-1.46	-0.51	-0.92
CKN1	-0.03	0.67	-0.79	-2.70
CHEK1	-2.04	0.44	-0.45	-0.19
CHEK1	-0.04	1.45	0.16	-0.38

CKS2	-0.39	1.28	-0.06	-0.84
CKS2	-0.73	0.08	-1.61	-2.09
CETN2	1.32	0.67	0.95	1.53
CETN2	-3.41	-2.38	-2.40	-3.13
CDKN3	0.87	-1.19	1.11	0.86
CDKN3	1.61	1.32	-0.20	-2.30
COL1A2	0.49	1.53	0.20	0.94
COL1A2	0.95	0.94	0.76	1.09
CRIP2	-0.63	-0.15	-2.95	-4.18
CRIP2	0.72	-0.15	-0.02	-2.05
COPB2	-0.20	0.16	-1.34	-5.09
COPB2	1.05	0.03	4.08	-5.93
DDB2	0.47	-1.60	-1.09	0.50
DDB2	2.71	0.72	-0.06	-5.39
DNMT1	-0.02	1.20	-1.45	0.99
DNMT1	1.11	1.37	-0.56	0.97
DDB1	-0.18	1.08	-0.73	2.10
DDB1	-0.06	0.89	-0.90	-0.02
DMC1	0.05	0.75	-1.57	0.04
DMC1	2.99	0.54	-0.42	-2.70
DDX48	3.85	2.07	0.19	-6.90
DDX48	3.76	2.70	1.24	-6.84
DCLRE1A	0.75	2.14	0.18	0.87
DCLRE1A	0.43	1.55	-0.51	0.22
DCLRE1C	-0.17	2.48	0.66	1.12
DCLRE1C	-0.64	0.76	-1.17	-0.63
DCLRE1B	-2.24	-0.42	-0.17	0.46
DCLRE1B	0.81	1.82	0.88	-1.71
DEPC-1	-0.29	-0.79	-0.45	-1.37
DEPC-1	-1.30	-0.57	0.43	-2.23
DUT	-0.28	2.28	0.49	1.19
DUT	0.02	0.44	-0.75	0.13
E2F5	-0.57	1.57	-0.24	0.58
E2F5	-0.34	0.84	0.47	0.00
DVL3	0.50	-1.59	-0.37	-2.34
DVL3	-1.57	1.44	0.86	0.44
DOT1L	-2.40	-2.80	-1.18	-3.55
DOT1L	-0.45	0.09	0.11	-0.55

EHMT1	-0.14	1.70	-0.64	-2.25
EHMT1	-0.82	0.39	-1.00	0.27
ERCC3	-1.16	-0.13	-0.24	0.41
ERCC3	-0.09	0.24	-0.07	-0.52
ERCC2	0.30	0.16	-0.53	-0.22
ERCC2	0.27	1.14	0.55	1.18
ERCC4	-0.33	0.61	-1.00	-0.37
ERCC4	0.45	0.87	0.04	0.52
ERCC5	0.40	0.40	-0.89	-0.19
ERCC5	-0.15	-0.27	-0.56	-1.09
ERCC6	0.44	0.93	0.66	-0.46
ERCC6	-0.52	-1.32	0.47	-1.08
FANCA	-0.63	-0.87	-1.53	-0.82
FANCA	-0.13	0.06	1.51	0.43
FANCC	-0.31	0.25	-1.07	-0.20
FANCC	-0.40	-0.15	-0.47	0.21
FAP	-0.01	-0.14	-0.27	-0.20
FAP	0.65	0.06	0.58	0.47
FANCG	-0.53	-0.52	-1.02	-1.77
FANCG	0.63	0.77	-1.16	1.80
FANCE	0.06	0.30	-1.18	-0.32
FANCE	0.06	-0.27	0.13	0.85
FANCF	0.18	0.29	0.04	0.19
FANCF	-0.58	-0.63	-0.23	-0.40
FANCD2	0.51	-0.26	0.98	0.70
FANCD2	1.34	-0.08	1.10	0.35
FEN1	0.89	-0.61	0.20	0.42
FEN1	-0.24	-1.24	-1.72	0.94
FLJ10858	0.23	1.67	-0.20	-1.08
FLJ10858	0.76	0.04	1.75	0.69
FLJ35220	0.48	0.11	1.53	0.90
FLJ35220	-0.10	-0.95	-0.38	-0.90
G22P1	0.23	-1.63	-0.58	-1.01
G22P1	-0.01	-1.37	0.47	-0.67
GTF2H2	-0.07	-2.49	-0.42	-1.78
GTF2H2	1.08	-1.01	-0.50	-0.03
GTF2H3	0.69	1.49	-0.65	0.43
GTF2H3	-1.19	-0.79	0.37	0.51

H2AFZ	-0.94	-0.08	-0.02	0.19
H2AFZ	-0.05	-0.12	-0.01	0.23
GTF2H1	0.75	-0.31	0.95	0.44
GTF2H1	0.73	-0.46	0.98	0.08
HDAC2	0.57	-1.32	0.70	-1.52
HDAC2	0.83	0.07	-0.79	1.32
HDAC1	-0.06	0.45	0.20	0.85
HDAC1	-0.68	-0.21	0.45	-0.41
HDAC4	0.54	1.14	0.42	0.64
HDAC4	-0.47	-0.14	-0.38	-0.81
HDAC6	0.52	0.21	1.30	0.54
HDAC6	0.20	-0.50	0.48	-0.14
ZDHHC17	-0.21	-1.30	0.68	-0.04
ZDHHC17	-0.24	-0.07	2.24	-0.21
HDAC11	-1.07	-0.34	-1.45	-1.46
HDAC11	-1.52	0.02	1.45	0.84
HDAC10	-0.68	-0.27	-0.46	0.41
HDAC10	-0.06	-0.04	-0.67	-0.17
HSPE1	-0.46	-0.67	1.16	0.17
HSPE1	-2.45	-2.09	1.04	-0.47
HUS1	0.21	-1.61	0.79	-0.22
HUS1	0.84	-1.39	1.10	2.33
ILF2	0.86	1.23	1.29	1.22
ILF2	1.37	0.89	1.14	0.35
IFNGR2	0.20	1.18	0.79	0.48
IFNGR2	-0.50	0.48	-0.11	-0.46
HSU24186	-1.02	-0.75	-0.38	-0.40
HSU24186	1.65	0.92	-0.92	-0.88
KDELR2	0.27	0.44	-0.67	0.23
KDELR2	1.30	0.67	0.54	-1.43
KIAA0101	0.70	-2.16	-0.86	-0.27
KIAA0101	0.72	0.10	-0.26	0.34
LIG1	-0.44	-0.05	0.44	0.54
LIG1	-0.39	0.37	-1.85	-0.12
KPNA2	0.33	-0.83	-0.71	0.14
KPNA2	0.13	-0.71	-1.97	-1.68
LDHA	1.06	-0.18	-0.73	0.27
LDHA	1.34	1.62	0.32	0.68

MAD2L2	-0.14	0.60	-0.57	-0.09
MAD2L2	0.15	-1.07	-3.34	-0.15
MCM3	-2.07	-1.40	-0.14	-0.15
MCM3	-0.04	1.59	-0.81	-0.07
MBD4	-0.44	1.75	0.17	0.00
MBD4	-1.56	-0.50	-0.59	-0.16
MBD3	-0.48	0.45	-0.85	-0.98
MBD3	0.11	0.59	-0.11	-0.26
MECP2	0.35	0.99	-1.50	0.37
MECP2	-0.30	-0.27	-0.09	0.98
MLH1	-0.96	-0.39	-1.25	1.61
MLH1	0.66	-2.53	0.09	-0.83
MGC90512	-1.87	0.01	0.25	0.07
MGC90512	1.58	1.20	0.85	-0.17
MNAT1	0.07	0.41	-0.48	-1.30
MNAT1	-0.89	0.50	-0.41	-0.77
MPG	1.32	0.33	0.11	0.64
MPG	0.12	1.50	0.39	0.26
MMP9	0.78	1.35	1.06	0.54
MMP9	-0.90	-2.74	-3.34	-2.27
MLL	-0.07	1.11	0.78	0.55
MLL	0.54	0.47	0.32	0.17
MRPL3	0.39	1.33	0.06	-0.40
MRPL3	1.35	1.33	-1.07	-0.20
MLH3	-1.18	0.62	0.14	-1.01
MLH3	0.48	-0.12	0.37	0.17
MMS19L	-0.17	-0.38	0.91	1.13
MMS19L	1.13	-1.50	1.20	0.46
MSH6	1.16	1.01	0.84	1.20
MSH6	0.49	-0.22	-0.95	-0.55
MSH2	0.21	0.89	-1.07	0.50
MSH2	1.85	0.75	1.33	0.87
MSH3	0.66	0.57	1.66	2.03
MSH3	1.14	-0.28	0.58	1.41
MSH4	-0.62	-0.85	1.84	0.81
MSH4	-0.35	-1.34	-2.10	1.86
MTHFD2	-0.30	0.67	0.69	0.86
MTHFD2	0.32	0.80	0.21	1.70

MUTYH	0.40	0.07	0.87	0.94
MUTYH	0.05	-0.58	-0.77	-0.01
NBS1	0.57	-0.08	0.53	-0.14
NBS1	1.55	-0.67	0.86	0.40
NCBP2	-1.64	-1.14	1.26	-0.73
NCBP2	0.34	-1.50	-0.46	-0.67
NONO	1.34	1.04	0.04	0.05
NONO	-3.60	-2.74	-4.15	-3.05
NEIL1	1.01	0.40	-0.93	0.06
NEIL1	1.25	-0.39	-1.02	-0.10
NEIL2	0.48	-0.72	0.04	-0.95
NEIL2	0.55	-0.37	0.66	0.09
NTHL1	0.39	0.15	1.49	1.00
NTHL1	2.55	-0.63	0.81	1.41
OK/SW-cl.56	0.33	0.05	-0.97	0.42
OK/SW-cl.56	1.01	-0.28	-0.18	-0.50
PAFAH1B3	-0.20	0.21	0.23	-0.41
PAFAH1B3	-1.24	-1.39	-0.69	-0.35
PAICS	-0.24	-0.46	0.47	0.22
PAICS	0.37	-1.03	0.60	0.70
PLK1	-0.88	-2.63	0.78	-0.22
PLK1	0.81	-2.64	0.27	0.30
PMS1	0.39	0.73	-0.67	0.48
PMS1	-0.76	0.14	-0.76	0.21
PMS2	-0.61	-0.71	-0.63	0.28
PMS2	-2.15	-1.65	-0.69	0.19
POLB	0.27	-0.92	0.06	0.09
POLB	0.28	-0.99	1.32	0.91
POLD1	0.44	-0.33	1.81	0.80
POLD1	0.73	-0.70	1.05	0.30
POLG	0.77	1.40	-0.20	0.96
POLG	-3.29	-1.55	0.44	-0.38
POLE	-0.49	0.78	0.78	1.01
POLE	-0.59	-0.03	0.14	0.69
POLH	0.56	-0.84	0.97	0.07
POLH	-0.57	-1.30	1.04	0.30
POLI	0.41	0.32	0.55	0.28
POLI	-0.62	-1.31	0.86	0.46

PNKP	0.12	0.60	-0.20	-0.48
PNKP	-0.56	0.02	1.19	-0.52
POLL	0.34	0.77	0.12	0.24
POLL	-2.65	0.23	-0.70	0.62
POLM	1.63	0.02	0.08	0.70
POLM	2.13	1.18	-2.51	1.29
POLK	-0.55	1.58	-0.03	0.84
POLK	-1.32	-0.30	-1.53	0.27
POLN	2.17	0.29	-1.54	0.26
POLN	-4.82	-0.90	-0.63	-0.27
PRDX4	-0.70	-0.71	-0.55	-1.67
PRDX4	0.05	0.02	0.94	2.46
PRKDC	-0.20	0.27	-1.83	0.26
PRKDC	-2.46	0.09	-1.56	0.21
RAD23B	-1.44	0.61	-1.31	0.27
RAD23B	3.39	0.80	0.44	0.33
RAD54L	2.07	-0.51	-1.11	-0.18
RAD54L	1.61	0.28	0.15	1.23
RAD9A	0.59	0.02	-0.19	-0.33
RAD9A	2.75	1.16	1.42	4.83
RAD23A	-2.15	-1.73	-0.41	0.11
RAD23A	4.15	1.30	-1.13	0.47
RAD18	-0.05	0.93	0.03	0.54
RAD18	1.87	-1.34	-1.70	-1.02
RBM4	-2.02	-3.02	-2.72	-1.87
RBM4	0.50	-1.47	-0.15	-1.71
RECQL4	1.26	-0.70	1.28	-0.18
RECQL4	1.64	0.95	1.37	3.97
REV3L	-3.08	1.72	-0.01	1.60
REV3L	2.79	-0.43	-0.98	-0.19
RPA1	8.38	1.82	2.41	1.98
RPA1	-1.20	2.88	2.04	1.54
RPA2	-0.14	-4.10	-1.32	-0.07
RPA2	4.14	-0.77	0.34	1.04
RPA3	3.16	-3.09	-0.22	-1.69
RPA3	2.81	-0.52	1.74	3.47
REV1L	-4.11	-0.58	-1.77	-0.07
REV1L	-1.09	-0.96	-0.62	0.40

SDHC	-1.44	-0.56	-0.48	-0.07
SDHC	-4.13	0.66	-1.57	0.42
RRM2B	-1.86	0.56	-1.44	1.26
RRM2B	-2.48	-0.32	0.40	-0.16
SET8	5.41	-1.81	1.00	-2.39
SET8	3.14	-0.03	2.28	3.04
SET7	-2.38	0.28	3.29	0.88
SET7	0.47	-0.21	-0.07	0.87
SMARCA4	-2.49	-0.30	0.51	1.15
SMARCA4	-0.47	0.36	0.07	-0.47
SNRPF	-4.06	0.57	-0.09	1.52
SNRPF	-5.00	1.64	-0.11	0.81
SOX4	3.01	-1.16	2.19	0.19
SOX4	-3.90	0.33	0.29	1.04
SMUG1	0.72	-0.42	0.08	0.05
SMUG1	1.45	0.06	-0.59	0.92
SND1	-1.75	1.53	-1.03	0.34
SND1	-0.85	0.99	-0.04	1.06
SSBP1	2.54	-0.04	-0.17	-0.43
SSBP1	5.37	2.34	1.11	0.88
SSR1	-11.80	1.23	-0.08	-3.17
SSR1	-10.91	2.90	1.60	0.63
SUV39H1	1.52	0.16	-2.05	-0.13
SUV39H1	0.01	-0.32	-1.78	0.44
SUV39H2	-0.95	0.30	-1.41	0.21
SUV39H2	-2.97	-1.28	-0.74	0.73
TDG	-1.05	1.11	0.42	0.93
TDG	-4.58	-1.09	0.81	0.38
TDP1	-3.66	-0.04	-1.71	-0.83
TDP1	-1.61	-0.73	1.21	-1.38
TARS	-1.76	0.49	-1.12	0.03
TARS	0.00	-1.25	-1.87	-0.37
TMEM30A	4.11	-3.86	-4.25	-3.53
TMEM30A	-1.09	-0.69	-1.29	-0.79
TOP2A	-5.18	0.52	0.10	0.43
TOP2A	-2.39	-0.03	1.30	0.31
TRA1	-1.98	-0.42	0.90	-1.51
TRA1	0.34	2.07	0.66	-0.05

TP53BP1	-4.95	0.93	-1.54	-0.16
TP53BP1	1.63	0.08	-0.19	0.56
TPX2	2.84	0.81	-0.25	0.00
TPX2	-0.18	0.63	1.12	0.72
TSTA3	-0.43	0.29	-1.13	0.00
TSTA3	-0.75	-0.25	0.09	0.54
UBE2B	0.62	0.98	1.86	1.63
UBE2B	1.45	0.26	0.64	1.74
UBE2N	0.55	-0.50	-0.13	0.34
UBE2N	-0.84	-2.61	0.21	0.76
UBE2V2	-0.25	-2.31	0.91	0.27
UBE2V2	1.16	-0.23	3.29	2.09
XPA	-1.89	-0.28	-0.76	-0.83
XPA	-0.72	-0.84	0.62	-0.11
WRN	-1.78	0.27	-0.29	-1.20
WRN	0.58	1.13	0.78	0.21
XPC	-0.09	0.45	0.48	-0.22
XPC	-0.60	-0.35	0.38	-0.62
XRCC2	0.17	-0.81	0.40	0.29
XRCC2	1.34	1.36	1.88	1.16
XRCC3	-1.46	-0.60	-1.03	-1.63
XRCC3	0.30	1.39	0.39	1.19
XRCC1	-0.76	0.10	1.21	-0.27
XRCC1	1.06	2.29	0.49	-0.45
XAB2	3.06	2.52	1.43	1.61
XAB2	1.61	1.04	1.22	0.34
XRCC5	0.73	-0.42	0.84	-0.59
XRCC5	1.57	-0.52	2.12	1.58
PMS2L4	-0.53	0.37	-0.54	0.73
PMS2L4	-1.27	0.15	-1.51	-0.27
H2AFX	-0.90	-0.24	-0.60	-0.35
H2AFX	0.24	0.70	-0.26	-0.26
MGMT	0.32	0.17	0.75	0.79
MGMT	-1.25	-2.54	-0.12	-0.13
PTMA	3.17	1.18	2.06	1.64
PTMA	-0.38	-2.00	0.87	0.91
RPL27	0.94	1.16	0.75	0.75
RPL27	0.40	2.04	-0.33	-0.16

PSME2	0.51	0.57	0.47	-0.77
PSME2	0.54	0.16	1.19	1.21
SNRPE	2.99	1.96	0.67	1.50
SNRPE	0.74	0.67	0.19	0.93
UBE2S	1.54	0.17	2.28	-0.55
UBE2S	0.42	-0.62	2.71	1.65
RPL35	1.05	1.78	-1.58	-0.39
RPL35	0.62	2.22	-1.89	0.16
GTF2H4	-1.29	1.52	0.34	-0.34
GTF2H4	0.62	1.44	2.19	2.11
ATM	-0.18	0.40	0.03	0.05
ATM	0.39	0.47	1.39	0.84
NME1	0.41	0.04	2.47	-0.67
NME1	0.12	0.71	2.74	0.83
RPL13	-0.35	1.56	-0.05	0.62
RPL13	-2.21	1.05	-3.16	-0.38
ACLY	-1.87	0.59	-1.67	-1.21
ACLY	-0.06	0.82	0.75	1.65
HRMT1L2	3.17	1.79	1.09	1.61
HRMT1L2	3.60	0.44	2.24	2.39
APEX1	-0.35	-0.01	0.21	-0.37
APEX1	2.18	-0.14	3.02	2.60
CDC2	-0.66	0.60	-0.55	-0.26
CDC2	-0.45	1.04	-2.25	-0.91
ERCC1	-1.05	-0.32	-1.17	-0.66
ERCC1	-1.77	-1.50	0.36	0.52
HNRPA2B1	-0.81	-1.14	-1.09	1.96
HNRPA2B1	-0.68	-1.82	-0.54	-1.17
HSPD1	1.15	-1.31	0.63	-2.38
HSPD1	1.71	-0.26	2.07	-1.18
IARS	1.20	1.44	-0.53	1.14
IARS	0.17	1.81	0.37	0.63
LIG3	0.61	1.28	-1.50	-0.40
LIG3	-2.05	-0.19	-1.47	0.11
LIG4	3.84	2.19	-1.46	0.28
LIG4	-1.46	-1.42	-0.82	-1.39
MBD1	-2.18	-1.76	-0.25	-3.67
MBD1	0.57	-0.88	0.97	-3.14

MSH5	-0.39	2.00	-0.73	0.96
MSH5	1.16	1.53	0.71	1.57
NUDT1	1.47	1.97	-2.05	0.85
NUDT1	0.78	0.89	-0.61	1.50
OGG1	0.83	0.00	0.18	1.21
OGG1	0.48	-1.03	-0.60	-1.48
PCNA	1.31	1.06	-0.32	0.46
PCNA	1.33	1.47	1.04	0.79
PPP2R5C	-2.29	-1.04	-1.00	-0.13
PPP2R5C	-0.46	0.82	0.24	-0.04
PSMA1	1.07	1.58	-0.33	0.77
PSMA1	0.45	1.80	2.69	1.78
RAD1	0.46	0.54	0.16	1.06
RAD1	1.16	-0.05	0.34	0.95
RAD17	1.47	1.00	-0.20	1.04
RAD17	-0.90	-0.54	-1.18	-0.80
RAD51	-0.08	0.89	0.68	1.34
RAD51	0.58	0.59	-0.34	-1.21
RAD51C	0.93	2.07	-0.44	0.02
RAD51C	-2.05	0.76	-0.69	-1.45
RAD51L1	1.15	0.45	-0.11	1.02
RAD51L1	2.67	-0.27	1.16	0.77
RAD51L3	-2.65	-2.47	-0.73	-0.84
RAD51L3	-1.52	-1.71	1.10	0.11
RAD52	-0.50	-0.46	1.40	-0.11
RAD52	0.32	-1.17	0.99	0.08
RFC4	0.10	0.23	1.90	-0.66
RFC4	-0.50	1.38	3.15	1.56
SMARCA3	1.97	0.60	0.85	1.04
SMARCA3	1.89	0.48	0.26	0.94
TGIF	0.21	-0.70	-1.39	0.73
TGIF	1.26	0.44	-0.10	0.91
UBE2A	1.40	0.97	-0.59	-0.39
UBE2A	0.27	0.76	0.52	-0.66
UNG	0.03	-0.08	-0.91	-0.48
UNG	-1.55	0.16	0.32	0.02
XRCC4	-0.70	-0.63	-0.65	-0.57
XRCC4	0.55	0.66	-0.45	2.19

OGT	-0.40	0.13	-0.86	0.39
OGT	1.99	1.44	0.76	0.34
EXO1	1.34	1.51	-0.46	0.23
EXO1	0.02	0.58	0.69	-0.59
MBD2	-0.41	-2.18	0.73	0.45
MBD2	-1.34	-0.27	1.49	-0.42
TRAF4	2.15	0.03	-0.02	1.50
TRAF4	1.17	-0.16	0.47	0.49
DNMT2	0.48	-0.16	0.09	0.49
DNMT2	0.72	-0.41	-0.09	0.29
EZH2	1.15	0.32	0.41	0.08
EZH2	1.28	1.29	1.13	0.85
MRE11A	1.09	-0.56	0.00	0.61
MRE11A	-0.79	-0.47	3.25	0.38
RAD50	1.83	0.62	-0.11	1.02
RAD50	2.72	0.27	-0.37	-0.13
G3BP	1.93	1.68	-0.88	0.52
G3BP	1.30	0.04	1.28	0.32
PRDX2	0.26	-0.48	0.92	0.52
PRDX2	1.77	0.62	0.99	1.14
PSMC4	1.62	0.89	-0.56	-1.30
PSMC4	0.99	1.38	2.61	0.01
POLQ	2.15	0.42	0.52	1.43
POLQ	1.58	-0.03	0.23	-0.33
DNMT3B	-0.98	-0.75	-0.32	-0.25
DNMT3B	0.67	0.52	-0.21	0.14
CHEK2	-3.07	-1.88	0.06	-0.06
CHEK2	0.10	-0.76	-0.55	-0.09
CBX3	0.32	-1.63	-0.36	-1.43
CBX3	-0.16	2.36	0.87	-2.37
BRCA1	1.12	0.48	-0.49	1.75
BRCA1	1.77	-0.32	0.48	-0.11
RAD54B	-0.03	0.15	-0.34	-0.62
RAD54B	-0.59	-0.22	0.19	0.23
SPO11	1.15	0.69	0.45	2.21
SPO11	-3.46	-1.81	-2.30	-0.50
TREX1	-1.74	-2.06	-0.98	-0.35
TREX1	-1.77	-1.55	2.17	0.64

MRPS12	2.12	1.07	-0.09	0.78
MRPS12	0.28	-0.77	0.94	-0.81
NUP205	2.34	1.09	0.93	0.87
NUP205	2.30	1.10	1.21	0.33
DNMT3A	-0.61	0.68	0.23	0.47
DNMT3A	0.08	-0.83	-0.52	-0.31
DNMT3A	-4.56	-3.11	-0.41	-0.91
DNMT3A	0.52	-0.12	0.13	-0.03
TREX2	-1.55	-2.00	0.76	-0.33
TREX2	-0.39	-1.72	2.03	0.72
TREX2	1.14	-0.19	0.25	-0.46
TREX2	0.51	1.30	0.99	-1.62
TREX2	-0.38	0.83	-0.08	-0.41
TREX2	-0.25	0.16	-0.08	-1.54

BIBLIOGRAPHY

Ackrill AM, Foster GR, Laxton CD, Flavell DM, Stark GR, et al. (1991) Inhibition of the cellular response to interferons by products of the adenovirus type 5 E1A oncogene. Nucleic Acids Res 19: 4387–93. (Cited on page 83.)

Adams SF, Marsh EB, Elmasri W, Halberstadt S, Vandecker S, et al. (2011) A high response rate to liposomal doxorubicin is seen among women with BRCA mutations treated for recurrent epithelial ovarian cancer. Gynecol Oncol 123: 486–91. (Cited on page 63.)

Aghajanian C, Blank SV, Goff BA, Judson PL, Teneriello MG, et al. (2012) OCEANS: a randomized, double-blind, placebo-controlled phase III trial of chemotherapy with or without bevacizumab in patients with platinum-sensitive recurrent epithelial ovarian, primary peritoneal, or fallopian tube cancer. J Clin Oncol 30: 2039–45. (Cited on page 44.)

Ahmed AA, Etemadmoghadam D, Temple J, Lynch AG, Riad M, et al. (2010) Driver mutations in TP53 are ubiquitous in high grade serous carcinoma of the ovary. J Pathol 221: 49–56. (Cited on page 33.)

Ahnesorg P, Smith P, Jackson SP (2006) XLF interacts with the XRCC4-DNA ligase IV complex to promote DNA nonhomologous end-joining. Cell 124: 301–13. (Cited on page 51.)

Akiyama M, Thorne S, Kirn D, Roelvink PW, Einfeld DA, et al. (2004) Ablating CAR and integrin binding in adenovirus vectors reduces nontarget organ transduction and permits sustained bloodstream persistence following intraperitoneal administration. Mol Ther 9: 218–30. (Cited on page 74.)

Alberts DS, Markman M, Muggia F, Ozols RF, Eldermire E, et al. (2006) Proceedings of a GOG workshop on intraperitoneal therapy for ovarian cancer. Gynecol Oncol 103: 783–92. (Cited on page 43.)

Alekseev O, Donovan K, Azizkhan-Clifford J (2014) Inhibition of ataxia telangiectasia mutated (ATM) kinase suppresses herpes simplex virus type 1 (HSV-1) keratitis. Invest Ophthalmol Vis Sci 55: 706–15. (Cited on page 204.)

Alemany R, Balague C, Curiel DT (2000) Replicative adenoviruses for cancer therapy. Nat Biotechnol 18: 723–7. (Cited on page 69.)

Alsop K, Fereday S, Meldrum C, deFazio A, Emmanuel C, et al. (2012) BRCA mutation frequency and patterns of treatment response in BRCA mutation-positive women with ovarian cancer: a report from the Australian Ovarian Cancer Study Group. J Clin Oncol 30: 2654–63. (Cited on page 153.)

Andtbacka RH, Kaufman HL, Collichio F, Amatruda T, Senzer N, et al. (2015) Talimogene Laherparepvec Improves Durable Response Rate in Patients With Advanced Melanoma. J Clin Oncol 33: 2780–8. (Cited on page 239.)

Anglesio MS, George J, Kulbe H, Friedlander M, Rischin D, et al. (2011) IL6-STAT3-HIF signaling and therapeutic response to the angiogenesis inhibitor sunitinib in ovarian clear cell cancer. Clin Cancer Res 17: 2538–48. (Cited on page 33.)

Antoniou A, Pharoah PD, Narod S, Risch HA, Eyfjord JE, et al. (2003) Average risks of breast and ovarian cancer associated with BRCA1 or BRCA2 mutations detected in case Series unselected for family history: a combined analysis of 22 studies. Am J Hum Genet 72: 1117–30. (Cited on page 29.)

Araki M, Masutani C, Takemura M, Uchida A, Sugasawa K, et al. (2001) Centrosome protein centrin 2/caltractin 1 is part of the xero-

derma pigmentosum group C complex that initiates global genome nucleotide excision repair. J Biol Chem 276: 18665–18672. (Cited on page 221.)

Arany Z, Newsome D, Oldread E, Livingston DM, Eckner R (1995) A family of transcriptional adaptor proteins targeted by the E1A oncoprotein. Nature 374: 81–4. (Cited on page 77.)

Araujo FD, Stracker TH, Carson CT, Lee DV, Weitzman MD (2005) Adenovirus type 5 E4orf3 protein targets the Mre11 complex to cytoplasmic aggresomes. J Virol 79: 11382–91. (Cited on pages 90, 203, and 205.)

Armstrong DK, Bundy B, Wenzel L, Huang HQ, Baergen R, et al. (2006) Intraperitoneal cisplatin and paclitaxel in ovarian cancer. N Engl J Med 354: 34–43. (Cited on page 43.)

Aylon Y, Liefshitz B, Kupiec M (2004) The CDK regulates repair of double-strand breaks by homologous recombination during the cell cycle. EMBO J 23: 4868–75. (Cited on page 59.)

Baird SK, Aerts JL, Eddaoudi A, Lockley M, Lemoine NR, et al. (2008) Oncolytic adenoviral mutants induce a novel mode of programmed cell death in ovarian cancer. Oncogene 27: 3081–90. (Cited on pages 92, 149, 152, and 240.)

Baker A, Rohleder KJ, Hanakahi LA, Ketner G (2007) Adenovirus E4 34k and E1b 55k oncoproteins target host DNA ligase IV for proteasomal degradation. J Virol 81: 7034–40. (Cited on pages 90, 177, and 203.)

Balasubramanian N, Bai P, Buchek G, Korza G, Weller SK (2010) Physical interaction between the herpes simplex virus type 1 exonuclease, UL12, and the DNA double-strand break-sensing MRN complex. J Virol 84: 12504–14. (Cited on page 204.)

Baldwin RL, Nemeth E, Tran H, Shvartsman H, Cass I, et al. (2000) BRCA1 promoter region hypermethylation in ovarian carcinoma: a population-based study. Cancer Res 60: 5329–33. (Cited on page 34.)

Bamias A, Psaltopoulou T, Sotiropoulou M, Haidopoulos D, Lianos E, et al. (2010) Mucinous but not clear cell histology is associated with inferior survival in patients with advanced stage ovarian carcinoma treated with platinum-paclitaxel chemotherapy. Cancer 116: 1462–8. (Cited on page 32.)

Barbeau D, Marcellus RC, Bacchetti S, Bayley ST, Branton PE (1992) Quantitative analysis of regions of adenovirus E1A products involved in interactions with cellular proteins. Biochem Cell Biol 70: 1123–34. (Cited on page 77.)

Baumann P, Benson FE, West SC (1996) Human Rad51 protein promotes ATP-dependent homologous pairing and strand transfer reactions in vitro. Cell 87: 757–66. (Cited on page 201.)

Baumann P, West SC (1998) Role of the human RAD51 protein in homologous recombination and double-stranded-break repair. Trends Biochem Sci 23: 247–51. (Cited on page 179.)

Baumbusch LO, Helland A, Wang Y, Liestol K, Schaner ME, et al. (2013) High levels of genomic aberrations in serous ovarian cancers are associated with better survival. PLoS One 8: e54356. (Cited on page 36.)

Ben-Israel H, Kleinberger T (2002) Adenovirus and cell cycle control. Front Biosci 7: d1369–95. (Cited on page 80.)

Benedict CA (2003) Viruses and the TNF-related cytokines, an evolving battle. Cytokine Growth Factor Rev 14: 349–57. (Cited on page 84.)

Berek J, Taylor P, McGuire W, Smith LM, Schultes B, et al. (2009) Oregovomab maintenance monoimmunotherapy does not improve out-

comes in advanced ovarian cancer. J Clin Oncol 27: 418–25. (Cited on page 45.)

Bergelson JM, Cunningham JA, Droguett G, Kurt-Jones EA, Krithivas A, et al. (1997) Isolation of a common receptor for Coxsackie B viruses and adenoviruses 2 and 5. Science 275: 1320–3. (Cited on page 73.)

Berk AJ (2005) Recent lessons in gene expression, cell cycle control, and cell biology from adenovirus. Oncogene 24: 7673–85. (Cited on pages 77, 78, 80, 81, 120, and 232.)

Bhattacharyya M, Francis J, Eddouadi A, Lemoine NR, Hallden G (2011) An oncolytic adenovirus defective in pRb-binding (dl922-947) can efficiently eliminate pancreatic cancer cells and tumors in vivo in combination with 5-FU or gemcitabine. Cancer Gene Ther 18: 734–43. (Cited on page 247.)

Bieler A, Mantwill K, Holzmüller R, Jürchott K, Kaszubiak A, et al. (2008) Impact of radiation therapy on the oncolytic adenovirus dl520: implications on the treatment of glioblastoma. Radiother Oncol 86: 419–27. (Cited on page 240.)

Birmingham A, Anderson EM, Reynolds A, Ilsley-Tyree D, Leake D, et al. (2006) 3' UTR seed matches, but not overall identity, are associated with RNAi off-targets. Nature methods 3: 199–204. (Cited on page 231.)

Birrer MJ (2010) The origin of ovarian cancer-is it getting clearer? N Engl J Med 363: 1574–5. (Cited on page 33.)

Bischoff JR, Kirn DH, Williams A, Heise C, Horn S, et al. (1996) An adenovirus mutant that replicates selectively in p53-deficient human tumor cells. Science 274: 373–6. (Cited on page 81.)

Blackford AN, Bruton RK, Dirlik O, Stewart GS, Taylor AMR, et al. (2008) A role for E1B-AP5 in ATR signaling pathways during ade-

novirus infection. J Virol 82: 7640–52. (Cited on pages 81, 90, 91, and 203.)

Blackford AN, Patel RN, Forrester NA, Theil K, Groitl P, et al. (2010) Adenovirus 12 E4orf6 inhibits ATR activation by promoting TOPBP1 degradation. Proc Natl Acad Sci USA 107: 12251–6. (Cited on page 91.)

Bolton KL, Chenevix-Trench G, Goh C, Sadetzki S, Ramus SJ, et al. (2012) Association between BRCA1 and BRCA2 mutations and survival in women with invasive epithelial ovarian cancer. JAMA 307: 382–90. (Cited on pages 63, 67, 153, and 200.)

Bonadona V, Bonaiti B, Olschwang S, Grandjouan S, Huiart L, et al. (2011) Cancer risks associated with germline mutations in MLH1, MSH2, and MSH6 genes in Lynch syndrome. JAMA 305: 2304–10. (Cited on page 29.)

Bookman MA, Brady MF, McGuire WP, Harper PG, Alberts DS, et al. (2009) Evaluation of new platinum-based treatment regimens in advanced-stage ovarian cancer: a Phase III Trial of the Gynecologic Cancer Intergroup. J Clin Oncol 27: 1419–25. (Cited on page 42.)

Bookman MA, Malmstrom H, Bolis G, Gordon A, Lissoni A, et al. (1998) Topotecan for the treatment of advanced epithelial ovarian cancer: an open-label phase II study in patients treated after prior chemotherapy that contained cisplatin or carboplatin and paclitaxel. J Clin Oncol 16: 3345–52. (Cited on page 44.)

Boulton S, Kyle S, Durkacz BW (1999) Interactive effects of inhibitors of poly(ADP-ribose) polymerase and DNA-dependent protein kinase on cellular responses to DNA damage. Carcinogenesis 20: 199–203. (Cited on page 64.)

Bowtell DD (2010) The genesis and evolution of high-grade serous ovarian cancer. Nat Rev Cancer 10: 803–8. (Cited on pages 32, 34, 36, and 37.)

Bowtell DD, Böhm S, Ahmed AA, Aspuria PJ, Bast RC Jr, et al. (2015) Rethinking ovarian cancer II: reducing mortality from high-grade serous ovarian cancer. Nat Rev Cancer 15: 668–79. (Cited on page 244.)

Boyd J, Sonoda Y, Federici MG, Bogomolniy F, Rhei E, et al. (2000) Clinicopathologic features of BRCA-linked and sporadic ovarian cancer. JAMA 283: 2260–5. (Cited on pages 28 and 153.)

Boyer J, Rohleder K, Ketner G (1999a) Adenovirus E4 34k and E4 11k inhibit double strand break repair and are physically associated with the cellular DNA-dependent protein kinase. Virology 263: 307–12. (Cited on pages 89, 90, 177, and 203.)

Boyer TG, Martin ME, Lees E, Ricciardi RP, Berk AJ (1999b) Mammalian Srb/Mediator complex is targeted by adenovirus E1A protein. Nature 399: 276–9. (Cited on page 77.)

Branzei D, Foiani M (2008) Regulation of DNA repair throughout the cell cycle. Nat Rev Mol Cell Biol 9: 297–308. (Cited on pages 51 and 201.)

Bressy C, Benihoud K (2014) Association of oncolytic adenoviruses with chemotherapies: an overview and future directions. Biochem Pharmacol 90: 97–106. (Cited on page 247.)

Bringhurst R (2004) The elements of typographic style. 3rd ed., Point Roberts, WA: Hartley and Marks, Publishers. (Cited on page 354.)

Browne A, Tookman LA, Ingemarsdotter CK, Bouwman RD, Pirlo K, et al. (2015) Pharmacological Inhibition of beta3 Integrin Reduces the Inflammatory Toxicities Caused by Oncolytic Adenovirus

without Compromising Anticancer Activity. Cancer Res 75: 2811–21. (Cited on page 85.)

Bruton RK, Rasti M, Mapp KL, Young N, Carter RZ, et al. (2007) C-terminal-binding protein interacting protein binds directly to adenovirus early region 1A through its N-terminal region and conserved region 3. Oncogene 26: 7467–79. (Cited on page 77.)

Bryant HE, Schultz N, Thomas HD, Parker KM, Flower D, et al. (2005) Specific killing of BRCA2-deficient tumours with inhibitors of poly(ADP-ribose) polymerase. Nature 434: 913–7. (Cited on pages 64, 146, 151, and 200.)

Bunting SF, Callen E, Wong N, Chen HT, Polato F, et al. (2010) 53BP1 inhibits homologous recombination in Brca1-deficient cells by blocking resection of DNA breaks. Cell 141: 243–54. (Cited on pages 49, 53, 57, and 61.)

Burger RA, Brady MF, Bookman MA, Fleming GF, Monk BJ, et al. (2011) Incorporation of bevacizumab in the primary treatment of ovarian cancer. N Engl J Med 365: 2473–83. (Cited on page 42.)

Burgert HG, Kvist S (1987) The E3/19K protein of adenovirus type 2 binds to the domains of histocompatibility antigens required for CTL recognition. EMBO J 6: 2019–26. (Cited on page 83.)

Burma S, Chen BP, Murphy M, Kurimasa A, Chen DJ (2001) ATM phosphorylates histone H2AX in response to DNA double-strand breaks. J Biol Chem 276: 42462–7. (Cited on page 150.)

Caldecott KW (2014) DNA single-strand break repair. Exp Cell Res 329: 2–8. (Cited on page 46.)

Campeau E, Gobeil S (2011) RNA interference in mammals: behind the screen. Brief Funct Genomics 10: 215–226. (Cited on page 231.)

Cantin GT, Stevens JL, Berk AJ (2003) Activation domain-mediator interactions promote transcription preinitiation complex assembly

on promoter DNA. Proc Natl Acad Sci USA 100: 12003–8. (Cited on page 77.)

Carmody RJ, Maguschak K, Chen YH (2006) A novel mechanism of nuclear factor-kappaB regulation by adenoviral protein 14.7K. Immunology 117: 188–95. (Cited on page 84.)

Carnevale J, Ashworth A (2015) Assessing the Significance of BRCA1 and BRCA2 Mutations in Pancreatic Cancer. J Clin Oncol 33: 3080–1. (Cited on page 61.)

Carr AM, Lambert S (2013) Replication stress-induced genome instability: the dark side of replication maintenance by homologous recombination. J Mol Biol 425: 4733–44. (Cited on page 201.)

Carreira A, Hilario J, Amitani I, Baskin RJ, Shivji MK, et al. (2009) The BRC repeats of BRCA2 modulate the DNA-binding selectivity of RAD51. Cell 136: 1032–43. (Cited on page 56.)

Carson CT, Orazio NI, Lee DV, Suh J, Bekker-Jensen S, et al. (2009) Mislocalization of the MRN complex prevents ATR signaling during adenovirus infection. EMBO J 28: 652–62. (Cited on page 203.)

Carson CT, Schwartz RA, Stracker TH, Lilley CE, Lee DV, et al. (2003) The Mre11 complex is required for ATM activation and the G2/M checkpoint. EMBO J 22: 6610–20. (Cited on pages 89, 90, 154, and 203.)

Carter SL, Eklund AC, Kohane IS, Harris LN, Szallasi Z (2006) A signature of chromosomal instability inferred from gene expression profiles predicts clinical outcome in multiple human cancers. Nat Genet 38: 1043–8. (Cited on page 36.)

Carvalho T, Seeler JS, Ohman K, Jordan P, Pettersson U, et al. (1995) Targeting of adenovirus E1A and E4-ORF3 proteins to nuclear matrix-associated PML bodies. J Cell Biol 131: 45–56. (Cited on page 205.)

Ceccaldi R, Rondinelli B, D'Andrea AD (2016) Repair Pathway Choices and Consequences at the Double-Strand Break. Trends Cell Biol 26: 52–64. (Cited on pages 48, 52, 56, 58, 59, and 60.)

Cerullo V, Pesonen S, Diaconu I, Escutenaire S, Arstila PT, et al. (2010) Oncolytic adenovirus coding for granulocyte macrophage colony-stimulating factor induces antitumoral immunity in cancer patients. Cancer Res 70: 4297–309. (Cited on pages 86 and 243.)

Chahal JS, Gallagher C, DeHart CJ, Flint SJ (2013) The repression domain of the E1B 55-kilodalton protein participates in countering interferon-induced inhibition of adenovirus replication. J Virol 87: 4432–44. (Cited on page 83.)

Chao WR, Lee MY, Lin WL, Chen CK, Lin JC, et al. (2014) HER2 amplification and overexpression are significantly correlated in mucinous epithelial ovarian cancer. Hum Pathol 45: 810–6. (Cited on page 32.)

Charames GS, Bapat B (2003) Genomic instability and cancer. Curr Mol Med 3: 589–96. (Cited on page 37.)

Charrier JD, Durrant SJ, Golec JM, Kay DP, Knegtel RM, et al. (2011) Discovery of potent and selective inhibitors of ataxia telangiectasia mutated and Rad3 related (ATR) protein kinase as potential anticancer agents. J Med Chem 54: 2320–30. (Cited on page 67.)

Chattopadhyay D, Ghosh MK, Mal A, Harter ML (2001) Inactivation of p21 by E1A leads to the induction of apoptosis in DNA-damaged cells. J Virol 75: 9844–56. (Cited on page 77.)

Chen HY, Shao CJ, Chen FR, Kwan AL, Chen ZP (2010) Role of ERCC1 promoter hypermethylation in drug resistance to cisplatin in human gliomas. Int J Cancer 126: 1944–54. (Cited on page 246.)

Cheng CY, Gilson T, Dallaire F, Ketner G, Branton PE, et al. (2011) The E4orf6/E1B55K E3 ubiquitin ligase complexes of human aden-

oviruses exhibit heterogeneity in composition and substrate specificity. J Virol 85: 765–75. (Cited on page 204.)

Cherubini G, Petouchoff T, Grossi M, Piersanti S, Cundari E, et al. (2006) E1B55K-deleted adenovirus (ONYX-015) overrides G1/S and G2/M checkpoints and causes mitotic catastrophe and endoreduplication in p53-proficient normal cells. Cell Cycle 5: 2244–52. (Cited on pages 149 and 205.)

Chi DS, Eisenhauer EL, Zivanovic O, Sonoda Y, Abu-Rustum NR, et al. (2009) Improved progression-free and overall survival in advanced ovarian cancer as a result of a change in surgical paradigm. Gynecol Oncol 114: 26–31. (Cited on page 41.)

Chittenden BG, Fullerton G, Maheshwari A, Bhattacharya S (2009) Polycystic ovary syndrome and the risk of gynaecological cancer: a systematic review. Reprod Biomed Online 19: 398–405. (Cited on page 30.)

Choi IK, Yun CO (2013) Recent developments in oncolytic adenovirus-based immunotherapeutic agents for use against metastatic cancers. Cancer Gene Ther 20: 70–6. (Cited on page 70.)

Chung N, Zhang XD, Kreamer A, Locco L, Kuan PF, et al. (2008) Median absolute deviation to improve hit selection for genome-scale RNAi screens. Journal of biomolecular screening 13: 149–158. (Cited on page 233.)

Ciccia A, Elledge SJ (2010) The DNA damage response: making it safe to play with knives. Mol Cell 40: 179–204. (Cited on pages 48 and 49.)

Cimprich KA, Cortez D (2008) ATR: an essential regulator of genome integrity. Nat Rev Mol Cell Biol 9: 616–27. (Cited on page 48.)

Ciriello G, Miller ML, Aksoy BA, Senbabaoglu Y, Schultz N, et al. (2013) Emerging landscape of oncogenic signatures across human cancers. Nat Genet 45: 1127–33. (Cited on pages 35 and 36.)

Clark J, Lu YJ, Sidhar SK, Parker C, Gill S, et al. (1997) Fusion of splicing factor genes PSF and NonO (p54nrb) to the TFE3 gene in papillary renal cell carcinoma. Oncogene 15: 2233–2239. (Cited on page 234.)

Clauson C, Schärer OD, Niedernhofer L (2013) Advances in understanding the complex mechanisms of DNA interstrand cross-link repair. Cold Spring Harb Perspect Biol 5: a012732. (Cited on page 62.)

Coleman MP, Forman D, Bryant H, Butler J, Rachet B, et al. (2011) Cancer survival in Australia, Canada, Denmark, Norway, Sweden, and the UK, 1995-2007 (the International Cancer Benchmarking Partnership): an analysis of population-based cancer registry data. Lancet 377: 127–38. (Cited on page 28.)

Connell CM, Shibata A, Tookman LA, Archibald KM, Flak MB, et al. (2011) Genomic DNA damage and ATR-Chk1 signaling determine oncolytic adenoviral efficacy in human ovarian cancer cells. J Clin Invest 121: 1283–97. (Cited on pages 93, 121, 125, 131, 148, 149, 150, 170, and 248.)

Connell CM, Wheatley SP, McNeish IA (2008) Nuclear survivin abrogates multiple cell cycle checkpoints and enhances viral oncolysis. Cancer Res 68: 7923–31. (Cited on pages 121, 149, and 205.)

Cooke SL, Ng CKY, Melnyk N, Garcia MJ, Hardcastle T, et al. (2010) Genomic analysis of genetic heterogeneity and evolution in high-grade serous ovarian carcinoma. Oncogene 29: 4905–13. (Cited on page 170.)

Cousineau I, Abaji C, Belmaaza A (2005) BRCA1 regulates RAD51 function in response to DNA damage and suppresses spontaneous

sister chromatid replication slippage: implications for sister chromatid cohesion, genome stability, and carcinogenesis. Cancer Res 65: 11384–91. (Cited on page 235.)

Coward J, Kulbe H, Chakravarty P, Leader D, Vassileva V, et al. (2011) Interleukin-6 as a therapeutic target in human ovarian cancer. Clin Cancer Res 17: 6083–96. (Cited on page 40.)

Coyne CB, Bergelson JM (2005) CAR: a virus receptor within the tight junction. Adv Drug Deliv Rev 57: 869–82. (Cited on page 73.)

Crum CP, Drapkin R, Miron A, Ince TA, Muto M, et al. (2007) The distal fallopian tube: a new model for pelvic serous carcinogenesis. Curr Opin Obstet Gynecol 19: 3–9. (Cited on page 34.)

Cuconati A, Mukherjee C, Perez D, White E (2003) DNA damage response and MCL-1 destruction initiate apoptosis in adenovirus-infected cells. Genes Dev 17: 2922–32. (Cited on pages 80 and 81.)

Cunningham JM, Kim CY, Christensen ER, Tester DJ, Parc Y, et al. (2001) The frequency of hereditary defective mismatch repair in a prospective series of unselected colorectal carcinomas. Am J Hum Genet 69: 780–90. (Cited on page 246.)

Curtin NJ (2012) DNA repair dysregulation from cancer driver to therapeutic target. Nat Rev Cancer 12: 801–17. (Cited on pages 50, 62, 67, 208, and 232.)

Daley JM, Kwon Y, Niu H, Sung P (2013) Investigations of homologous recombination pathways and their regulation. Yale J Biol Med 86: 453–61. (Cited on page 201.)

D'Andrilli G, Kumar C, Scambia G, Giordano A (2004) Cell cycle genes in ovarian cancer: steps toward earlier diagnosis and novel therapies. Clin Cancer Res 10: 8132–41. (Cited on page 78.)

Dantas TJ, Daly OM, Morrison CG (2012) Such small hands: the roles of centrins/caltractins in the centriole and in genome maintenance. Cell Mol Life Sci 69: 2979–2997. (Cited on page 221.)

Davar D, Beumer JH, Hamieh L, Tawbi H (2012) Role of PARP inhibitors in cancer biology and therapy. Curr Med Chem 19: 3907–21. (Cited on pages 146 and 151.)

de Gramont A, Watson S, Ellis LM, Rodón J, Tabernero J, et al. (2015) Pragmatic issues in biomarker evaluation for targeted therapies in cancer. Nat Rev Clin Oncol 12: 197–212. (Cited on page 241.)

De Jong R, Van der Vliet P (1999) Mechanism of DNA replication in eukaryotic cells: cellular host factors stimulating adenovirus DNA replication. Gene 236: 1–12. (Cited on pages 79, 80, and 206.)

de Jong RN, van der Vliet PC, Brenkman AB (2003) Adenovirus DNA replication: protein priming, jumping back and the role of the DNA binding protein DBP. Curr Top Microbiol Immunol 272: 187–211. (Cited on pages 79 and 245.)

De Lorenzo SB, Patel AG, Hurley RM, Kaufmann SH (2013) The Elephant and the Blind Men: Making Sense of PARP Inhibitors in Homologous Recombination Deficient Tumor Cells. Front Oncol 3: 228. (Cited on page 64.)

De Picciotto N, Cacheux W, Roth A, Chappuis PO, Labidi-Galy SI (2016) Ovarian cancer: Status of homologous recombination pathway as a predictor of drug response. Crit Rev Oncol Hematol 101: 50–9. (Cited on page 242.)

Delacôte F, Lopez BS (2008) Importance of the cell cycle phase for the choice of the appropriate DSB repair pathway, for genome stability maintenance: the trans-S double-strand break repair model. Cell Cycle 7: 33–8. (Cited on page 202.)

DelloRusso C, Welcsh PL, Wang W, Garcia RL, King MC, et al. (2007) Functional characterization of a novel BRCA1-null ovarian cancer cell line in response to ionizing radiation. Mol Cancer Res 5: 35–45. (Cited on page 162.)

Deriano L, Roth DB (2013) Modernizing the nonhomologous end-joining repertoire: alternative and classical NHEJ share the stage. Annu Rev Genet 47: 433–55. (Cited on page 52.)

Deryckere F, Burgert HG (1996) Tumor necrosis factor alpha induces the adenovirus early 3 promoter by activation of NF-kappaB. J Biol Chem 271: 30249–55. (Cited on page 84.)

Di Y, Seymour L, Fisher K (2014) Activity of a group B oncolytic adenovirus (ColoAd1) in whole human blood. Gene Ther 21: 440–3. (Cited on page 85.)

Dianov GL, Hubscher U (2013) Mammalian base excision repair: the forgotten archangel. Nucleic Acids Res 41: 3483–90. (Cited on page 64.)

Difilippantonio MJ, Zhu J, Chen HT, Meffre E, Nussenzweig MC, et al. (2000) DNA repair protein Ku80 suppresses chromosomal aberrations and malignant transformation. Nature 404: 510–4. (Cited on page 51.)

Domchek SM, Aghajanian C, Shapira-Frommer R, Schmutzler RK, Audeh MW, et al. (2016) Efficacy and safety of olaparib monotherapy in germline BRCA1/2 mutation carriers with advanced ovarian cancer and three or more lines of prior therapy. Gynecol Oncol 140: 199–203. (Cited on page 65.)

Domcke S, Sinha R, Levine DA, Sander C, Schultz N (2013) Evaluating cell lines as tumour models by comparison of genomic profiles. Nat Commun 4: 2126. (Cited on pages 162, 185, 209, 210, and 244.)

Dong HP, Elstrand MB, Holth A, Silins I, Berner A, et al. (2006) NK- and B-cell infiltration correlates with worse outcome in metastatic ovarian carcinoma. Am J Clin Pathol 125: 451–8. (Cited on page 39.)

Doucas V, Ishov AM, Romo A, Juguilon H, Weitzman MD, et al. (1996) Adenovirus replication is coupled with the dynamic properties of the PML nuclear structure. Genes Dev 10: 196–207. (Cited on pages 87 and 205.)

du Bois A, Floquet A, Kim JW, Rau J, del Campo JM, et al. (2014) Incorporation of pazopanib in maintenance therapy of ovarian cancer. J Clin Oncol 32: 3374–82. (Cited on page 42.)

du Bois A, Reuss A, Pujade-Lauraine E, Harter P, Ray-Coquard I, et al. (2009) Role of surgical outcome as prognostic factor in advanced epithelial ovarian cancer: a combined exploratory analysis of 3 prospectively randomized phase 3 multicenter trials: by the Arbeitsgemeinschaft Gynaekologische Onkologie Studiengruppe Ovarialkarzinom (AGO-OVAR) and the Groupe d'Investigateurs Nationaux Pour les Etudes des Cancers de l'Ovaire (GINECO). Cancer 115: 1234–44. (Cited on page 41.)

Echeverri CJ, Beachy PA, Baum B, Boutros M, Buchholz F, et al. (2006) Minimizing the risk of reporting false positives in large-scale RNAi screens. Nature methods 3: 777–779. (Cited on page 225.)

Edwards SM, Kote-Jarai Z, Meitz J, Hamoudi R, Hope Q, et al. (2003) Two percent of men with early-onset prostate cancer harbor germline mutations in the BRCA2 gene. Am J Hum Genet 72: 1–12. (Cited on page 61.)

Eisenhauer EA, Vermorken JB, van Glabbeke M (1997) Predictors of response to subsequent chemotherapy in platinum pretreated ovarian cancer: a multivariate analysis of 704 patients. Ann Oncol 8: 963–8. (Cited on page 43.)

Emili A, Shales M, McCracken S, Xie W, Tucker PW, et al. (2002) Splicing and transcription-associated proteins PSF and p54nrb/nonO bind to the RNA polymerase II CTD. RNA 8: 1102–1111. (Cited on pages 220 and 234.)

Esteller M, Levine R, Baylin SB, Ellenson LH, Herman JG (1998) MLH1 promoter hypermethylation is associated with the microsatellite instability phenotype in sporadic endometrial carcinomas. Oncogene 17: 2413–7. (Cited on page 246.)

Etemadmoghadam D, deFazio A, Beroukhim R, Mermel C, George J, et al. (2009) Integrated genome-wide DNA copy number and expression analysis identifies distinct mechanisms of primary chemoresistance in ovarian carcinomas. Clin Cancer Res 15: 1417–27. (Cited on page 34.)

Etemadmoghadam D, Weir BA, Au-Yeung G, Alsop K, Mitchell G, et al. (2013) Synthetic lethality between CCNE1 amplification and loss of BRCA1. Proc Natl Acad Sci USA 110: 19489–94. (Cited on page 35.)

Evans JD, Hearing P (2005) Relocalization of the Mre11-Rad50-Nbs1 complex by the adenovirus E4 ORF3 protein is required for viral replication. J Virol 79: 6207–15. (Cited on pages 90, 203, and 205.)

Fagotti A, Ferrandina G, Vizzielli G, Fanfani F, Gallotta V, et al. (2016) Phase III randomised clinical trial comparing primary surgery versus neoadjuvant chemotherapy in advanced epithelial ovarian cancer with high tumour load (SCORPION trial): Final analysis of peri-operative outcome. Eur J Cancer 59: 22–33. (Cited on page 41.)

Farmer H, McCabe N, Lord CJ, Tutt ANJ, Johnson DA, et al. (2005) Targeting the DNA repair defect in BRCA mutant cells as a therapeutic strategy. Nature 434: 917–21. (Cited on pages 146 and 151.)

Fattaey A, Harlow E, Helin K (1993) Independent regions of adenovirus E1A are required for binding to and dissociation of E2F-protein complexes. Mol Cell Biol 13: 7267–7277. (Cited on page 120.)

Fattah F, Lee EH, Weisensel N, Wang Y, Lichter N, et al. (2010) Ku regulates the non-homologous end joining pathway choice of DNA double-strand break repair in human somatic cells. PLoS Genet 6: e1000855. (Cited on page 202.)

Felsani A, Mileo AM, Paggi MG (2006) Retinoblastoma family proteins as key targets of the small DNA virus oncoproteins. Oncogene 25: 5277–85. (Cited on page 75.)

Ferguson MS, Lemoine NR, Wang Y (2012) Systemic delivery of oncolytic viruses: hopes and hurdles. Adv Virol 2012: 805629. (Cited on page 243.)

Fisher KD, Seymour LW (2010) HPMA copolymers for masking and retargeting of therapeutic viruses. Adv Drug Deliv Rev 62: 240–5. (Cited on page 85.)

Flak MB, Connell CM, Chelala C, Archibald K, Salako MA, et al. (2010) p21 Promotes oncolytic adenoviral activity in ovarian cancer and is a potential biomarker. Mol Cancer 9: 175. (Cited on pages 149 and 242.)

Fleisher AS, Esteller M, Wang S, Tamura G, Suzuki H, et al. (1999) Hypermethylation of the hMLH1 gene promoter in human gastric cancers with microsatellite instability. Cancer Res 59: 1090–5. (Cited on page 246.)

Flint J, Enquist l, Racaniello V, Skalka A (2004) Principles of virology. 2nd ed., ASM Press, 253-297 pp. (Cited on pages 70 and 72.)

Flint J, Shenk T (1989) Adenovirus E1A protein paradigm viral transactivator. Annu Rev Genet 23: 141–61. (Cited on pages 75, 148, and 232.)

Flint J, Shenk T (1997) Viral transactivating proteins. Annual review of genetics 31: 177–212. (Cited on pages 75 and 77.)

Folkins AK, Jarboe EA, Saleemuddin A, Lee Y, Callahan MJ, et al. (2008) A candidate precursor to pelvic serous cancer (p53 signature) and its prevalence in ovaries and fallopian tubes from women with BRCA mutations. Gynecol Oncol 109: 168–73. (Cited on page 34.)

Fong PC, Boss DS, Yap TA, Tutt A, Wu P, et al. (2009) Inhibition of poly(ADP-ribose) polymerase in tumors from BRCA mutation carriers. N Engl J Med 361: 123–34. (Cited on page 64.)

Forrester NA, Sedgwick GG, Thomas A, Blackford AN, Speiseder T, et al. (2011) Serotype-specific inactivation of the cellular DNA damage response during adenovirus infection. J Virol 85: 2201–11. (Cited on pages 81, 91, 204, and 246.)

Friedberg EC, Aguilera A, Gellert M, Hanawalt PC, Hays JB, et al. (2006) DNA repair: from molecular mechanism to human disease. DNA Repair (Amst) 5: 986–96. (Cited on pages 45 and 202.)

Friedman LS, Ostermeyer EA, Lynch ED, Szabo CI, Anderson LA, et al. (1994) The search for BRCA1. Cancer Res 54: 6374–82. (Cited on page 57.)

Frisch SM, Mymryk JS (2002) Adenovirus-5 E1A: paradox and paradigm. Nat Rev Mol Cell Biol 3: 441–52. (Cited on pages 76 and 77.)

Fueyo J, Gomez-Manzano C, Alemany R, Lee PS, McDonnell TJ, et al. (2000) A mutant oncolytic adenovirus targeting the Rb pathway produces anti-glioma effect in vivo. Oncogene 19: 2–12. (Cited on page 79.)

Gallimore PH, Turnell AS (2001) Adenovirus E1A: remodelling the host cell, a life or death experience. Oncogene 20: 7824–35. (Cited on page 80.)

Gelmon KA, Tischkowitz M, Mackay H, Swenerton K, Robidoux A, et al. (2011) Olaparib in patients with recurrent high-grade serous or poorly differentiated ovarian carcinoma or triple-negative breast cancer: a phase 2, multicentre, open-label, non-randomised study. Lancet Oncol 12: 852–61. (Cited on page 65.)

Geoerger B, Grill J, Opolon P, Morizet J, Aubert G, et al. (2003) Potentiation of radiation therapy by the oncolytic adenovirus dl1520 (ONYX-015) in human malignant glioma xenografts. Br J Cancer 89: 577–84. (Cited on page 240.)

Gershenson DM, Sun CC, Bodurka D, Coleman RL, Lu KH, et al. (2009) Recurrent low-grade serous ovarian carcinoma is relatively chemoresistant. Gynecol Oncol 114: 48–52. (Cited on page 31.)

Gilks CB (2010) Molecular abnormalities in ovarian cancer subtypes other than high-grade serous carcinoma. J Oncol 2010: 740968. (Cited on page 32.)

Gilks CB, Prat J (2009) Ovarian carcinoma pathology and genetics: recent advances. Hum Pathol 40: 1213–23. (Cited on page 32.)

Goktug AN, Chai SC, Chen T (2013) Data analysis approaches in high throughput screening. INTECH Open Access Publisher. (Cited on page 233.)

Gonzalez RA, Flint SJ (2002) Effects of mutations in the adenoviral E1B 55-kilodalton protein coding sequence on viral late mRNA metabolism. J Virol 76: 4507–19. (Cited on page 87.)

Gordon AN, Granai CO, Rose PG, Hainsworth J, Lopez A, et al. (2000) Phase II study of liposomal doxorubicin in platinum- and paclitaxel-refractory epithelial ovarian cancer. J Clin Oncol 18: 3093–100. (Cited on page 44.)

Gorodnova TV, Sokolenko AP, Ivantsov AO, Iyevleva AG, Suspitsin EN, et al. (2015) High response rates to neoadjuvant platinum-

based therapy in ovarian cancer patients carrying germ-line BRCA mutation. Cancer Lett 369: 363–7. (Cited on page 154.)

Grand RJ, Ibrahim AP, Taylor AM, Milner AE, Gregory CD, et al. (1998) Human cells arrest in S phase in response to adenovirus 12 E1A. Virology 244: 330–42. (Cited on page 148.)

Grawunder U, Wilm M, Wu X, Kulesza P, Wilson TE, et al. (1997) Activity of DNA ligase IV stimulated by complex formation with XRCC4 protein in mammalian cells. Nature 388: 492–5. (Cited on page 51.)

Hallden G, Portella G (2012) Oncolytic virotherapy with modified adenoviruses and novel therapeutic targets. Expert Opin Ther Targets 16: 945–58. (Cited on page 247.)

Hamanishi J, Mandai M, Iwasaki M, Okazaki T, Tanaka Y, et al. (2007) Programmed cell death 1 ligand 1 and tumor-infiltrating CD8+ T lymphocytes are prognostic factors of human ovarian cancer. Proc Natl Acad Sci USA 104: 3360–5. (Cited on pages 40 and 45.)

Hande KR (1998) Etoposide: four decades of development of a topoisomerase II inhibitor. Eur J Cancer 34: 1514–21. (Cited on pages 146 and 151.)

Hankinson SE, Hunter DJ, Colditz GA, Willett WC, Stampfer MJ, et al. (1993) Tubal ligation, hysterectomy, and risk of ovarian cancer. A prospective study. JAMA 270: 2813–8. (Cited on page 30.)

Harada JN, Shevchenko A, Shevchenko A, Pallas DC, Berk AJ (2002) Analysis of the adenovirus E1B-55K-anchored proteome reveals its link to ubiquitination machinery. J Virol 76: 9194–206. (Cited on pages 87, 90, and 202.)

Harper JW, Elledge SJ (2007) The DNA damage response: ten years after. Mol Cell 28: 739–45. (Cited on pages 46, 49, and 131.)

Hashimoto Y, Ray Chaudhuri A, Lopes M, Costanzo V (2010) Rad51 protects nascent DNA from Mre11-dependent degradation and promotes continuous DNA synthesis. Nat Struct Mol Biol 17: 1305–11. (Cited on page 206.)

Heise C, Ganly I, Kim YT, Sampson-Johannes A, Brown R, et al. (2000) Efficacy of a replication-selective adenovirus against ovarian carcinomatosis is dependent on tumor burden, viral replication and p53 status. Gene Ther 7: 1925–9. (Cited on pages 78 and 97.)

Helland A, Anglesio MS, George J, Cowin PA, Johnstone CN, et al. (2011) Deregulation of MYCN, LIN28B and LET7 in a molecular subtype of aggressive high-grade serous ovarian cancers. PloS one 6: e18064. (Cited on page 35.)

Helleday T, Petermann E, Lundin C, Hodgson B, Sharma RA (2008) DNA repair pathways as targets for cancer therapy. Nature Reviews Cancer 8: 193–204. (Cited on page 208.)

Hendrickx R, Stichling N, Koelen J, Kuryk L, Lipiec A, et al. (2014) Innate immunity to adenovirus. Hum Gene Ther 25: 265–84. (Cited on page 82.)

Heo J, Reid T, Ruo L, Breitbach CJ, Rose S, et al. (2013) Randomized dose-finding clinical trial of oncolytic immunotherapeutic vaccinia JX-594 in liver cancer. Nat Med 19: 329–36. (Cited on page 239.)

Hernández L, Terradas M, Martín M, Tusell L, Genescà A (2013) Highly sensitive automated method for DNA damage assessment: gamma-H2AX foci counting and cell cycle sorting. Int J Mol Sci 14: 15810–26. (Cited on page 151.)

Hickson I, Zhao Y, Richardson CJ, Green SJ, Martin NM, et al. (2004) Identification and characterization of a novel and specific inhibitor of the ataxia-telangiectasia mutated kinase ATM. Cancer Res 64: 9152–9. (Cited on page 67.)

Hinkula M, Pukkala E, Kyyronen P, Kauppila A (2006) Incidence of ovarian cancer of grand multiparous women–a population-based study in Finland. Gynecol Oncol 103: 207–11. (Cited on page 30.)

Hoeijmakers JH (2001) Genome maintenance mechanisms for preventing cancer. Nature 411: 366–74. (Cited on page 151.)

Hoeijmakers JH (2009) DNA damage, aging, and cancer. N Engl J Med 361: 1475–85. (Cited on page 46.)

Holmes K, Williams CM, Chapman EA, Cross MJ (2010) Detection of siRNA induced mRNA silencing by RT-qPCR: considerations for experimental design. BMC research notes 3: 53. (Cited on page 232.)

Holstege H, Joosse SA, van Oostrom CT, Nederlof PM, de Vries A, et al. (2009) High incidence of protein-truncating TP53 mutations in BRCA1-related breast cancer. Cancer Res 69: 3625–33. (Cited on page 36.)

Holthausen JT, Wyman C, Kanaar R (2010) Regulation of DNA strand exchange in homologous recombination. DNA Repair (Amst) 9: 1264–72. (Cited on page 155.)

Hou JY, Kelly MG, Yu H, McAlpine JN, Azodi M, et al. (2007) Neoadjuvant chemotherapy lessens surgical morbidity in advanced ovarian cancer and leads to improved survival in stage IV disease. Gynecol Oncol 105: 211–7. (Cited on page 41.)

Howe JA, Bayley ST (1992) Effects of Ad5 E1A mutant viruses on the cell cycle in relation to the binding of cellular proteins including the retinoblastoma protein and cyclin A. Virology 186: 15–24. (Cited on page 148.)

Huang J, Schneider RJ (1991) Adenovirus inhibition of cellular protein synthesis involves inactivation of cap-binding protein. Cell 65: 271–280. (Cited on page 179.)

Huarte E, Cubillos-Ruiz JR, Nesbeth YC, Scarlett UK, Martinez DG, et al. (2008) Depletion of dendritic cells delays ovarian cancer progression by boosting antitumor immunity. Cancer Res 68: 7684–91. (Cited on page 40.)

Inaba T, Ino K, Kajiyama H, Yamamoto E, Shibata K, et al. (2009) Role of the immunosuppressive enzyme indoleamine 2,3-dioxygenase in the progression of ovarian carcinoma. Gynecol Oncol 115: 185–92. (Cited on page 40.)

Ingemarsdotter CK, Tookman LA, Browne A, Pirlo K, Cutts R, et al. (2015) Paclitaxel resistance increases oncolytic adenovirus efficacy via upregulated CAR expression and dysfunctional cell cycle control. Mol Oncol 9: 791–805. (Cited on pages 148, 149, and 170.)

Ip SC, Rass U, Blanco MG, Flynn HR, Skehel JM, et al. (2008) Identification of Holliday junction resolvases from humans and yeast. Nature 456: 357–61. (Cited on page 54.)

Jackson SP, Bartek J (2009) The DNA-damage response in human biology and disease. Nature 461: 1071–8. (Cited on page 46.)

Jayson GC, Kohn EC, Kitchener HC, Ledermann JA (2014) Ovarian cancer. Lancet 384: 1376–88. (Cited on pages 32 and 43.)

Jeggo P, Lavin MF (2009) Cellular radiosensitivity: how much better do we understand it? Int J Radiat Biol 85: 1061–81. (Cited on page 51.)

Jelovac D, Armstrong DK (2011) Recent progress in the diagnosis and treatment of ovarian cancer. CA Cancer J Clin 61: 183–203. (Cited on pages 28 and 29.)

Jemal A, Bray F, Center MM, Ferlay J, Ward E, et al. (2011) Global cancer statistics. CA Cancer J Clin 61: 69–90. (Cited on page 28.)

Jemal A, Siegel R, Xu J, Ward E (2010) Cancer statistics, 2010. CA Cancer J Clin 60: 277–300. (Cited on page 28.)

Jensen RB, Carreira A, Kowalczykowski SC (2010) Purified human BRCA2 stimulates RAD51-mediated recombination. Nature 467: 678–83. (Cited on page 201.)

Jiang H, Conrad C, Fueyo J, Gomez-Manzano C, Liu TJ (2003) Oncolytic adenoviruses for malignant glioma therapy. Front Biosci 8: d577–88. (Cited on page 74.)

Jiang H, Gomez-Manzano C, Lang FF, Alemany R, Fueyo J (2009) Oncolytic adenovirus: preclinical and clinical studies in patients with human malignant gliomas. Curr Gene Ther 9: 422–7. (Cited on page 74.)

Jiricny J (2006) The multifaceted mismatch-repair system. Nat Rev Mol Cell Biol 7: 335–46. (Cited on page 47.)

Kakarougkas A, Jeggo PA (2014) DNA DSB repair pathway choice: an orchestrated handover mechanism. Br J Radiol 87: 20130685. (Cited on pages 59 and 61.)

Kaneko S, Rozenblatt-Rosen O, Meyerson M, Manley JL (2007) The multifunctional protein p54nrb/PSF recruits the exonuclease XRN2 to facilitate pre-mRNA 3′ processing and transcription termination. Genes and Dev 21: 1779–1789. (Cited on page 234.)

Kanerva A, Mikheeva GV, Krasnykh V, Coolidge CJ, Lam JT, et al. (2002) Targeting adenovirus to the serotype 3 receptor increases gene transfer efficiency to ovarian cancer cells. Clin Cancer Res 8: 275–80. (Cited on page 75.)

Kantoff PW, Schuetz TJ, Blumenstein BA, Glode LM, Bilhartz DL, et al. (2010) Overall survival analysis of a phase II randomized controlled trial of a Poxviral-based PSA-targeted immunotherapy in metastatic castration-resistant prostate cancer. J Clin Oncol 28: 1099–105. (Cited on page 239.)

Karen KA, Hoey PJ, Young CS, Hearing P (2009a) Temporal regulation of the Mre11-Rad50-Nbs1 complex during adenovirus infection. J Virol 83: 4565–73. (Cited on page 89.)

Karen KA, Hoey PJ, Young CSH, Hearing P (2009b) Temporal regulation of the Mre11-Rad50-Nbs1 complex during adenovirus infection. J Virol 83: 4565–73. (Cited on page 90.)

Karpenshif Y, Bernstein KA (2012) From yeast to mammals: recent advances in genetic control of homologous recombination. DNA Repair (Amst) 11: 781–8. (Cited on page 155.)

Katsumata N, Yasuda M, Isonishi S, Takahashi F, Michimae H, et al. (2013) Long-term results of dose-dense paclitaxel and carboplatin versus conventional paclitaxel and carboplatin for treatment of advanced epithelial ovarian, fallopian tube, or primary peritoneal cancer (JGOG 3016): a randomised, controlled, open-label trial. Lancet Oncol 14: 1020–6. (Cited on page 42.)

Kaufman B, Shapira-Frommer R, Schmutzler RK, Audeh MW, Friedlander M, et al. (2015a) Olaparib monotherapy in patients with advanced cancer and a germline BRCA1/2 mutation. J Clin Oncol 33: 244–50. (Cited on page 65.)

Kaufman HL, Kohlhapp FJ, Zloza A (2015b) Oncolytic viruses: a new class of immunotherapy drugs. Nat Rev Drug Discov 14: 642–62. (Cited on pages 86, 243, 248, and 249.)

Kaye SB, Lubinski J, Matulonis U, Ang JE, Gourley C, et al. (2012) Phase II, open-label, randomized, multicenter study comparing the efficacy and safety of olaparib, a poly (ADP-ribose) polymerase inhibitor, and pegylated liposomal doxorubicin in patients with BRCA1 or BRCA2 mutations and recurrent ovarian cancer. J Clin Oncol 30: 372–9. (Cited on page 65.)

Kehoe S, Hook J, Nankivell M, Jayson GC, Kitchener H, et al. (2015) Primary chemotherapy versus primary surgery for newly diagnosed advanced ovarian cancer (CHORUS): an open-label, randomised, controlled, non-inferiority trial. Lancet 386: 249–57. (Cited on page 41.)

Kelemen LE, Kobel M (2011) Mucinous carcinomas of the ovary and colorectum: different organ, same dilemma. Lancet Oncol 12: 1071–80. (Cited on page 32.)

Kelkar SA, Pfister KK, Crystal RG, Leopold PL (2004) Cytoplasmic dynein mediates adenovirus binding to microtubules. J Virol 78: 10122–32. (Cited on page 74.)

Kelly E, Russell SJ (2007) History of oncolytic viruses: genesis to genetic engineering. Mol Ther 15: 651–9. (Cited on page 68.)

Khuri FR, Nemunaitis J, Ganly I, Arseneau J, Tannock IF, et al. (2000) a controlled trial of intratumoral ONYX-015, a selectively-replicating adenovirus, in combination with cisplatin and 5-fluorouracil in patients with recurrent head and neck cancer. Nat Med 6: 879–85. (Cited on page 238.)

Kimball KJ, Preuss MA, Barnes MN, Wang M, Siegal GP, et al. (2010) A phase I study of a tropism-modified conditionally replicative adenovirus for recurrent malignant gynecologic diseases. Clin Cancer Res 16: 5277–87. (Cited on pages 75 and 249.)

King MC, Marks JH, Mandell JB, New York Breast Cancer Study G (2003) Breast and ovarian cancer risks due to inherited mutations in BRCA1 and BRCA2. Science 302: 643–6. (Cited on page 29.)

Kirn D (2001) Oncolytic virotherapy for cancer with the adenovirus dl1520 (Onyx-015): results of phase I and II trials. Expert Opin Biol Ther 1: 525–38. (Cited on page 82.)

Kitchingman GR (1995) Mutations in the adenovirus-encoded single-stranded DNA binding protein that result in altered accumulation of early and late viral RNAs. Virology 212: 91–101. (Cited on page 206.)

Kiyohara C, Yoshimasu K (2007) Genetic polymorphisms in the nucleotide excision repair pathway and lung cancer risk: a meta-analysis. Int J Med Sci 4: 59–71. (Cited on page 246.)

Knutson KL, Karyampudi L, Lamichhane P, Preston C (2015) Targeted immune therapy of ovarian cancer. Cancer Metastasis Rev 34: 53–74. (Cited on pages 30, 38, 39, and 40.)

Ko SY, Naora H (2014) HOXA9 promotes homotypic and heterotypic cell interactions that facilitate ovarian cancer dissemination via its induction of P-cadherin. Mol Cancer 13: 170. (Cited on page 40.)

Konner JA, Bell-McGuinn KM, Sabbatini P, Hensley ML, Tew WP, et al. (2010) Farletuzumab, a humanized monoclonal antibody against folate receptor alpha, in epithelial ovarian cancer: a phase I study. Clin Cancer Res 16: 5288–95. (Cited on page 44.)

Konstantinopoulos PA, Spentzos D, Karlan BY, Taniguchi T, Fountzilas E, et al. (2010) Gene expression profile of BRCAness that correlates with responsiveness to chemotherapy and with outcome in patients with epithelial ovarian cancer. J Clin Oncol 28: 3555–61. (Cited on pages 66 and 242.)

Korkmaz T, Seber S, Basaran G (2016) Review of the current role of targeted therapies as maintenance therapies in first and second line treatment of epithelial ovarian cancer; In the light of completed trials. Crit Rev Oncol Hematol 98: 180–8. (Cited on page 237.)

Krejci L, Altmannova V, Spirek M, Zhao X (2012) Homologous recombination and its regulation. Nucleic Acids Res 40: 5795–818. (Cited on pages 47, 53, 54, 55, 56, 57, 61, and 62.)

Krietsch J, Caron MC, Gagne JP, Ethier C, Vignard J, et al. (2012) PARP activation regulates the RNA-binding protein NONO in the DNA damage response to DNA double-strand breaks. Nucleic Acids Res 40: 10287–10301. (Cited on pages 220 and 234.)

Kroeger DR, Milne K, Nelson BH (2016) Tumor-Infiltrating Plasma Cells Are Associated with Tertiary Lymphoid Structures, Cytolytic T-Cell Responses, and Superior Prognosis in Ovarian Cancer. Clin Cancer Res . (Cited on page 39.)

Kruijer W, Nicolas JC, van Schaik FM, Sussenbach JS (1983) Structure and function of DNA binding proteins from revertants of adenovirus type 5 mutants with a temperature-sensitive DNA replication. Virology 124: 425–33. (Cited on page 80.)

Kubota H, Hynes G, Carne A, Ashworth A, Willison K (1994) Identification of six Tcp-1-related genes encoding divergent subunits of the TCP-1-containing chaperonin. Current Biol 4: 89–99. (Cited on page 221.)

Kudoh A, Iwahori S, Sato Y, Nakayama S, Isomura H, et al. (2009) Homologous recombinational repair factors are recruited and loaded onto the viral DNA genome in Epstein-Barr virus replication compartments. J Virol 83: 6641–51. (Cited on page 204.)

Kulbe H, Chakravarty P, Leinster DA, Charles KA, Kwong J, et al. (2012) A dynamic inflammatory cytokine network in the human ovarian cancer microenvironment. Cancer Res 72: 66–75. (Cited on page 40.)

Kuo KT, Guan B, Feng Y, Mao TL, Chen X, et al. (2009) Analysis of DNA copy number alterations in ovarian serous tumors identifies new molecular genetic changes in low-grade and high-grade carcinomas. Cancer Res 69: 4036–42. (Cited on pages 32 and 33.)

Kurman RJ, McConnell TG (2010) Precursors of endometrial and ovarian carcinoma. Virchows Archiv 456: 1–12. (Cited on page 30.)

Lai MC, Kuo HW, Chang WC, Tarn WY (2003) A novel splicing regulator shares a nuclear import pathway with SR proteins. EMBO J 22: 1359–1369. (Cited on page 221.)

Lamfers MLM, Grill J, Dirven CMF, Van Beusechem VW, Geoerger B, et al. (2002) Potential of the conditionally replicative adenovirus Ad5-Delta24RGD in the treatment of malignant gliomas and its enhanced effect with radiotherapy. Cancer Res 62: 5736–42. (Cited on page 240.)

Larson C, Oronsky B, Scicinski J, Fanger GR, Stirn M, et al. (2015) Going viral: a review of replication-selective oncolytic adenoviruses. Oncotarget 6: 19976–89. (Cited on pages 68, 82, 238, 245, and 249.)

Lawrie TA, Winter-Roach BA, Heus P, Kitchener HC (2015) Adjuvant (post-surgery) chemotherapy for early stage epithelial ovarian cancer. Cochrane Database Syst Rev 12: CD004706. (Cited on page 42.)

Ledermann J, Harter P, Gourley C, Friedlander M, Vergote I, et al. (2012) Olaparib maintenance therapy in platinum-sensitive relapsed ovarian cancer. N Engl J Med 366: 1382–92. (Cited on page 65.)

Lee J, Ledermann J, Kohn E (2013) PARP Inhibitors for BRCA1/2 mutation-associated and BRCA-like malignancies. Ann Oncol 25: 32–40. (Cited on page 172.)

Lee KR, Young RH (2003) The distinction between primary and metastatic mucinous carcinomas of the ovary: gross and histologic findings in 50 cases. Am J Surg Pathol 27: 281–92. (Cited on page 32.)

Lee N, Yario TA, Gao JS, Steitz JA (2016) EBV noncoding RNA EBER2 interacts with host RNA-binding proteins to regulate viral gene

expression. Proc Natl Acad Sci USA 113: 3221–3226. (Cited on page 235.)

Lee Y, Miron A, Drapkin R, Nucci MR, Medeiros F, et al. (2007) A candidate precursor to serous carcinoma that originates in the distal fallopian tube. J Pathol 211: 26–35. (Cited on pages 33 and 34.)

Lengyel E (2010) Ovarian cancer development and metastasis. Am J Pathol 177: 1053–64. (Cited on page 37.)

Leopold PL, Kreitzer G, Miyazawa N, Rempel S, Pfister KK, et al. (2000) Dynein- and microtubule-mediated translocation of adenovirus serotype 5 occurs after endosomal lysis. Hum Gene Ther 11: 151–65. (Cited on page 74.)

Levanon K, Crum C, Drapkin R (2008) New insights into the pathogenesis of serous ovarian cancer and its clinical impact. J Clin Oncol 26: 5284–93. (Cited on page 33.)

Li E, Stupack D, Bokoch GM, Nemerow GR (1998) Adenovirus endocytosis requires actin cytoskeleton reorganization mediated by Rho family GTPases. J Virol 72: 8806–12. (Cited on page 74.)

Li K, Mandai M, Hamanishi J, Matsumura N, Suzuki A, et al. (2009a) Clinical significance of the NKG2D ligands, MICA/B and ULBP2 in ovarian cancer: high expression of ULBP2 is an indicator of poor prognosis. Cancer Immunol Immunother 58: 641–52. (Cited on page 39.)

Li S, Kuhne WW, Kulharya A, Hudson FZ, Ha K, et al. (2009b) Involvement of p54 (nrb), a PSF partner protein, in DNA double-strand break repair and radioresistance. Nucleic Acids Res 37: 6746–6753. (Cited on page 234.)

Li X, Heyer WD (2008) Homologous recombination in DNA repair and DNA damage tolerance. Cell Res 18: 99–113. (Cited on page 54.)

Li X, Ye DF, Xie X, Chen HZ, Lu WG (2005) Proportion of CD4+CD25+ regulatory T cell is increased in the patients with ovarian carcinoma. Cancer Invest 23: 399–403. (Cited on page 40.)

Lichtenstein DL, Toth K, Doronin K, Tollefson AE, Wold WS (2004) Functions and mechanisms of action of the adenovirus E3 proteins. Int Rev Immunol 23: 75–111. (Cited on page 83.)

Lieber MR (2010) The mechanism of double-strand DNA break repair by the nonhomologous DNA end-joining pathway. Annu Rev Biochem 79: 181–211. (Cited on pages 172 and 201.)

Lieberman HB (2006) Rad9, an evolutionarily conserved gene with multiple functions for preserving genomic integrity. J Cell Biochem 97: 690–697. (Cited on page 222.)

Lilley CE, Carson CT, Muotri AR, Gage FH, Weitzman MD (2005) DNA repair proteins affect the lifecycle of herpes simplex virus 1. Proc Natl Acad Sci USA 102: 5844–9. (Cited on page 204.)

Lin JC, Hsu M, Tarn WY (2007) Cell stress modulates the function of splicing regulatory protein RBM4 in translation control. Proc Natl Acad Sci USA 104: 2235–2240. (Cited on page 221.)

Lin JC, Tarn WY (2009) RNA-binding motif protein 4 translocates to cytoplasmic granules and suppresses translation via argonaute2 during muscle cell differentiation. J Biol Chem 284: 34658–34665 (Cited on page 221.)

Liu TC, Galanis E, Kirn D (2007) Clinical trial results with oncolytic virotherapy: a century of promise, a decade of progress. Nat Clin Pract Oncol 4: 101–17. (Cited on page 248.)

Liu X, Erikson RL (2003) Polo-like kinase (Plk) 1 depletion induces apoptosis in cancer cells. Proc Natl Acad Sci USA 100: 5789–5794. (Cited on pages 109 and 213.)

Löbrich M, Shibata A, Beucher A, Fisher A, Ensminger M, et al. (2010) gammaH2AX foci analysis for monitoring DNA double-strand break repair: strengths, limitations and optimization. Cell Cycle 9: 662–9. (Cited on page 150.)

Lockley M, Fernandez M, Wang Y, Li NF, Conroy S, et al. (2006) Activity of the adenoviral E1A deletion mutant dl922-947 in ovarian cancer: comparison with E1A wild-type viruses, bioluminescence monitoring, and intraperitoneal delivery in icodextrin. Cancer Res 66: 989–98. (Cited on pages 78, 85, 120, and 121.)

Lopez-Serra L, Ballestar E, Fraga MF, Alaminos M, Setien F, et al. (2006) A profile of methyl-CpG binding domain protein occupancy of hypermethylated promoter CpG islands of tumor suppressor genes in human cancer. Cancer Res 66: 8342–8346. (Cited on page 222.)

Lord CJ, Ashworth A (2012) The DNA damage response and cancer therapy. Nature 481: 287–94. (Cited on page 47.)

Lord CJ, McDonald S, Swift S, Turner NC, Ashworth A (2008) A high-throughput RNA interference screen for DNA repair determinants of PARP inhibitor sensitivity. DNA Repair 7: 2010–2019. (Cited on page 209.)

Lorusso PM, Edelman MJ, Bever SL, Forman KM, Pilat M, et al. (2012) Phase I study of folate conjugate EC145 (Vintafolide) in patients with refractory solid tumors. J Clin Oncol 30: 4011–6. (Cited on page 44.)

Lowe KA, Chia VM, Taylor A, O'Malley C, Kelsh M, et al. (2013) An international assessment of ovarian cancer incidence and mortality. Gynecol Oncol 130: 107–14. (Cited on pages 28 and 29.)

Lowe SW, Ruley HE (1993) Stabilization of the p53 tumor suppressor is induced by adenovirus 5 E1A and accompanies apoptosis. Genes Dev 7: 535–45. (Cited on page 80.)

Lu W, Zheng S, Li XF, Huang JJ, Zheng X, et al. (2004) Intra-tumor injection of H101, a recombinant adenovirus, in combination with chemotherapy in patients with advanced cancers: a pilot phase II clinical trial. World J Gastroenterol 10: 3634–8. (Cited on page 82.)

Lu Y, Kucharski TJ, Gamache I, Blanchette P, Branton PE, et al. (2014) Interaction of adenovirus type 5 E4orf4 with the nuclear pore subunit Nup205 is required for proper viral gene expression. J Virol 88: 13249–13259. (Cited on page 223.)

Machida YJ, Dutta A (2005) Cellular checkpoint mechanisms monitoring proper initiation of DNA replication. J Biol Chem 280: 6253–6. (Cited on page 149.)

Maine CJ, Aziz NH, Chatterjee J, Hayford C, Brewig N, et al. (2014) Programmed death ligand-1 over-expression correlates with malignancy and contributes to immune regulation in ovarian cancer. Cancer Immunol Immunother 63: 215–24. (Cited on page 45.)

Makharashvili N, Tubbs AT, Yang SH, Wang H, Barton O, et al. (2014) Catalytic and noncatalytic roles of the CtIP endonuclease in double-strand break end resection. Mol Cell 54: 1022–33. (Cited on page 205.)

Malo N, Hanley JA, Carlile G, Liu J, Pelletier J, et al. (2010) Experimental design and statistical methods for improved hit detection in high-throughput screening. J Biomol Screen 15: 990–1000. (Cited on page 233.)

Malpica A, Deavers MT, Lu K, Bodurka DC, Atkinson EN, et al. (2004) Grading ovarian serous carcinoma using a two-tier system. Am J Surg Pathol 28: 496–504. (Cited on page 31.)

Manie E, Vincent-Salomon A, Lehmann-Che J, Pierron G, Turpin E, et al. (2009) High frequency of TP53 mutation in BRCA1 and sporadic basal-like carcinomas but not in BRCA1 luminal breast tumors. Cancer Res 69: 663–71. (Cited on page 36.)

Mantia-Smaldone GM, Edwards RP, Vlad AM (2011) Targeted treatment of recurrent platinum-resistant ovarian cancer: current and emerging therapies. Cancer Manag Res 3: 25–38. (Cited on page 44.)

Maréchal A, Zou L (2015) RPA-coated single-stranded DNA as a platform for post-translational modifications in the DNA damage response. Cell Res 25: 9–23. (Cited on page 222.)

Markman M, Webster K, Zanotti K, Kulp B, Peterson G, et al. (2003) Phase 2 trial of single-agent gemcitabine in platinum-paclitaxel refractory ovarian cancer. Gynecol Oncol 90: 593–6. (Cited on page 44.)

Martin SA, Hewish M, Lord CJ, Ashworth A (2010) Genomic instability and the selection of treatments for cancer. J Pathol 220: 281–9. (Cited on page 37.)

Mastrangelo MJ, Lattime EC (2002) Virotherapy clinical trials for regional disease: in situ immune modulation using recombinant poxvirus vectors. Cancer Gene Ther 9: 1013–21. (Cited on page 243.)

Matthews DA, Russell WC (1998) Adenovirus core protein V is delivered by the invading virus to the nucleus of the infected cell and later in infection is associated with nucleoli. J Gen Virol 79 (Pt 7): 1671–5. (Cited on page 74.)

McCabe N, Turner NC, Lord CJ, Kluzek K, Bialkowska A, et al. (2006) Deficiency in the repair of DNA damage by homologous recombination and sensitivity to poly(ADP-ribose) polymerase inhibition. Cancer Res 66: 8109–15. (Cited on page 64.)

McConnell MJ, Imperiale MJ (2004) Biology of adenovirus and its use as a vector for gene therapy. Hum Gene Ther 15: 1022–33. (Cited on page 72.)

McNeish IA, Oza AM, Coleman RL, Scott CL, Konecny GE, et al. (2015) Results of ARIEL2: Phase 2 trial to prospectively identify ovarian cancer patients likely to response to rucaparib using tumour genetic analysis. J Clin Oncol 33: S5508. (Cited on page 66.)

McNeish IA, Tenev T, Bell S, Marani M, Vassaux G, et al. (2001) Herpes simplex virus thymidine kinase/ganciclovir-induced cell death is enhanced by co-expression of caspase-3 in ovarian carcinoma cells. Cancer Gene Ther 8: 308–19. (Cited on page 97.)

McSharry BP, Burgert HG, Owen DP, Stanton RJ, Prod'homme V, et al. (2008) Adenovirus E3/19K promotes evasion of NK cell recognition by intracellular sequestration of the NKG2D ligands major histocompatibility complex class I chain-related proteins A and B. J Virol 82: 4585–94. (Cited on page 83.)

Mehta A, Haber JE (2014) Sources of DNA double-strand breaks and models of recombinational DNA repair. Cold Spring Harb Perspect Biol 6: a016428. (Cited on page 52.)

Melcher A, Parato K, Rooney CM, Bell JC (2011) Thunder and lightning: immunotherapy and oncolytic viruses collide. Mol Ther 19: 1008–16. (Cited on page 243.)

Menzel T, Nahse-Kumpf V, Kousholt AN, Klein DK, Lund-Andersen C, et al. (2011) A genetic screen identifies BRCA2 and PALB2 as key regulators of G2 checkpoint maintenance. EMBO Rep 12: 705–12. (Cited on page 57.)

Meyer T, Rustin GJ (2000) Role of tumour markers in monitoring epithelial ovarian cancer. Br J Cancer 82: 1535–8. (Cited on page 43.)

Milne K, Köbel M, Kalloger SE, Barnes RO, Gao D, et al. (2009) Systematic analysis of immune infiltrates in high-grade serous ovarian cancer reveals CD20, FoxP3 and TIA-1 as positive prognostic factors. PLoS One 4: e6412. (Cited on page 39.)

Mocellin S, Provenzano M (2004) RNA interference: learning gene knock-down from cell physiology. J Transl Med 2: 39. (Cited on page 232.)

Mohr SE, Perrimon N (2012) RNAi screening: new approaches, understandings, and organisms. Wiley Interdiscip Rev RNA 3: 145–158. (Cited on page 231.)

Monferran S, Paupert J, Dauvillier S, Salles B, Muller C (2004) The membrane form of the DNA repair protein Ku interacts at the cell surface with metalloproteinase 9. EMBO J 23: 3758–3768. (Cited on page 221.)

Morch LS, Lokkegaard E, Andreasen AH, Kruger-Kjaer S, Lidegaard O (2009) Hormone therapy and ovarian cancer. JAMA 302: 298–305. (Cited on page 30.)

Moynahan ME, Jasin M (2010) Mitotic homologous recombination maintains genomic stability and suppresses tumorigenesis. Nat Rev Mol Cell Biol 11: 196–207. (Cited on page 201.)

Mozlin AM, Fung CW, Symington LS (2008) Role of the Saccharomyces cerevisiae Rad51 paralogs in sister chromatid recombination. Genetics 178: 113–26. (Cited on page 206.)

Mukhopadhyay A, Elattar A, Cerbinskaite A, Wilkinson SJ, Drew Y, et al. (2010) Development of a functional assay for homologous recombination status in primary cultures of epithelial ovarian tumor and correlation with sensitivity to poly(ADP-ribose) polymerase inhibitors. Clin Cancer Res 16: 2344–51. (Cited on pages 67, 155, 210, and 241.)

Mukhopadhyay A, Plummer ER, Elattar A, Soohoo S, Uzir B, et al. (2012) Clinicopathological features of homologous recombination-deficient epithelial ovarian cancers: sensitivity to PARP inhibitors, platinum, and survival. Cancer Res 72: 5675–82. (Cited on pages 154 and 200.)

Mund A, Schubert T, Staege H, Kinkley S, Reumann K, et al. (2012) SPOC1 modulates DNA repair by regulating key determinants of chromatin compaction and DNA damage response. Nucleic Acids Res 40: 11363–79. (Cited on page 91.)

Munksgaard PS, Blaakaer J (2012) The association between endometriosis and ovarian cancer: a review of histological, genetic and molecular alterations. Gynecol Oncol 124: 164–9. (Cited on page 30.)

Murai J, Huang SY, Das BB, Renaud A, Zhang Y, et al. (2012) Trapping of PARP1 and PARP2 by Clinical PARP Inhibitors. Cancer Res 72: 5588–99. (Cited on page 64.)

Nagase H, Woessner JF (1999) Matrix metalloproteinases. J Biol Chem 274: 21491–21494. (Cited on page 221.)

Naipal KAT, Verkaik NS, Ameziane N, van Deurzen CHM, Ter Brugge P, et al. (2014) Functional ex vivo assay to select homologous recombination-deficient breast tumors for PARP inhibitor treatment. Clin Cancer Res 20: 4816–26. (Cited on pages 67 and 241.)

Natrajan R, Lambros MB, Rodriguez-Pinilla SM, Moreno-Bueno G, Tan DS, et al. (2009) Tiling path genomic profiling of grade 3 invasive ductal breast cancers. Clin Cancer Res 15: 2711–22. (Cited on page 36.)

Nemajerova A, Talos F, Moll UM, Petrenko O (2008) Rb function is required for E1A-induced S-phase checkpoint activation. Cell Death Differ 15: 1440–9. (Cited on page 149.)

Nevins JR (1992) E2F: a link between the Rb tumor suppressor protein and viral oncoproteins. Science 258: 424–9. (Cited on page 149.)

Ng HH, Jeppesen P, Bird A (2000) Active repression of methylated genes by the chromosomal protein MBD1. Mol Cell Biol 20: 1394–1406. (Cited on page 222.)

Nichols GJ, Schaack J, Ornelles DA (2009) Widespread phosphorylation of histone H2AX by species C adenovirus infection requires viral DNA replication. J Virol 83: 5987–98. (Cited on pages 131, 135, 150, and 151.)

Nomura H, Sawada Y, Ohtaki S (1998) Interaction of p27 with E1A and its effect on CDK kinase activity. Biochem Biophys Res Commun 248: 228–34. (Cited on page 77.)

Nutley B, Smith N, Hayes A, Kelland L, Brunton L, et al. (2005) Preclinical pharmacokinetics and metabolism of a novel prototype DNA-PK inhibitor NU7026. Br J Cancer 93: 1011–1018. (Cited on page 177.)

O'Connor MJ (2015) Targeting the DNA damage response in cancer. Mol Cell 60: 547–560 (Cited on pages 47 and 208.)

Orazio NI, Naeger CM, Karlseder J, Weitzman MD (2011) The adenovirus E1b55K/E4orf6 complex induces degradation of the Bloom helicase during infection. J Virol 85: 1887–92. (Cited on page 90.)

O'Shea CC, Johnson L, Bagus B, Choi S, Nicholas C, et al. (2004) Late viral RNA export, rather than p53 inactivation, determines ONYX-015 tumor selectivity. Cancer Cell 6: 611–23. (Cited on pages 81 and 82.)

Oza AM, Cibula D, Benzaquen AO, Poole C, Mathijssen RH, et al. (2015) Olaparib combined with chemotherapy for recurrent platinum-sensitive ovarian cancer: a randomised phase 2 trial. Lancet Oncol 16: 87–97. (Cited on page 66.)

Ozols RF, Bundy BN, Greer BE, Fowler JM, Clarke-Pearson D, et al. (2003) Phase III trial of carboplatin and paclitaxel compared with cisplatin and paclitaxel in patients with optimally resected stage III ovarian cancer: a Gynecologic Oncology Group study. J Clin Oncol 21: 3194–200. (Cited on page 42.)

Panier S, Boulton SJ (2014) Double-strand break repair: 53BP1 comes into focus. Nat Rev Mol Cell Biol 15: 7–18. (Cited on pages 49, 61, and 202.)

Park BH, Hwang T, Liu TC, Sze DY, Kim JS, et al. (2008) Use of a targeted oncolytic poxvirus, JX-594, in patients with refractory primary or metastatic liver cancer: a phase I trial. Lancet Oncol 9: 533–42. (Cited on page 239.)

Park EJ, Chan DW, Park JH, Oettinger MA, Kwon J (2003) DNA-PK is activated by nucleosomes and phosphorylates H2AX within the nucleosomes in an acetylation-dependent manner. Nucleic Acids Res 31: 6819–27. (Cited on page 150.)

Parmar MK, Ledermann JA, Colombo N, du Bois A, Delaloye JF, et al. (2003) Paclitaxel plus platinum-based chemotherapy versus conventional platinum-based chemotherapy in women with relapsed ovarian cancer: the ICON4/AGO-OVAR-2.2 trial. Lancet 361: 2099–106. (Cited on page 43.)

Passaro C, Abagnale A, Libertini S, Volpe M, Botta G, et al. (2013) Ionizing radiation enhances dl922-947-mediated cell death of anaplastic thyroid carcinoma cells. Endocr Relat Cancer 20: 633–47. (Cited on page 240.)

Passon DM, Lee M, Rackham O, Stanley WA, Sadowska A, et al. (2012) Structure of the heterodimer of human NONO and paraspeckle protein component 1 and analysis of its role in subnuclear body formation. Proc Natl Acad Sci USA 109: 4846–4850. (Cited on page 234.)

Patankar MS, Jing Y, Morrison JC, Belisle JA, Lattanzio FA, et al. (2005) Potent suppression of natural killer cell response mediated by the ovarian tumor marker CA125. Gynecol Oncol 99: 704–13. (Cited on page 40.)

Patch AM, Christie EL, Etemadmoghadam D, Garsed DW, George J, et al. (2015) Whole-genome characterization of chemoresistant ovarian cancer. Nature 521: 489–94. (Cited on pages 34, 35, and 36.)

Patel AG, Sarkaria JN, Kaufmann SH (2011) Nonhomologous end joining drives poly(ADP-ribose) polymerase (PARP) inhibitor lethality in homologous recombination-deficient cells. Proc Natl Acad Sci USA 108: 3406–11. (Cited on page 65.)

Patel KJ, Yu VP, Lee H, Corcoran A, Thistlethwaite FC, et al. (1998) Involvement of Brca2 in DNA repair. Mol Cell 1: 347–57. (Cited on page 36.)

Paull TT, Rogakou EP, Yamazaki V, Kirchgessner CU, Gellert M, et al. (2000) A critical role for histone H2AX in recruitment of repair factors to nuclear foci after DNA damage. Curr Biol 10: 886–95. (Cited on pages 131 and 150.)

Pellegrini L, Yu DS, Lo T, Anand S, Lee M, et al. (2002) Insights into DNA recombination from the structure of a RAD51-BRCA2 complex. Nature 420: 287–93. (Cited on page 56.)

Pennington KP, Swisher EM (2012) Hereditary ovarian cancer: beyond the usual suspects. Gynecol Oncol 124: 347–53. (Cited on page 29.)

Pennington KP, Walsh T, Harrell MI, Lee MK, Pennil CC, et al. (2014) Germline and somatic mutations in homologous recombination genes predict platinum response and survival in ovarian, fallopian tube, and peritoneal carcinomas. Clin Cancer Res 20: 764–75. (Cited on page 242.)

Perren TJ, Swart AM, Pfisterer J, Ledermann JA, Pujade-Lauraine E, et al. (2011) A phase 3 trial of bevacizumab in ovarian cancer. N Engl J Med 365: 2484–96. (Cited on page 42.)

Perrimon N, Mathey-Prevot B (2007) Applications of high-throughput RNA interference screens to problems in cell and developmental biology. Genetics 175: 7–16. (Cited on page 232.)

Petermann E, Orta ML, Issaeva N, Schultz N, Helleday T (2010) Hydroxyurea-stalled replication forks become progressively inactivated and require two different RAD51-mediated pathways for restart and repair. Mol Cell 37: 492–502. (Cited on pages 146, 151, and 201.)

Pfisterer J, Plante M, Vergote I, du Bois A, Hirte H, et al. (2006) Gemcitabine plus carboplatin compared with carboplatin in patients with platinum-sensitive recurrent ovarian cancer: an intergroup trial of the AGO-OVAR, the NCIC CTG, and the EORTC GCG. J Clin Oncol 24: 4699–707. (Cited on page 44.)

Pierce AJ, Johnson RD, Thompson LH, Jasin M (1999) XRCC3 promotes homology-directed repair of DNA damage in mammalian cells. Genes and Dev 13: 2633–2638. (Cited on pages 113 and 114.)

Pignata S, Ferrandina G, Scarfone G, Scollo P, Odicino F, et al. (2008) Activity of chemotherapy in mucinous ovarian cancer with a recurrence free interval of more than 6 months: results from the SOCRATES retrospective study. BMC Cancer 8: 252. (Cited on page 32.)

Piver MS, Jishi MF, Tsukada Y, Nava G (1993) Primary peritoneal carcinoma after prophylactic oophorectomy in women with a family history of ovarian cancer. A report of the Gilda Radner Familial Ovarian Cancer Registry. Cancer 71: 2751–5. (Cited on page 29.)

Plante M, Rubin SC, Wong GY, Federici MG, Finstad CL, et al. (1994) Interleukin-6 level in serum and ascites as a prognostic factor in patients with epithelial ovarian cancer. Cancer 73: 1882–8. (Cited on page 40.)

Podhorecka M, Skladanowski A, Bozko P (2010) H2AX phosphorylation: its role in DNA damage response and cancer therapy. J Nucleic Acids 2010. (Cited on pages 140 and 151.)

Preston CC, Maurer MJ, Oberg AL, Visscher DW, Kalli KR, et al. (2013) The ratios of CD8+ T cells to CD4+CD25+ FOXP3+ and FOXP3- T cells correlate with poor clinical outcome in human serous ovarian cancer. PLoS One 8: e80063. (Cited on page 40.)

Pujade-Lauraine E, Wagner U, Aavall-Lundqvist E, Gebski V, Heywood M, et al. (2010) Pegylated liposomal Doxorubicin and Carboplatin compared with Paclitaxel and Carboplatin for patients with platinum-sensitive ovarian cancer in late relapse. J Clin Oncol 28: 3323–9. (Cited on page 44.)

Pujade-Lauraine E WB Hilpert F (2012) AURELIA: a randomized phase III trial evaluating bevacizumab (BEV) plus chemotherapy (CT) for platinum (PT)-resistant recurrent ovarian cancer (OC). J Clin Oncol ASCO. (Cited on page 44.)

Puzanov I, Milhem M, Andtbacka R, Minor D, Hamid O, et al. (2014) Primary analysis of a phase 1b multicenter trial to evaluate safety and efficacy of talimogene laherparepvec (T-VEC) and ipilimumab (ipi) in previously untreated, unresected stage IIIB-IV melanoma. J Clin Oncol 32 abstr 9029. (Cited on page 247.)

Querido E, Blanchette P, Yan Q, Kamura T, Morrison M, et al. (2001) Degradation of p53 by adenovirus E4orf6 and E1B55K proteins occurs via a novel mechanism involving a Cullin-containing complex. Genes Dev 15: 3104–17. (Cited on pages 80 and 202.)

Raderschall E, Stout K, Freier S, Suckow V, Schweiger S, et al. (2002) Elevated levels of Rad51 recombination protein in tumor cells. Cancer Res 62: 219–25. (Cited on page 61.)

Radhakrishnan SK, Jette N, Lees-Miller SP (2014) Non-homologous end joining: emerging themes and unanswered questions. DNA Repair (Amst) 17: 2–8. (Cited on page 51.)

Rajagopalan S, Andreeva A, Rutherford TJ, Fersht AR (2010) Mapping the physical and functional interactions between the tumor suppressors p53 and BRCA2. Proc Natl Acad Sci USA 107: 8587–92. (Cited on page 57.)

Rao L, Debbas M, Sabbatini P, Hockenbery D, Korsmeyer S, et al. (1992) The adenovirus E1A proteins induce apoptosis, which is inhibited by the E1B 19-kDa and Bcl-2 proteins. Proc Natl Acad Sci USA 89: 7742–6. (Cited on page 80.)

Raper SE, Chirmule N, Lee FS, Wivel NA, Bagg A, et al. (2003) Fatal systemic inflammatory response syndrome in a ornithine transcarbamylase deficient patient following adenoviral gene transfer. Mol Genet Metab 80: 148–58. (Cited on page 84.)

Reaper PM, Griffiths MR, Long JM, Charrier JD, Maccormick S, et al. (2011) Selective killing of ATM- or p53-deficient cancer cells through inhibition of ATR. Nat Chem Biol 7: 428–30. (Cited on page 67.)

Rebbeck TR, Lynch HT, Neuhausen SL, Narod SA, Van't Veer L, et al. (2002) Prophylactic oophorectomy in carriers of BRCA1 or BRCA2 mutations. N Engl J Med 346: 1616–22. (Cited on page 29.)

Rebbeck TR, Mitra N, Wan F, Sinilnikova OM, Healey S, et al. (2015) Association of type and location of BRCA1 and BRCA2 mutations with risk of breast and ovarian cancer. JAMA 313: 1347–61. (Cited on page 34.)

Reich NC, Sarnow P, Duprey E, Levine AJ (1983) Monoclonal antibodies which recognize native and denatured forms of the adenovirus DNA-binding protein. Virology 128: 480–4. (Cited on page 180.)

Reid T, Galanis E, Abbruzzese J, Sze D, Wein LM, et al. (2002) Hepatic arterial infusion of a replication-selective oncolytic adenovirus (dl1520): phase II viral, immunologic, and clinical endpoints. Cancer Res 62: 6070–9. (Cited on pages 84, 243, and 249.)

Richardson C, Stark JM, Ommundsen M, Jasin M (2004) Rad51 overexpression promotes alternative double-strand break repair pathways and genome instability. Oncogene 23: 546–53. (Cited on page 62.)

Robert-Guroff M (2007) Replicating and non-replicating viral vectors for vaccine development. Curr Opin Biotechnol 18: 546–56. (Cited on page 69.)

Robertson KA, Bullock HA, Xu Y, Tritt R, Zimmerman E, et al. (2001) Altered expression of Ape1/ref-1 in germ cell tumors and overexpression in NT2 cells confers resistance to bleomycin and radiation. Cancer Res 61: 2220–5. (Cited on page 246.)

Rogakou EP, Pilch DR, Orr AH, Ivanova VS, Bonner WM (1998) DNA double-stranded breaks induce histone H2AX phosphorylation on serine 139. J Biol Chem 273: 5858–68. (Cited on page 150.)

Rosonina E, Ip JY, Calarco JA, Bakowski MA, Emili A, et al. (2005) Role for PSF in mediating transcriptional activator-dependent stimulation of pre-mRNA processing in vivo. Mol Cell Biol 25: 6734–6746. (Cited on page 234.)

Roy R, Chun J, Powell SN (2012) BRCA1 and BRCA2: different roles in a common pathway of genome protection. Nat Rev Cancer 12: 68–78. (Cited on pages 53, 56, 57, and 58.)

Russell SJ, Peng KW, Bell JC (2012) Oncolytic virotherapy. Nat Biotechnol 30: 658–70. (Cited on pages 68, 69, 82, 239, and 248.)

Russell WC (2000) Update on adenovirus and its vectors. J Gen Virol 81: 2573–604. (Cited on pages 71, 73, 74, 87, and 232.)

Russell WC (2009) Adenoviruses: update on structure and function. J Gen Virol 90: 1–20. (Cited on page 71.)

Rustin GJ, van der Burg ME, Griffin CL, Guthrie D, Lamont A, et al. (2010) Early versus delayed treatment of relapsed ovarian cancer (MRC OV05/EORTC 55955): a randomised trial. Lancet 376: 1155–63. (Cited on page 43.)

Safra T, Borgato L, Nicoletto MO, Rolnitzky L, Pelles-Avraham S, et al. (2011) BRCA mutation status and determinant of outcome in women with recurrent epithelial ovarian cancer treated with pegylated liposomal doxorubicin. Mol Cancer Ther 10: 2000–7. (Cited on page 63.)

Sakai W, Swisher EM, Jacquemont C, Chandramohan KV, Couch FJ, et al. (2009) Functional restoration of BRCA2 protein by secondary BRCA2 mutations in BRCA2-mutated ovarian carcinoma. Cancer Res 69: 6381–6. (Cited on pages 155 and 162.)

Sakai W, Swisher EM, Karlan BY, Agarwal MK, Higgins J, et al. (2008) Secondary mutations as a mechanism of cisplatin resistance in BRCA2-mutated cancers. Nature 451: 1116–20. (Cited on pages 63, 154, and 200.)

Salako MA, Kulbe H, Ingemarsdotter CK, Pirlo KJ, Williams SL, et al. (2011) Inhibition of the inflammatory cytokine TNF-alpha increases

adenovirus activity in ovarian cancer via modulation of cIAP1/2 expression. Mol Ther 19: 490–9. (Cited on page 85.)

Saleh-Gohari N, Bryant HE, Schultz N, Parker KM, Cassel TN, et al. (2005) Spontaneous homologous recombination is induced by collapsed replication forks that are caused by endogenous DNA single-strand breaks. Mol Cell Biol 25: 7158–69. (Cited on page 149.)

Salehi F, Dunfield L, Phillips KP, Krewski D, Vanderhyden BC (2008) Risk factors for ovarian cancer: an overview with emphasis on hormonal factors. J Toxicol Environ Health B Crit Rev 11: 301–21. (Cited on page 30.)

Salisbury JL, Suino KM, Busby R, Springett M (2002) Centrin-2 is required for centriole duplication in mammalian cells. Current Biol 12: 1287–1292. (Cited on page 221.)

Sandhu SK, Schelman WR, Wilding G, Moreno V, Baird RD, et al. (2013) The poly(ADP-ribose) polymerase inhibitor niraparib (MK4827) in BRCA mutation carriers and patients with sporadic cancer: a phase 1 dose-escalation trial. Lancet Oncol 14: 882–92. (Cited on page 66.)

Sarnow P, Hearing P, Anderson CW, Halbert DN, Shenk T, et al. (1984) Adenovirus early region 1B 58,000-dalton tumor antigen is physically associated with an early region 4 25,000-dalton protein in productively infected cells. J Virol 49: 692–700. (Cited on page 81.)

Satisbury JL (1995) Centrin, centrosomes, and mitotic spindle poles. Curr Opin Cell Biol 7: 39–45. (Cited on page 221.)

Sato E, Olson SH, Ahn J, Bundy B, Nishikawa H, et al. (2005) Intraepithelial CD8+ tumor-infiltrating lymphocytes and a high CD8+/regulatory T cell ratio are associated with favorable prognosis in ovarian cancer. Proc Natl Acad Sci USA 102: 18538–43. (Cited on page 39.)

Schild D, Wiese C (2010) Overexpression of RAD51 suppresses recombination defects: a possible mechanism to reverse genomic instability. Nucleic Acids Res 38: 1061–70. (Cited on page 62.)

Schlacher K, Christ N, Siaud N, Egashira A, Wu H, et al. (2011) Double-strand break repair-independent role for BRCA2 in blocking stalled replication fork degradation by MRE11. Cell 145: 529–42. (Cited on pages 56 and 206.)

Schorge JO, McCann C, Del Carmen MG (2010) Surgical debulking of ovarian cancer: what difference does it make? Rev Obstet Gynecol 3: 111–7. (Cited on page 41.)

Schreiner S, Kinkley S, Burck C, Mund A, Wimmer P, et al. (2013) SPOC1-mediated antiviral host cell response is antagonized early in human adenovirus type 5 infection. PLoS Pathog 9: e1003775. (Cited on page 91.)

Senzer NN, Kaufman HL, Amatruda T, Nemunaitis M, Reid T, et al. (2009) Phase II clinical trial of a granulocyte-macrophage colony-stimulating factor-encoding, second-generation oncolytic herpesvirus in patients with unresectable metastatic melanoma. J Clin Oncol 27: 5763–71. (Cited on page 249.)

Shaltiel IA, Krenning L, Bruinsma W, Medema RH (2015) The same, only different - DNA damage checkpoints and their reversal throughout the cell cycle. J Cell Sci 128: 607–20. (Cited on page 131.)

Shayakhmetov DM, Gaggar A, Ni S, Li ZY, Lieber A (2005) Adenovirus binding to blood factors results in liver cell infection and hepatotoxicity. J Virol 79: 7478–91. (Cited on page 85.)

Shenk T (2001) Adenoviridae: The Viruses and their Replication In: Fields Virology. Fields Virology, Lippincott Williams and Wilkins. (Cited on page 72.)

Sherr CJ, McCormick F (2002) The RB and p53 pathways in cancer. Cancer Cell 2: 103–12. (Cited on pages 78, 81, and 120.)

Shibata A, Conrad S, Birraux J, Geuting V, Barton O, et al. (2011) Factors determining DNA double-strand break repair pathway choice in G2 phase. EMBO J 30: 1079–92. (Cited on pages 61 and 202.)

Shibata A, Jeggo PA (2014) DNA double-strand break repair in a cellular context. Clin Oncol (R Coll Radiol) 26: 243–9. (Cited on pages 49, 51, 52, and 59.)

Shrivastav M, De Haro LP, Nickoloff JA (2008) Regulation of DNA double-strand break repair pathway choice. Cell Res 18: 134–47. (Cited on pages 202 and 235.)

Singer G, Oldt R 3rd, Cohen Y, Wang BG, Sidransky D, et al. (2003) Mutations in BRAF and KRAS characterize the development of low-grade ovarian serous carcinoma. J Natl Cancer Inst 95: 484–6. (Cited on page 32.)

Singer G, Stöhr R, Cope L, Dehari R, Hartmann A, et al. (2005) Patterns of p53 mutations separate ovarian serous borderline tumors and low- and high-grade carcinomas and provide support for a new model of ovarian carcinogenesis: a mutational analysis with immunohistochemical correlation. Am J Surg Pathol 29: 218–24. (Cited on page 32.)

Singhal G, Leo E, Setty SKG, Pommier Y, Thimmapaya B (2013) Adenovirus E1A oncogene induces rereplication of cellular DNA and alters DNA replication dynamics. J Virol 87: 8767–78. (Cited on pages 148, 149, and 150.)

Siu KT, Rosner MR, Minella AC (2012) An integrated view of cyclin E function and regulation. Cell Cycle 11: 57–64. (Cited on page 35.)

Soerjomataram I, Lortet-Tieulent J, Parkin DM, Ferlay J, Mathers C, et al. (2012) Global burden of cancer in 2008: a systematic analysis of

disability-adjusted life-years in 12 world regions. Lancet 380: 1840–50. (Cited on page 28.)

Sowd GA, Li NY, Fanning E (2013) ATM and ATR activities maintain replication fork integrity during SV40 chromatin replication. PLoS Pathog 9: e1003283. (Cited on page 204.)

Sowd GA, Mody D, Eggold J, Cortez D, Friedman KL, et al. (2014) SV40 utilizes ATM kinase activity to prevent non-homologous end joining of broken viral DNA replication products. PLoS Pathog 10: e1004536. (Cited on page 204.)

Stewart PL, Chiu CY, Huang S, Muir T, Zhao Y, et al. (1997) Cryo-EM visualization of an exposed RGD epitope on adenovirus that escapes antibody neutralization. EMBO J 16: 1189–98. (Cited on page 74.)

Stone RL, Nick AM, McNeish IA, Balkwill F, Han HD, et al. (2012) Paraneoplastic thrombocytosis in ovarian cancer. N Engl J Med 366: 610–8. (Cited on page 40.)

Stracker TH, Carson CT, Weitzman MD (2002) Adenovirus oncoproteins inactivate the Mre11-Rad50-NBS1 DNA repair complex. Nature 418: 348–52. (Cited on pages 89, 90, 175, and 202.)

Stracker TH, Lee DV, Carson CT, Araujo FD, Ornelles DA, et al. (2005) Serotype-specific reorganization of the Mre11 complex by adenoviral E4orf3 proteins. J Virol 79: 6664–73. (Cited on pages 90 and 203.)

Suh DH, Kim JW, Kang S, Kim HJ, Lee KH (2014) Major clinical research advances in gynecologic cancer in 2013. J Gynecol Oncol 25: 236–48. (Cited on page 42.)

Sung P (1994) Catalysis of ATP-dependent homologous DNA pairing and strand exchange by yeast RAD51 protein. Science 265: 1241–3. (Cited on page 201.)

Sung P, Krejci L, Van Komen S, Sehorn MG (2003) Rad51 recombinase and recombination mediators. J Biol Chem 278: 42729–32. (Cited on pages 52 and 54.)

Swanton C, Nicke B, Schuett M, Eklund AC, Ng C, et al. (2009) Chromosomal instability determines taxane response. Proc Natl Acad Sci USA 106: 8671–6. (Cited on page 36.)

Swisher EM, Sakai W, Karlan BY, Wurz K, Urban N, et al. (2008) Secondary BRCA1 mutations in BRCA1-mutated ovarian carcinomas with platinum resistance. Cancer Res 68: 2581–6. (Cited on pages 63 and 201.)

Symington LS, Gautier J (2011) Double-strand break end resection and repair pathway choice. Annu Rev Genet 45: 247–71. (Cited on pages 59 and 202.)

Synowiec A, Wcisło G, Bodnar L, Górski B, Szenajch J, et al. (2016) Clinical features and outcomes of germline mutation BRCA1-linked versus sporadic ovarian cancer patients. Hered Cancer Clin Pract 14: 1. (Cited on page 153.)

Tagliaferri P, Ventura M, Baudi F, Cucinotto I, Arbitrio M, et al. (2009) BRCA1/2 genetic background-based therapeutic tailoring of human ovarian cancer: hope or reality? J Ovarian Res 2: 14. (Cited on page 63.)

Takeda T, Nakajima K, Kojima H, Hirano T (1994) E1A repression of IL-6-induced gene activation by blocking the assembly of IL-6 response element binding complexes. J Immunol 153: 4573–82. (Cited on page 83.)

Tan DS, Kaye SB (2015) Chemotherapy for Patients with BRCA1 and BRCA2-Mutated Ovarian Cancer: Same or Different? Am Soc Clin Oncol Educ Book pp. 114–21. (Cited on pages 63 and 66.)

Tan DSP, Rothermundt C, Thomas K, Bancroft E, Eeles R, et al. (2008) "BRCAness" syndrome in ovarian cancer: a case-control study describing the clinical features and outcome of patients with epithelial ovarian cancer associated with BRCA1 and BRCA2 mutations. J Clin Oncol 26: 5530–6. (Cited on page 154.)

Tan DSP, Yap TA, Hutka M, Roxburgh P, Ang J, et al. (2013) Implications of BRCA1 and BRCA2 mutations for the efficacy of paclitaxel monotherapy in advanced ovarian cancer. Eur J Cancer 49: 1246–53. (Cited on page 63.)

Tan TR, Kanaar R, Wyman C (2003) Rad54, a Jack of all trades in homologous recombination. DNA Repair 2: 787–794. (Cited on pages 222 and 235.)

Tarsounas M, Davies D, West SC (2003) BRCA2-dependent and independent formation of RAD51 nuclear foci. Oncogene 22: 1115–1123. (Cited on page 206.)

TGCA (2011) Integrated genomic analyses of ovarian carcinoma. Nature 474: 609–15. (Cited on pages 33, 34, 35, 36, 153, 200, and 232.)

Theerthagiri G, Eisenhardt N, Schwarz H, Antonin W (2010) The nucleoporin Nup188 controls passage of membrane proteins across the nuclear pore complex. J Cell Biol 189: 1129–1142. (Cited on page 223.)

Thigpen JT, Blessing JA, Ball H, Hummel SJ, Barrett RJ (1994) Phase II trial of paclitaxel in patients with progressive ovarian carcinoma after platinum-based chemotherapy: a Gynecologic Oncology Group study. J Clin Oncol 12: 1748–53. (Cited on page 44.)

Thimmappaya B, Weinberger C, Schneider RJ, Shenk T (1982) Adenovirus VAI RNA is required for efficient translation of viral mRNAs at late times after infection. Cell 31: 543–51. (Cited on page 72.)

Thomas MA, Spencer JF, La Regina MC, Dhar D, Tollefson AE, et al. (2006) Syrian hamster as a permissive immunocompetent animal model for the study of oncolytic adenovirus vectors. Cancer Res 66: 1270–6. (Cited on page 244.)

Titus-Ernstoff L, Perez K, Cramer DW, Harlow BL, Baron JA, et al. (2001) Menstrual and reproductive factors in relation to ovarian cancer risk. Br J Cancer 84: 714–21. (Cited on pages 29 and 30.)

Tollefson AE, Scaria A, Hermiston TW, Ryerse JS, Wold LJ, et al. (1996) The adenovirus death protein (E3-11.6K) is required at very late stages of infection for efficient cell lysis and release of adenovirus from infected cells. J Virol 70: 2296–306. (Cited on page 84.)

Tothill RW, Tinker AV, George J, Brown R, Fox SB, et al. (2008) Novel molecular subtypes of serous and endometrioid ovarian cancer linked to clinical outcome. Clin Cancer Res 14: 5198–208. (Cited on page 35.)

Touchefeu Y, Vassaux G, Harrington KJ (2011) Oncolytic viruses in radiation oncology. Radiother Oncol 99: 262–70. (Cited on page 240.)

Trotman LC, Mosberger N, Fornerod M, Stidwill RP, Greber UF (2001) Import of adenovirus DNA involves the nuclear pore complex receptor CAN/Nup214 and histone H1. Nat Cell Biol 3: 1092–100. (Cited on page 74.)

Truong LN, Wu X (2011) Prevention of DNA re-replication in eukaryotic cells. J Mol Cell Biol 3: 13–22. (Cited on page 131.)

Tsai CJ, Kim SA, Chu G (2007) Cernunnos/XLF promotes the ligation of mismatched and noncohesive DNA ends. Proc Natl Acad Sci USA 104: 7851–6. (Cited on page 51.)

Turnbull S, West EJ, Scott KJ, Appleton E, Melcher A, et al. (2015) Evidence for Oncolytic Virotherapy: Where Have We Got to and

Where Are We Going? Viruses 7: 6291–312. (Cited on pages 85, 86, 245, 247, and 248.)

Turnell AS, Grand RJ (2012) DNA viruses and the cellular DNA-damage response. J Gen Virol 93: 2076–97. (Cited on pages 88, 92, 203, 204, and 246.)

Tutt A, Robson M, Garber JE, Domchek SM, Audeh MW, et al. (2010) Oral poly (ADP-ribose) polymerase inhibitor olaparib in patients with BRCA1 or BRCA2 mutations and advanced breast cancer: a proof-of-concept trial. Lancet 376: 235–244 (Cited on page 208.)

Udayakumar D, Dynan WS (2015) Characterization of DNA binding and pairing activities associated with the native SFPQÂ·NONO DNA repair protein complex. Biochem Biophys Res Commun 463: 473–8. (Cited on page 234.)

Ushijima K (2010) Treatment for recurrent ovarian cancer-at first relapse. J Oncol 2010: 497429. (Cited on page 44.)

Uusi-Kerttula H, Hulin-Curtis S, Davies J, Parker AL (2015) Oncolytic Adenovirus: Strategies and Insights for Vector Design and Immuno-Oncolytic Applications. Viruses 7: 6009–42. (Cited on page 85.)

Van Gorp T, Amant F, Neven P, Vergote I, Moerman P (2004) Endometriosis and the development of malignant tumours of the pelvis. A review of literature. Best Pract Res Clin Obstet Gynaecol 18: 349–71. (Cited on page 30.)

Vasey PA, Shulman LN, Campos S, Davis J, Gore M, et al. (2002) Phase I trial of intraperitoneal injection of the E1B-55-kd-gene-deleted adenovirus ONYX-015 (dl1520) given on days 1 through 5 every 3 weeks in patients with recurrent/refractory epithelial ovarian cancer. J Clin Oncol 20: 1562–9. (Cited on page 249.)

Vaughan S, Coward JI, Bast J R C, Berchuck A, Berek JS, et al. (2011) Rethinking ovarian cancer: recommendations for improving

outcomes. Nat Rev Cancer 11: 719–25. (Cited on pages 31, 237, and 244.)

Venkitaraman AR (2009) Linking the cellular functions of BRCA genes to cancer pathogenesis and treatment. Annu Rev Pathol 4: 461–87. (Cited on page 29.)

Vergote I, Trope CG, Amant F, Kristensen GB, Ehlen T, et al. (2010) Neoadjuvant chemotherapy or primary surgery in stage IIIC or IV ovarian cancer. N Engl J Med 363: 943–53. (Cited on page 41.)

Verhaak RGW, Tamayo P, Yang JY, Hubbard D, Zhang H, et al. (2013) Prognostically relevant gene signatures of high-grade serous ovarian carcinoma. J Clin Invest 123: 517–25. (Cited on page 35.)

Wan Y, Han J, Fan G, Zhang Z, Gong T, et al. (2013) Enzyme-responsive liposomes modified adenoviral vectors for enhanced tumor cell transduction and reduced immunogenicity. Biomaterials 34: 3020–30. (Cited on page 85.)

Wang ZC, Birkbak NJ, Culhane AC, Drapkin R, Fatima A, et al. (2012) Profiles of genomic instability in high-grade serous ovarian cancer predict treatment outcome. Clin Cancer Res 18: 5806–15. (Cited on page 36.)

Ward IM, Chen J (2001) Histone H2AX is phosphorylated in an ATR-dependent manner in response to replicational stress. J Biol Chem 276: 47759–62. (Cited on page 150.)

Ward JD, Muzzini DM, Petalcorin MI, Martinez-Perez E, Martin JS, et al. (2010) Overlapping mechanisms promote postsynaptic RAD-51 filament disassembly during meiotic double-strand break repair. Mol Cell 37: 259–72. (Cited on page 58.)

Watkins JA, Irshad S, Grigoriadis A, Tutt ANJ (2014) Genomic scars as biomarkers of homologous recombination deficiency and drug

response in breast and ovarian cancers. Breast Cancer Res 16: 211. (Cited on page 242.)

Wei S, Kryczek I, Zou L, Daniel B, Cheng P, et al. (2005) Plasmacytoid dendritic cells induce CD8+ regulatory T cells in human ovarian carcinoma. Cancer Res 65: 5020–6. (Cited on page 40.)

Weiden MD, Ginsberg HS (1994) Deletion of the E4 region of the genome produces adenovirus DNA concatemers. Proc Natl Acad Sci USA 91: 153–7. (Cited on page 89.)

Weitzman MD, Ornelles DA (2005) Inactivating intracellular antiviral responses during adenovirus infection. Oncogene 24: 7686–96. (Cited on pages 73, 87, 88, 89, 91, 120, 154, 155, 209, and 232.)

White E (2001) Regulation of the cell cycle and apoptosis by the oncogenes of adenovirus. Oncogene 20: 7836–46. (Cited on page 80.)

Wiegand KC, Shah SP, Al-Agha OM, Zhao Y, Tse K, et al. (2010) ARID1A mutations in endometriosis-associated ovarian carcinomas. N Engl J Med 363: 1532–43. (Cited on page 33.)

Wiggans AJ, Cass GKS, Bryant A, Lawrie TA, Morrison J (2015) Poly(ADP-ribose) polymerase (PARP) inhibitors for the treatment of ovarian cancer. Cochrane Database Syst Rev 5: CD007929. (Cited on page 154.)

Williams RS, Williams JS, Tainer JA (2007) Mre11-Rad50-Nbs1 is a keystone complex connecting DNA repair machinery, double-strand break signaling, and the chromatin template. Biochem Cell Biol 85: 509–20. (Cited on pages 48 and 90.)

Wolchok JD, Hoos A, O'Day S, Weber JS, Hamid O, et al. (2009) Guidelines for the evaluation of immune therapy activity in solid tumors: immune-related response criteria. Clin Cancer Res 15: 7412–20. (Cited on page 249.)

Wong HH, Lemoine NR, Wang Y (2010) Oncolytic Viruses for Cancer Therapy: Overcoming the Obstacles. Viruses 2: 78–106. (Cited on page 69.)

Wood RD, Mitchell M, Lindahl T (2005) Human DNA repair genes, 2005. Mutation Research/Fundamental and Molecular Mechanisms of Mutagenesis 577: 275–283. (Cited on page 209.)

Wu L, Hickson ID (2003) The Bloom's syndrome helicase suppresses crossing over during homologous recombination. Nature 426: 870–4. (Cited on page 54.)

Xia B, Sheng Q, Nakanishi K, Ohashi A, Wu J, et al. (2006) Control of BRCA2 cellular and clinical functions by a nuclear partner, PALB2. Mol Cell 22: 719–29. (Cited on page 56.)

Xia F, Taghian DG, DeFrank JS, Zeng ZC, Willers H, et al. (2001) Deficiency of human BRCA2 leads to impaired homologous recombination but maintains normal nonhomologous end joining. Proc Natl Acad Sci USA 98: 8644–9. (Cited on page 177.)

Xiao X, Melton DW, Gourley C (2014) Mismatch repair deficiency in ovarian cancer – molecular characteristics and clinical implications. Gynecol Oncol 132: 506–12. (Cited on page 246.)

Xu J, Zhu W, Xu W, Cui X, Chen L, et al. (2013) Silencing of MBD1 reverses pancreatic cancer therapy resistance through inhibition of DNA damage repair. Int J Oncol 42: 2046–2052. (Cited on page 222.)

Xu X, Weaver Z, Linke SP, Li C, Gotay J, et al. (1999) Centrosome amplification and a defective G2-M cell cycle checkpoint induce genetic instability in BRCA1 exon 11 isoform-deficient cells. Mol Cell 3: 389–95. (Cited on page 36.)

Yang D, Khan S, Sun Y, Hess K, Shmulevich I, et al. (2011) Association of BRCA1 and BRCA2 mutations with survival, chemotherapy

sensitivity, and gene mutator phenotype in patients with ovarian cancer. JAMA 306: 1557–65. (Cited on pages 63, 185, and 200.)

Yang Y, Hanke J, Carayannopoulos L, Craft C, Capra J, et al. (1993) NonO, a non-POU-domain-containing, octamer-binding protein, is the mammalian homolog of Drosophila nonAdiss. Mol Cell Biol 13: 5593–5603. (Cited on page 220.)

Yang Z, Zhang Q, Xu K, Shan J, Shen J, et al. (2012) Combined therapy with cytokine-induced killer cells and oncolytic adenovirus expressing IL-12 induce enhanced antitumor activity in liver tumor model. PLoS One 7: e44802. (Cited on page 86.)

Yap TA, Sandhu SK, Carden CP, de Bono JS (2011) Poly (ADP-Ribose) polymerase (PARP) inhibitors: Exploiting a synthetic lethal strategy in the clinic. CA Cancer J Clin 61: 31–49. (Cited on page 172.)

Young AM, Archibald KM, Tookman LA, Pool A, Dudek K, et al. (2012) Failure of translation of human adenovirus mRNA in murine cancer cells can be partially overcome by L4-100K expression in vitro and in vivo. Mol Ther 20: 1676–88. (Cited on pages 86 and 244.)

Yu W, Fang H (2007) Clinical trials with oncolytic adenovirus in China. Curr Cancer Drug Targets 7: 141–8. (Cited on page 238.)

Yuan SS, Lee SY, Chen G, Song M, Tomlinson GE, et al. (1999) BRCA2 is required for ionizing radiation-induced assembly of Rad51 complex in vivo. Cancer Res 59: 3547–51. (Cited on page 56.)

Zhang JH, Chung TD, Oldenburg KR (1999a) A simple statistical parameter for use in evaluation and validation of high throughput screening assays. J Biomol Screen 4: 67–73. (Cited on page 214.)

Zhang L, Conejo-Garcia JR, Katsaros D, Gimotty PA, Massobrio M, et al. (2003a) Intratumoral T cells, recurrence, and survival in epithe-

lial ovarian cancer. N Engl J Med 348: 203–13. (Cited on pages 37 and 45.)

Zhang M, Li S, Li J, Ensminger WD, Lawrence TS (2003b) Ionizing radiation increases adenovirus uptake and improves transgene expression in intrahepatic colon cancer xenografts. Mol Ther 8: 21–8. (Cited on page 240.)

Zhang X, Turnell AS, Gorbea C, Mymryk JS, Gallimore PH, et al. (2004) The targeting of the proteasomal regulatory subunit S2 by adenovirus E1A causes inhibition of proteasomal activity and increased p53 expression. J Biol Chem 279: 25122–33. (Cited on page 80.)

Zhang XD, Heyse JF (2009) Determination of sample size in genome-scale RNAi screens. Bioinformatics 25: 841–844. (Cited on page 233.)

Zhang XD, Kuan PF, Ferrer M, Shu X, Liu YC, et al. (2008) Hit selection with false discovery rate control in genome-scale RNAi screens. Nucleic Acids Res 36: 4667–4679. (Cited on page 233.)

Zhang XY, Pettengell R, Nasiri N, Kalia V, Dalgleish AG, et al. (1999b) Characteristics and growth patterns of human peritoneal mesothelial cells: comparison between advanced epithelial ovarian cancer and non-ovarian cancer sources. J Soc Gynecol Investig 6: 333–40. (Cited on pages 115 and 117.)

Zhang Z, Huang J, Zhang C, Yang H, Qiu H, et al. (2015) Infiltration of dendritic cells and T lymphocytes predicts favorable outcome in epithelial ovarian cancer. Cancer Gene Ther 22: 198–206. (Cited on page 45.)

Zhou BB, Elledge SJ (2000) The DNA damage response: putting checkpoints in perspective. Nature 408: 433–9. (Cited on page 48.)

Zhu J, Zhou L, Wu G, Konig H, Lin X, et al. (2013) A novel small molecule RAD51 inactivator overcomes imatinib-resistance in chronic myeloid leukaemia. EMBO Mol Med 5: 353–365. (Cited on page 179.)

Zhu Z, Zhao X, Zhao L, Yang H, Liu L, et al. (2015) p54nrb/NONO regulates lipid metabolism and breast cancer growth through SREBP-1A. Oncogene 35: 1399–1410. (Cited on page 234.)

COLOPHON

This thesis was typeset in Lyx with LaTeX 2ε using Hermann Zapf's *Palatino* and *Euler* type faces (Type 1 PostScript fonts *URW Palladio L* and *FPL* were used).

The typographic style, developed by André Miede, was inspired by Bringhurst's *The Elements of Typographic Style* (2004). It is available for LaTeX via CTAN as "classicthesis".

Final Version as of September 17, 2016 (`classicthesis` version 4.2).